Carbon Metabolism of Methylotrophic Methanogens and Asgard Archaea in Marine Sediments

DISSERTATION

zur

Erlangung des Grades eines

Doktors der Naturwissenschaften

−Dr. rer. nat.−

dem Fachbereich Biologie/Chemie der

Universität Bremen vorgelegt von

Xiuran Yin

Bremen 2019

Universität Bremen

This PhD thesis was conducted in the frame work
of the International Max Planck Research
School of Marine Microbiology (MarMic) and
supported by the China Scholarship Council.

Gutachter: Prof. Dr. Michael W. Friedrich (Universität Bremen)
Gutachter: Prof. Dr. Jens Harder (Max-Planck-Institut für Marine Mikrobiologie)

Prüfer: Dr. Marcus Elvert (Marum)
Prüfer: Tilmann Harder (Universität Bremen)

Contents

Abbreviation

AAI: amino acid identity

alkB: alkane hydroxylase gene

ANMEs: anaerobic methanotrophs

AQDS: anthraquinone-2,6-disulfonic acid

AR: archaeol; AR-OH: hydroxyarchaeol

ASW: artificial sea water

CBB cycle: Calvin-Benson-Bassham cycle

CH_3-H_4MPT: methyl-tetrahydromethanopterin

CsCl: cesium chloride

CsTFA: cesium trifluoroacetate

DIC: dissolved inorganic carbon

EMP: Embden-Meyerhof-Parnas pathway

EtOH: ethanol

GB: gradient buffer

GC-c-IRMS: gas chromatography combustion isotope ratio mass spectrometry

LPA: linear polyacrylamide

MAGs: metagenome-assembled genomes

MBGD: marine benthic group D

mcrA: methyl-coenzyme M reductase subunit alpha

MeOH: methanol

MZ: methanogenic zone

PCI: phenol:chloroform:isoamylalcohol

PEG: polyethylene glycol

RMSD: root mean square deviation

RubisCO: ribulose-1,5-bisphosphate carboxylase/oxygenase

SIP: stable isotope probing

SMTZ: sulfate-methane transition zone

SRZ: sulfate reduction zone

TCA cycle: tricarboxylic acid cycle

THF-WL: tetrahydrofolate dependent Wood-Ljungdahl

THMPT-WL: tetrahydromethanopterin dependent Wood-Ljungdahl

TIC: total inorganic carbon

TNS: tris-NaCl-sodium dodecyl sulfate

TOC: sulfate-methane transition zone

WL: Wood-Ljungdahl pathway

Summary

Carbon is the central element of life, as it is involved in building up of biological constituents and energy metabolisms in the cell. Archaea, - the most recently recognized domain of life - hold a crucial phylogenetic position in the evolution of life, but for most archaeal phyla, little is known about their role and activity in carbon metabolism. Archaea inhabit a variety of environments such as soils, sediments, sea water, and the guts of animals. Specifically in marine sediments, Thaumarchaeota, Euryarchaeota, Bathyarchaeota, Woesearchaeota and Asgard archaea are commonly found in archaeal communities.

Methanogens affiliated to Euryarchaeota are well-known players in carbon metabolism, i.e., acetoclastic, hydrogenotrophic, and methylotrophic methanogenesis. Based on pure culture studies and genomic evidence, significant amounts of the biomass of methylotrophic methanogens growing on methyl substrates is derived from inorganic carbon. However, the *in situ* activity of these methanogens in carbon assimilation is unclear as the large inorganic carbon pool in marine sediment potentially affects carbon utilization patterns. To address this hypothesis, we initially applied nucleic acid stable isotope probing (SIP) to detect methylotrophic methanogens in marine sediment incubations. SIP results showed that ^{13}C-labeled dissolved inorganic carbon (DIC) is necessary to identify methylotrophic methanogens, as illustrated by the nucleic acid synthesis pathway in these methanogens that 70-80% of carbon stems from DIC rather than methanol.

In parallel, lipid-SIP suggested that DIC contributed to more than 60% from incubations with sediment from the sulfate reduction zone (SRZ), i.e., 20% higher than expected from lipid synthesis pathway. We further unexpectedly found that up to 12% methane was formed from DIC in autoclaved slurry incubations inoculated with the marine methylotrophic methanogen *Methanococcoides methylutens*. Similarly, methane formation from CO_2 during methylotrophic methanogenesis was also observed with SRZ sediment incubations. In the same sediment incubations a higher amount of inorganic carbon was incorporated into lipids than expected, indicating that more DIC was assimilated into biomass than expected. Thus, the CO_2 conversion to methane and biomass may play an important role in marine sediments.

In the most recently discovered super phylum of the Archaea, the Asgard archaea might hold the key to understand the evolutionary origin of eukaryotes. Unlike methanogens, however, the diversity, carbon metabolism and the activity of Asgard archaea in marine sediments are still unknown. In this study, five new groups of Asgard archaea namely Kariarchaeota, Balderarchaeota, Hodarchaeota, Lagarchaeota and Gerdarchaeota are reported. In experiments with ^{13}C-DIC, potential electron donors and electron acceptors, subgroup of Asgard archaea i.e., Lokiarchaeota was detected in the heavy SIP fractions from the incubations amended with organic polymers or sulfur, suggesting their activities of carbon fixation, organic polymers (cellulose, lignin and humic acid) degradation and sulfur

metabolism. Furthermore, metagenomes were sequenced from heavy fractions of DNA-SIP samples obtained in the aforementioned experiments and from DNA extracted from mangrove sediments in the southeast coast of China. These metagenomes indicate that Asgard archaea harbor pathways of inorganic carbon fixation and degradation of cellulose, protein, short-chain and medium-chain alkane as well as assimilatory sulfate reduction. Crucially, the methyl coenzyme M reductase genes found in Helarchaeota have extended the potential of short-chain hydrocarbon oxidation to the Asgard archaea in this study. Overall, these findings illustrate that Asgard archaea actively utilize organic and inorganic carbon at the same time in mixotrophic fashion, which might play critical roles in carbon cycling of marine sediments.

In particular, the successful detection of methylotrophic methanogens and Asgard archaea in marine sediments by nucleic acid-SIP with ^{13}C-DIC suggested a crucial role of inorganic carbon in carbon metabolisms of these archaea. Given that many archaea harbor the acetyl-CoA associated carbon fixation pathway, my findings indicate that inorganic carbon assimilation might be ubiquitous in archaea when supply or availability of organic carbon are not sufficient in marine sediments.

Zusammenfassung

Kohlenstoff ist für alles Leben auf der Erde von zentraler Bedeutung: Er bildet das Grundgerüst aller zellulärer Komponenten und ist am Energiestoffwechsel beteiligt. Archaeen – die zuletzt entdeckte Domäne irdischen Lebens – besetzen eine Schlüsselposition innerhalb der organismischen Evolution, aber über die physiologische Rolle der meisten Stämme der Archaeen im Kohlenstoffkreislauf ist noch sehr wenig bekannt. Archaeen kommen in einer Vielzahl von Habitaten vor, beispielsweise in Böden, Sedimenten, aquatischen Lebensräumen oder im gastrointestinalen Trakt vieler Metazoa.

Innerhalb dieser wichtigen Gruppe von Organismen sind methanogene Euryarchaeota als Teilnehmer des Kohlenstoffkreislaufes gut bekannt, zum Beispiel in der acetoklastischen, hydrogenotrophen und methylotrophen Methanbildung. Durch Studien an Reinkulturen und Genomanalysen weiß man, dass methylotrophe Methanogene einen nicht unerheblichen Anteil ihrer Biomasse aus anorganischen Kohlenstoffquellen bestreiten, wenn sie auf methylierten Verbindungen wachsen. Jedoch ist nicht bekannt, ob diese Stoffwechselwege auch *in situ* beschritten werden; allerdings ist zu vermuten, dass die großen Mengen anorganisch gebundenen Kohlenstoffs in der Umwelt auch Auswirkungen auf die Strategie der Kohlenstoffaufnahme dieser Mikroorganismen haben. Um diese Hypothese zu prüfen, benutzten wir eine Technik zur stabilen Isotopenbeprobung (SIP). Zunächst wurden marine Sedimente mit ^{13}C-markierten Substraten inkubiert, um methylotrophe Methanogene zu detektieren. Dabei zeigte sich, dass die Markierung mit gelöstem anorganischen Kohlenstoff (engl. DIC) notwendig ist, um dieses Ziel zu erreichen, da zwischen 70 – 80% des in den Nukleinsäuren dieser Organismen gebundenen Kohlenstoffs aus anorganischen Quellen stammt – nicht aus Methanol.

Parallel dazu konnte in Inkubationen mit Sedimenten aus der Sulfatreduktionszone (SRZ) mit Hilfe der Isotopenanalyse der zellulären Fettsäuren (Lipid-SIP) gezeigt werden, dass der gelöste anorganische Kohlenstoff zu mehr als 60% des in den Fettsäuren gebundenen Kohlenstoffs beiträgt, also etwa 20% mehr als durch den Fettsäuresyntheseweg vorhergesagt. Wir konnten auch die unerwartete Entdeckung machen, dass in Inkubationen mit inokuliertem *Methanococcoides methylutens*, einem methylotrophen Methanbildners, mit autoklaviertem Sediment 12% des hergestellten Methans aus dem DIC-Reservoir stammt. In ähnlicher Weise konnte die Methansynthese aus CO_2 auch während der eigentlich methylotrophen Methanogenese in SRZ-Sedimenten beobachtet werden. Hierbei wurde ebenfalls mehr anorganischer Kohlenstoff in die zellulären Fettsäuren, also Biomasse, eingebaut als erwartet. Daraus folgend lässt sich eine wichtige Rolle der CO_2-Fixierung und -Konversion zu Methan und Biomasse in marinen Sedimenten vermuten.

Der erst kürzlich entdeckte archaeale Superstamm (engl. super phylum) der Asgard-Archaeen könnte eine Schlüsselrolle beim evolutionären Übergang von den Pro- zu den Eukaryonten gespielt haben. Im Gegensatz zu den Methanogenen jedoch ist sehr wenig über Diversität, Physiologie und Aktivitäten

dieser Gruppe bekannt. In der vorliegenden Arbeit werden 5 neue Gruppen innerhalb dieses Superstammes eingeführt, namentlich Kariarchaeota, Balderarchaeota, Hodarchaeota, Lagarchaeota und Gerdarchaeota. In Experimenten mit ^{13}C-markiertem DIC und verschiedenen potentiellen Elektronendonoren und –akzeptoren wurden Asgard-Archaeen, zum Beispiel Lokiarchaeota, in den schweren Nukleinsäurefraktionen derjenigen Inkubationen gefunden, die unter Zugabe von organischen Polymeren oder Schwefel abliefen. Dies zeigt eine ökophysiologische Funktion dieser Organismen im Abbau von organischen Polymeren (z.B. Lignin, Cellulose und Huminsäuren), in der Kohlenstofffixierung und im Schwefelstoffwechsel an. Weiterhin wurden Metagenome aus den schweren Fraktionen dieser Experimente und aus DNA aus Mangrovensedimenten von der chinesischen Südostküste gebildet. Die Analyse dieser Metagenome zeigte, dass Asgard-Archaeen über das genetische Potential verfügen, um Cellulose, Proteine, kurz- und mittelkettige Alkane zu verstoffwechseln, anorganischen Kohlenstoff zu fixieren, und assimilatorische Sulfatreduktion zu betreiben. Besonders wichtig ist die Detektion von Genen für die Methyl-Coenzym-M-Reduktase in Helarchaeota, was das funktionelle Spektrum der Asgard-Archaeen um die Fähigkeit der Oxidation kurzkettiger Kohlenwasserstoffe erweitert. Insgesamt konnte gezeigt werden, dass Asgard-Archaeen mixotroph sowohl organische als auch anorganische Kohlenstoffverbindungen gleichzeitig aufnehmen können, was für den Kohlenstoffkreislauf in marinen Sedimenten eine wichtige Rolle spielen könnte.

Besonders die Entdeckung von methylotrophen und Asgard-Archaeen in marinen Sedimenten mit Hilfe der Beprobung mit ^{13}C-DIC deutet auf eine wesentliche Funktion von anorganischen Kohlenstoffverbindungen im Stoffwechsel dieser Archaeen hin. Zieht man in Betracht, dass viele Archaeen über den Acetyl-CoA-assoziierten Kohlenstofffixierungsweg verfügen, zeigen meine Befunde, dass anorganischer Kohlenstoff ubiquitär von allen Archaeen assimiliert wird, wenn der Kohlenstoffbedarf nicht aus organischen Quellen gedeckt werden kann.

Chapter 1

Introduction

1.1. Carbon utilization in marine sediments

Marine sediments are the sink of particles in suspension settling down from the water column. These particles contain aggregates of organic compounds, which mainly originate from terrestrial or aquatic primary production as dominant autotrophic process (Burdige 2005; Schlünz and Schneider 2000; Schubert and Calvert 2001). For our study site at Helgoland Mud Area in the German Bight of North Sea (Fig. 1), the input of fresh water provided relatively rich organic carbon and minerals with high sedimentation rates of above 13 mm/year prior to 1250 A.D and 7.7 mm/year during the last century (Dominik et al., 1978; Hebbeln et al., 2003). In contrast, sedimentation in the deep sea sediments occurred over millions of years (Roy et al., 2012; Zhou and Kyte 1992). However, these sedimentations are responsible for organic carbon input and feed microorganisms in marine sediments.

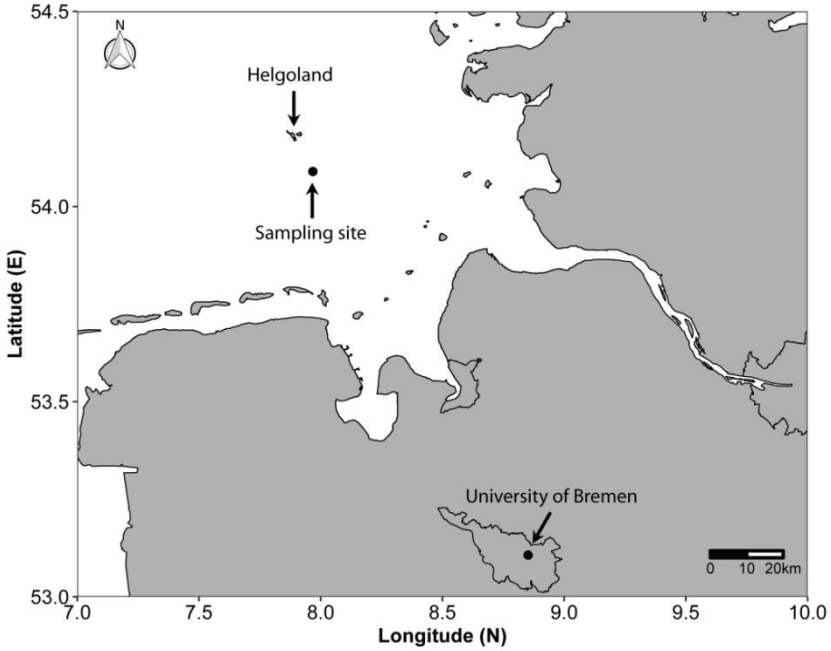

Fig. 1 Sampling site in the Helgoland Mud Area

(The map data was obtained from the Database of Global Administrative Areas (GADM) (http://www.gadm.org/country) and the figure was made in R3.5.2)

Global deposition of organic carbon in the ocean reaches 169×10^{12} g C yr^{-1} of which ~75% organic carbon originates from continental shelf, (Smith et al., 2015), providing a large amount of organic carbon as C source for microbial metabolism. The composition of organic compounds in marine sediments is complex, mainly comprising of carbohydrates, aromatics (humic substances and lignin), aliphatic compounds, lipids, protein and amino acids (Arndt et al., 2013; Carter and Mitterer 1978;

Colombo et al., 1996; Goni et al., 1997; Guerzoni and Rovatti 1987; Mayer et al., 1986; Oni et al., 2015b; Prahl et al., 1994; Smith et al., 2015; Volkman et al., 1987). These organic compounds harbor versatile functional groups, indicating a variety of degradability by microorganisms (De Leeuw and Largeau 1993). Thus, this organic carbon can serve as electron donor and carbon source through the sediment core and likely shapes microbial communities and activities. In the upper layers, microorganisms preferentially take up easily degradable organic compounds (Wakeham et al., 1997), which is coupled with the reduction of oxygen, nitrate, manganese oxides, iron oxides and sulfate. As general rule, oxygen and nitrate is quickly depleted, followed by metal (manganese and iron oxides) and sulfate reduction, according to the availabilities and redox potentials of electron acceptors from upper to deeper sediment layers (Jørgensen and Kasten 2006). For example in the Helgoland Mud sediments, the concentration of dissolved manganese quickly increases from the top of sediment core (~2 cm), followed by Fe^{2+} (~4 cm) (Fig. 2). Sulfate depletion is observed from approximately 10 – 86 cm below subsurface (Fig. 2 and Fig. 3). The dynamics of the geochemical profile in marine sediments reflects that these electron acceptors fuel microbial metabolisms by organic carbon degradation. In the deeper sediment below 100 cm in the Helgoland Mud sediments, the occurrence of methane indicates organic carbon that can be consumed and that fermentation intermediates are used for methanogenesis (Fig. 3). Furthermore, diffusion of methane from the lower sediment to the upper layers feed methane oxidizers when electron acceptor (sulfate) is available. Therefore, in the Helgoland Mud area, although the content of total organic carbon fluctuates through sediment core (Fig. 3), recalcitrance such as aromatic compounds and unsaturated compounds with low hydrogen to carbon ratios accumulates in deeper sediments (Oni et al., 2015b), resulting in a low degradability in deeper sediments.

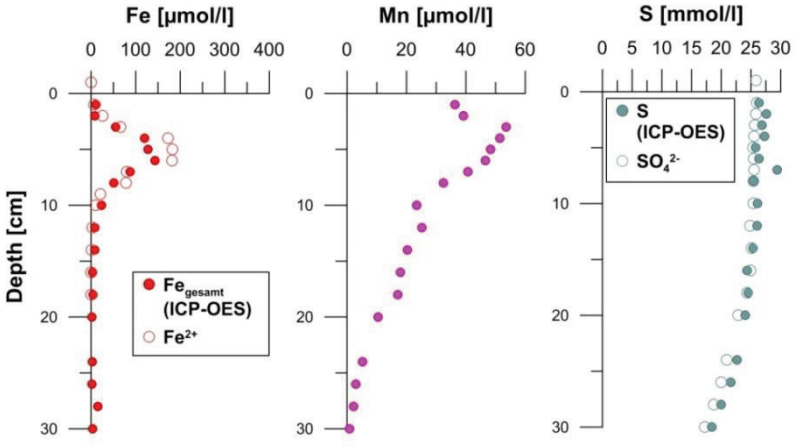

Fig. 2 Geochemical profiles of dissolved iron, manganese and sulfur in the Helgoland Mud sediment in the upper sediment layers (down to 30 cm depths, data were obtained from multicorer sampling). Sediment cores were collected in 2015 during the RV HEINCKE cruise HE443. This data is unpublished and kindly provided by Dr. Susann Henkel (AWI, Bremerhaven).

Anaerobic degradation of organic matter in marine sediments involves fermentation, sulfate reduction, iron reduction and manganese reduction (Canfield et al., 1993). Organic compounds such as carbohydrates can be fermented to short-chain fatty acids or H_2, and the terminal degraders (methanogens) will utilize these carbon sources or electron donors for methane formation when electron acceptors are unavailable (Schink 1997; Tromp et al., 1995). In the presence of electron acceptors, long-chain fatty acids and recalcitrant compounds can be used for microbial growth anaerobically (Annweiler et al., 2000; Coates et al., 1995; Egland et al., 1997). Consequently, turning over of organic carbon in deep marine sediments leads to the accumulation of methane and CO_2.

Besides organic carbon, CO_2 is an important carbon source as suggested by presence of hydrogenotrophic methanogens in deeper layers (Lazar et al., 2011; Zeleke et al., 2013), since CO_2 fixation by hydrogenotrophic methanogens represents an input of inorganic carbon into biosphere. Inorganic carbon is a large pool (up to 40 mM (Zhuang et al., 2018)) in deeper sediment (Fig. 3) including CO_2, mineral inorganic carbon and dissolved inorganic carbon (DIC). Except for methanogens, DIC is also an important carbon source for autotrophs and mixotrophs in sediments such as sulfur-oxidizing *Gammaproteobacteria*, anaerobic methanotrophs (ANMEs) and Bathyarchaeota via the ribulose-1,5-bisphosphate carboxylase/oxygenase (RubisCO) pathway or Wood-Ljungdahl pathway (Dyksma et al., 2016; Kellermann et al., 2012; Yu et al., 2018).

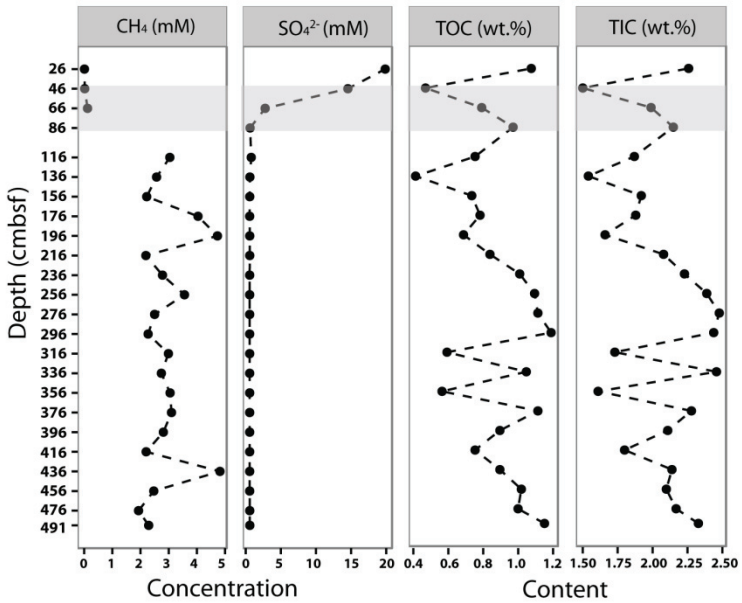

Fig. 3 Geochemical profiles of methane, sulfate, total organic carbon (TOC) and total inorganic carbon (TIC) in the Helgoland Mud sediment from the gravity corer. Sediment was collected during the RV HEINCKE cruise HE443. Gray bar denotes the sulfate-methane transition zone (SMTZ). This data is unpublished and is kindly provided by Dr. Susann Henkel (AWI, Bremerhaven).

Additionally, CO_2 fixation during pyruvate formation from acetyl-CoA for gluconeogenesis and anaplerotic reactions for replenishing citric acid cycle intermediates elevate the contribution of inorganic carbon to biomass substantially in both archaea and bacteria (Perez and Matin 1982; Deppenmeier et al., 2002).

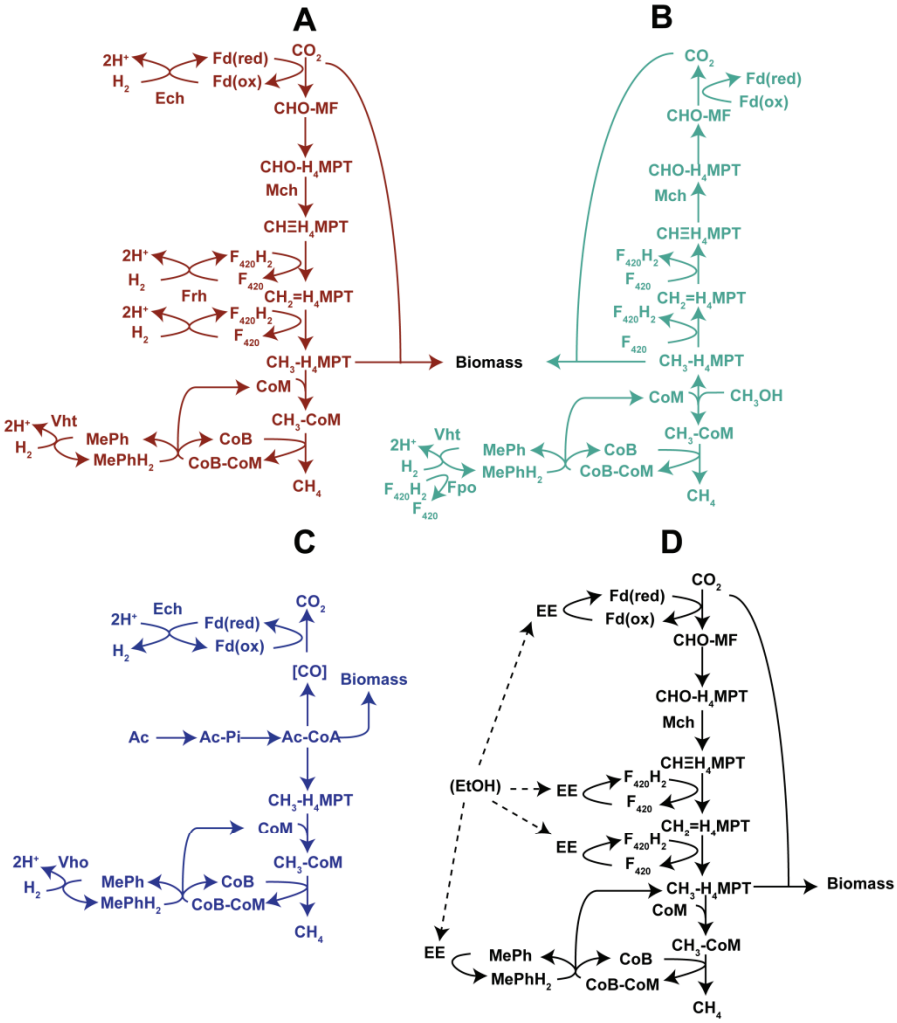

Fig. 4 Methanogenic pathways in *Methanosarcina barkeri* including hydrogenotrophic (H_2/CO_2; A), methylotrophic (e.g., methanol; B), acetoclastic (acetate; C) methanogenesis and syntrophic methane production via extracellular electron transfer (D).

The pathways were constructed according to previous studies (Guss et al., 2005; Rotaru et al., 2014; Thauer 1998). Abbreviations: Ech, ferredoxin-dependent hydrogenase; Frh, F_{420}-dependent hydrogenase; Vho, methanophenazine-dependent hydrogenase; Fpo, F_{420} dehydrogenase; CHO-MF, formyl-methanofuran; CHO-H_4MPT, formyl-tetrahydromethanopterin; CH≡H_4MPT, methenyl-tetrahydromethanopterin; CH_2=H_4MPT, methylene-tetrahydromethanopterin; CH_3-H_4MPT, methyl-tetrahydromethanopterin; CH_3-CoM, methyl-coenzyme M; CoM, coenzyme M; CoB, coenzyme B; CoM-CoB, mixed disulfide of CoM and CoB; Mph/$MphH_2$, oxidized and reduced methanophenazine; $F_{420}/F_{420}H_2$, oxidized and reduced Factor 420; Fd(ox)/Fd(red), oxidized and reduced ferredoxin; Ac, acetate; Ac-Pi, acetyl-phosphate; Ac-CoA, acetyl-Coenzyme A; EE, extracellular electron; EtOH, ethanol. Dashed lines indicate extracellular electron transfer. The figure was made by Weichao Wu (Marum) and Xiuran Yin.

1.2. Carbon metabolisms in methanogenesis

Methanogenesis, as an ancient pathway diverged before 3.51 billion years (Wolfe and Fournier 2018), is the terminal step of organic carbon degradation when the simple compounds or electron donors such as CO_2/H_2, methanol and acetate are accumulated (Ferry and Lessner 2008). As one of green-house gases, annual methane emission can reach 500 – 600 Tg globally, in which 5 – 6% methane is originated from ocean (Reay et al., 2018). These large amounts of methane are generated via three main pathways: hydrogenotrophic, methylotrophic and acetoclastic methanogenesis.

1.2.1. Hydrogenotrophic methanogens

Most orders of methanogens are capable of methane formation from H_2 and CO_2, including *Methanopyrales*, *Methanococcales*, *Methanobacteriales*, *Methanomicrobiales*, *Methanocellales* and *Methanosarcinales* (Liu and Whitman 2008; Thauer et al., 2008). Hydrogenotrophic methanogenesis is CO_2-dependent. During methanogenesis, CO_2 is reduced to CH_4 with H_2 as electron donor according to the following reaction:

$4\ H_2 + CO_2 \rightarrow CH_4 + 2\ H_2O$ $\Delta G^{\circ\prime} = -131$ kJ/mol CH_4 (Thauer et al., 2008) (1)

In this pathway (Fig. 4A), a range of hydrogenases in *Methanosarcinales* (Ech, Frh, Vht) or obligate hydrogenotrophic methanogens (Eha, Frh, Mvh) (Thauer et al., 2010) are used to catalyze reduction reactions with H_2 as electron donor and obtain electron carriers such as reduced ferredoxin and $F_{420}H_2$. These electron carriers further reduce CO_2 to formyl groups (CHO-MF and CHO-H_4MPT), methenyl group (CH≡H_4MPT), methylene group (CH_2=H_4MPT), methyl groups (CH_3-H_4MPT and CH_3-CoM) and CH_4, subsequently. In versatile methanogens (*Methanosarcinales*), methanophenazine-dependent hydrogenase (Vht) catalyzes the reduction of methanophenazine, with which reduced coenzyme B (CoB) is formed, required for catalyzing methyl coenzyme M (CH_3-CoM) reduction to CH_4. The last step of methane formation (reduction of CH_3-CoM to methane) is catalyzed by another hydrogenase, i.e., F_{420}-non-reducing hydrogenase (Mvh) in obligate hydrogenotrophic methanogens as methanophenazine-dependent hydrogenase is restricted to the order of *Methanosarcinales* containing cytochromes (Thauer et al., 2010; Thauer et al., 2008).

Under standard conditions, hydrogenotrophic methanogenesis produces sufficient energy for cell growth (reaction 1). In fact, obligate hydrogenotrophic methanogenesis without cytochromes are more efficient in obtaining ATP than *Methanosarcinales* (Thauer et al., 2008), promoting the adaption of these methanogens to utilization of low H_2 partial pressures (≥5 Pa) (Thauer et al., 2010). As hydrogenotrophic methanogens are observed in a variety of anoxic environments, methane formation from H_2 and CO_2 is regarded as main methanogenic pathway in marine sediments (Katayama et al., 2015; Lazar et al., 2011).

Carbon assimilation by hydrogenotrophic methanogens involves CO_2 reduction, overlapping partly with the dissimilatory pathway, i.e., all the way to the formation of methyl-tetrahydromethanopterin (CH_3-H_4MPT) (Fig. 4). As the key precursor for biomass synthesis, acetyl-CoA is synthesized from CH_3-H_4MPT as methyl group donor and CO_2 as carboxyl group donor (Fig. 4). Both obligate and facultative hydrogenotrophic methanogens harbor the same pathway for autotrophic carbon assimilation.

1.2.2. Methylotrophic methanogens

There are two types of methyl-dependent methanogenesis pathways: disproportionation of C-1 compounds into methane and CO_2, and reduction of methyl group by H_2 to methane (Borrel et al., 2013; Lang et al., 2015) (Fig. 4B). The reactions are as follows:

$4\ CH_3OH \rightarrow 3\ CH_4 + CO_2 + 2\ H_2O$ $\Delta G^{\circ\prime} = -105$ kJ/mol CH_4 (Liu and Whitman 2008) (3)

$CH_3OH + H_2 \rightarrow CH_4 + H_2O$ $\Delta G^{\circ\prime} = -113$ kJ/mol CH_4 (Liu and Whitman 2008) (4)

Disproportionation of methyl substrates was found in the family of *Methanosarcinaceae* and *Methermicoccaceae*. In this pathway, the methyl group is delivered to CH_3-H_4MPT or methyl-tetrahydrosarcinapterin (CH_3-H_4SPT) and subsequently to CO_2 via the reverse CO_2 reduction pathway. On the other hand, reducing equivalents ($F_{420}H_2$) stemming from methyl group oxidation are used to reduce the methyl group and generate CH_4. For H_2-dependent methylotrophic methanogenesis, however, reduction of methyl substrates by H_2 to methane is not involved in oxidation of methyl group to CO_2. The methyl group can be reduced with electrons from H_2 to CH_4 directly. For this pathway, the versatile methanogens in the family of *Methanosarcinaceae*, the genus of *Methanosphaera* and the order of *Methanomassiliicoccales* have the capability of methanol reduction to methane using H_2 as electron donor; in fact, in the latter, hydrogen is obligatory for methylotrophic methanogenesis (Borrel et al., 2014; Lambie et al., 2015; Poehlein et al., 2018).

Methanogens having the ability to use methyl substrates for methanogenesis are identified in different orders. For example, in the order of *Methanosarcinales*, the obligate methylotrophic methanogens only using C1 compounds for methane formation such as the genus of *Methanococcoides*, *Methanolobus*, *Methanomethylovorans* and *Methermicoccus*, as well as the versatile *Methanosarcina* (Cheng et al., 2007; Liu and Whitman 2008). Methylotrophic methanogens placed into other groups including *Methanomassiliicoccales*, *Candidatus* Methanofastidiosa and the newly proposed phylum Verstraetearchaeota, in which H_2 is required to reduce methyl group to methane because of the lack of methyl group oxidation capability to CO_2 (Borrel et al., 2014; Nobu et al., 2016; Vanwonterghem et al., 2016).

Methylotrophic methanogens are able to utilize a variety of methyl substrates including methanol, methyl amines, methionine, methyl sulfides, glycine betaine, choline and dimethylethanolamine for methanogenesis (Cha et al., 2013; Mochimaru et al., 2009; Watkins et al., 2014; Watkins et al., 2012). Specifically in marine sediments, methyl compounds are detectable. For instance, methanol originates from degradation of pectin and lignin (Fall and Benson 1996; Schink and Zeikus 1980). Methylated amines are derived from glycine betaine and choline, which are organic osmoprotectants in marine organisms (King 1984). Dimethylsulfide is formed by decomposition of dimethylsulfoniopropionate, an osmoprotectant in algae (Dacey and Wakeham 1986). These methyl substrates even harbor a high concentration, i.e., up to 69 μM of methanol, 3 μmol/kg trimethylamine and 15 μmol/kg of dimethylsulfoniopropionate (Yanagawa et al., 2016; Zhuang et al., 2016; Zhuang et al., 2018; Zhuang et al., 2014). These observations highlight the important role of methylotrophic methanogenesis in marine sediments, especially in SRZ and hypersaline sediments (Zhuang et al., 2016). Notably, methyl compounds are considered as non-competitive substrates for methanogenesis, since sulfate reducing microorganisms apparently do not compete with methanogens for these compounds (Oremland and Polcin 1982).

In methylotrophic methanogens, acetyl-CoA is formed from CH_3-H_4SPT and CO_2, indicating both CO_2 and methyl group are the main carbon sources. Mixotrophic growth, i.e. utilizing both methyl group carbon and CO_2 for assimilation, was observed in pure cultures of *Methanosarcina barkeri*, with equivalent proportions of methanol and CO_2 contributing to total cell carbon (Weimer and Zeikus 1978).

1.2.3. Acetoclastic methanogens

Acetoclastic methanogens utilize acetate for energy and carbon source. For methanogenesis, acetate is disproportionated to CO_2 and CH_4, which can be performed by the order of *Methanosarcinales* (*Methanosarcinaceae* and *Methanosaetaceae*). The reaction is as follows:

$CH_3COOH \rightarrow CH_4 + CO_2$ $\Delta G^{\circ\prime} = -35.6$ kJ/mol CH_4 (Conrad 1999) (2)

In acetoclastic methanogens, acetate is converted to acetyl-phosphate and further to acetyl-CoA via acetate kinase and phosphate acetyltransferase, respectively. As an important intermediate, acetyl-CoA can be disproportionated to CO_2 and CH_4 under catalysis of a series of enzymes. Regarding carbon assimilation, acetyl-CoA is the key precursor for pyruvate synthesis and further for macromolecule biosynthesis, i.e., protein, nucleic acids and lipids (Fig. 4C).

Compared with hydrogenotrophic and methylotrophic methanogenesis, acetoclastic methanogens generate less energy under standard conditions. However, acetate is the one of the major intermediates of organic polymer degradation formed by fermenting and syntrophic bacteria, and subsequently used

for methane formation in marine sediments (Beulig et al., 2018; Carr et al., 2018; Sorensen et al., 1981; Yoshioka et al., 2015). Acetate concentrations range from 2 – 23 μM in marine sediments (Iniri et al., 2010; Zhuang et al., 2018), indicating the availability as energy and carbon source for these methanogens.

In addition, methanogenesis involved in ethanol metabolisms also occurs in a syntrophic pathway by *Methanosaeta* spp. (Fig. 4D) (Lovley 2017; Rotaru et al., 2014). In this pathway, extracellular electrons generated from degradation of ethanol by *Geobacter* species are transferred via conductive pili to methanogens (Rotaru et al., 2014). In the presence of these extracellular electrons, CO_2 will be reduced to methane via the hydrogenotrophic methanogenesis pathway. On the other hand, the generated byproduct of ethanol degradation, i.e., acetate, is also used by *Methanosaeta* for methane formation via the acetoclastic methanogenesis pathway.

1.3. Carbon metabolisms in other uncultured archaea

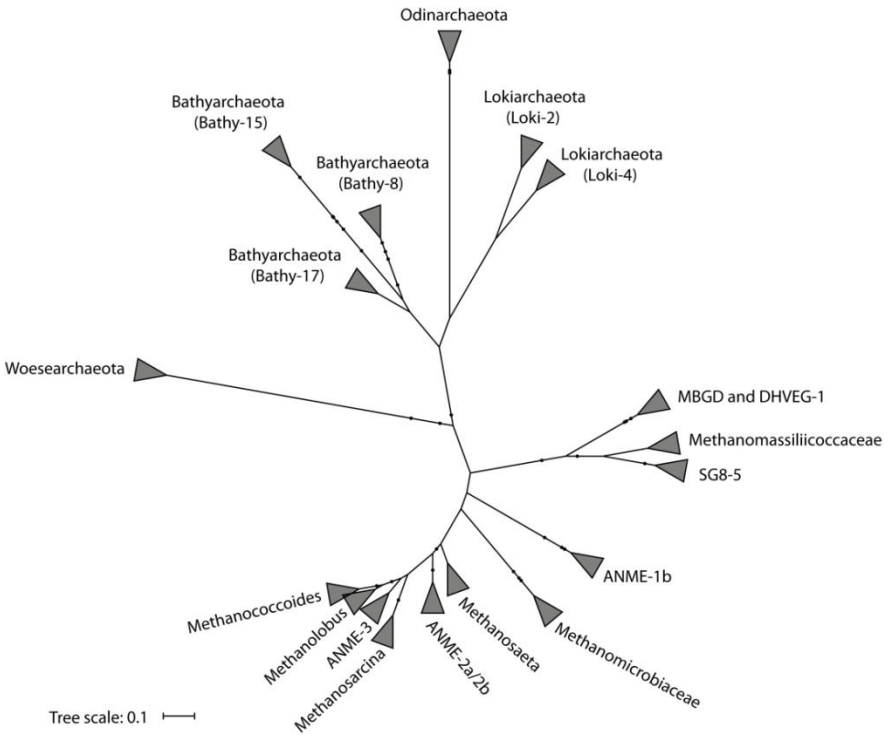

Fig. 5 The unrooted 16S rRNA tree of archaea found in Helgoland Mud sediment and sediment incubations based on clone sequences. The raw tree contained about 300 clones was built by using maximum likelihood algorithm and bootstrapping (n=1000). 2 clones from each branch were picked from the original tree to generate this pruned tree. The tree was built by Ajinkya Kulkarni and Xiuran Yin.

1.3.1. Archaeal diversity in the Helgoland Mud sediments

Archaea affiliated to marine benthic group D (MBGD), Bathyarchaeota and Lokiarchaeota (phylum of Asgard archaea) tend to be found in organic-rich sediments (Durbin and Teske 2012). With a high sedimentation rate and organic carbon input, these archaea are also detected in Helgoland Mud sediments and incubations, including Thaumarchaeota, Euryarchaeota, Bathyarchaeota and Asgard archaea (Lokiarchaeota and Odinarchaeota). Among Euryarchaeota, methanogens with the three methanogenic pathways are found from archaea clones and next-generation sequencing (Fig. 5) (Oni et al., 2015a; Oni et al., 2015b). These methanogens comprised the family of *Methanosarcinaceae* (*Methanococcoides*, *Methanolobus* and *Methanosarcina*), *Methanosaetaceae*, *Methanomicrobiaceae* and *Methanomassiliicoccales*-like group. Except for methanogens, anaerobic methanotrophs (ANMEs) including three subgroups are also found (ANME-1b, ANME-2a/2b and ANME-3), indicating the activities of anaerobic methane oxidation in Helgoland Mud sediments. The other Euryarchaeota such as MBGD, SG8-5 are also detectable in original sediment and incubations (Fig. 5). High relative abundance of Thaumarchaeota is detected from the surface sediment, suggesting oxygen-dependent ammonia oxidation by members of this phylum.

Bathyarchaeota and Asgard archaea are important archaeal subgroups in marine sediments. The *in situ* activities of Bathyarchaeota and Lokiarchaeota are not well known, but evidence exists that Bathyarchaeota is the most dominant archaeal phylum in deep sediments of Helgoland Mud Area (> 50%) (Oni et al., 2015b) and perform CO_2 fixation and degradation of aromatic compounds such as lignin by the subgroup of Bathy-8 (Meng et al., 2014; Yu et al., 2018). By contrast, activity of Asgard archaea is unknown in marine sediments. Asgard archaea is the newly described archaeal super phylum, which include Lokiarchaeota, Thorarchaeota, Odinarchaeota, Heimdallarchaeota and Helarchaeota. These archaea harbor eukaryotic signature proteins and have a crucial phylogenetic position close to eukaryotes, suggesting a role as close relatives of eukaryotes (Spang et al., 2015; Zaremba-Niedzwiedzka et al., 2017). The metagenome-assembled genomes detected from marine sediments suggest Lokiarchaeota and Thorarchaeota might fix CO_2 associating with organic carbon degradation; Heimdallarchaeota potentially utilize nitrate or oxygen to breakdown organic compounds; Odinarchaeota can ferment carbohydrates and Helarchaeota have the capability of hydrocarbon oxidation (Bulzu et al., 2019; Seitz et al., 2019; Seitz et al., 2016; Spang et al., 2019). However, these predicted metagenomic evidences directly obtained from original marine sediments showed all the abilities of Asgard archaea, while the activity in marine sediments is still unknown.

1.3.2. Carbon fixation

Carbon fixation is ubiquitous in methanogens, e.g., autotrophic growth of hydrogenotrophic methanogens and mixotrophic growth of methylotrophic methanogens. In these methanogens, CO_2 is

incorporated into biomass by the Wood-Ljungdahl pathway (reductive acetyl-CoA pathway) and reduced to acetyl-CoA under catalysis of carbon monoxide dehydrogenase/acetyl-CoA synthase (CODH/ACS). Specifically, the complete Wood-Ljungdahl pathway is widespread in most archaea in anoxic Helgoland Mud sediment (Table 1), indicating the potential capability of these archaea in carbon fixation. Methanogens, ANMEs, MBGD, Bathyarchaeota, Woesearchaeota and Lokiarchaeota have the genes encoding the type III ribulose-1,5-bisphosphate carboxylase/oxygenase (RubisCO), the key enzyme catalyzing the CO_2 fixation in the Calvin-Benson-Bassham (CBB) cycle (Table 1). However, the CBB cycle in these archaea is incomplete (Table 1) since the gene encoding Phosphoribulokinase is not present. Although the RubisCO gene is detected and expressed in methanogens (Table 1) (Allen et al., 2009; Goodchild et al., 2004), its function is still enigmatic; potentially RubisCO is involved in metabolism of adenosine 5-monophosphate (Sato et al., 2007) or a new carbon fixation pathway (reductive hexulose-phosphate pathway) (Kono et al., 2017). Similarly, the tricarboxylic acid (TCA) cycle is also incomplete in most archaea with the exception of the MBGD (Table 1) (Lazar et al., 2017; Zhou et al., 2018). In addition, some archaea are "organo-autotrophs" such as ANME-1 and Bathyarchaeota since they specifically utilize CO_2 for carbon source and methane and lignin for energy, respectively (Kellermann et al., 2012; Yu et al., 2018), although the details of their carbon-fixing pathways are unclear.

1.3.3. Alkane and fatty acids degradation

The *mcr* genes, encoding methyl coenzyme M reductase, have been found to be central in both methanogenesis and alkane oxidation. In marine sediments, methane and short-chain alkanes will be formed via the mediation of biological process (Hinrichs et al., 2006) and subsequently oxidized by other archaea in anoxic sediments when electron acceptors are available (Ettwig et al., 2016; Hinrichs et al., 1999; Jørgensen et al., 2004; Laso-Perez et al., 2016). These alkane oxidizing archaea are mainly placed within the group of ANMEs. For example, ANME-1 and ANME-2 archaea perform methane oxidation associated with sulfate reduction by the *Desulfosarcina*/*Desulfococcus* group (Blumenberg et al., 2004; Michaelis et al., 2002; Schreiber et al., 2010). Besides, short-chain hydrocarbons such as butane potentially can be degraded by novel ANME-1, Bathyarchaeota and Asgard archaea (Table 1), since the phylogenetic position of detected *mcr* genes are close to the putative butane oxidizer (Syntrophoarchaea) (Dombrowski et al., 2018; Evans et al., 2015; Laso-Perez et al., 2016; Seitz et al., 2019). The expansive and divergent *mcr* genes found in recent years reflect the wide distribution and complex metabolisms encoded by in *mcr* genes in the kingdom of archaea (Evans et al., 2019).

Interestingly, beta-oxidation is detected in some archaea (novel ANME-1, Bathyarchaeota and Asgardarchaeota) (Table 1) (Dombrowski et al., 2018; He et al., 2016; Seitz et al., 2019). Specifically, these archaea harbor the capability of alkane oxidization, potentially involving alkane oxidation to

fatty acids and further conversion to acetyl-CoA via beta-oxidation. Additionally, beta-oxidation in these archaea may be also associated with the degradation of fatty acids, which are the important class of compounds in marine sediments (Kniemeyer et al., 2007; Pearson et al., 2001; Sinninghe Damsté et al., 2003).

1.3.4. Fermentation and organic polymer degradation

In many archaea, most steps of Embden-Meyerhof-Parnas (EMP) pathway are present (Table 1). However, except for Woesearchaeota (Lazar et al., 2017; Liu et al., 2018), the lack of evidence of sugar degradation and fermentation to acetate indicates that these archaea might use the reverse pathway to obtain sugar-phosphate, which is further used for nucleotide synthesis. Therefore, although acetate metabolism is present in these archaea, it is unclear whether acetate is produced or incorporated acetate as the relevant enzymes (acetyl-CoA synthetase) catalyze acetate metabolism are reversible (Schäfer et al., 1993).

Functional genes encoding protein breaking down and incorporating into cells were detected in MBGD and DHVEG-1, Bathyarchaeota and Asgard archaea (Table 1) (He et al., 2016; Lazar et al., 2016; Lazar et al., 2017; MacLeod et al., 2019; Zhou et al., 2018). Protein degradation might be an important survival strategy for these archaea, since protein can provide both carbon and nitrogen source for growth. Nevertheless, the direct evidence about the activities of protein degradation by these archaea is unclear to date. More promisingly, Bathyarchaeota is active in lignin degradation as subgroup of Bathy-8 is enriched in a long-term incubation amended with lignin (Yu et al., 2018). Considering divergent carbon metabolic pathways in archaea found from anoxic Helgoland Mud sediment, archaea might have versatile strategies in carbon utilization, potentially including carbon fixation, alkane degradation, aromatic compound degradation and the intermediates utilization.

Table 1 Summary of the main carbon metabolism pathways in archaea found in anoxic sediment of Helgoland Mud Area

	WL	CBB	TCA	Alkane metabol.	β-oxid.	EMP	Acetate metabol.	Protein degrad.	Aromatic degrad.	Ethanol metabol.
Methanosarcinaceae	+++	++	++	+++[a]	-	++	+++[e]	-	-	+++[g]
Methanosaetaceae	+++	++	++	+++[a]	-	++	+++[e]	-	-	+++[g]
Methanomicrobiaceae	+++	++	++	+++[a]	-	++	++[f]	-	-	-
Methanomassiliicoccaceae	+	++	++	++ [a]	-	++	++[f]	-	-	-
ANME-1	+++	-	++	+++[a,b,c]	+++	++	++[f]	+	-	-
ANME-2a/2b	+++	++	++	+++[b]	-	++	++[f]	-	-	-
MBGD and DHVEG-1	+++	-	+++	-	-	++	+++[f]	+++	-	+++[h]
Woesearchaeota	++	-	+	-	-	++	+++[f]	-	-	+++[h]
Bathyarchaeota	+++	-	++	+++ [a,c]	+++[d]	++	+++[f]	+++	+++	+++[h]
Asgard archaea	+++	++	++	+++	+++[d]	++	+++[f]	+++	-	+++[h]

TCA, tricarboxylic acid cycle; CBB, Calvin-Benson-Bassham cycle; 3-HP/4-HB, 3-hydroxypropionate/4-hydroxybutyrate cycle; WL, Wood-Ljungdahl pathway; Alkane metabol., Alkane metabolisms; EMP, Embden–Meyerhof–Parnas pathway; Protein degrad., Protein degradation; β-oxid., β-oxidation; Aromatic degrad., Aromatic compounds degradation; Acetate metabol., Acetate metabolisms; Ethanol metabol., Ethanol metabolisms.

+++, pathway complete; ++, main gene cluster detected; +, few gene cluster detected; -, no relevant gene detected; na, not applicable.

a, methanogenesis; b, methane oxidation; c, short-chain alkane degradation; d, long-chain alkane degradation; e, acetoclastic methanogenesis; f, acetogenesis or acetate utilization; g, extracellular electron transfer mediated methanogenesis; h, ethanol generation.

The summary is based on the KEGG metabolic pathways and the previous studies (Allen et al., 2009; Beulig et al., 2019; Deppenmeier et al., 2002; Dombrowski et al., 2018; Evans et al., 2015; He et al., 2016; Lazar et al., 2016; Lazar et al., 2017; Liu et al., 2018; MacLeod et al., 2019; Meng et al., 2014; Meyerdierks et al., 2010; Rotaru et al., 2014; Seitz et al., 2019; Spring et al., 2010; Wang et al., 2014; Zhou et al., 2018).

1.4. Identification of active microorganisms by stable isotope probing

Stable isotope probing (SIP) is an incubation-dependent technique that uses substrates labelled with stable isotopes such as ^{13}C-carbon, ^{15}N-nitrogen or ^{18}O-oxygen for detecting microbial activities by tracking the incorporated labeled substrates into macromolecules such as nucleic acids and lipids, i.e., DNA-SIP, RNA-SIP and lipid-SIP.

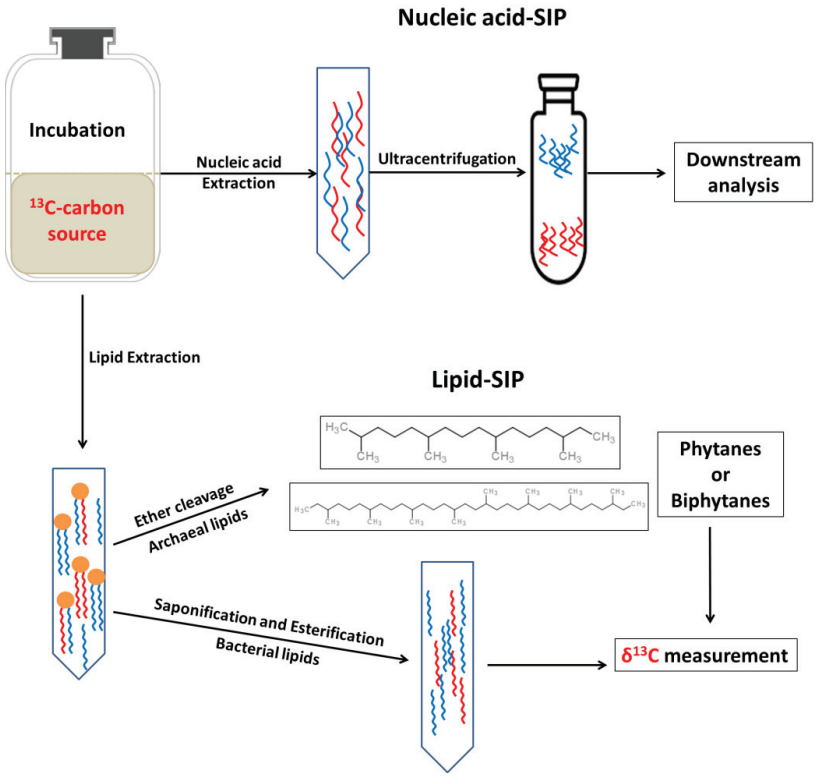

Fig. 6 Workflow of nucleic acid- and lipid-SIP based on ^{13}C-carbon incorporation

1.4.1. Nucleic acid-SIP

For detecting active microbial members in environmental samples by nucleic acid-SIP, ^{13}C-carbon, ^{15}N-nitrogen or ^{18}O-oxygen substrates can be assimilated into nucleic acids, thereby increasing the density of DNA and RNA (Cadisch et al., 2005; Lueders et al., 2004; Schwartz et al., 2016). This is the basis for separating labeled nucleic acids with higher density from unlabeled ones (lower density) by isopycnic centrifugation (Fig. 6) (Radajewski et al., 2000). Considering the difference of DNA and RNA densities, nucleic acid-SIP is conducted in cesium chloride and cesium trifluoroacetate gradients, respectively (Lueders et al., 2003; Manefield et al., 2002; Radajewski et al., 2000). In combination with next generation sequencing of the labeled and unlabeled nucleic acids, nucleic acid-SIP harbors a high

resolution and sensitivity in identification of taxonomic levels (Aoyagi et al., 2015; Aoyagi et al., 2018; Singer et al., 2017). Furthermore, combining nucleic acid-SIP with metagenomics and metatranscriptomics provides the direct evidence for construction and characterization of carbon metabolic pathways (Bradford et al., 2018; Chemerys et al., 2014; Coyotzi et al., 2016; Fortunato and Huber 2016; Kalyuhznaya et al., 2009). Except for ^{13}C-carbon substrates, ^{15}N-nucleic acid-SIP is conducted to track nitrogen metabolisms in environmental samples (Buckley et al., 2007; Roh et al., 2009), but with a higher threshold level (atom% >50%) than ^{13}C-nucleic acid-SIP (>10 %) (Cadisch et al., 2005; Manefield et al., 2002). In addition, by amending with $H_2{}^{18}O$ into soils or sediments, the *in situ* microbial growth and activity have been detected by using ^{18}O-nucleic acid-SIP (Rettedal and Brozel 2015; Schwartz et al., 2016). However, most of these studies detected bacteria activities based on carbon and nitrogen assimilation. For identifying archaeal activity, it is necessary and worthy to try the nucleic acid-SIP method because of its sensitivity for detecting uncultured archaea with low activity.

1.4.2. Lipid-SIP

Unlike the taxonomic identification of active microorganisms by nucleic acid-SIP, lipid-SIP harbors a lower phylogenetic resolution but measurement of δ^{13}C or δD-values by gas chromatography combustion isotope ratio mass spectrometry (GC-c-IRMS) in lipids allows us to track carbon and hydrogen assimilation into biomass quantitatively and high-sensitively (Berry et al., 2015; Boschker et al., 1998; Kopf et al., 2016; Wegener et al., 2016). Before δ^{13}C and δD lipid measurement from environmental samples, fatty acids or isoprenoid chains are obtained by saponification/esterification and ether cleavage, respectively (Fig. 6) (Elvert et al., 2003; Liu et al., 2012). Lipid-SIP has been used for assessing carbon assimilation patterns, carbon fixation and organic carbon degradation in a variety of environments (Blaser et al., 2015; Boschker and Middelburg 2002; Hinrichs et al., 1999; Wegener et al., 2012).

1.5. Objectives and structure of the thesis

A number of studies about methanogenesis in marine sediments in recent years have indicated the importance of methylotrophic methanogenesis. Methylotrophic methanogens can utilize methyl substrates for methane formation in presence of sulfate and sulfate reducers successfully because it is regarded as non-competitive substrate. However, it is unclear, which methylotrophic methanogens are active in the sulfate reduction zone and the methanogenic zone of marine sediments, although methyl substrates and methanogenic methylotrophic activity are detected. Marine sediment harbor a large pool of inorganic carbon, and thus, this ambient CO_2 may affect carbon utilization by methylotrophic methanogens. Hence, identifying and characterizing methylotrophic methanogens in marine sediments allows us to know how carbon can be used in marine sediments by these archaea.

Apart from methylotrophic methanogens, uncultured archaea such as Bathyarchaeota, Asgard archaea and MBGD and DHVEG-1 are found in the Helgoland sediments while their activities are not well studied. Especially for Asgard archaea, studying their activity will help us understand the survival strategy of these archaea. Because Asgard archaea are the closest relatives of Eukarya, even their carbon metabolism can provide insight into evolutionary relationships between Archaea and Eukarya. Nevertheless, some studies suggest that these uncultured archaea might utilize a decent amount of CO_2 for carbon assimilation.

In this study, I used SIP methods including nucleic acid- and lipid-SIP to further understand the carbon utilization patterns in methylotrophic methanogens and uncultured archaea. Specifically, I worked on the following objectives:

1) Identify methylotrophic methanogens in different depths of marine sediment by RNA and DNA-SIP (sulfate reduction zone and methanogenic zone).
2) Quantify carbon utilization patterns in methylotrophic methanogens by nucleic acid-SIP and lipid-SIP.
3) Identify uncultured archaea in deep marine sediment by nucleic acid-SIP with providing potential electron donor, electron acceptor and ^{13}C-labeled dissolved inorganic carbon.

In brief, this thesis contains three manuscript chapters (chapter 2 to 5):

Chapter 2: **DNA and RNA stable isotope probing of methylotrophic methanogenic archaea**. In this chapter, we developed a labeling strategy to identify methylotrophic methanogens by amendment with ^{13}C-DIC using nucleic acid-SIP. In combination with Illumina sequencing of nucleic acid samples from the "heavy" and "light" fractions, we showed that ^{13}C-DIC is necessary to use in order to obtain sufficient labeled nucleic acids in heavy gradient fractions after density separation of nucleic acids.

Chapter 3: **CO_2 conversion to methane and biomass in obligate methylotrophic methanogens in marine sediments.** In order to identify methylotrophic methanogens in the Helgoland Mud sediments, we applied RNA-SIP on the incubations amended with ^{13}C-DIC and unlabeled methanol and successfully detected methylotrophic methanogens. By analyzing carbon assimilation into biomass using lipid-SIP, we found that the contribution of inorganic carbon was higher than that of methanol. The further study of the autoclaved slurry incubations with inoculated *Methanococcoides methylutens* suggested that obligate methylotrophic methanogens have the unexpected ability of using CO_2 for methane formation during methylotrophic methanogenesis. The CO_2-dependent methanogenesis in methylotrophic methanogens may play an important role in environment.

Chapter 4: Asgard archaea are key participants in marine sediment carbon cycling. In this study, we showed that amendment of ^{13}C-DIC and electron donors into the SIP incubations was an effective strategy on identifying uncultured archaea (Asgard archaea). In the presence of organic polymers (lignin, cellulose and humic acid) or sulfur, we found that Asgard archaea were incorporating ^{13}C-DIC in these SIP incubations. Combining metagenomes and metatranscriptomes of the Asgard archaea obtained from SIP samples and mangrove sediment in the southeast coast of China, we demonstrated that Asgard archaea harbor genes for alkane, protein, fatty acids and cellulose degradation, and are actively involved in organic polymer degradation as well as CO_2 fixation.

1.6. Reference

Allen, M. A., Lauro, F. M., Williams, T. J., Burg, D., Siddiqui, K. S., De Francisci, D., Chong, K. W., Pilak, O., Chew, H. H., De Maere, M. Z., Ting, L., Katrib, M., Ng, C., Sowers, K. R., Galperin, M. Y., Anderson, I. J., Ivanova, N., Dalin, E., Martinez, M., Lapidus, A., Hauser, L., Land, M., Thomas, T. and Cavicchioli, R. (2009) The genome sequence of the psychrophilic archaeon, *Methanococcoides burtonii*: the role of genome evolution in cold adaptation. *ISME J.,* 3, 1012-1035.

Annweiler, E., Materan, A., Safinowski, M., Kappler, A., Richnow, H. H., Michaelis, W. and Meckenstock, R. U. (2000) Anaerobic degradation of 2-methylnaphthalene by a sulfate-reducing enrichment culture. *Appl. Environ. Microbiol.,* 66, 5329–5333.

Aoyagi, T., Hanada, S., Itoh, H., Sato, Y., Ogata, A., Friedrich, M. W., Kikuchi, Y. and Hori, T. (2015) Ultra-high-sensitivity stable-isotope probing of rRNA by high-throughput sequencing of isopycnic centrifugation gradients. *Environ Microbiol Rep,* 7, 282-287.

Aoyagi, T., Morishita, F., Sugiyama, Y., Ichikawa, D., Mayumi, D., Kikuchi, Y., Ogata, A., Muraoka, K., Habe, H. and Hori, T. (2018) Identification of active and taxonomically diverse 1,4-dioxane degraders in a full-scale activated sludge system by high-sensitivity stable isotope probing. *ISME J,* 12, 2376-2388.

Arndt, S., Jørgensen, B. B., LaRowe, D. E., Middelburg, J. J., Pancost, R. D. and Regnier, P. (2013) Quantifying the degradation of organic matter in marine sediments: A review and synthesis. *Earth-Sci. Rev.,* 123, 53-86.

Berry, D., Mader, E., Lee, T. K., Woebken, D., Wang, Y., Zhu, D., Palatinszky, M., Schintlmeister, A., Schmid, M. C., Hanson, B. T., Shterzer, N., Mizrahi, I., Rauch, I., Decker, T., Bocklitz, T., Popp, J., Gibson, C. M., Fowler, P. W., Huang, W. E. and Wagner, M. (2015) Tracking heavy water (D_2O) incorporation for identifying and sorting active microbial cells. *Proc. Natl. Acad. Sci. U. S. A.,* 112, 194-203.

Beulig, F., Roy, H., Glombitza, C. and Jorgensen, B. B. (2018) Control on rate and pathway of anaerobic organic carbon degradation in the seabed. *Proc. Natl. Acad. Sci. U. S. A.,* 115, 367-372.

Beulig, F., Roy, H., McGlynn, S. E. and Jorgensen, B. B. (2019) Cryptic CH_4 cycling in the sulfate-methane transition of marine sediments apparently mediated by ANME-1 archaea. *ISME J.,* 13, 250-262.

Blaser, M. B., Dreisbach, L. K. and Conrad, R. (2015) Carbon isotope fractionation of *Thermoanaerobacter kivui* in different growth media and at different total inorganic carbon concentration. *Org. Geochem.,* 81, 45-52.

Blumenberg, M., Seifert, R., Reitner, J., Pape, T. and Michaelis, W. (2004) Membrane lipid patterns typify distinct anaerobic methanotrophic consortia. *Proc. Natl. Acad. Sci. U. S. A.,* 101, 11111–11116.

Borrel, G., O'Toole, P. W., Harris, H. M., Peyret, P., Brugere, J. F. and Gribaldo, S. (2013) Phylogenomic data support a seventh order of Methylotrophic methanogens and provide insights into the evolution of methanogenesis. *Genome Biol. Evol.,* 5, 1769-1780.

Borrel, G., Parisot, N., Harris, H. M., Peyretaillade, E., Gaci, N., Tottey, W., Bardot, O., Raymann, K., Gribaldo, S., Peyret, P., O'Toole, P. W. and Brugere, J. F. (2014) Comparative genomics highlights the unique biology of *Methanomassiliicoccales*, a *Thermoplasmatales*-related seventh order of methanogenic archaea that encodes pyrrolysine. *BMC Genomics,* 15, 679, doi: 10.1186/1471-2164-15-679.

Boschker, H. T. S. and Middelburg, J. J. (2002) Stable isotopes and biomarkers in microbial ecology. *FEMS Microbiol Ecol.,* 40, 85–95.

Boschker, H. T. S., Nold, S. C., Wellsbury, P., Bos, D., de Graaf, W., Pel, R., Parkes, R. J. and Cappenberg, T. E. (1998) Direct linking of microbial populations to specific biogeochemical processes by ^{13}C-labelling of biomarkers. *Nature,* 392, 801-805.

Bradford, L. M., Vestergaard, G., Tancsics, A., Zhu, B., Schloter, M. and Lueders, T. (2018) Transcriptome-stable isotope probing provides targeted functional and taxonomic insights into microaerobic oollutant-degrading aquifer microbiota. *Front. Microbiol.,* 9, 2696, doi: 10.3389/fmicb.2018.02696.

Buckley, D. H., Huangyutitham, V., Hsu, S. F. and Nelson, T. A. (2007) Stable isotope probing with $^{15}N_2$ reveals novel noncultivated diazotrophs in soil. *Appl. Environ. Microbiol.,* 73, 3196-3204.

Bulzu, P. A., Andrei, A. S., Salcher, M. M., Mehrshad, M., Inoue, K., Kandori, H., Beja, O., Ghai, R. and Banciu, H. L. (2019) Casting light on Asgardarchaeota metabolism in a sunlit microoxic niche. *Nat Microbiol*. doi: 10.1038/s41564-019-0404-y.

Burdige, D. J. (2005) Burial of terrestrial organic matter in marine sediments: A re-assessment. *Global Biogeochem. Cy.,* 19, GB4011, doi: 10.1029/2004gb002368.

Cadisch, G., Espana, M., Causey, R., Richter, M., Shaw, E., Morgan, J. A., Rahn, C. and Bending, G. D. (2005) Technical considerations for the use of ^{15}N-DNA stable-isotope probing for functional microbial activity in soils. *Rapid. Commun. Mass. Spectrom.,* 19, 1424-1428.

Canfield, D. E., Thamdrup, B. and Hansen, J. W. (1993) The anaerobic degradation of organic matter in Danish coastal sediments iron reduction, manganese reduction, and sulfate reduction. *Geochim. Cosmochim. Acta,* 57, 3867-3883.

Carr, S. A., Schubotz, F., Dunbar, R. B., Mills, C. T., Dias, R., Summons, R. E. and Mandernack, K. W. (2018) Acetoclastic *Methanosaeta* are dominant methanogens in organic-rich Antarctic marine sediments. *ISME J.,* 12, 330-342.

Carter, P. W. and Mitterer, R. M. (1978) Amino acid composition of organic matter associated with carbonate and non-carbonate sediments. *Geochim. Cosmochim. Acta,* 42, 1231-1238.

Cha, I. T., Min, U. G., Kim, S. J., Yim, K. J., Roh, S. W. and Rhee, S. K. (2013) *Methanomethylovorans uponensis* sp. nov., a methylotrophic methanogen isolated from wetland sediment. *Antonie Leeuwenhoek.,* 104, 1005-1012.

Chemerys, A., Pelletier, E., Cruaud, C., Martin, F., Violet, F. and Jouanneau, Y. (2014) Characterization of novel polycyclic aromatic hydrocarbon dioxygenases from the bacterial metagenomic DNA of a contaminated soil. *Appl. Environ. Microbiol.,* 80, 6591-6600.

Cheng, L., Qiu, T. L., Yin, X. B., Wu, X. L., Hu, G. Q., Deng, Y. and Zhang, H. (2007) *Methermicoccus shengliensis* gen. nov., sp. nov., a thermophilic, methylotrophic methanogen isolated from oil-production water, and proposal of *Methermicoccaceae* fam. nov. *Int J Syst Evol Microbiol,* 57, 2964-2969.

Coates, J. D., Lonergan, D. J., Philips, E. J. P., Jenter, H. and Lovley, D. R. (1995) *Desulfuromonas palmitatis* sp. nov., a marine dissimilatory Fe(III) reducer that can oxidize long-chain fatty acids. *Arch. Microbiol.,* 164, 406-413.

Colombo, J. C., Silverberg, N. and Gearing, J. N. (1996) Biogeochemistry of organic matter in the Laurentian Trough, II. Bulk composition of the sediments and relative reactivity of major components during early diagenesis. *Mar. Chem.,* 51, 295-314.

Conrad, R. (1999) Contribution of hydrogen to methane production and control of hydrogen concentrations in methanogenic soils and sediments. *FEMS Microbiol Ecol.,* 28, 193-202.

Coyotzi, S., Pratscher, J., Murrell, J. C. and Neufeld, J. D. (2016) Targeted metagenomics of active microbial populations with stable-isotope probing. *Curr. Opin. Biotechnol.,* 41, 1-8.

Dacey, J. W. H. and Wakeham, S. G. (1986) Oceanic dimethylsulfide: production during zooplankton grazing on phytoplankton. *Science,* 233, 1314-1316.

De Leeuw, J. W. and Largeau, C. (1993) A review of macromolecular organic compounds that comprise living organisms and their role in kerogen, coal, and petroleum formation. *Org. Geochem.*, 23-72.

Deppenmeier, U., Johann, A., Martinez-Arias, R., Henne, A., Wiezer, A., Bäumer, S., Jacobi, C., Brüggemann, H., Lienard, T., Christmann, A., Bömeke, M., Steckel, S., Bhattacharyya, A., Lykidis, A., Overbeek, R., Klenk, H. P., Gunsalus, R. P., Fritz, H. J. and Gottschalk, G. (2002) The genome of *Methanosarcina mazei*: evidence for lateral gene transfer between bacteria and archaea. *J. Mol. Microbiol. Biotechnol.,* 4, 453-461.

Dombrowski, N., Teske, A. P. and Baker, B. J. (2018) Expansive microbial metabolic versatility and biodiversity in dynamic Guaymas Basin hydrothermal sediments. *Nat. Commun.,* 9, 4999.

Dominik, J., Förstner, U., Mangini, A. and Reineck, H. E. (1978) ^{210}Pb and ^{137}Cs chronology of heavy metal pollution in a sediment core from the German Bight (North Sea). *Senckenberg. mar.,* 10, 213-227.

Durbin, A. M. and Teske, A. (2012) Archaea in organic-lean and organic-rich marine subsurface sediments: an environmental gradient reflected in distinct phylogenetic lineages. *Front Microbiol,* 3, 168, doi: 10.3389/fmicb.2012.00168.

Dyksma, S., Bischof, K., Fuchs, B. M., Hoffmann, K., Meier, D., Meyerdierks, A., Pjevac, P., Probandt, D., Richter, M., Stepanauskas, R. and Mussmann, M. (2016) Ubiquitous *Gammaproteobacteria* dominate dark carbon fixation in coastal sediments. *ISME J.,* 10, 1939-1953.

Egland, P. G., Pelletier, D. A., Dispensa, M., Gibson, J. and Harwood, C. S. (1997) A cluster of bacterial genes for anaerobic benzene ring biodegradation. *Proc. Natl. Acad. Sci. U. S. A.,* 94, 6484–6489.

Elvert, M., Boetius, A., Knittel, K. and Jorgensen, B. B. (2003) Characterization of specific membrane fatty acids as chemotaxonomic markers for sulfate-reducing bacteria involved in anaerobic oxidation of methane. *Geomicrobiol.,* 20, 403–419.

Ettwig, K. F., Zhu, B., Speth, D., Keltjens, J. T., Jetten, M. S. M. and Kartal, B. (2016) Archaea catalyze iron-dependent anaerobic oxidation of methane. *Proc. Natl. Acad. Sci. U. S. A.,* 113, 12792-12796.

Evans, P. N., Boyd, J. A., Leu, A. O., Woodcroft, B. J., Parks, D. H., Hugenholtz, P. and Tyson, G. W. (2019) An evolving view of methane metabolism in the Archaea. *Nat. Rev. Microbiol.*, 219–232.

Evans, P. N., Parks, D. H., Chadwick, G. L., Robbins, S. J., Orphan, V. J., Golding, S. D. and Tyson, G. W. (2015) Methane metabolism in the archaeal phylum Bathyarchaeota revealed by genome-centric metagenomics. *Science,* 350, 432-438.

Fall, R. and Benson, A. A. (1996) Leaf methanol-the simplest natural product from plants. *Trends Plant Sci,* 1, 296–301.

Ferry, J. G. and Lessner, D. J. (2008) Methanogenesis in marine sediments. *Ann. NY. Acad. Sci.,* 1125, 147-157.

Fortunato, C. S. and Huber, J. A. (2016) Coupled RNA-SIP and metatranscriptomics of active chemolithoautotrophic communities at a deep-sea hydrothermal vent. *ISME J.,* 10, 1925-1938.

Goni, M. A., Ruttenberg, K. C. and Eglinton, T. I. (1997) Sources and contribution of terrigenous organic carbon to surface sediments in the Gulf of Mexico. *Nature,* 389, 275-278.

Goodchild, A., Raftery, M., Saunders, N. F. W., Guilhaus, M. and Cavicchioli, R. (2004) Biology of the cold adapted archaeon, *Methanococcoides burtonii* determined by proteomics using liquid chromatography-tandem mass spectrometry. *J. Proteome. Res.,* 3, 1164-1176.

Guerzoni, S. and Rovatti, G. (1987) Organic matter composition in coastal marine sediments from different depositional areas, Italy. *Sci. Total. Environ.,* 62, 477-479.

Guss, A. M., Mukhopadhyay, B., Zhang, J. K. and Metcalf, W. W. (2005) Genetic analysis of *mch* mutants in two *Methanosarcina* species demonstrates multiple roles for the methanopterin-dependent C-1 oxidation/reduction pathway and differences in H_2 metabolism between closely related species. *Mol. Microbiol.,* 55, 1671-1680.

He, Y., Li, M., Perumal, V., Feng, X., Fang, J., Xie, J., Sievert, S. M. and Wang, F. (2016) Genomic and enzymatic evidence for acetogenesis among multiple lineages of the archaeal phylum Bathyarchaeota widespread in marine sediments. *Nat. Microbiol.,* 1, 16035, doi: 10.1038/nmicrobiol.2016.35.

Hebbeln, D., Scheurle, C. and Lamy, F. (2003) Depositional history of the Helgoland mud area, German Bight, North Sea. *Geo-Mar. Lett.,* 23, 81-90.

Hinrichs, K. U., Hayes, J. M., Bach, W., spivack, A. J., Hmelo, L. R., Holm, N. G., Johnson, C. G. and Sylva, S. P. (2006) Biological formation of ethane and propane in the deep marine subsurface. *Proc. Natl. Acad. Sci. U. S. A.,* 103, 14684–14689.

Hinrichs, K. U., Hayes, J. M., Sylva, S. P., Brewer, P. G. and DeLong, E. F. (1999) Methane-consuming archaebacteria in marine sediments. *Nature,* 389, 802-805.

Iniri, A., Harada, N., Ogawa, N. O., Sakamoto, T. and Nakatsuka, T. (2010) Carbon isotope biogeochemistry of acetate in sub-sea floor sediments in the Sea of Okhotsk near Sakhalin Island, Russia. *Res. Org. Geochem.,* 26, 95-105.

Jørgensen, B. B., Böttcher, M. E., Lüschen, H., Neretin, L. N. and Volkov, I. I. (2004) Anaerobic methane oxidation and a deep H_2S sink generate isotopically heavy sulfides in Black Sea sediments. *Geochim. Cosmochim. Acta,* 68, 2095-2118.

Jørgensen, B. B. and Kasten, S. 2006. Sulfur cycling and methane oxidation. In *Mar. Geochem.*, 271-309.

Kalyuhznaya, M. G., Martens-Habbena, W., Wang, T., Hackett, M., Stolyar, S. M., Stahl, D. A., Lidstrom, M. E. and Chistoserdova, L. (2009) *Methylophilaceae* link methanol oxidation to denitrification in freshwater lake sediment as suggested by stable isotope probing and pure culture analysis. *Environ. Microbiol. Rep.,* 1, 385-392.

Katayama, T., Yoshioka, H., Muramoto, Y., Usami, J., Fujiwara, K., Yoshida, S., Kamagata, Y. and Sakata, S. (2015) Physicochemical impacts associated with natural gas development on methanogenesis in deep sand aquifers. *ISME J.,* 9, 436-446.

Kellermann, M. Y., Wegener, G., Elvert, M., Yoshinaga, M. Y., Lin, Y. S., Holler, T., Mollar, X. P., Knittel, K. and Hinrichs, K. U. (2012) Autotrophy as a predominant mode of carbon fixation in anaerobic methane-oxidizing microbial communities. *Proc. Natl. Acad. Sci. U. S. A.,* 109, 19321-19326.

King, G. M. (1984) Metabolism of trimethylamine, choline, and glycine betaine by sulfate-reducing and methanogenic bacteria in marine sediments. *Appl Environ Microbiol,* 48, 719-725.

Kniemeyer, O., Musat, F., Sievert, S. M., Knittel, K., Wilkes, H., Blumenberg, M., Michaelis, W., Classen, A., Bolm, C., Joye, S. B. and Widdel, F. (2007) Anaerobic oxidation of short-chain hydrocarbons by marine sulphate-reducing bacteria. *Nature,* 449, 898-901.

Kono, T., Mehrotra, S., Endo, C., Kizu, N., Matusda, M., Kimura, H., Mizohata, E., Inoue, T., Hasunuma, T., Yokota, A., Matsumura, H. and Ashida, H. (2017) A RuBisCO-mediated carbon metabolic pathway in methanogenic archaea. *Nat. Commun.,* 8, 14007, doi: 10.1038/ncomms14007.

Kopf, S. H., Sessions, A. L., Cowley, E. S., Reyes, C., Van Sambeek, L., Hu, Y., Orphan, V. J., Kato, R. and Newman, D. K. (2016) Trace incorporation of heavy water reveals slow and heterogeneous pathogen growth rates in cystic fibrosis sputum. *Proc. Natl. Acad. Sci. U. S. A.,* 113, 110-116.

Lambie, S. C., Kelly, W. J., Leahy, S. C., Li, D., Reilly, K., McAllister, T. A., Valle, E. R., Attwood, G. T. and Altermann, E. (2015) The complete genome sequence of the rumen methanogen *Methanosarcina barkeri* CM1. *Stand Genomic Sci,* 10, 57, doi: 10.1186/s40793-015-0038-5.

Lang, K., Schuldes, J., Klingl, A., Poehlein, A., Daniel, R. and Brunea, A. (2015) New mode of energy metabolism in the seventh order of methanogens as revealed by comparative genome analysis of "*Candidatus Methanoplasma termitum*". *Appl. Environ. Microbiol.,* 81, 1338-1352.

Laso-Perez, R., Wegener, G., Knittel, K., Widdel, F., Harding, K. J., Krukenberg, V., Meier, D. V., Richter, M., Tegetmeyer, H. E., Riedel, D., Richnow, H. H., Adrian, L., Reemtsma, T., Lechtenfeld, O. J. and Musat, F. (2016) Thermophilic archaea activate butane via alkyl-coenzyme M formation. *Nature,* 539, 396-401.

Lazar, C. S., Baker, B. J., Seitz, K., Hyde, A. S., Dick, G. J., Hinrichs, K. U. and Teske, A. P. (2016) Genomic evidence for distinct carbon substrate preferences and ecological niches of Bathyarchaeota in estuarine sediments. *Environ. Microbiol.,* 18, 1200-1211.

Lazar, C. S., Baker, B. J., Seitz, K. W. and Teske, A. P. (2017) Genomic reconstruction of multiple lineages of uncultured benthic archaea suggests distinct biogeochemical roles and ecological niches. *ISME J.,* 11, 1118-1129.

Lazar, C. S., Parkes, R. J., Cragg, B. A., L'Haridon, S. and Toffin, L. (2011) Methanogenic diversity and activity in hypersaline sediments of the centre of the Napoli mud volcano, Eastern Mediterranean Sea. *Environ. Microbiol.,* 13, 2078-2091.

Liu, X., Li, M., Castelle, C. J., Probst, A. J., Zhou, Z., Pan, J., Liu, Y., Banfield, J. F. and Gu, J. D. (2018) Insights into the ecology, evolution, and metabolism of the widespread Woesearchaeotal lineages. *Microbiome,* 6, 102, doi: 10.1186/s40168-018-0488-2.

Liu, X. L., Lipp, J. S., Simpson, J. H., Lin, Y. S., Summons, R. E. and Hinrichs, K. U. (2012) Mono- and dihydroxyl glycerol dibiphytanyl glycerol tetraethers in marine sediments: Identification of both core and intact polar lipid forms. *Geochim. Cosmochim. Acta,* 89, 102-115.

Liu, Y. and Whitman, W. B. (2008) Metabolic, phylogenetic, and ecological diversity of the methanogenic archaea. *Ann. NY. Acad. Sci.,* 1125, 171-189.

Lovley, D. R. (2017) Happy together: microbial communities that hook up to swap electrons. *ISME J.,* 11, 327-336.

Lueders, T., Manefield, M. and Friedrich, M. W. (2003) Enhanced sensitivity of DNA- and rRNA-based stable isotope probing by fractionation and quantitative analysis of isopycnic centrifugation gradients. *Environ. Microbiol.,* 6, 73-78.

Lueders, T., Pommerenke, B. and Friedrich, M. W. (2004) Stable-isotope probing of microorganisms thriving at thermodynamic limits: syntrophic propionate oxidation in flooded soil. *Appl. Environ. Microbiol.,* 70, 5778-5786.

MacLeod, F., S. Kindler, G., Lun Wong, H., Chen, R. and P. Burns, B. (2019) Asgard archaea: Diversity, function, and evolutionary implications in a range of microbiomes. *AIMS Microbiol.,* 5, 48-61.

Manefield, M., Whiteley, A. S., Griffiths, R. I. and Bailey, M. J. (2002) RNA stable isotope probing, a novel means of linking microbial community function to phylogeny. *Appl. Environ. Microbiol.,* 68, 5367-5373.

Mayer, L. M., Schick, L. L. and Setchell, F. W. (1986) Measurement of protein in nearshore marine sediments. *Mar. Ecol. Prog. Ser.,* 30, 159-165.

Meng, J., Xu, J., Qin, D., He, Y., Xiao, X. and Wang, F. (2014) Genetic and functional properties of uncultivated MCG archaea assessed by metagenome and gene expression analyses. *ISME J.,* 8, 650-659.

Meyerdierks, A., Kube, M., Kostadinov, I., Teeling, H., Glockner, F. O., Reinhardt, R. and Amann, R. (2010) Metagenome and mRNA expression analyses of anaerobic methanotrophic archaea of the ANME-1 group. *Environ. Microbiol.,* 12, 422-439.

Michaelis, W., Seifert, R., Nauhaus, K., Treude, T., Thiel, V., Blumenberg, M., Knittel, K., Gieseke, A., Peterknecht, K., Pape, T., Boetius, A., Amann, R., Jorgensen, B. B., Widdel, F., Peckmann, J., Pimenov, N. V. and Gulin, M. B. (2002) Microbial feefs in the Black Sea fueled by anaerobic oxidation of methane. *Science,* 297, 1013-1015.

Mochimaru, H., Tamaki, H., Hanada, S., Imachi, H., Nakamura, K., Sakata, S. and Kamagata, Y. (2009) *Methanolobus profundi* sp. nov., a methylotrophic methanogen isolated from deep subsurface sediments in a natural gas field. *Int. J Syst. Evol. Microbiol.,* 59, 714-718.

Nobu, M. K., Narihiro, T., Kuroda, K., Mei, R. and Liu, W. T. (2016) Chasing the elusive Euryarchaeota class WSA2: genomes reveal a uniquely fastidious methyl-reducing methanogen. *ISME J,* 10, 2478-2487.

Oni, O., Miyatake, T., Kasten, S., Richter-Heitmann, T., Fischer, D., Wagenknecht, L., Kulkarni, A., Blumers, M., Shylin, S. I., Ksenofontov, V., Costa, B. F., Klingelhofer, G. and Friedrich, M. W. (2015a) Distinct microbial populations are tightly linked to the profile of dissolved iron in the methanic sediments of the Helgoland mud area, North Sea. *Front. Microbiol.,* 6, 365, doi: 10.3389/fmicb.2015.00365.

Oni, O. E., Schmidt, F., Miyatake, T., Kasten, S., Witt, M., Hinrichs, K. U. and Friedrich, M. W. (2015b) Microbial communities and organic matter composition in surface and subsurface sediments of the Helgoland Mud Area, North Sea. *Front. Microbiol.,* 6, 1290, doi: 10.3389/fmicb.2015.01290.

Oremland, R. S. and Polcin, S. (1982) Methanogenesis and sulfate reduction: competitive and noncompetitive substrates in estuarine sediments. *Appl. Environ. Microbiol.,* 44, 1270-1276.

Pearson, A., Mcnichol, A. P., Benitez-Nelson, B. C., Hayes, J. M. and Eglinton, T. I. (2001) Origins of lipid biomarkers in Santa Monica Basin surface sediment: a case study using compound-specific $\Delta^{14}C$ analysis. *Geochim. Cosmochim. Acta,* 65, 3123–3137.

Perez, R. C. and Matin, A. (1982) Carbon dioxide assimilation by *Thiobacillus novellus* under nutrient-limited mixotrophic conditions. *J. Bacteriol.,* 150, 46-51.

Poehlein, A., Schneider, D., Soh, M., Daniel, R. and Seedorf, H. (2018) Comparative genomic analysis of members of the genera *Methanosphaera* and *Methanobrevibacter* reveals distinct clades with specific potential metabolic functions. *Archaea,* 2018, 7609847, doi: 10.1155/2018/7609847.

Prahl, F. G., Ertel, J. R., Goni, M. A., Sparrow, M. A. and Eversmeyer, B. E. (1994) Terrestrial organic carbon contributions to sediments on the Washington margin. *Geochim. Cosmochim. Acta,* 58, 3035-3048.

Radajewski, S., Ineson, P., Parekh, N. R. and Murrell, J. C. (2000) Stable-isotope probing as a tool in microbial ecology. *Nature,* 403, 464-469.

Reay, D. S., Smith, P., Christensen, T. R., James, R. H. and Clark, H. (2018) Methane and global environmental change. *Annu. Rev. Environ. Resour.,* 43, 165-192.

Rettedal, E. A. and Brozel, V. S. (2015) Characterizing the diversity of active bacteria in soil by comprehensive stable isotope probing of DNA and RNA with $H_2{}^{18}O$. *Microbiologyopen.,* 4, 208-219.

Roh, H., Yu, C. P., Fuller, M. E. and Chu, K. H. (2009) Identification of hexahydro-1,3,5-trinitro-1,3,5-triazine-degrading microorganisms via ^{15}N-stable isotope probing. *Environ. Sci. Technol.,* 43, 2505–2511.

Rotaru, A. E., Shrestha, P. M., Liu, F., Shrestha, M., Shrestha, D., Embree, M., Zengler, K., Wardman, C., Nevin, K. P. and Lovley, D. R. (2014) A new model for electron flow during anaerobic digestion: direct interspecies electron transfer to *Methanosaeta* for the reduction of carbon dioxide to methane. *Energy Environ. Sci.,* 7, 408-415.

Roy, H., Kallmeyer, J., Adhikari, R. R., Pockalny, R., Jorgensen, B. B. and D'Hondt, S. (2012) Aerobic microbial respiration in 86-million-year-old deep-sea red clay. *Science,* 336, 922-925.

Sato, T., Atomi, H. and Imanaka, T. (2007) Archaeal type III RuBisCOs function in a pathway for AMP methabolism. *Science,* 315, 1003–1006.

Schäfer, T., Selig, M. and Schönheit, P. (1993) Acetyl-CoA synthetase (ADP forming) in archaea, a novel enzyme involved in acetate formation and ATP synthesis. *Arch. Microbiol.,* 159, 72-83.

Schink, B. (1997) Energetics of syntrophic cooperation in methanogenic degradation. *Microbiol. Mol. Biol. Rev.,* 61, 262-280.

Schink, B. and Zeikus, J. G. (1980) Microbial methanol formation: a major end product of pectin metabolism. *Curr Microbiol,* 4, 387-389.

Schlünz, B. and Schneider, R. R. (2000) Transport of terrestrial organic carbon to the oceans by rivers: re-estimating flux- and burial rates. *IRJES,* 88, 599-606.

Schreiber, L., Holler, T., Knittel, K., Meyerdierks, A. and Amann, R. (2010) Identification of the dominant sulfate-reducing bacterial partner of anaerobic methanotrophs of the ANME-2 clade. *Environ. Microbiol.,* 12, 2327-2340.

Schubert, C. J. and Calvert, S. E. (2001) Nitrogen and carbon isotopic composition of marine and terrestrial organic matter in Arctic Ocean sediments: implications for nutrient utilization and organic matter composition. *Deep Sea Res. Part 1,* 48, 789-810.

Schwartz, E., Hayer, M., Hungate, B. A., Koch, B. J., McHugh, T. A., Mercurio, W., Morrissey, E. M. and Soldanova, K. (2016) Stable isotope probing with ^{18}O-water to investigate microbial growth and death in environmental samples. *Curr. Opin. Biotechnol.,* 41, 14-18.

Seitz, K. W., Dombrowski, N., Eme, L., Spang, A., Lombard, J., Sieber, J. R., Teske, A. P., Ettema, T. J. G. and Baker, B. J. (2019) Asgard archaea capable of anaerobic hydrocarbon cycling. *Nat Commun,* 10, 1822, doi: 10.1038/s41467-019-09364-x.

Seitz, K. W., Lazar, C. S., Hinrichs, K. U., Teske, A. P. and Baker, B. J. (2016) Genomic reconstruction of a novel, deeply branched sediment archaeal phylum with pathways for acetogenesis and sulfur reduction. *ISME J,* 10, 1696-1705.

Singer, E., Wagner, M. and Woyke, T. (2017) Capturing the genetic makeup of the active microbiome *in situ*. *ISME J.,* 11, 1949-1963.

Sinninghe Damsté, J. S., Rampen, S., Irene, W., Rijpstra, C., Abbas, B., Muyzer, G. and Schouten, S. (2003) A diatomaceous origin for long-chain diols and mid-chain hydroxy methyl alkanoates widely occurring in quaternary marine sediments: indicators for high-nutrient conditions. *Geochim. Cosmochim. Acta,* 67, 1339-1348.

Smith, R. W., Bianchi, T. S., Allison, M., Savage, C. and Galy, V. (2015) High rates of organic carbon burial in fjord sediments globally. *Nat. Geosci.,* 8, 450-453.

Sorensen, J., Christensen, D. and Jorgensen, B. B. (1981) Volatile fatty acids and hydrogen as substrates for sulfate-reducing bacteria in anaerobic marine sediment. *Appl. Environ. Microbiol.,* 42, 5-11.

Spang, A., Saw, J. H., Jorgensen, S. L., Zaremba-Niedzwiedzka, K., Martijn, J., Lind, A. E., van Eijk, R., Schleper, C., Guy, L. and Ettema, T. J. G. (2015) Complex archaea that bridge the gap between prokaryotes and eukaryotes. *Nature,* 521, 173-179.

Spang, A., Stairs, C. W., Dombrowski, N., Eme, L., Lombard, J., Caceres, E. F., Greening, C., Baker, B. J. and Ettema, T. J. G. (2019) Proposal of the reverse flow model for the origin of the eukaryotic cell based on comparative analyses of Asgard archaeal metabolism. *Nat Microbiol* , doi: 10.1038/s41564-019-0406-9.

Spring, S., Scheuner, C., Lapidus, A., Lucas, S., Glavina Del Rio, T., Tice, H., Copeland, A., Cheng, J. F., Chen, F., Nolan, M., Saunders, E., Pitluck, S., Liolios, K., Ivanova, N., Mavromatis, K., Lykidis, A., Pati, A., Chen, A., Palaniappan, K., Land, M., Hauser, L., Chang, Y. J., Jeffries, C. D., Goodwin, L., Detter, J. C., Brettin, T., Rohde, M., Goker, M., Woyke, T., Bristow, J., Eisen, J. A., Markowitz, V., Hugenholtz, P., Kyrpides, N. C. and Klenk, H. P. (2010) The genome sequence of *Methanohalophilus mahii* SLP(T) reveals differences in the energy metabolism among members of the *Methanosarcinaceae* inhabiting freshwater and saline environments. *Arch.,* 2010, 690737, doi: doi: 10.1155/2010/690737..

Thauer, R. K. (1998) Biochemistry of methanogenesis: a tribute to Marjory Stephenson. *Microbiol.,* 144, 2377-2406.

Thauer, R. K., Kaster, A. K., Goenrich, M., Schick, M., Hiromoto, T. and Shima, S. (2010) Hydrogenases from methanogenic archaea, nickel, a novel cofactor, and H_2 storage. *Annu. Rev. Biochem.,* 79, 507-536.

Thauer, R. K., Kaster, A. K., Seedorf, H., Buckel, W. and Hedderich, R. (2008) Methanogenic archaea: ecologically relevant differences in energy conservation. *Nat. Rev. Microbiol.,* 6, 579-591.

Tromp, T. K., Van Cappellen, P. and Key, R. M. (1995) A global model for the early diagenesis of organic carbon and organic phosphorus in marine sediments. *Geochim. Cosmochim. Acta,* 59, 1259-1284.

Vanwonterghem, I., Evans, P. N., Parks, D. H., Jensen, P. D., Woodcroft, B. J., Hugenholtz, P. and Tyson, G. W. (2016) Methylotrophic methanogenesis discovered in the archaeal phylum Verstraetearchaeota. *Nat Microbiol,* 1, 16170, doi: doi: 10.1038/nmicrobiol.2016.170.

Volkman, J. K., Farrington, J. W. and Gagosian, R. B. (1987) Marine and terrigenous lipids in coastal sediments from the Peru upwelling region at 15°S: Sterols and triterpene alcohols. *Org. Geochem.,* 11, 463-477.

Wakeham, S. G., Lee, C., He, J. I., Hernes, P. J. and Peterson, M. J. (1997) Molecular indicators of diagenetic status in marine organic matter. *Geochim. Cosmochim. Acta,* 61, 5363-5369.

Wang, F. P., Zhang, Y., Chen, Y., He, Y., Qi, J., Hinrichs, K. U., Zhang, X. X., Xiao, X. and Boon, N. (2014) Methanotrophic archaea possessing diverging methane-oxidizing and electron-transporting pathways. *ISME J.,* 8, 1069-1078.

Watkins, A. J., Roussel, E. G., Parkes, R. J. and Sass, H. (2014) Glycine betaine as a direct substrate for methanogens (*Methanococcoides* spp.). *Appl. Environ. Microbiol.,* 80, 289-293.

Watkins, A. J., Roussel, E. G., Webster, G., Parkes, R. J. and Sass, H. (2012) Choline and N,N-dimethylethanolamine as direct substrates for methanogens. *Appl. Environ. Microbiol.,* 78, 8298-8303.

Wegener, G., Bausch, M., Holler, T., Thang, N. M., Prieto Mollar, X., Kellermann, M. Y., Hinrichs, K. U. and Boetius, A. (2012) Assessing sub-seafloor microbial activity by combined stable isotope probing with deuterated water and ^{13}C-bicarbonate. *Environ. Microbiol.,* 14, 1517-1527.

Wegener, G., Kellermann, M. Y. and Elvert, M. (2016) Tracking activity and function of microorganisms by stable isotope probing of membrane lipids. *Curr. Opin. Biotechnol.,* 41, 43-52.

Weimer, P. J. and Zeikus, J. G. (1978) One carbon metabolism in methanogenic bacteria. *Arch. Microbiol.,* 119, 47-57.

Wolfe, J. M. and Fournier, G. P. (2018) Horizontal gene transfer constrains the timing of methanogen evolution. *Nat. Ecol. Evol.,* 2, 897-903.

Yanagawa, K., Tani, A., Yamamoto, N., Hachikubo, A., Kano, A., Matsumoto, R. and Suzuki, Y. (2016) Biogeochemical cycle of methanol in anoxic deep-sea sediments. *Microbes Environ,* 31, 190-193.

Yoshioka, H., Mochimaru, H., Sakata, S., Takeda, H. and Yoshida, S. (2015) Methane production potential of subsurface microbes in Pleistocene sediments from a natural gas field of the dissolved-in-water type, central Japan. *Chem. Geol.,* 419, 92-101.

Yu, T., Wu, W., Liang, W., Lever, M. A., Hinrichs, K. U. and Wang, F. (2018) Growth of sedimentary Bathyarchaeota on lignin as an energy source. *Proc. Natl. Acad. Sci. U. S. A.,* 115, 6022-6027.

Zaremba-Niedzwiedzka, K., Caceres, E. F., Saw, J. H., Backstrom, D., Juzokaite, L., Vancaester, E., Seitz, K. W., Anantharaman, K., Starnawski, P., Kjeldsen, K. U., Stott, M. B., Nunoura, T., Banfield, J. F., Schramm, A., Baker, B. J., Spang, A. and Ettema, T. J. (2017) Asgard archaea illuminate the origin of eukaryotic cellular complexity. *Nature,* 541, 353-358.

Zeleke, J., Lu, S. L., Wang, J. G., Huang, J. X., Li, B., Ogram, A. V. and Quan, Z. X. (2013) Methyl coenzyme M reductase A (*mcrA*) gene-based investigation of methanogens in the mudflat sediments of Yangtze River estuary, China. *Microb. Ecol.,* 66, 257-267.

Zhou, L. and Kyte, F. T. (1992) Sedimentation history of the South Pacific pelagic clay province over the last 85 million years Inferred from the geochemistry of Deep Sea Drilling Project Hole 596. *Paleoceanography.,* 7, 441-465.

Zhou, Z., Liu, Y., Lloyd, K. G., Pan, J., Yang, Y., Gu, J. D. and Li, M. (2018) Genomic and transcriptomic insights into the ecology and metabolism of benthic archaeal cosmopolitan, *Thermoprofundales* (MBG-D archaea). *ISME J.* 13, 1751-7370.

Zhuang, G.-C., Elling, F. J., Nigro, L. M., Samarkin, V., Joye, S. B., Teske, A. and Hinrichs, K.-U. (2016) Multiple evidence for methylotrophic methanogenesis as the dominant methanogenic pathway in hypersaline sediments from the Orca Basin, Gulf of Mexico. *Geochim. Cosmochim. Acta,* 187, 1-20.

Zhuang, G.-C., Heuer, V. B., Lazar, C. S., Goldhammer, T., Wendt, J., Samarkin, V. A., Elvert, M., Teske, A. P., Joye, S. B. and Hinrichs, K.-U. (2018) Relative importance of methylotrophic methanogenesis in sediments of the Western Mediterranean Sea. *Geochim. Cosmochim. Acta,* 224, 171-186.

Zhuang, G.-C., Lin, Y.-S., Elvert, M., Heuer, V. B. and Hinrichs, K.-U. (2014) Gas chromatographic analysis of methanol and ethanol in marine sediment pore waters: Validation and implementation of three pretreatment techniques. *Marine Chemistry,* 160, 82-90.

Chapter 2

DNA and RNA stable isotope probing of methylotrophic methanogenic archaea

Xiuran Yin[1,2,3], Ajinkya C. Kulkarni[1,2,3], and Michael W. Friedrich[1,2*]

[1]Microbial Ecophysiology Group, Faculty of Biology/Chemistry, University of Bremen, Bremen, Germany

[2]MARUM – Center for Marine Environmental Sciences, University of Bremen, Bremen, Germany

[3]International Max Planck Research School for Marine Microbiology, Max Planck Institute for Marine Microbiology, Bremen, Germany

*Correspondence to:

Michael W. Friedrich

michael.friedrich@uni-bremen.de

(In press in Springer protocol handbook)

Contribution to the manuscript:

Experimental concept and design	80%
Acquisition of experimental data	80%
Data analysis and interpretation	80%
Preparation of figures and tables	70%
Drafting of manuscript	50%

Abstract

Methylotrophic methanogenic archaea are an integral part of the carbon cycle in various anaerobic environments. Different from methylotrophic bacteria, methylotrophic methanogens assimilate both, the methyl compound and dissolved inorganic carbon. Here, we present DNA- and RNA-stable isotope probing (SIP) methods involving an effective labeling strategy using ^{13}C-labeled dissolved inorganic carbon (DIC) as carbon source along with methanol as dissimilatory substrate.

Keywords Methylotrophic methanogens, Stable isotope probing (SIP), Labeling strategy, Dissolved inorganic carbon, Methanol

Running head: SIP of methylotrophic methanogens

2.1. Introduction

A large part of the globally emitted climate relevant trace gas methane is produced by methanogenic archaea, which use three main groups of substrate: hydrogen (formate) and CO_2, acetate, and methyl compounds (e.g., methanol, methyl amine) [1, 2]. Using ^{13}C-labeled acetate and CO_2, acetoclastic and hydrogenotrophic methanogens have been identified using stable isotope-probing (SIP) of nucleic acids [3, 4, 5]. Conversely, methylotrophic methanogens have not been studied using SIP of nucleic acids.

SIP of nucleic acids capitalizes on assimilation of isotopically labeled compounds (e.g., ^{13}C, ^{15}N) into DNA and RNA, density separation of differently labeled nucleic acid, and identification of actively assimilating microorganisms in isotopically "heavy" DNA or RNA [6, 7, 8]. Originally, the method was described for identifying methylotrophic bacteria with ^{13}C-labeled methanol in soil microcosms [6], but has been extended to a wide range of labeled compounds used and physiological guilds traced. Methylotrophic bacteria use C-1 compounds as carbon and energy source [9], and^{13}C-labeled methyl substrates have been demonstrated to be highly effective in labeling nucleic acids of methylotrophs using SIP of nucleic acids [10, 11]. Contrastingly, methylotrophic methanogens assimilate carbon mixotrophically, for example, using both, organic and inorganic carbon sources at the same time. In methanogenic archaea, *de novo* nucleotide biosynthesis is based on acetyl-CoA synthesis from methyl-tetrahydrosarcinopterin and CO_2 via the Wood-Ljungdahl pathway [12, 13], with 50% of acetyl carbon originating from inorganic carbon in methylotrophic methanogens [14]. Pyruvate, a precursor for nucleic acid synthesis in methanogens, is formed by further incorporation of CO_2 into acetyl-CoA [15], elevating the inorganic carbon contribution to 67% in nucleic acids. Thus in case of methylotrophic methanogens, the typical assumption in SIP labeling that the dissimilated substrate (here, ^{13}C-methyl compounds) will also be dominantly present in the biomass formed, will result in low levels of labeling of DNA and RNA. As a remedy, we have developed a labeling strategy for targeting methylotrophic methanogens involving a mixture of ^{13}C-CO_2 and a C-1 compound such as methanol to ensure sufficient labeling of these methanogens in DNA- and RNA-SIP [16]. Here, we present the workflow for labeling of methlyotrophic methanogenic archaea by DNA- and RNA-SIP using a combination of ^{13}C-labeled and unlabeled methanol and DIC with marine sediment incubations as an example. Major steps of the method encompass (i) labeling of methylotrophic methanogens in sediment incubations, (ii) nucleic acid extraction, and (iii) density separation of differently labeled DNA or RNA. The chapter is concluded by discussing anticipated results of the method.

2.2. Materials

Chemicals used for sediment slurry incubations are prepared using Milli-Q water and are 'pro analysi (p. a.)' (*see* **Note 1**). Chemicals and reagents used for DNA and RNA based processing are ultrapure, molecular biology grade and devoid of DNA and RNA nucleases. They are prepared in diethyl pyrocarbonate (DEPC) treated, autoclaved water (*see* **Note 2**). All solutions are sterilized by autoclaving (120 °C for 20 min, 103 kPa) and filtered through 0.22 µm polyethersulfone filters into sterilized glass bottles (*see* **Note 3**). All glassware, spoons, spatulas, and magnetic stir bars are sterilized and made nuclease-free by baking at 180 °C, 3 hours.

2.2.1. Sediment slurry incubations

Incubations for SIP of methylotrophic methanogens are performed in slurries prepared with anoxic marine sediment (*see* **Note 4)**.

1. Artificial Sea Water (ASW): Dissolve 26.4 g NaCl, 11.2 g $MgCl_2 \cdot 6H_2O$, 1.5 g $CaCl_2 \cdot 2H_2O$, and 0.7 g KCl in 1 L Milli-Q water (*see* **Note 5**). Transfer into 1-L serum bottle and crimp-seal with butyl rubber stopper. Solution is sterilized and made anoxic (*see* **Note 6**).
2. 500 mM Methanol stock solution: Add 98.7 mL Milli-Q water into a sterile serum bottle, crimp-seal with a butyl rubber stopper, and make it anoxic. Weigh out solutions of ^{13}C-methanol (1.652 g) or unlabeled methanol (1.602 g) and transfer to anoxic water using a N_2 flushed, sterile needle (0.8 x 40 mm, 21G) and syringe and autoclave (*see* **Note 7**).
3. 500 mM DIC solution: Transfer 4.25 g sodium ^{13}C-bicarbonate or 4.20 g unlabeled sodium bicarbonate into 120-mL serum bottle and crimp-seal with butyl rubber stopper. The bottle is made anoxic by flushing with N_2 for 10 min (*see* **Note 8**). Prepare anoxic water by flushing 100 mL Milli-Q water with N_2. Using a N_2 flushed sterile needle and syringe, add 99 mL anoxic water to dissolve the bicarbonate and autoclave.
4. Environmental samples: Marine sediment sample (*see* **Note 9**).

2.2.2. Media

1. Lysogeny broth (LB) medium (100 mL): Dissolve 1 g tryptone, 0.5 g yeast extract and 0.5 g NaCl in 90 mL Milli-Q water. Adjust pH to 7 and volume to 100 mL. Transfer the medium to 150-mL glass flasks and seal with cotton plugs. Sterilize by autoclaving.
2. *E. coli* OD 2, ^{13}C-labeled medium (*E. Coli*-OD2 C, Silantes, Germany): Ready to use *E. coli* medium. Transfer the medium to 150-mL Erlenmeyer flasks and seal with cotton plugs. Sterilize by autoclaving.

2.2.3. Nucleic acid extraction

1. 0.1 mm zirconium beads (Carl Roth, Karlsruhe): Sterilized by baking at 180˚C for 3 hours in a glass bottle.
2. 120 mM sodium phosphate buffer (pH 8): 112.87 mM Na_2HPO_4 and 7.12 mM NaH_2PO_4.
3. Tris-NaCl-sodium dodecyl sulfate (TNS): 500 mM Tris-HCl pH 8.0, 100 mM NaCl, 10% sodium dodecyl sulfate (SDS) (w/v).
4. Phenol:chloroform:isoamylalcohol pH 8 (PCI; 25:24:1; v/v/v)
5. Chloroform:isoamylalcohol (CI; 24:1; v/v) (*see* **Note 10**).
6. 30% Polyethylene glycol (PEG) 6000 (w/v): Slowly dissolve 60 g of PEG 6000 in 100 mL 1.6 M NaCl and make up volume to 200 mL. Sterilize by autoclaving (*see* **Note 11**).
7. 70% ethanol (v/v): Prepare using DEPC treated water and store at 4 °C.
8. Quant-iT PicoGreen dsDNA assay kit (Invitrogen-Thermo Fischer Scientific) (*see* **Note 12**).
9. Quant-iT RiboGreen kit (Invitrogen-Thermo Fischer Scientific).
10. RNase-free DNase.
11. Bead beater (Fast-Prep 24, MP Biomedicals).
12. Refrigerated centrifuge.
13. NanoDrop spectrophotometer (ND-1000, Peqlab Biotechnologie).
14. Microplate fluorometer (Fluoroskan Ascent FC, Thermo labsystems)

2.2.4. DNA- and RNA-SIP

1. Gradient Buffer (GB): 0.1 M Tris-HCl (pH 8), 0.1 M KCl, 1 mM ethylenediaminetetraacetic acid. Prepare using DEPC-treated water, autoclave in baked glassware.
2. 7.163 M Cesium chloride solution (CsCl, 1.847 g/mL): 217.07 g Cesium chloride dissolved in 180 mL Milli-Q water. Filter sterilize into serum bottles crimp-sealed with butyl rubber stoppers (*see* **Note 13**).
3. Cesium trifluoroacetate (2 ± 0.05 g/mL): Cesium trifluoroacetate solution is directly obtained from GE Healthcare, United Kingdom, in 120-mL rubber stopper sealed serum bottles.
4. Formamide (≥ 99.5%, deionized): Stored at -20 °C until use. (*see* **Note 14**)
5. Digital refractometer (AR200, Reichert Technologies).
6. Vertical ultracentrifuge rotor (VTi 65.1, Beckman Coulter) with tube adapters and seals.
7. Ultracentrifuge (Optima XE-90, Beckman Coulter).
8. Quick seal 16 x 45 mm tubes (Beckman Coulter).
9. Microbalance.
10. Beckman cordless tube topper.

11. Syringe pump (Aladdin syringe pump, AL-1000, WPI).
12. Stop watch.
13. 7.5 M ammonium acetate.
14. 100% isopropanol.
15. GenElute-Linear polyacrylamide (LPA, 25 μg/mL; Merck).
16. RNaseZap (Thermo Fischer Scientific).

2.3. Methods

SIP experiments start with the incubation of the microbial community, ideally, under close to natural conditions and in triplicate biological replicates (3.1), followed by the nucleic acid extraction (3.2), density separation of nucleic acids by ultracentrifugation (3.3.1–3.3.6), and precipitation, quantification and analysis of DNA and RNA from "light" and "heavy" density fractions (3.3.7–3.3.8, 3.5) (*see* **Note 15**).

2.3.1. SIP incubations

1. Transfer 200 g sediment into glass bottle under constant flushing of N_2 (or use an anaerobic glove box when available). Transfer 800 mL of ASW to prepare a 1:4 (w/v) sediment slurry dilution. Flush the headspace of the bottle with N_2 for 3 min and seal with a butyl stopper. Mix sediment slurry until homogeneity is achieved (*see* **Note 16**).
2. To set up anoxic sediment slurry incubations (n=3), flush 120-mL serum bottles with N_2 for 2 min and crimp-seal using a butyl rubber stopper. Under continuous N_2 flushing and stirring, transfer 50 mL of sediment slurry to each 120-mL serum bottle using a sterile needle (0.8 x 40 mm, 21G) and syringe.
3. To remove residual oxygen and ambient CO_2 in serum bottles, sediment slurries are made anoxic as stated in Note 6.
4. Pre-incubate sediment slurries for 10 days at 30 °C in the dark (*see* **Note 17**).
5. Prepare a working methanol solution (50 mM) by transferring stock solution (500 mM) to a serum bottle containing sterile anoxic water. Add 1 mL of ^{13}C-labeled or unlabeled methanol solution (50 mM) to the respective sediment slurries using a sterile needle (0.8 x 40 mm, 21G) and syringe (Table 1; Fig. 1). Similarly, add 1 mL of ^{13}C-DIC or unlabeled DIC to sediment slurries (*see* **Note 18**).
6. Incubate the sediment slurries at 30 °C (*see* **Note 19**).
7. Track methane concentration in headspace by gas chromatography (GC) [17], and stop the incubation when methane concentrations in the headspace stop increasing (Fig. 2A) (*see* **Note 20**).

8. Up to 8 mL of slurry is transferred in 2-mL aliquots into sterile Eppendorf tubes, per biological replicate incubation and stored at -80 °C (*see* **Note 21**).

2.3.2. Nucleic acids extraction

1. 2 mL sediment slurries (see step 8, Section 3.1) are centrifuged for 5 min to obtain sediment pellets after discarding the supernatant.
2. Add 750 µL of 120 mM sodium phosphate buffer (pH 8) to the sediment pellet and vortex to re-suspend the pellet.
3. Transfer the re-suspended sediment to a 2-mL sterile screw cap vial containing 0.5 g of sterile zirconium beads.
4. Add 250 µL TNS solution and gently mix the tubes without vortexing (*see* **Note 22**).
5. Disrupt cells by bead beating for 1 min at 6.5 m/s and centrifuge for 10 min (*see* **Note 23**).
6. Carefully transfer the supernatant to a 2-mL tube.
7. Add 1 volume PCI and gently vortex for 10 seconds (*see* **Note 24**).
8. Incubate for 10 min at room temperature and centrifuge for 5 min.
9. Transfer upper aqueous phase to a 2-mL tube (*see* **Note 25**).
10. Add 1 volume CI to the aqueous phase and gently vortex for 10 seconds and centrifuge for 5 min.
11. Transfer the aqueous phase to a 2-mL tube and fill the tube up to the 2 mL mark with 30% PEG solution. Gently mix by turning the tube up and down and incubate for 30 min at room temperature to precipitate the nucleic acids.
12. Pellet the precipitated nucleic acids by centrifuging at 45 min.
13. Discard supernatant and add 1 mL cold 70% ethanol to wash pellet (*see* **Note 26**).
14. Centrifuge for 5 min and repeat step 13.
15. Discard supernatant and air dry pellet under a fume hood for 5 min (*see* **Note 27**).
16. Dissolve DNA or RNA pellet in 50 µL DEPC treated water (*see* **Note 28**).
17. Quantify DNA with Quant-iT PicoGreen dsDNA assay kit and assess its quality using NanoDrop spectrophotometer.

Steps 18–21for RNA extraction only:

18. To remove DNA from extracts for RNA-SIP, extracts are treated with DNase using RQ1 DNase.
19. For removal of DNases, add 500 µL of DEPC treated water and repeat steps 7–16.
20. Quantify RNA with Quant-iT RiboGreen kit and assess its quality using NanoDrop spectrophotometer.

21. Conduct PCR with archaeal primers to confirm absence of DNA after DNase treatment (*see* **Note 29**).

2.3.3. Density separation of isotopically labeled nucleic acids

2.3.3.1 Preparation of *Escherichia coli* DNA and RNA standards

1. Inoculate a culture of *E. coli* DSM 498 strain into 50 mL of liquid LB medium and 50 mL of ^{13}C-labeled *E. coli* medium under a sterile clean bench.
2. Incubate cultures at 37 °C overnight at 150 rpm in a shaker incubator. Collect cells by centrifugation.
3. Repeat steps from section 3.2 to obtain ^{13}C-labeled and unlabeled *E. coli* DNA and RNA.

2.3.3.2 Preparation of samples for DNA-SIP

1. Gently mix 1.5 µg of DNA from SIP incubations with 1.5 mL GB. Similarly, mix 1.5 µg of ^{13}C- and unlabeled *E. coli* DNA (a total of 3 µg) with 1.5 mL GB (*see* **Note 30**).
2. Add 6.16 mL CsCl to the DNA-GB mixture.
3. Vortex gently and measure refractive index (RI) of each mixture (75 µL from each fraction) using the refractometer in "nD-TC" mode after calibrating with Milli-Q water. Adjust the RI of the mixtures to 1.4022 by adding 30 µL of GB or CsCl (*see* **Note 31**).

2.3.3.3 Preparation of samples for RNA-SIP

1. Mix 750 ng of RNA from sediment slurries with 1.3 mL GB. Similarly, mix 375 ng of ^{13}C- and unlabeled *E. coli* RNA (a total of 750 ng) with 1.3 mL GB.
2. Add 240 µL formamide and 6 mL of CsTFA to the RNA-GB mixture (*see* **Note 32**).
3. Gently mix, measure RI of each mixture as stated above (3.3.2) and adjust the RI to 1.7328 by adding 30 µL aliquots of GB or CsTFA.

2.3.3.4 Preparation of ultracentrifugation

1. Transfer sample mixtures to 6.9 mL Quick Seal tubes using a 10-mL sterile syringe and needle (0.8 x 40 mm, 21G). Fill the Quick Seal tubes up to their shoulder mark (*see* **Note 33**).
2. Balance (with tube adapters and rotor seals for the rotor) the weight of two tubes against each other on a microbalance so that the weight difference is ± 0.01 g. Use leftover sample mixtures from before. (*see* **Note 34**).
3. Seal tubes with Beckman cordless tube topper (*see* **Note 35**).

4. Place the tubes into the vertical rotor (VTi 65.1) and fit the tube adapters and rotor seals.
5. Tighten the rotor seals using a wrench and a pressure not greater than 120 psi.
6. Centrifuge for 40 hours at 20 °C and 192,600 *g* for DNA-SIP and for 65 hours at 20 °C and 124,000 *g* for RNA-SIP (*see* **Note 36**).

2.3.3.5 Fractionation of nucleic acids

1. After centrifugation, carry rotor from centrifuge to bench with minimum disturbance. Remove the tubes from rotor using a wrench and attach one of the tubes to a clamp stand such that the tube is stable but not under high pressure (*see* **Note 37**). Prepare 16 sterile, 1.5-mL Eppendorf tubes below the fixed sample tube to collect gradient fractions.
2. Fill a 20-mL sterile syringe, attached to a long tube, with DEPC treated water and attach it to the pre-calibrated syringe pump (pump rate of 1 mL/min).
3. Attach a sterile needle (0.5 x 16 mm, 25G) to the end of the tube. Pump water to remove any air bubbles from the setup. Refill syringe if necessary.
4. Carefully pierce the needle into the shoulder of Quick Seal tube such that the needle opening faces the solution in the tube (*see* **Note 38**).
5. Pierce the bottom of the tube with another sterile needle (0.5 x 16 mm, 25G) and remove it.
6. Pump the Milli-Q water from the needle at the top by starting the syringe pump and collect 16 fractions (420 µL) in 1.5-mL Eppendorf tubes placed below the tube by manual shifting each tube every 25 sec (using preset stopwatches) (*see* **Note 39**).

2.3.3.6 Density measurement of gradient fractions

1. Measure RI of fractions (30 µL from each fraction) starting with the lightest fraction (*see* **Note 40**).
2. For fractions where only GB was added, density of each fraction was estimated by weighing out 100 µL of each fraction medium three times on a microbalance (*see* **Note 41**).
3. Plot the RI and density values against each other and obtain a linear curve equation. Determine the densities of sample fractions using the RI values of each fraction in this equation.

2.3.3.7 DNA precipitation and quantification from fractions

1. Add 2 volumes PEG and 1 µL (25 µg) linear polyacrylamide (LPA) to each fraction and mix by inverting the tubes (*see* **Note 42**).
2. Incubate for 2 hours at room temperature to precipitate the DNA and centrifuge for 30 min at 20 °C. Discard supernatant.

3. Wash the DNA pellet with 500 µL cold 70% ethanol and centrifuge for 10 min at 20 °C.
4. Air-dry the pellet under a fume hood and elute DNA in 30 µL DEPC treated water.
5. Quantify DNA using Quant-iT PicoGreen dsDNA kit.
6. Plot DNA quantities against the fraction densities to analyze the outcome of SIP (Fig. 2B).

2.3.3.8 RNA precipitation and quantification from fractions

1. Precipitate RNA from fractions by adding 1 volume of isopropanol and 1/5 volume of 7.5 M ammonium acetate each.
2. Mix by inverting the tubes and incubate at room temperature for 20 min.
3. Centrifuge the tubes for 1 hour at 4 °C. Discard supernatant.
7. Wash the RNA pellet with 500 µL cold 70% ethanol and centrifuge for 5 min at 4 °C.
4. Air-dry the pellet under a fume hood and elute RNA in 15 µL DEPC water.
5. Quantify RNA using Quant-iT RiboGreen kit.
6. Plot RNA quantities against the fraction densities to analyze the outcome of SIP (Fig. 2C).

2.3.4. Anticipated results

In our laboratory, we have successfully labeled both, DNA and RNA, of methylotrophic methanogens in marine sediment incubations using ^{13}C-DIC as substrates. Labeling of RNA was strongest, when ^{13}C-DIC was used as substrate as indicated by the larger amount of heavy RNA compared to ^{13}C-methanol (Fig. 2C). Illumina sequencing of 16S rRNA showed that members of the *Methanococcoides,* a genus known to harbor methylotrophs, were predominantly present in heavy RNA from both ^{13}C-DIC, and ^{13}C-methanol; the occurrence of these *Methanococcoides* spp. in the light fractions of ^{13}C-methanol incubations might be explained with their strong enrichment, however, the lower degree of labeling from ^{13}C-methanol.

Labeling of DNA was much less pronounced regardless of labeled substrate used, as expected because of longer incubation times required for DNA replication and incorporation of label. Still, the power of PCR and Illumina sequencing of16S rRNA genes showed that *Methanococcoides* were the active methylotrophic methanogens in DNA-SIP (Fig. 3). Similar trends were observed in control incubations where no methanol was amended confirming the necessity to use ^{13}C-DIC as a carbon source to track methylotrophic methanogens from environments.

In general, the total recovery of nucleic acids after density separation can be expected to be much lower than what was loaded into the gradient (between 10-30%); especially the labeled nucleic acids in the heavy fractions have a low yield as often only small amounts of labeled nucleic acids are formed, which affects recovery by nucleic acid precipitation substantially (*see* **Note 42**). To identify potentially active

methylotrophic methanogens, nucleic acids from one or more fractions can be pooled (to counteract low yields) and used as templates for downstream processes such as metagenomics and next generation sequencing.

2.3.5. Experimental run time

DNA- and RNA-SIP experiments (sections 3.2–3.3.8) for 6 samples can be performed ideally over the course of 5–6 days respectively. The breakdown is as follows: (i) nucleic acid extraction and quantification - 1 day; (ii) preparation of SIP samples and ultracentrifugation - 2 days for DNA-SIP, 3 days for RNA-SIP; (iii) gradient fractionation, RI and density measurements - 1 day; and (iv) nucleic acid quantification from fractions - 1 day. We recommend starting the ultracentrifuge runs at 16:00 h to ensure that it ends in the morning giving ample time to process the fractions on the same day. It takes 2–3 hours for the ultracentrifuge to stop as the deceleration is set to coast. Incubation times for your samples may vary based on activity rates of methylotrophic methanogens. Before starting the experiment, running test incubations using DIC and methanol and measuring CH_4 formation gives a good estimate of incubation time.

2.4. Notes

1. Chemicals and reagents can also be prepared using double distilled water instead of Milli-Q water if necessary.
2. Treatment with DEPC is useful for inactivating RNA nucleases. To prepare DEPC treated nuclease-free water, add 1 mL to 1000 mL Milli-Q water. Shake vigorously and incubate at 37 °C for 12 hours. Autoclave for 15 minutes to remove traces of DEPC and inactivate DNases. Filter sterilize through a 0.22 μm filter in a sterile bottle.
3. Avoid using cellulose or acetate based filter for sterilizing solutions as they can contaminate the solutions with unwanted carbon traces.
4. The protocol described here uses marine sediment samples but the labeling strategy can also be used with other samples, e.g., lake sediment, anoxic soil etc. The solution for preparing anoxic slurries has to be adjusted accordingly for the habitat type, e.g. marine, brackish, or freshwater.
5. Since sulfate reduction is more thermodynamically favorable over methylotrophic methanogenesis, ASW is prepared without the addition of sulfate to prevent the preferential enrichment of sulfate reducing microorganisms which are found in many environments.
6. Solutions and sediment slurry incubations in serum bottles are made anoxic by replacing the headspace gas with N_2 (99.999%) and removing dissolved O_2 from the solution by three repetitive cycles of gassing and vacuum. N_2 gas is introduced into the bottle by penetrating the butyl rubber

stopper with a sterile needle (0.8 x 40 mm, 21G) attached to a sterile filter (0.2 µm, cellulose acetate) up to a pressure of max. 0.5 bar. Fitted to the same line via a 3-way stop cock with Luer lock adapters, vacuum is applied to remove gas from the headspace and the solution until no gas bubbles appear from within the solution (~ 5–10 minutes). Safety note: wear safety goggles at all time when working with compressed gases and glassware.

7. No vacuum is used while making methanol and DIC stock solutions anoxic as suggested in Note 6 due to their volatile nature.
8. The bottle is made anoxic by flushing with N_2, as mentioned in Note 6, but without the use of vacuum. Instead, another needle (0.55 x 25 mm, 24G) is introduced into the bottle through the rubber septa to allow the headspace air to be exchanged ("chimney method").
9. We collected marine sediment samples in the form of a 5 m long gravity core from the Helgoland Mud Area, North Sea, on board of the RV HEINCKE (Cruise 443; core HE443-077-1). This core was cut immediately on board into 1 m long sections, sealed and stored at 4 ºC and brought to the lab. Finally, cores were sectioned into 25 cm sections which were homogenized and stored anoxically (see Note 6.) in 2.5 L jars at 4 ºC until use.
10. Both PCI and CI are commercially available. Due to their hazardous nature, all steps involving these chemicals should be done under a fume hood along with the recommended protective gear (gloves, eye protection).
11. Since PEG solution is highly viscous, it forms two phases after autoclaving: the lower dense PEG 6000 phase and the upper aqueous NaCl phase. Upon cooling, gently shake the bottle to mix these phases completely.
12. Kits are used as per manufacturer's instructions.
13. Dissolution of cesium chloride into water can be enhanced by continuous stirring on a magnetic stirring device set at a temperature between 50–100 ºC. The solution is filtered in 30–50 mL stocks using a sterile needle (0.8 x 40 mm, 21G), 0.22 µm filter, and a 50-mL syringe. The solution is stored in butyl rubber stopper sealed serum bottles to prevent cesium chloride crust formation due to evaporation [18].
14. Storage of formamide at -20 °C prevents it from decomposing and lengthens its storage time. Storing in 2 mL aliquots allows for faster thawing times before use.
15. Disinfect all working benches and micropipettes with 70% ethanol before beginning any lab work. Treat working benches with RNaseZap before conducting RNA extraction procedures and working with RNA samples. Cool table top centrifuges to 4 °C before using them for DNA and RNA related work. All centrifugation steps in this section are carried out between 15,294–20,817 *g* at 4 °C unless specified.

16. Mixing of sediment samples with ASW helps to mimic *in situ* conditions and ensures homogenization of the sediment sample and the microbial community within. As the sediment samples are dense in nature, dilution (1:4 with ASW) also helps easier sub-sampling of the incubations for DNA and RNA extractions.
17. Pre-incubation of sediment slurries is helpful in activating the microbial community, which was surviving on minimum metabolic activity at 4 °C. Storing in dark prevents the growth of phototrophic microorganisms.
18. Having an estimate of indigenous DIC in the sample can be helpful in determining the amount of ^{13}C-DIC that should be added to sediment slurry incubations. Since indigenous DIC is preferably assimilated by microbes over ^{13}C-DIC, the latter should be added in excess in order to successfully label the active populations. In this study, supplementing 10 mM of ^{13}C-DIC elevated the ^{13}C-DIC level to 70% - 85% based on GC coupled combustion isotope ratio mass spectrometer (GC-c-IRMS) measurements. Samples from different environments may have variable DIC concentrations. Thus, quantifying ^{13}C-DIC in the slurry incubations after amending ^{13}C-DIC is highly recommended.
19. We incubated the sediment slurries at 30 ºC as the process of methanogenesis is thermodynamically favorable at mesophilic temperatures [19].
20. Preferably, stop the incubations immediately once the methanogenesis is complete (i.e. no increase of methane over 1–2 time points of measurement; Fig. 2A) to avoid cross-feeding of label and the degradation of primarily labeled microorganisms. Track changes in methane concentration in the headspace on a daily basis.
21. It can be difficult to obtain high amounts of labeled nucleic acids, especially RNA, from certain environmental samples due to many factors: low microbial activity rates, low starting biomass and loss of nucleic acids during extraction due to physical or enzyme based denaturation. We collected large amounts of slurry (up to 8 mL for DNA and RNA, respectively, per replicate treatment) from each biological replicate incubation to ensure that sufficient amounts of nucleic acids could be extracted. Here, nucleic acid extracts from all replicates were pooled together to obtain DNA and RNA in one tube in order to have sufficient amounts of nucleic acids. Otherwise, nucleic acids from biological replicates can be treated separately to check for community differences in parallel treatments.
22. Avoid vortexing after addition of TNS solution to prevent foaming from SDS. Make sure that there is at least 500 µL headspace left after addition of TNS for efficient cell disruption during bead beating.

23. After bead beating, samples must always be placed on ice or in cold blocks (+4 °C) to prevent denaturation of DNA and RNA by exo- and endonucleases present within the samples.
24. Avoid strong vortexing of samples during the extraction of total nucleic acids as shearing forces can fragment DNA and RNA.
25. It is important to avoid disturbing the aqueous and organic phases formed after centrifugation on PCI treatment. Since phenol is partially miscible in the aqueous phase, traces of phenol originating from the organic phase can inhibit downstream processes such as PCR. Transferring small volumes of the aqueous phase using low-volume micropipette is useful to avoid uptake of phenol from the organic phase. If the aqueous phase after PCI treatment looks brownish due to high amount of organic content coming from the sediment samples, repeat the PCI treatment to obtain higher quality of nucleic acids.
26. Use of "cold" 70% ethanol improves DNA precipitation efficiency and ensures that the precipitated DNA is not denatured.
27. Air drying is done to remove residual ethanol. Preferably, remove traces of ethanol using a 100 µL micropipette to expedite drying. However, avoid "over-drying" (i.e. extended periods of drying), which renders resuspension of the nucleic acid pellet more difficult.
28. Dissolution of nucleic acids can be enhanced by slow and steady mixing of 50 µL nuclease-free water for 1–2 minutes using the micropipette. This prevents shearing of nucleic acids and ensures complete dissolution of the nucleic acids into the water. 50 µL of dissolved nucleic acids are transferred from one replicate tube to another and the dissolution procedure is repeated in order to pool all nucleic acids together.
29. PCR using general archaeal primer pairs such as Arc109f [20] and Arc912rt [21] must be conducted on DNase treated samples to confirm the absence of DNA in the samples. This is done to prevent DNA contamination into the RNA fractions after SIP. If the archaeal PCR yields a product, then repeat the DNase treatment to remove any trace of DNA within the sample. Generally, 2 µL of DNase treated sample can be used to detect the presence of DNA. Appropriate controls must be tested along with the samples: (i) negative control, (ii) positive control (e.g., genomic DNA of *Methanosarcina barkeri*), (iii) DNase kit control where DNase treatment was carried out without the addition of sample to detect post process contaminants and (iv) spiking of some DNase treated samples with genomic DNA of *Methanosarcina barkeri* to detect inhibition of PCR.
30. For every first ultracentrifuge run using a fresh stock of either CsCl or CsTFA, it is necessary to centrifuge a GB sample without any nucleic acid as a standard. RI and densities of fractions obtained from the GB standard are plotted against each other to obtain a standard linear curve

equation to quantify densities of samples. Accuracy of density measurements rely on calibrated micropipettes. To obtain a "gold standard", *E. coli* standards should be always used with every sample run to check the consistency of density separation. At a time, we recommend to process only 4–6 samples (including *E. coli* standard) due to the high number of fractions obtained after fractionation (i.e. at least 16 fractions/ sample). Up to 5 µg DNA and 1.5 µg RNA can be used for ultracentrifugation. Higher quantities of DNA and RNA than recommended can lead to improper separation of labeled and unlabeled DNA and RNA post ultracentrifugation.

31. Estimates of RI and densities of mixtures can be done by mixing different volumes of GB to fixed volumes of CsCl or CsTFA [22]. This information is useful for determining the starting RI and density, where the density is ~1.705 g/mL for DNA-SIP and ~1.8 g/mL for RNA-SIP. This ensures the complete retrieval of labeled and unlabeled DNA and RNA after isopycnic separation (Fig 2B, 2C).
32. Formamide is specifically added to RNA-SIP samples to break secondary structures formed within the RNA molecules which can affect their migration of RNA along the CsTFA gradient. Mix the RNA-GB mixture with formamide before mixing the RNA with CsTFA to prevent RNA precipitation.
33. Avoid filling the Quick Seal tubes completely as the tubes have to be heat sealed later. Leaving a headspace ensures easier removal of air bubbles which can be removed by gently tapping the tubes or turning the tubes up and down after sealing. Always place the tubes on a suitable stand that can hold the ultracentrifuge tubes, their respective adapters, and centrifuge lids in order to avoid damage and disturbance within the tubes, especially post ultracentrifugation.
34. Balancing of two tubes against each other should be done very accurately using a microbalance (least count: 0.00001 g). A small imbalance will prevent the ultracentrifuge from starting and can cause it to break down (if started) owing to the high centrifugation speeds. Take utmost care to not mix the tubes, their adapters and centrifuge lids that have been balanced against each other.
35. Pre-heat (~20 seconds) the tube topper before use. Place the tube topper on the opening of the Quick Seal tube only briefly to seal the tube. Quickly place a small metallic lid to cool the sealed tube.
36. Ultracentrifugation is carried out at maximum acceleration and deceleration is set to coast so that the slowing of the ultracentrifuge does not disrupt the gradient. CsTFA protects RNA from degradation over the duration of ultracentrifugation run at 20 ºC.
37. From this step onwards, avoid shaking and disturbance of the ultracentrifuge tubes. Always place the tubes in their stands and avoid free handling of the tubes.

38. Pierce the needle into the ultracentrifuge tube in one stroke. This is done to prevent the formation of a bigger hole on top which can exert higher pressure within the tube thereby leading to a faster outflow of the liquid from the other end of the tube. Placing the tip of the needle on the opposing wall of the tube stabilizes it and prevents it from rotating inside the tube.
39. Refer to [18] for a video on SIP of nucleic acids.
40. Lighter fractions may contain some water and their RI will be much lower than the expected density range. Water containing fractions can be disregarded for further processing.
41. Instead of weighing 100 µL from each fraction in a separate new tube, remove 100 µL, record the difference, and put the sample back into the tube. Set microbalance to zero ("tare") and repeat estimation twice. As the microbalance is very sensitive and densities of the neighboring fractions are similar, pipetting should be done slowly, carefully and in the absence of any sudden movements.
42. LPA is a non-interfering agent which acts as a carrier for DNA precipitation and increases the efficiency of the process [18]. Owing to its dense nature, it also helps in locating the DNA pellet after precipitation.

2.5. Figures

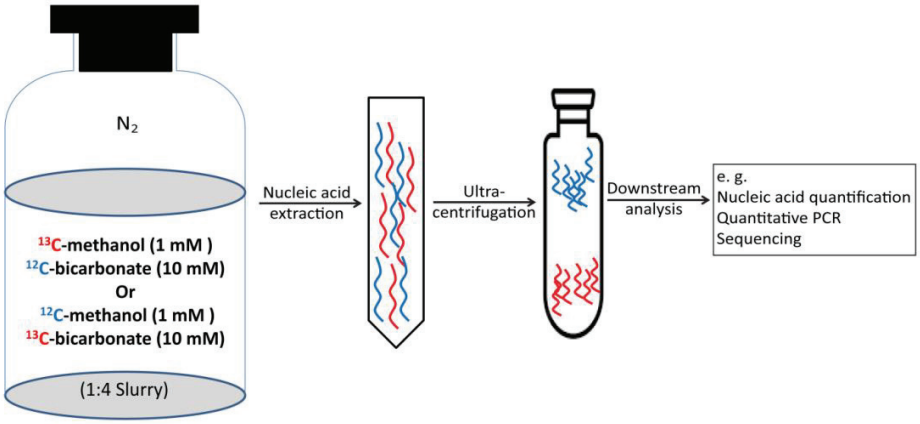

Figure 1. Workflow for DNA- and RNA-SIP for targeting methylotrophic methanogens in marine sediments.

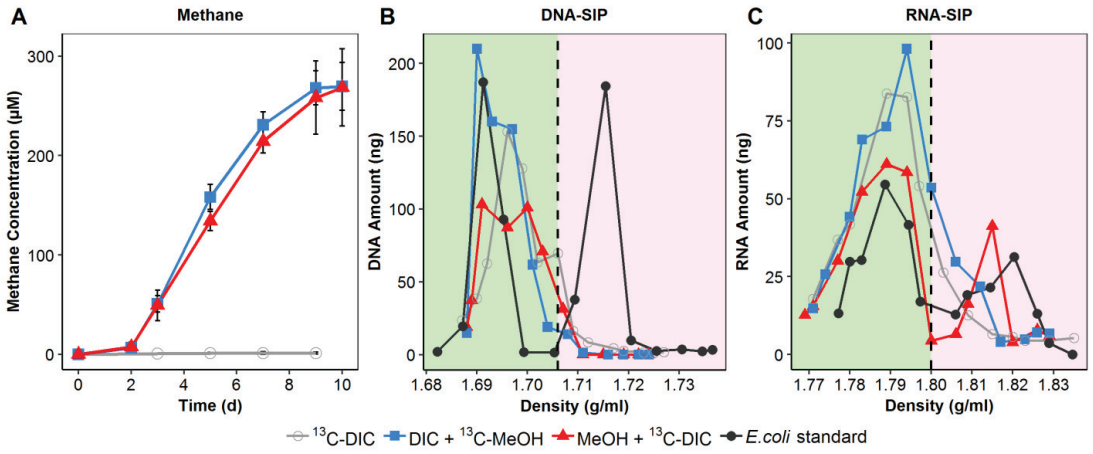

Figure 2. Isotope probing of methylotrophic methanogens in marine sediment incubations. (A) Kinetics of methane production over 10 days in sediment slurry incubations with different C1 substrates. (B) Isopycnic separation of unlabeled and labeled DNA and (C) RNA from sediment slurry incubations and controls (*E. coli*). Each data point represents the amount of DNA or RNA from a single fraction collected after density separation. Fractions containing unlabeled DNA or RNA are represented by the green area and fractions containing labeled DNA or RNA are represented by the pink area. The dotted line represents the density of the sample mixture before ultracentrifugation (**Note 31**).

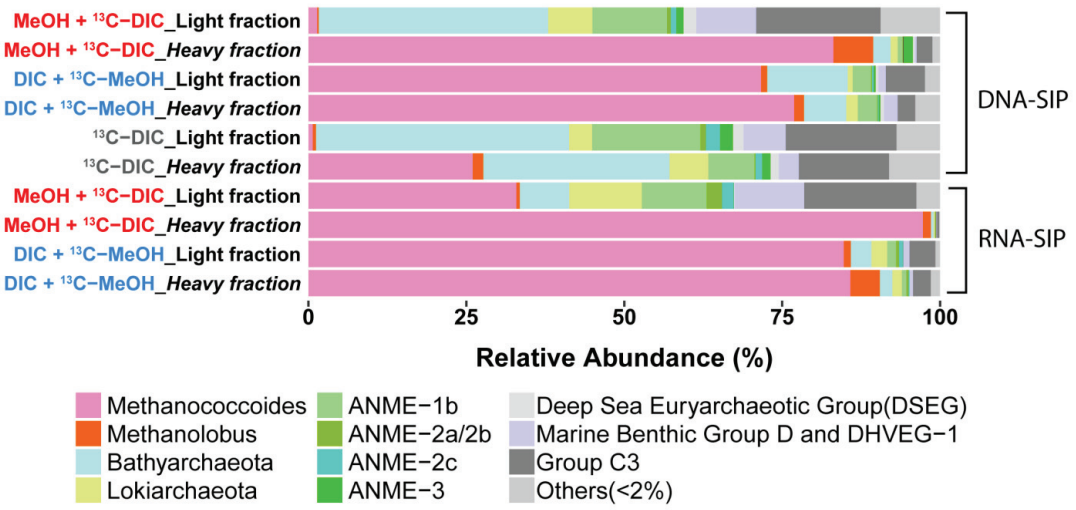

Figure 3. Total sum scaling of abundances of archaeal 16S rRNA gene sequences from selected light and heavy fractions of DNA- and RNA-SIP. Sequencing was done on an Illumina HiSeq 4000 platform as stated in [23]. Relative abundances of population < 2% were grouped together as "Others".

2.6. Table

Table 1. Sediment slurry incubation setup using different C-1 substrates, n=3 per treatment.

Incubation setup	Unlabeled methanol (1 mM)	^{13}C-methanol (1 mM)	Unlabeled DIC (10 mM)	^{13}C-DIC (10 mM)
^{13}C-DIC				X
DIC + ^{13}C-MeOH		X	X	
MeOH + ^{13}C-DIC	X			X

2.7. References

1. Ferry JG, Lessner DJ (2008) Methanogenesis in marine sediments. Ann N Y Acad Sci 1125: 147-157

2. Liu Y, Whitman WB (2008) Metabolic, phylogenetic, and ecological diversity of the methanogenic archaea. Ann N Y Acad Sci 1125: 171-189

3. Lu Y, Conrad R (2005) In situ stable isotope probing of methanogenic archaea in the rice rhizosphere. Science 309: 1088-1090

4. Schwarz JI, Lueders T, Eckert W, Conrad R (2007) Identification of acetate-utilizing bacteria and archaea in methanogenic profundal sediments of Lake Kinneret (Israel) by stable isotope probing of rRNA. Environ Microbiol 9: 223-237

5. Liu F, Conrad R (2010) *Thermoanaerobacteriaceae* oxidize acetate in methanogenic rice field soil at 50 degrees C. Environ Microbiol 12: 2341-2354

6. Radajewski S, Ineson P, Parekh NR, Murrell JC (2000) Stable-isotope probing as a tool in microbial ecology. Nature 403: 646-649

7. Manefield M, Whiteley AS, Ostle N, Ineson P, Bailey MJ (2002) Technical considerations for RNA-based stable isotope probing: an approach to associating microbial diversity with microbial community function. Rapid Commun Mass Spectrom 16: 2179-2183

8. Dumont MG, Murrell JC (2005) Stable isotope probing — linking microbial identity to function. Nat Rev Microbiol 3(6): 499-504

9. Chistoserdova L, Kalyuzhnaya MG, Lidstrom ME (2009) The expanding world of methylotrophic metabolism. Annu Rev Microbiol 63: 477-499

10. Neufeld JD, Schafer H, Cox MJ, Boden R, McDonald IR, Murrell JC (2007) Stable-isotope probing implicates *Methylophaga* spp and novel Gammaproteobacteria in marine methanol and methylamine metabolism. ISME J 1(6): 480-491

11. Grob C, Taubert M, Howat AM, Burns OJ, Dixon JL, Richnow HH, et al (2015) Combining metagenomics with metaproteomics and stable isotope probing reveals metabolic pathways used by a naturally occurring marine methylotroph. Environ Microbiol 17 (10): 4007-4018

12. Allen MA, Lauro FM, Williams TJ, Burg D, Siddiqui KS, De Francisci D, et al (2009) The genome sequence of the psychrophilic archaeon, *Methanococcoides burtonii*: the role of genome evolution in cold adaptation. ISME J 3(9): 1012-1035

13. Williams TJ, Burg D, Ertan H, Raftery MJ, Poljak A, Guilhaus M, et al(2010) Global proteomic analysis of the insoluble, soluble, and supernatant fractions of the psychrophilic archaeon *Methanococcoides burtonii*. Part II: the effect of different methylated growth substrates. J Proteome Res 9(2): 653-663

14. Weimer PJ, Zeikus JG (1978) One carbon metabolism in methanogenic bacteria. Arch. Microbiol. 119: 49-57

15. Goodchild A, Raftery MJ, Saunders NFW, Guilhaus M, Cavicchioli R (2004) Biology of the cold adapted archaeon, *Methanococcoides burtonii* determined by proteomics using liquid chromatography-tandem mass spectrometry. J Proteome Res 3(6): 1164-1176

16. Yin X, Wu W, Maeke M, Richter-Heitmann T, Kulkarni AC, Oni OE, Wendt J, Elvert M, Friedrich MW (2018) CO_2 conversion to methane and biomass in obligate methylotrophic methanogens in marine sediments. bioRxiv: doi.org/10.1101/528562.

17. van Rensburg MJ, Botha A, Ntsasa NG, Tshilongo J, Leshabane N (2009) Towards the simultaneous detection of the low nmol/mol range of CO, CH_4 and CO_2 in nitrogen using GC-FID. Accred Qual Assur 14: 665-670

18. Dunford EA, Neufeld JD (2010) DNA stable-isotope probing (DNA-SIP). J Vis Exp 42, e2027, doi: 10.3791/2027

19. Yao H, Conrad R. (2000) Effect of temperature on reduction of iron and production of carbon dioxide and methane in anoxic wetland rice soils. Biol Fertil Soils 32(2): 135-141

20. Grosskopf R, Janssen PH, Liesack W (1998) Diversity and structure of the methanogenic community in anoxic rice paddy soil microcosms as examined by cultivation and direct 16S rRNA gene sequence retrieval. Appl Environ Microbiol 64(3): 960–969

21. Lueders T, Friedrich M. (2000). Archaeal population dynamics during sequential reduction processes in rice field soil. Appl Environ Microbiol 66(7): 2732-2742

22. Fortney NW, He S, Kulkarni A, Friedrich MW et al (2018) Stable isotope probing for microbial iron reduction in chocolate pots hot spring, Yellowstone National Park. Appl Environ Microbiol 84(11): e02894-e02917

23. Aromokeye DA, Richter-Heitmann T, Oni OE, Kulkarni A, Yin X, Kasten S, Friedrich MW. (2018) Temperature controls crystalline iron oxide utilization by microbial communities in methanic ferruginous marine sediment incubations. Front Microbiol 2018;9:2574

Chapter 3

CO_2 conversion to methane and biomass in obligate methylotrophic methanogens in marine sediments

Xiuran Yin[1,2,3‡], Weichao Wu[2,4‡*], Mara Maeke[1,3], Tim Richter-Heitmann[1], Ajinkya C. Kulkarni[1,2,3], Oluwatobi E. Oni[1,2], Jenny Wendt[2,4], Marcus Elvert[2,4] and Michael W. Friedrich[1,2]

[1]Microbial Ecophysiology Group, Faculty of Biology/Chemistry, University of Bremen, Bremen, Germany

[2]MARUM - Center for Marine Environmental Sciences, Bremen, Germany

[3]International Max-Planck Research School for Marine Microbiology, Max Planck Institute for Marine Microbiology, Bremen, Germany

[4]Department of Geosciences, University of Bremen, Bremen, Germany

Running title: Methane formation from CO_2 in *Methanococcoides*

(Published in ISME J, 2019)

Contribution to the manuscript:

Experimental concept and design	70%
Acquisition of experimental data	60%
Data analysis and interpretation	60%
Preparation of figures and tables	60%
Drafting of manuscript	50%

Correspondence:

Michael W. Friedrich,

Microbial Ecophysiology Group, Faculty of Biology/Chemistry, University of Bremen, PO

Box 33 04 40, D-28334 Bremen, Germany

Email: michael.friedrich@uni-bremen.de

‡ These authors contributed equally to this work.

*Current address: Department of Biogeochemistry of Agroecosystems, University of Goettingen, Goettingen, Germany

Abstract

Methyl substrates are important compounds for methanogenesis in marine sediments but diversity and carbon utilization by methylotrophic methanogenic archaea have not been clarified. Here, we demonstrate that RNA-stable isotope probing (SIP) requires ^{13}C-labeled bicarbonate as co-substrate for identification of methylotrophic methanogens in sediment samples of the Helgoland mud area, North Sea. Using lipid-SIP, we found that methylotrophic methanogens incorporate 60 to 86% of dissolved inorganic carbon (DIC) into lipids, and thus considerably more than what can be predicted from known metabolic pathways (~40% contribution). In slurry experiments amended with the marine methylotroph *Methanococcoides methylutens*, up to 12% of methane was produced from CO_2, indicating that CO_2-dependent methanogenesis is an alternative methanogenic pathway and suggesting that obligate methylotrophic methanogens grow in fact mixotrophically on methyl compounds and DIC. Although methane formation from methanol is the primary pathway of methanogenesis, the observed high DIC incorporation into lipids is likely linked to CO_2-dependent methanogenesis, which was triggered when methane production rates were low. Since methylotrophic methanogenesis rates are much lower in marine sediments than under optimal conditions in pure culture, CO_2 conversion to methane is an important but previously overlooked methanogenic process in sediments for methylotrophic methanogens.

3.1. Introduction

Methanogenesis is the terminal step of organic matter mineralization in marine sediments [1]. There are three main pathways producing methane, i.e., hydrogenotrophic (H_2/CO_2), acetoclastic (acetate), and methylotrophic (e.g., methanol, methylamine, methoxylated benzoate) methanogenesis [2-4] with the former two pathways considered dominant. However, the importance of methylated compounds for methanogenesis in marine sediments has been acknowledged in recent years. Geochemical profiles and molecular analysis have shown that methylotrophic methanogenesis is the most significant pathway for methane formation in hypersaline sediments [5, 6] and in the sulfate reduction zone (SRZ) in marine environments [7, 8] where methanol concentration of up to 69 μM had been measured [9, 10]. Especially in the SRZ, methylated compounds are regarded as non-competitive substrates for methanogenesis, since sulfate reducing microorganisms apparently do not compete with methanogens for these compounds [11, 12]; in addition, methylated compounds can be used by marine homoacetogens [13] however, in marine sediments evidence for this activity in competition with methanogens has not been obtained so far [14]. In sediments of the Helgoland mud area, specifically, high relative abundances of potential methylotrophic methanogens were observed [15] of which many are unknown. The potential for methylotrophic methanogenesis was recently even predicted from two metagenome-assembled genomes of uncultivated Bathyarchaeota, assembled from a shotgun metagenome [16].

The formation of methane via the three main pathways in methanogenic archaea has been studied intensively [17-19]. Much less is known regarding assimilation of carbon into biomass under *in situ* conditions and to which extent different carbon sources in the environment are utilized. Discrepancies between the predicted pathways known and the actual carbon metabolism measured appear to be based on 1) different cellular functions of carbon dissimilation and assimilation originated from reaction equilibria operative, 2) intermediate carbon cross utilization, and 3) interplay between different microbial communities [18, 20-23]. For example, mixotrophically growing cultures of *Methanosarcina barkeri* form their biomass equally from methanol and CO_2, however, almost all the methane is formed from methanol rather than from CO_2 since methanol is disproportionated to methane and CO_2 according to the following reaction:

$$4\ CH_3OH \rightarrow 3\ CH_4 + CO_2 + 2\ H_2O \qquad (1)$$

But apart from such culture studies using the nutritionally versatile *Methanosarcina barkeri*, the respective contribution of CO_2 and methylated carbon substrates to biomass formation during

methylotrophic methanogenesis, especially for “obligate” methylotrophic methanogens, in natural sediments has not been studied to date.

Nucleic acids (RNA ~20%, DNA ~3%, of dry biomass, respectively), lipids (7–9%) and proteins (50–55%) are crucial cell components in living microorganisms [24], and thus, are suitable markers of carbon assimilation. In order to characterize carbon assimilation capabilities, stable isotope probing (SIP) techniques exist, among which RNA-SIP is very powerful for identifying active microorganisms based on separating ^{13}C-labeled from unlabeled RNA using isopycnic centrifugation [25, 26]. In combination with downstream sequencing analysis, RNA-SIP provides high phylogenetic resolution in detecting transcriptionally active microbes [27, 28] but is limited in its sensitivity by requiring more than 10% of ^{13}C incorporation into RNA molecules for separating ^{13}C-labeled from unlabeled RNA [29]. To date, a number of SIP studies successfully detected methylotrophic bacteria [30-32] but the detection of methylotrophic methanogens by RNA-SIP with ^{13}C labeled methyl compounds might be hampered by mixotrophic growth [33].

In contrast to RNA-SIP, lipid-SIP has a lower phylogenetic resolution, but can detect very sensitively δ^{13}C-values in lipid derivatives by gas chromatography combustion isotope ratio mass spectrometry (GC-c-IRMS), thereby facilitating quantitative determination of small amounts of assimilated carbon [34, 35].

In this study, we aimed to identify methylotrophic methanogens by RNA-SIP and elucidate carbon assimilation patterns in marine sediments. We hypothesized that the large pool of ambient dissolved inorganic carbon (DIC) in sediments [7] alters carbon utilization patterns in methylotrophic methanogens compared to pure cultures. To address this hypothesis, we tracked carbon dissimilation into methane and quantified assimilation into lipids by lipid-SIP in slurry incubations and pure cultures. In contrast to known pathways, we found a high degree of methane generation from DIC during methylotrophic methanogenesis by obligate methylotrophic methanogens, i.e., using only methyl groups for methane formation. This mixotrophic methanogenesis from both, methanol and DIC, might be the basis for our observation that more inorganic carbon was assimilated into biomass than could be expected from known pathways.

3.2. Materials and Methods

3.2.1. Sediment incubation setup for SIP

Sediment was collected from the Helgoland mud area (54°05.23'N, 007°58.04'E) by gravity coring in 2015 during the RV HEINCKE cruise HE443. The geochemical profiles were previously described [15].

Sediments of the SRZ (16–41 cm) and MZ (238–263 cm) from gravity core HE443/077-1 were selected for incubations; typically, sulfate concentration for SRZ sediment is in the range of ~3-25 mM and for MZ sediment is below the detection threshold (~50 µM) as reported in Oni et al. 2015 [15]. Anoxic slurries (1:4; w/v) were prepared by mixing sediments with sterilized artificial sea water without sulfate [36]. Slurries of 50 mL were dispensed into sterile 120-mL serum bottles and sealed with butyl rubber stoppers. Residual oxygen was removed by exchanging bottle headspace 3 times with N_2 gas. A 10-day pre-incubation was performed, followed by applying vacuum (3 min at 100 mbar) to remove most of the headspace CO_2. Triplicate incubations were conducted by supplementing 1 mM ^{13}C-labeled methanol (~33 mg L^{-1} slurry) and unlabeled 10 mM sodium bicarbonate (~610 mg L^{-1} slurry), or 1 mM unlabeled methanol and 10 mM ^{13}C-labeled sodium bicarbonate (^{13}C-labeled substrates provided by Cambridge Isotope Laboratories, Tewksbury, Massachusetts, USA) at 10 °C. The proportion of ^{13}C dissolved inorganic carbon (DIC) was determined by GC-c-IRMS.

3.2.2. Pure culture setup

The carbon assimilation patterns were compared between SIP sediment incubations and the obligate methylotrophic methanogen, *Methanococcoides methylutens*. *M. methylutens* strain MM1 (DSM 16625) was obtained from the German Collection of Microorganisms and Cell Cultures (DSMZ, Braunschweig, Germany). Initial cultivation was performed using Medium 280 according to DSMZ protocols. After several transfers of the culture in anoxic marine Widdel medium [37], 5% of the culture were inoculated into fresh Widdel medium supplemented with 30 mM methanol, trace element solution SL 10 [38], and 50 mM sodium bicarbonate (i.e., DIC) with carbon sources containing 5% of ^{13}C-label. Pure cultures were grown at 30 °C in triplicates.

3.2.3. Slurry incubations inoculated with M. methylutens

To test methanogenesis from CO_2, incubations were performed with *M. methylutens* in autoclaved (n=3) slurry from the SRZ with different amendments of electron donor (H_2), electron shuttles (humic acid; anthraquinone-2,6-disulfonic acid - AQDS), and electron acceptors/electron conductors (hematite, α-Fe_2O_3; magnetite, Fe_3O_4; Lanxess, Germany). Incubations were separately prepared with 50% H_2 in headspace, 100 µM AQDS, 30 mM magnetite, 30 mM hematite and 500 mg L^{-1} humic acid (Sigma-Aldrich, Steinheim, Germany). The pure culture (5%) was inoculated into these setups, and amended with 20 mM unlabeled methanol and ~10% of ^{13}C-labeled DIC (1 mM) for measuring carbon partitioning into methane. The control incubation comprised autoclaved slurry, 50% H_2 and 20 mM methanol without

addition of *M. methylutens*. All experiments were setup with a total volume of 50 mL in 120-mL serum bottles sealed with butyl rubber stoppers, and incubated at 30 °C in triplicates.

3.2.4. Gas analysis

The concentration of methane in the headspace was measured by gas chromatography as previously described [39]. Headspace H_2 was determined with a reduction gas detector (Trace Analytical, Menlo Park, California, USA). Gas samples of 100 µL and 1 mL from triplicate bottles were used for measuring methane and H_2, respectively. The parameters were as follows: carrier gas (nitrogen) 50 mL min^{-1}, injector temperature 110 °C, detector 230 °C, column (Porapak Q 80/100) 40 °C.

The $\delta^{13}C$ values of methane and CO_2 in the headspace, DIC as well as total dissolved inorganic carbon (TIC) in slurries were determined using a Thermo Finnigan Trace GC connected to a DELTA Plus XP IRMS (Thermo Scientific, Bremen, Germany) as described previously [40]. Prior to analyses of $\delta^{13}C$-DIC and -TIC, 1 mL of supernatant or slurry was converted to CO_2 by adding 1 mL phosphoric acid (85%, H_3PO_4) overnight at room temperature.

3.2.5. Nucleic acids extraction, quantification and DNase treatment

The nucleic acids were extracted according to Lueders et al. [41]. Briefly, 2 mL of wet sediment without supernatant from biological triplicates was used for cell lysis by bead beating, nucleic acid purification by phenol-chloroform-isoamyl alcohol extraction and precipitation with polyethylene glycol. For the RNA extract, DNA was removed by using the RQ1 DNase kit (Promega, Madison, Wisconsin, USA). DNA and RNA were quantified fluorimetrically using Quant-iT PicoGreen and Quant-iT RiboGreen (both Invitrogen, Eugene, Oregon, USA), respectively.

3.2.6. Isopycnic centrifugation, gradient fractionation and reverse transcription

Isopycnic centrifugation and gradient fractionation were performed according to the previously described method with modifications [41]. In brief, 600 to 800 ng RNA from biological replicates (n=3) was combined and loaded with 240 µL formamide, 6 mL cesium trifluoroacetate solution (CsTFA, GE Healthcare, Buckinghamshire, UK) and gradient buffer solution. RNA was density separated by centrifugation at 124 000 ×*g* at 20 °C for 65 h using an Optima L-90 XP ultracentrifuge (Beckman Coulter, Brea, California, USA). As standard, a mixture of equivalent amounts of fully ^{13}C-labeled and unlabeled *E. coli* RNA was used in density separation for defining heavy and light gradient fraction

density ranges. RNA was quantified and reverse transcription was conducted using the high capacity cDNA reverse transcription kit (Applied Biosystems, Foster City, California, USA).

3.2.7. Quantitative PCR (qPCR)

Archaeal 16S rRNA and *mcrA* genes were quantified from each biological replicate (n=3) using primer sets 806F/912R and ME2 mod/ME3´Fs 1011 (Table S1), respectively; *mcrA* encodes the alpha subunit of methyl coenzyme M reductase, a key enzyme of methanogenic and methanotrophic archaea [42]. Standard curves were based on the 16S rRNA gene of *M. barkeri* and the *mcrA* gene clone A4-67 for archaea and methanogens, respectively. The setup of PCR reaction was described previously [36]. The qPCR protocol comprised an initial denaturation for 5 min at 95 °C and 40 cycles amplification (95 °C for 30 sec, 58 °C for 30 sec and 72 °C for 40 sec). The detection thresholds were 100–1 000 gene copies with an efficiency of 90–110%.

3.2.8. Sequencing and bioinformatics analysis

Based on the RNA-SIP profiles of *E.coli* standard RNA (Figure S1) and a previously reported density shifts in SIP fractions [41], "heavy" (1.803–1.823 g mL^{-1}, combination of fraction 3, 4, and 5) and "light" (1.777–1.780 g mL^{-1}, fraction 11) fractions of RNA-SIP samples were selected. Library construction and sequence read processing were as described previously [39].

3.2.9. Lipid analysis

Total lipids were extracted from ~4 g of freeze-dried sediment samples from single labeling incubations (one substrate labeled, the other unlabeled) using a modified Bligh-Dyer protocol [43]. Intact polar archaeal ether lipids were purified by preparative high performance liquid chromatography with fraction collection according to the method by Zhu et al. [44]. Considering the origin and complexity of sediment samples and similar proportion of carbon atoms in lipid molecules (archaeol and hydroxyarchaeol), phytenes, biphytane, and biphytanes containing cycloalkyl rings (Figure 3C, Figure S2) were obtained from the intact archaeal lipid fraction [45]. The detailed chromatographic and mass spectrometric parameters were described by Kellermann et al. [46].

3.2.10. $\delta^{13}C$ calculation

The proportion of methane from DIC (f_{DIC/CH_4}) was calculated based on the fractional abundance of ^{13}C (^{13}F) of methane, methanol (MeOH) and DIC in the incubation with ^{13}C-DIC and MeOH. According to a

two-end member model, DIC and MeOH are two main carbon sources for methane production expressed as follows:

$$f_{DIC/CH_4}{}^{13}F_{DIC} + \left(1 - f_{DIC/CH_4}\right){}^{13}F_{MeOH} = {}^{13}F_{CH_4} \quad \text{(Eq.1)}$$

$$f_{DIC/CH_4} = \frac{{}^{13}F_{CH_4} - {}^{13}F_{MeOH}}{{}^{13}F_{DIC} - {}^{13}F_{MeOH}} \times 100\% \quad \text{(Eq.2)}$$

where ${}^{13}F$ is obtained from the δ notation according to F = R/(1+R) and R = (δ/1000+1) * 0.011180 [47]. ${}^{13}F_{CH_4}$ and ${}^{13}F_{DIC}$ were the fractional ^{13}C abundance of methane and DIC at harvest time, and ${}^{13}F_{MeOH}$ that of MeOH in the medium at the start.

^{13}C label incorporation ratios from MeOH or DIC in single labeling experiments were calculated from the ^{13}C abundance increase relative to the ^{13}C label strength via Eq. 3 and Eq. 4. X_{MeOH} and X_{DIC} signify the ^{13}C incorporation ratio from MeOH and DIC, respectively. ${}^{13}F_{t_{end}}$ and ${}^{13}F_{t_0}$ are the ^{13}C fractional abundance of lipids harvested at t_{end} and t_0.

$$X_{MeOH} = \frac{{}^{13}F_{t_{end}} - {}^{13}F_{t_0}}{{}^{13}F_{MeOH}} \quad \text{(Eq.3)}$$

$$X_{DIC} = \frac{{}^{13}F_{t_{end}} - {}^{13}F_{t_0}}{{}^{13}F_{DIC}} \quad \text{(Eq.4)}$$

Given that the single labeling incubations were conducted with the same treatment, i.e., 1 mM methanol and 10 mM DIC, the relative proportion of DIC for lipids biosynthesis ($f_{DIC/lipid}$) was estimated from the ^{13}C incorporation ratios (X_{MeOH} and X_{DIC}) in these single labeling incubations as follow:

$$f_{DIC/lipid} = \frac{X_{DIC}}{X_{DIC} + X_{Me}} \quad \text{(Eq.5)}$$

3.3. Results

3.3.1. Methylotrophic methanogenesis and increase in methanogenic archaea

In order to examine carbon labeling into RNA and lipids of methylotrophic methanogens in anoxic marine environments, sediment slurries amended with or without ^{13}C-methanol (1 mM) and ^{13}C-DIC (10 mM) were incubated at 10 °C. Sediment incubations from the zones of sulfate reduction (SRZ) and methanogenesis (MZ) showed a divergent methane production rate, i.e., methanogenesis finished after 40 and 20 days, respectively (Figure 1A). In incubations amended with DIC and ^{13}C-methanol, carbon recovery from methanol of ~80% was measured from both sediment incubations (Table S2). Amended

^{13}C-DIC was diluted into the sediment endogenous DIC pool to about 70–84%, which was more obvious in samples from MZ than SRZ (Table 1). In SRZ sediment incubations with ^{13}C-DIC and unlabeled methanol, up to 10.3% of methane originated from ^{13}C-DIC (Table 1).

The dynamics of the archaeal communities in all incubations was tracked by qPCR of archaeal 16S rRNA genes and *mcrA* genes after methanogenesis ceased (Figure 1B). Archaeal and *mcrA* gene copy numbers increased strongly by 10–14 and 19–30 times for all treatment incubations respectively, while gene copies in control incubations were not elevated (Figure 1B).

3.3.2. Carbon assimilation into RNA and identification of metabolically active archaea

In preliminary sediment incubations, SIP experiments with ^{13}C-methanol had shown that RNA could not be labeled to a sufficiently high extent to become detectable in heavy gradient fractions (e.g., >1.803 g mL^{-1}) after isopycnic separation of RNA. Contrastingly, methanol dissimilation was strong and archaeal and *mcrA* gene copies increased compared to that on day 0 and ^{13}C-DIC control, likewise indicating that methylotrophic methanogens were active (Figures 1A and B, Table S2). Because of mixotrophic assimilation capabilities in methylotrophic methanogens, i.e., utilizing methylated compounds and DIC, a series of SIP slurry experiments were conducted with combinations of methanol and DIC in order to improve the sensitivity of RNA-SIP: double ^{13}C-label (methanol + DIC), single ^{13}C-label (one of the substrates labeled), both substrates unlabeled, and a ^{13}C-DIC control (Figure 2, Figure S3). After density separation of RNA, different degrees of RNA labeling were detected in isotopically heavy gradient fractions, e.g., >1.803 g mL^{-1} (Figure 2). Strongest ^{13}C-labeling, as indicated by largest amounts of RNA found in gradient fractions > 1.803 g mL^{-1}, was detected in RNA from incubations with double ^{13}C-labeling (Figure 2A), followed by single-label incubations with ^{13}C-DIC. For single-label ^{13}C-methanol incubations, however, RNA fraction shifts according to density were minor compared to unlabeled incubations.

In order to estimate ^{13}C-labeling levels of methanogens in single SIP experiments (^{13}C-methanol or ^{13}C-DIC), a series of molecular techniques were applied including qPCR of cDNA in heavy fractions of RNA-SIP samples, archaeal 16S rRNA sequencing from RNA-SIP fractions and δ^{13}C value determination of methanogen lipids, e.g., phytanes derived from intact polar archaeol-based molecules. In incubations amended with ^{13}C-DIC and unlabeled methanol, archaeal gene copies were substantially higher than that of ^{13}C-DIC control and ^{13}C-methanol incubations (Figure 2B). Up to 49 000-fold more RNA molecules were present in the heavy fraction (i.e., 1.803–1.823 g mL^{-1}) compared to the incubation amended with unlabeled DIC and ^{13}C-methanol (Table S3). Correspondingly, Illumina sequencing of RNA revealed that sequences identified as related to the genera *Methanococcoides* were dominant in SRZ sediment

incubations, and the methylotrophic methanogens *Methanococcoides* and *Methanolobus* spp. were more dominant in MZ sediment incubations. In contrast to heavy fractions, the abundance of methanogens in the light fractions from double labeling incubations, i.e., ^{13}C-(DIC + methanol) were lowest (~30-60%) (Figure S3), followed by the incubations amended with methanol and ^{13}C-DIC (~50-70%) (Figure 2C). SIP incubations amended with DIC and ^{13}C-methanol harbored the highest relative abundance of methanogens in the light fraction, which ranged in abundance from 80 to 90% of total archaea (Figure 2C). Light fractions were overall mainly composed of anaerobic methanotrophic (ANME) archaea, Bathyarchaeota and Lokiarchaeota except for methylotrophic methanogens (Figure 2C). For ^{13}C-DIC control incubations, abundances of methanogens were low in SIP samples (Figure S3). For unlabeled methanol and DIC incubations, given the low amount of labeled RNA in heavy fractions, no amplicons were obtained, but light fractions showed a high abundance of methylotrophic methanogens (Figure S3). Classifications were confirmed by phylogenetic clustering of cloned 16S rRNA gene fragments (about 800 base pairs) with OTU sequences representing *Methanococcoides* and *Methanolobus* spp. (Figure S4). Sequences of these methanogens accounted for more than 97% of total archaea in heavy gradient fractions. However, known hydrogenotrophic methanogens were undetectable (Figure 2C) although 3 and 10% of methane was formed from DIC in incubations with MZ and SRZ sediments, respectively (Table 1).

In parallel to RNA-SIP, lipid-SIP incubations with SRZ sediment slurries demonstrated δ^{13}C values of phytane and phytenes being more positive in ^{13}C-DIC and unlabeled methanol treatment than that in ^{13}C-methanol amendments, while the opposite was found in MZ sediment incubations (Figure 3A). After elimination of ^{13}C-DIC dilution effects by ambient inorganic carbon, DIC contributions to lipids ranged from 59.3% to 86.1% in SRZ sediment incubations, which was constantly higher than that of MZ sediment incubations (52.7% to 56.4%).

To understand how carbon is assimilated into lipids by methylotrophic methanogens, pure culture incubations of *M. methylutens* were performed with 5% of the ^{13}C-labeled substrates (i.e., DIC or MeOH) and the dominating archaeal lipids archaeol (AR) and hydroxyarchaeol (OH-AR) were directly analyzed without cleavage. In contrast to sediment incubations, lipids showed lower $f_{DIC/lipid}$ (~49%) based on the carbon incorporation in single labeling incubations (Figure 3B).

3.3.3. Methane formation from DIC during methylotrophic methanogenesis

The high proportion of methane formed from DIC in methanol amended sediment slurry incubations (Table 1) prompted us to investigate the underlying mechanism in more detail. Thus, autoclaved sediment slurries were used as a surrogate of natural sediment, but with all microorganisms killed, and inoculated

with the obligate methylotroph *M. methylutens*. Hematite and magnetite known to serve as electron acceptors or conductors [48, 49] were added along with humic acid, and AQDS as electron shuttles, as well as an additional electron donor (H_2), which are all known to stimulate methanogenesis [48-51]; certain methylotrophic methanogens, e.g., *Methanomassiliicoccales* spp., require hydrogen for methanogenesis [52, 53].

Methane concentrations in incubations with hematite and humic acid were higher than that of the other incubations after 7 days (Figure 4A). Although methane production rates were low, methane proportions from DIC in treatments with *M. methylutens* alone, H_2, AQDS and magnetite were much higher ($f_{DIC/CH4}$, ~10%) than that in incubations with hematite and humic acid (~2%) (Figure 4B). Linear regression showed a strong correlation between methane production rate and CO_2-dependent methanogenesis by methylotrophic methanogens on day 3 and 5 of the incubations, indicating that lower methanogenesis rates triggered higher levels of methane formation derived from ^{13}C-DIC (Figure 4C).

3.4. Discussion

In this study, we utilized RNA-SIP employing ^{13}C-DIC and methanol and successfully identified methylotrophic methanogens in both, SRZ and MZ sediments of the Helgoland mud area in the North Sea. We demonstrated that the addition of ^{13}C-DIC is necessary to detect label in RNA of methylotrophic methanogens rather than using ^{13}C-methanol as energy substrate alone. We further evaluated carbon utilization patterns of the methylotrophic methanogens by lipid-SIP and identified a high DIC assimilation into characteristic lipids within the SRZ sediment. Isotope probing experiments revealed that up to 12% of methane was formed from DIC by the "obligate" methylotrophic methanogen, *M. methylutens*, thereby suggesting an explanation for the elevated DIC incorporation into biomass.

3.4.1. Carbon assimilation by methylotrophic methanogens in sediment incubations

Nucleic acids-SIP techniques depend on ^{13}C-labeling levels of DNA or RNA molecules, from which carbon assimilation can be reconstructed and compared to the known pathway of nucleic acid biosynthesis from methyl-groups in methanogens [54-59]. The current pathways show that only one carbon atom stems from methanol in ribose-5-phosphate while 25% to 40% of carbon in nucleobases originates from the methyl carbon of the substrate (Figure 5). This is corroborated by our RNA-SIP experiments using ^{13}C-labeled methanol alone, but RNA was not found to be labeled effectively enough for density separation and further sequence analysis. However, by additionally using ^{13}C-DIC, we found high 16S rRNA copy numbers (Figure 2B) and a high representation of known methylotrophic methanogens (Figure 2C) in the heavy RNA gradient fractions, successfully recovering ^{13}C-labeled RNA

of methylotrophic methanogens in the SRZ and MZ sediments of the Helgoland mud area. Combined with downstream analysis including qPCR, 16S rRNA sequencing and cloning, we directly show that members of the genus *Methanococcoides* were the predominantly active methylotrophic methanogens in SRZ incubations, while *Methanococcoides* together with *Methanolobus* were dominant in MZ incubations. In addition, archaea with an abundance less than 0.01% showed a higher proportion in light fractions than in heavy fractions (Table S4), excluding the populations under high-sensitivity SIP conditions [60]. A small peak at 1.808 g mL^{-1} was detected in RNA-SIP profiles from the SRZ incubations amended with ^{13}C-methanol and unlabeled DIC, which originated most likely from methylotrophic methanogens as shown by relative abundances of methanogens in the heavy fractions (Fig. 2C). However, at this density, RNA was partially labeled only because of the lower contribution of methanol carbon to nucleic acid biosynthesis, which resulted in lower RNA amounts in heavy fractions than that of ^{13}C-DIC and unlabeled methanol treatment. Consequently, RNA labeling will be more effective in methylotrophic methanogenic archaea by using DIC than by methanol.

The main reactions of inorganic carbon assimilation are the generation of acetyl-CoA and pyruvate, respectively (Figure 5). In principle, the generated CO_2 from methanol (Reaction 1) can be utilized for biomass synthesis but is in exchange with the large pool of ambient CO_2 (at least 10 mM in our experiments, up to 40 mM in marine sediment [7]. Thus, the methane formed by reduction of CO_2 will be largely recruited from ambient, unlabeled CO_2 molecules [61]. Hence, addition of ^{13}C-labeled DIC or a combination of both substrates labeled enables tracking of methylotrophic methanogens via RNA-SIP techniques. For carbon assimilation into nucleic acids of these methanogens, both proposed biosynthesis pathway of nucleic acid and labeling strategy of RNA-SIP confirmed inorganic carbon as the main carbon source for nucleic acids.

Because of its proven accuracy, lipid-SIP was used for the relative quantification of carbon assimilation into biomass. In lipid-SIP analysis, we evaluated ^{13}C-incorporation into intact polar archaeol- and hydroxyarchaeol diether molecules, which are the dominant lipids produced by moderately thermophilic methanogenic archaea [62-64], via phytane and phytene side-chain analysis (Figure 3). These moieties were the only ones being ^{13}C-labeled while tetraether-derived biphytane and cycloalkylated biphytanes as indicators of archaea such as Thaumarchaeota [65], anaerobic methanotrophs [66, 67] or Bathyarchaeota [68] did not show a ^{13}C incorporation (Figure S5). This was corroborated by our sequencing results demonstrating that methylotrophic methanogens were the dominant archaea in the heavy fractions and that the relative abundances of other archaea were very low or even below detection (Figure 2C).

By evaluating ^{13}C incorporation into methanogen-derived phytane and phytenes, lipid-SIP provides insight into methanogen activities and carbon utilization. As the main precursors of ether lipids in archaea, biosynthesis of isopentenyl diphosphate (IPP) and dimethylallyl diphosphate (DMAPP) proceeds via the modified mevalonate pathway [69-71]. In this pathway, mevalonate-5-phosphate is decarboxylated to IPP, in which three out of five carbon atoms are derived from methanol (Figure 6). DMAPP is further converted to geranylgeranyl diphosphate (GGPP), which receives 60% of its carbon from methanol, suggestive of a lower DIC contribution to isoprenoid chains than methanol. This was supported by the fact that archaeol and hydroxyarchaeol contained more methanol-derived than DIC-derived carbon using a pure culture of *M. methylutens* (Figure 3B). However, unlike the proposed lipid biosynthesis pathway and the pure culture, clearly more DIC was assimilated into lipids than methanol in both sediment incubations, which was most prominent in the sediment from the SRZ (Figure 3A). We, moreover, detected that ~10% of methane produced was derived from DIC during the SIP experiments and using *M. methylutens* in autoclaved sediment slurry incubations (Table 1, Figure 4). Because of the reversibility of all reactions from CO_2 to methyl-tetrahydrosarcinapterin (CH_3-H_4SPT) [23], it is very likely that part of the DIC is converted to CH_3-H_4SPT. Thus, CH_3-H_4SPT generated from CO_2 will be available for lipid biosynthesis (Figure 6) leading to the ^{13}C-enrichment of the lipid pool observed (Figure 3).

3.4.2. CO_2 reduction to methane by obligate methylotrophic methanogens

There are two types of CO_2-dependent methanogenesis: 1) Hydrogenotrophic methanogenesis [2, 4]. These methanogens contain F_{420}-reducing [NiFe]-hydrogenase to catalyze F_{420} reduction by H_2 [72]. 2) Mediation by interspecies electron transfer between bacteria and some members of the *Methanosarcinales*. CO_2 reduction to methane was observed in *Methanosaeta* and *Methanosarcina* during syntrophic growth with *Geobacter* species on alcohols (ethanol, propanol, and butanol), as electrons generated from *Geobacter* are directly transferred to methanogens to reduce CO_2 [73-76].

Based on our SIP incubations with SRZ sediment showing 10% of methane generation from DIC at low H_2 partial pressure (< 0.3 Pa) (Table 1) and the overall lack of hydrogenotrophic methanogens in RNA-SIP fractions (Figure 2C), we argue that H_2-dependent methanogenesis does not play a role [2]. Similarly, in autoclaved sediment slurry (Figure 4B), the "obligate" methylotroph *M. methylutens* generated methane from CO_2 without a hydrogen (or electron) supplying partner microorganism.

Members of the genus *Methanococcoides* are considered as obligate methylotrophic methanogens since no F_{420}-reducing [NiFe]-hydrogenase was detected in their genomes [69, 77] ruling out hydrogenotrophic methanogenesis in sediment incubations. Nevertheless, part of the methane formed during methylotrophic

methanogenesis by *M. methylutens* was from CO_2, especially when methane production rates were low (Figure 4C). Apparently, at high rates of methanol dissimilation to CO_2, the reverse pathway of CO_2 reduction to methane was outcompeted. Higher rates of methylotrophic methanogenesis can be achieved potentially by amendments in autoclaved slurries using hydrogen as electron donor, electron conductors (hematite, magnetite) and electron shuttles (humic acid, AQDS); in our incubations, we found humic acid and hematite most strongly stimulating methylotrophic methanogenesis. Although the underlying mechanism is beyond the scope of the current study, methylotrophic methanogens in our incubations could take advantage of hematite as potential electron conductor [48, 49] or humic acid as electron shuttle [51] as indicated by a higher rate of methanogenesis compared to the other treatments (Figure 4A).

It has been shown that 3% of methane was produced from CO_2 during methylotrophic methanogenesis of *Methanosarcina barkeri* (i.e., a facultative methylotroph) without the addition of H_2 [33], which is similar to about 2.5% of methane generated from CO_2 by *M. methylutens* (i.e., "obligate" methylotroph) in our study (Table S5). However, in SRZ sediment incubations the rate of methane production was lower than in MZ incubations, which resulted in a high proportion of methane generated from CO_2 (10%) (Table 1, Figure 1). Furthermore, CO_2 conversion to methane linked inorganic carbon assimilation into lipids, highlighting the importance of the activity of concomitant CO_2 reduction during methylotrophic methanogenesis in marine sediments. In contrast, we found that in pure cultures, under optimal growth conditions, a substantially higher methanogenesis rate decreases the amount of methane produced from CO_2. In marine sediment methylotrophic methanogenesis rates are likely lower than those in pure cultures because of the limitation in methylated substrates [7, 18], strongly suggesting that methane generation from CO_2 by obligate methylotrophic methanogens is underestimated under *in situ* conditions. Thus, CO_2 conversion to methane has to be considered when estimates of *in situ* methylotrophic methanogenesis in marine sediments are performed.

In summary, we have shown that ^{13}C-DIC is required as co-substrate for successful identification of methylotrophic methanogens by RNA-SIP in marine sediments. DIC is the main carbon source for biosynthesis of nucleic acids in these methanogens and thus using ^{13}C-methanol as energy and carbon substrate alone is insufficient in SIP experiments (Figure 5). Given the intricacies of known assimilatory pathways in methanogenic archaea as a functional group, it might be necessary to at least check for the possibility of DIC as a main assimilatory carbon component in all methanogens for successful SIP experiments. In general, it seems that archaea have a propensity for using DIC as a carbon source for assimilation [68, 78], possibly as an evolutionary adaptation to environments with limited availability of organic carbon [79]

But beyond known pathways, we detected an unexpectedly high amount of methane (> 10%) formed from DIC. Especially in SRZ incubations, the lower methane production rates resulted in increased CO_2 conversion to methane (~10%), which is linked to CO_2 conversion assimilation. This finding strongly suggests that the alleged obligate methylotroph studied here was rather mixotrophically converting both available substrates (DIC, methanol) to methane. Our detailed labeling studies showed that the kinetics of substrate utilization apparently is a decisive factor in channeling more or less CO_2 into the pathway of methanogenesis: more methane formed from CO_2 when the overall kinetics were slow, and vice versa. From an ecological perspective, DIC is a much more pertinent substrate than methanol (or other methyl compounds) in marine sediments [5, 7], and thus, we speculate that more DIC reduction by obligate methylotrophic methanogens occurs *in situ* than is currently known. A larger proportion of methane formed from DIC in methylotrophic methanogens should also impact interpretation of $\delta^{13}CH_4$ values and associated carbon isotope fractionations, which might be overprinted by such mixotrophic methanogenesis. Thus, the CO_2 reduction to methane and assimilation into biomass by obligate methylotrophic methanogens plays a much more important role in the environment than was previously known.

3.5. Acknowledgments

This study was supported by the Research Center/Cluster of Excellence 'The Ocean in the Earth System' (MARUM) funded by the Deutsche Forschungsgemeinschaft (DFG) and by the University of Bremen. Xiuran Yin and Weichao Wu were funded by the scholarship from China Scholarship Council (CSC). We thank the captain, crew and scientists of R/V HEINCKE expeditions HE443.

3.6. Conflict of interest

The authors declare that they have no conflict of interest.

3.7. Data availability

Sequencing data have been submitted to GenBank Short Reads Archive with accession numbers from SRR8207425 to SRR8207442.

3.8. Table

Table 1. ^{13}C fractional abundance and H_2 partial pressures in SIP incubations. Data is presented as average values (n = 3).

Sediment	Substrates	$^{13}F_{DIC}$ (%)	f_{DIC/CH_4} (%)[a]	H_2 (Pa)[b]	Incubation time (d)
SRZ	DIC + ^{13}C-MeOH	3.7 ± 0.4	89.3 ± 0.3	NA	43
MZ	DIC + ^{13}C-MeOH	3.0 ± 0.0	96.4 ± 0.1	NA	19
SRZ	MeOH + ^{13}C-DIC	83.6 ± 0.6	10.3 ± 0.2	0.1 ± 0.1	43
MZ	MeOH + ^{13}C-DIC	69.8 ± 0.7	3.4± 0.1	0.3 ± 0.0	19

[a]Methane proportion from DIC (f_{DIC/CH_4}) in "methanol + ^{13}C-DIC" incubations was based on Eq.2. [b]H_2 partial pressure was measured on day 23 and 16 for incubation SRZ and MZ sediments, respectively. NA, not analyzed.

3.9. Figures

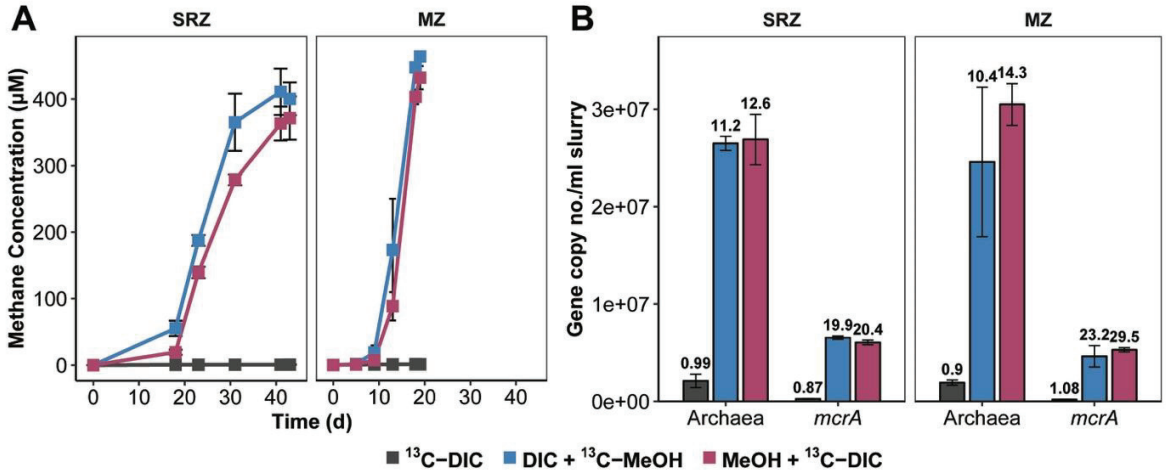

Figure 1. Dynamics of methane formation and archaeal populations in stable isotope probing (SIP) incubations with SRZ and MZ sediment samples. (A) Methane concentrations in SIP incubations. Methane data is presented as average values (n = 3, error bar = SD). (B) Gene copy numbers of archaea (16S rRNA genes) and methanogens (*mcrA* gene). Gene copies were quantified based on DNA extracts at harvest. Fold increase of gene copies were indicated above each histogram by comparing gene copies on day 0 after preincubation (n = 3, error bar = SD). DIC: dissolved inorganic carbon, i.e. bicarbonate; MeOH: methanol.

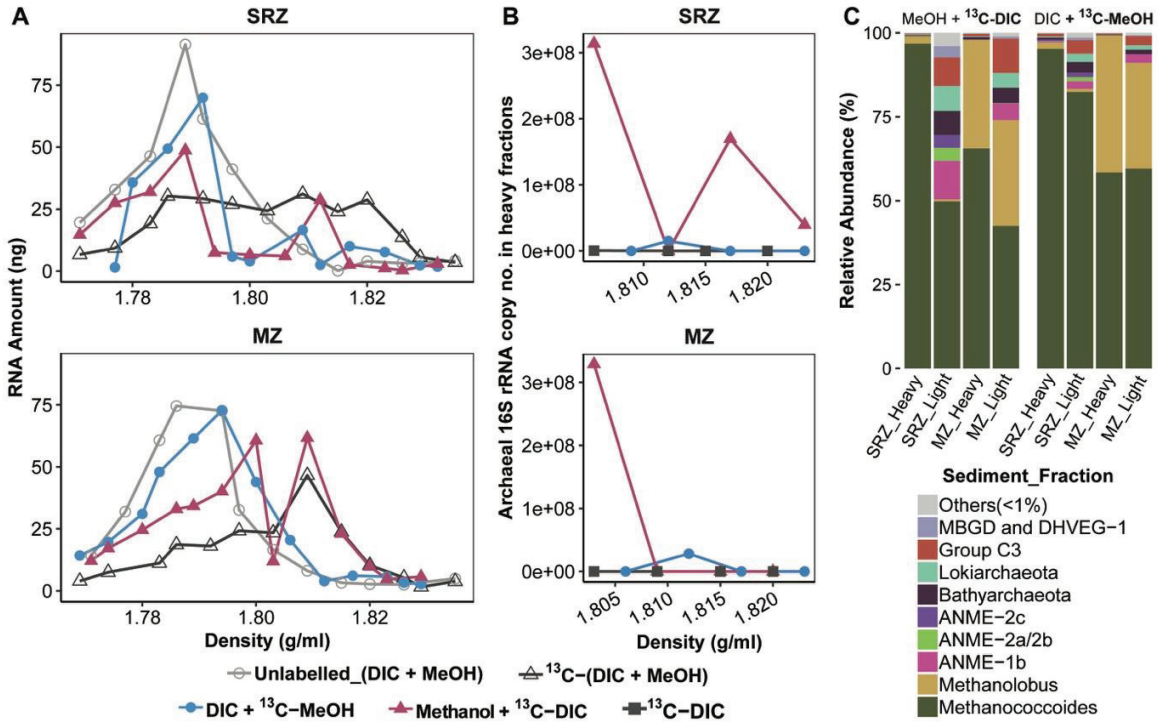

Figure 2. Density distribution of RNA, gene copy numbers, and community composition from SIP incubations with SRZ and MZ sediment after isopycnic separation. (A) RNA profiles from different RNA-SIP experiments. (B) Gene copy numbers of archaeal cDNA in heavy fractions (1.803 g mL^{-1} to 1.823 g mL^{-1}) from RNA-SIP experiments. Archaeal gene copy numbers refer to the absolute abundance of 16S rRNA gene copies in cDNA from gradient fractions. (C) Relative abundances of density separated archaeal 16S rRNA from single-labeling incubations in light (1.771 g mL^{-1} to 1.800 g mL^{-1}) and heavy (1.803 g mL^{-1} to 1.835 g mL^{-1}) gradient fractions.

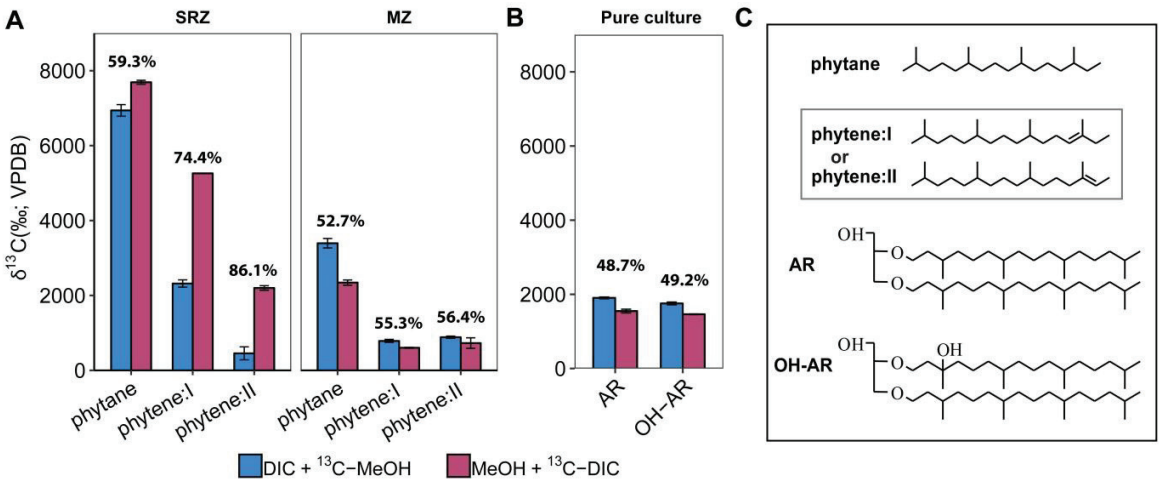

Figure 3. Lipid-SIP experiments from sediment incubations (natural community) and pure cultures in Widdel medium. Lipid $\delta^{13}C$ values were measured in homogenized samples after methanogenesis had ceased. (A) $\delta^{13}C$ values of phytanes in sediment incubations with 70% ^{13}C-DIC. Phytane originates from intact polar archaeol lipids, phytenes (phytene I and phytene (II) derive from intact polar hydroxyarchaeol lipids. $f_{DIC/lipid}$ are indicated on the top of bars from single labeling incubations based on Eq.5. (B) $\delta^{13}C$ values of archaeol (AR) and hydroxyarchaeol (AR-OH) in pure culture of *M. methylutens* treated with 5% ^{13}C-labeled substrates (methanol or DIC) (C) Structures of archaeal lipids. Enclosed structures of phytenes in Figure C were tentatively assigned according to GC-MS mass spectra (Figure S6) [80]. Data is expressed as average values (n = 3, error bar=SD).

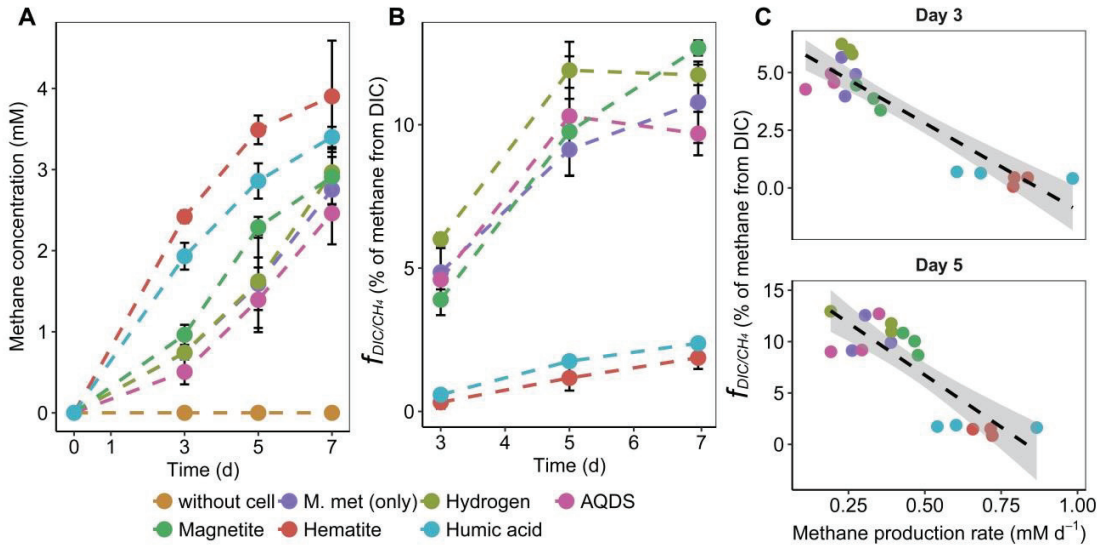

Figure 4. Methane production from DIC during methylotrophic methanogenesis in autoclave slurry supplemented with pure culture of *M. methylutens*. (A) Total methane concentrations in headspace. (B) Proportion of methane derived from DIC. Methane proportion from DIC (f_{DIC/CH_4}) was calculated according to Eq.2. Data is expressed as average values (n = 3, error bar = SD). (C) Linear correlation between methanogenesis rate and methane proportion from DIC after 3 and 5 days. Day 3: Pearson's r = -0.92, P < 0.001, CI (0.95) = -0.79 > r > -0.97; Day 5: Pearson's r = -0.85, P < 0.001, CI (0.95) = -0.62 > r > -0.94.

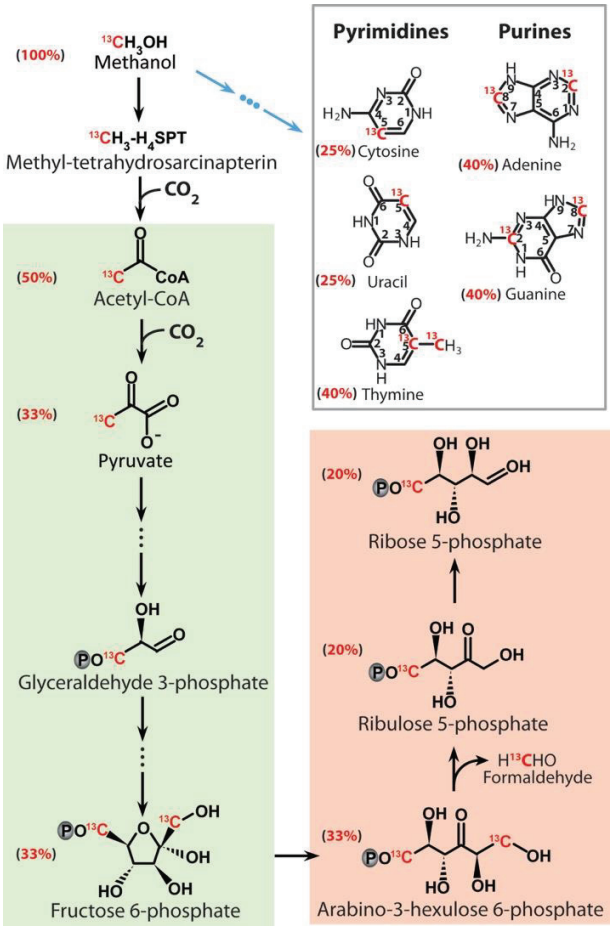

Figure 5. Biosynthesis of nucleotide moieties, the pyrimidine and purine bases, as well as the C5-carbon from ^{13}C-labelled methanol in methylotrophic methanogens based on previous studies [54-59] with final carbon contribution from methanol added besides the compounds. Black arrows indicate ribose synthesis and the blue arrows represent synthesis of base moieties in nucleosides. The reverse gluconeogenesis pathway is displayed in green and the reverse ribulose monophosphate pathway in pink.

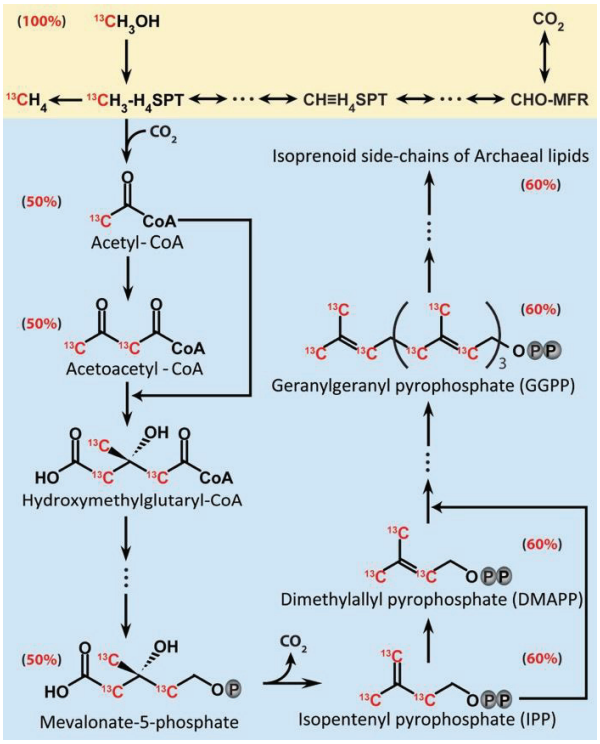

Figure 6. Methylotrophic methanogenesis pathway from methanol (yellow) and carbon assimilation pattern into isoprenoid chains of archaeal lipids (blue) with carbon contribution from ^{13}C-methanol added besides the compounds. The pathway of archaeal lipid biosynthesis is based on previous studies [69, 81, 82].

3.10. Supplementary figures

Clone library construction

A clone library of archaeal 16S rRNA gene fragments (~800 bp) was constructed to confirm the accuracy of classification by using short Illumina sequences (143 base pairs). PCR was conducted with primer set of 109F/912R (Table S1) and ALLin RPH polymerase Kit (highQu, Kraichtal, Germany) according to the protocol of the manufacturer. The template cDNA was used from the heavy fractions of RNA-SIP sample of the MZ incubations amended with ^{13}C-DIC and unlabeled methanol. Thermocycling was performed as follows: 95 °C for 3 min; 40 cycles at 95 °C for 30 sec, 58 °C for 45 sec and 72 °C for 45 sec; 72 °C for 10 min. Purified PCR products were ligated into the pGEM-T vector (Promega, Mannheim, Germany) and transformed into *Escherichia coli* JM109 competent cells (Promega, Mannheim, Germany) according to the manufacturer. White colonies were randomly picked and cell material directly subjected to colony PCR with the following cycling parameters: 95 °C for 5 min; 28 cycles at 95 °C for 30 sec, 55 °C for 45 sec and 72 °C for 1 min; 72 °C for 5 min. Amplicons of 8 clones were submitted to LGC Genomics (Berlin, Germany) for Sanger sequencing. Sequences have been deposited at GenBank with accession numbers from MK434328 to MK434335.

Table S1. Primers used in this study

Target gene	Primer	Reference
Archaeal 16S rRNA gene	806F (5'-ATTAGATACCCSBGTAGTCC-3')	[1]
Archaeal 16S rRNA gene	912R (5'-GTGCTCCCCCGCCAATTCCTTTA-3')	[2]
*mcr*A	ME2 mod (5'-TCATBGCRTAGTTNGGRTAGT-3')	[3]
*mcr*A	ME3'Fs (5'-GTCNGGTGGHGTMGGSTTYAC -3')	[4]
Archaeal 16S rRNA gene	Arch519F (5'-CAGCMGCCGCGGTAA-3')	[5]
Archaeal 16S rRNA gene	Arch806R (5'-GGACTACVSGGGTATCTAAT-3')	[6]
Archaeal 16S rRNA gene	109F (5'-ACKGCTCAGTAACACGT-3')	[7]

Table.S2 Carbon recovery of methanol from incubations amended with DIC and ^{13}C-methanol

Sediment	methane, μmol	^{13}C-TIC, μmol	Ratio of methane to CO_2	Carbon recovery, %
SRZ	27.0 ± 1.4	10.8 ± 0.7	2.5 ± 0.3	81.3 ± 1.7
MZ	28.6 ± 0.4	8.8 ± 0.3	3.2 ± 0.1	80.4 ± 0.4

^{13}C-TIC (total inorganic carbon in bottle) and ^{13}C-methane were quantified at harvest. Data is presented as average values (n = 3, error bar = SD). A total amount of 46.5 μmol ^{13}C-methanol was amended into SIP incubation.

Table S3. Comparison of fold increase of archaeal 16S rRNA gene copy number in heavy fractions between "MeOH + ^{13}C-DIC" and "DIC + ^{13}C-MeOH" incubations

Sample	Density (g/mL)	Archaeal 16S rRNA copy number	Fold increase compared to ^{13}C-MeOH incubation
MZ_ DIC+^{13}C-MeOH	1.823	9.04E+00	-
	1.817	3.05E+01	-
	1.812	2.82E+07	-
	1.806	1.59E+03	-
MZ_ MeOH+^{13}C-DIC	1.82	1.43E+01	1.59E+00
	1.815	3.67E+02	1.21E+01
	1.809	2.31E+02	8.20E-06
	1.803	3.29E+08	2.07E+05
SMZ_ DIC+^{13}C-MeOH	1.823	1.69E+02	-
	1.817	3.46E+02	-
	1.812	1.50E+07	-
	1.809	1.32E+04	-
SMZ_ MeOH+^{13}C-DIC	1.823	3.96E+07	2.35E+05
	1.817	1.70E+08	4.90E+05
	1.812	7.69E+03	5.11E-04
	1.806	3.14E+08	2.37E+04

Table S4. Relative abundance of archaeal reads above 0.01%.

taxonomy	SRZ DIC+13C-MeOH Heavy fraction	SRZ DIC+13C-MeOH Light fraction	MZ DIC+13C-MeOH Heavy fraction	MZ DIC+13C-MeOH Light fraction	SRZ MeOH+13C-DIC Heavy fraction	SRZ MeOH+13C-DIC Light fraction	MZ MeOH+13C-DIC Heavy fraction	MZ MeOH+13C-DIC Light fraction
Methanococcoides	95.2564	79.2561	58.4216	61.3458	96.7867	67.7758	65.5494	56.4008
Methanolobus	1.8769	1.1343	40.8147	36.9315	2.0298	1.6736	32.3346	36.3824
Group C3	0.8410	8.1593	0.2845	0.5795	0.2740	2.5437	0.6668	3.8382
Bathyarchaeota	0.6359	4.5811	0.1385	0.1736	0.2198	6.7875	0.7557	1.2871
ANME-2c	0.4051	0.2629	0.0075	0.0000	0.0181	3.7059	0.0178	0.0460
Lokiarchaeota	0.3385	4.6054	0.0936	0.2706	0.1897	3.0418	0.2400	0.7584
ANME-1b	0.2974	0.4576	0.0899	0.3721	0.0602	5.3995	0.0889	0.5516
ANME-2a/2b	0.1538	0.0633	0.0112	0.0135	0.2018	4.1841	0.0445	0.0230
Marine Benthic Group D and DHVEG-1	0.0154	0.1022	0.0262	0.0992	0.0843	2.0456	0.1245	0.1379
Thermoplasmatales_CCA47	0.0359	0.2629	0.0000	0.0000	0.0120	0.4251	0.0178	0.0000
Marine Hydrothermal Vent Group(MHVG)	0.0359	0.5696	0.0037	0.0113	0.0181	0.6907	0.0000	0.0689
Methanosarcina	0.0308	0.0097	0.0225	0.0316	0.0211	0.0199	0.0267	0.0230
ANME-3	0.0256	0.0195	0.0112	0.0225	0.0181	0.0731	0.0267	0.0230
Candidatus Nitrosopumilus	0.0205	0.0487	0.0112	0.0135	0.0060	0.0797	0.0178	0.0919
Unclassified Archaea	0.0103	0.0584	0.0037	0.0135	0.0030	0.0531	0.0089	0.0460
Thermoplasmatales_ANT06-05	0.0051	0.1753	0.0075	0.0068	0.0120	0.4649	0.0089	0.0000
Methanosaeta	0.0051	0.0146	0.0075	0.0248	0.0000	0.1195	0.0000	0.0919
Woesearchaeota (DHVEG-6)	0.0051	0.0682	0.0150	0.0338	0.0271	0.0930	0.0089	0.0460
Thermoplasmatales_20c-4	0.0000	0.0243	0.0000	0.0023	0.0000	0.1461	0.0000	0.0000
Archaea_AK8	0.0000	0.0049	0.0000	0.0000	0.0000	0.0066	0.0178	0.0000
Altiarchaeales	0.0000	0.0049	0.0037	0.0045	0.0000	0.0066	0.0178	0.0000
Thermoplasmatales_AMOS1A-4113-D04	0.0000	0.0097	0.0037	0.0000	0.0000	0.0332	0.0000	0.0000
Ancient Archaeal Group(AAG)	0.0000	0.0000	0.0000	0.0023	0.0030	0.0797	0.0000	0.0000
Candidatus Aenigmarchaeum	0.0000	0.0000	0.0000	0.0000	0.0000	0.0199	0.0000	0.0230
Deep Sea Euryarchaeotic Group(DSEG)	0.0000	0.0487	0.0000	0.0045	0.0120	0.1328	0.0089	0.0689
Marine Group I	0.0000	0.0000	0.0000	0.0023	0.0000	0.0000	0.0000	0.0230
Marine Group II	0.0000	0.0049	0.0037	0.0090	0.0000	0.0000	0.0089	0.0460
Thermoplasmatales_MKCST-A3	0.0000	0.0049	0.0000	0.0023	0.0000	0.0465	0.0000	0.0000
Soil Crenarchaeotic Group(SCG)	0.0000	0.0097	0.0000	0.0000	0.0030	0.0133	0.0089	0.0230
Terrestrial Miscellaneous Gp(TMEG)	0.0000	0.0292	0.0037	0.0090	0.0000	0.3121	0.0000	0.0000
Thermoplasmatales_VC2.1 Arc6	0.0000	0.0000	0.0000	0.0000	0.0000	0.0133	0.0000	0.0000
Others(<0.01%)	0.0051	0.0097	0.0150	0.0203	0.0000	0.0133	0.0000	0.0000

The gray color denotes archaea taxonomy showed in Figure 2. Pink and green colors indicate the scale of archaeal relative abundance.

Table S5. Methanogenesis from methanol and DIC in pure culture of *M. methylutens* grown in Widdel medium. Data is expressed as average values (n = 3).

Substrates	δ^{13}C-methane, (‰; VPDB)	δ^{13}C-DIC_day 0, (‰; VPDB)	δ^{13}C-DIC_day 11, (‰; VPDB)	Methane from labeled substrate, %
DIC + 5% ^{13}C-MeOH	4620 ± 160	NA	NA	97.1 ± 3.2
MeOH + 5% ^{13}C-DIC	63.8 ± 5.5	4170 ± 80	3520 ± 82.0	2.3 ± 0.1 ~ 2.6 ± 0.2

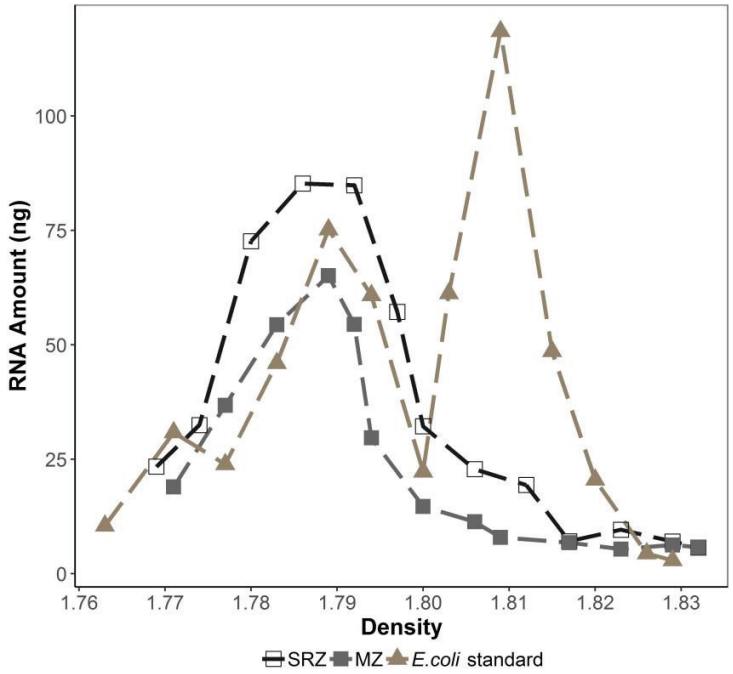

Figure S1. RNA-SIP profiles from slurry incubations amended with ^{13}C-DIC only (no methanol added) and *E.coli* standard. Samples were harvested in parallel to methanol amended incubations.

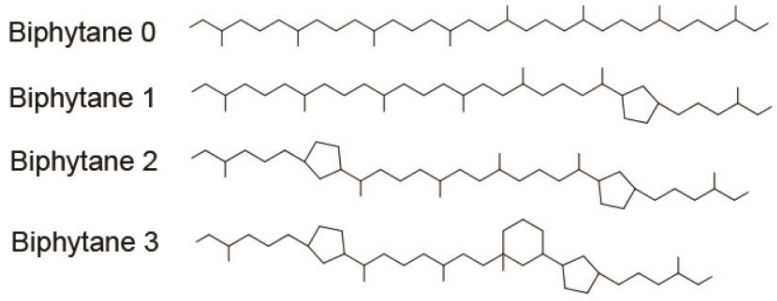

Figure S2. Structures of biphytane moieties released from the intact polar glycerol diphytanoyl glycerol tetraether fraction.

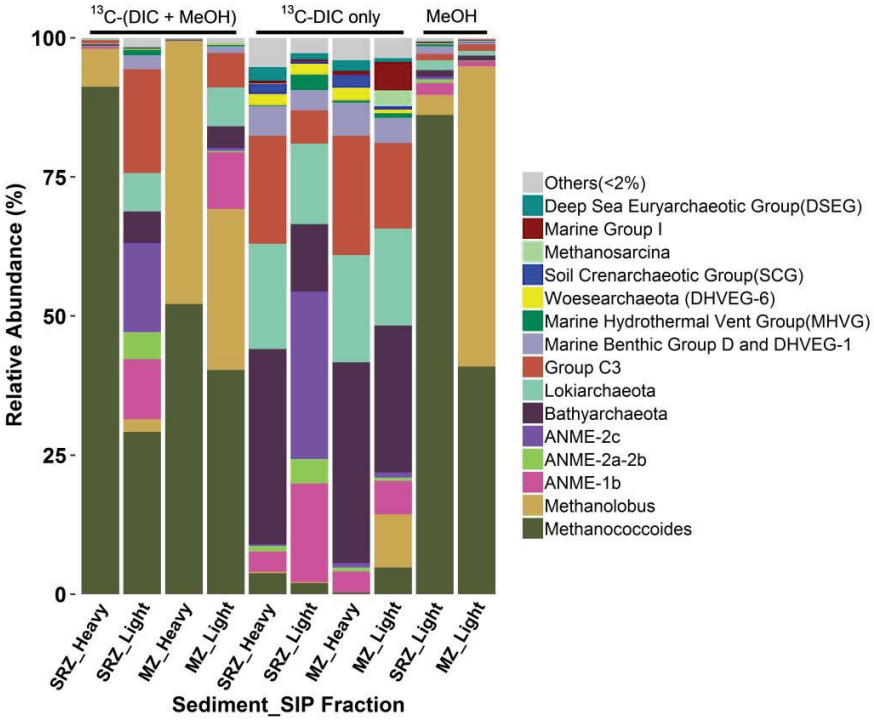

Figure S3. Relative abundance of archaeal 16S rRNA in the RNA-SIP samples from double-labeling incubations (^{13}C-DIC + ^{13}C-methanol) and control incubations (^{13}C-DIC or unlabeled-methanol). No data are shown for the unlabeled-methanol controls from the SRZ and MZ due to low amount of RNA in the heavy fraction.

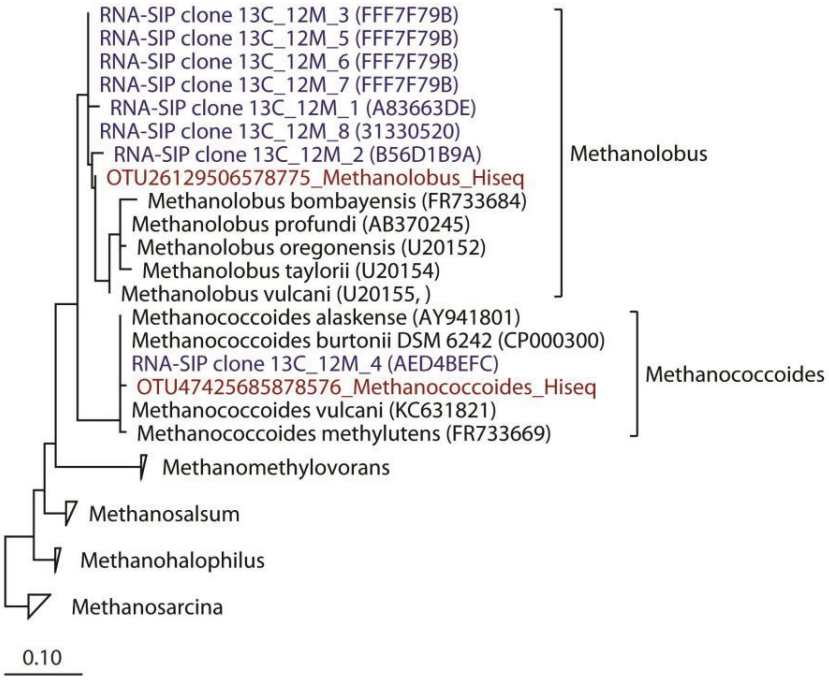

Figure S4. Phylogenetic tree of 16S rRNA genes from clone library (blue) and Illumina sequencing (red). Clone sequences were assembled by using SeqMan software (Version 8.0.2) and aligned online by Silva aligner (https://www.arb-silva.de/aligner/). The aligned sequences were input into ARB (Version 6.0.2). Aligned clone sequences and know sequences of *Methanosarcinaceae* in SILVA SSURef database (Release 132) were selected to build a phylogenetic tree using maximum likelihood algorithm and bootstrapping (n=1000). The two dominant OTUs of *Methanosarcinaceae* from Hiseq Illumina sequencing (red) were aligned and added to the tree using the ARB parismony tool.

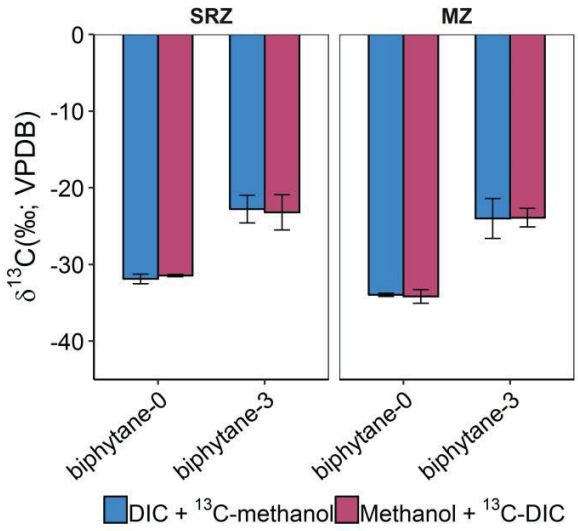

Figure S5. $\delta^{13}C$ values of biphytanes released from the intact ploar glycerol diphytanoyl glycerol tetraether fraction. Biphytane-1 and biphytane-2 concentrations were too low to be measured accurately. Determiantion of carbon isotope values was performed after methanogenesis had ceased. Data is expressed as average values (n = 3, error bar = SD).

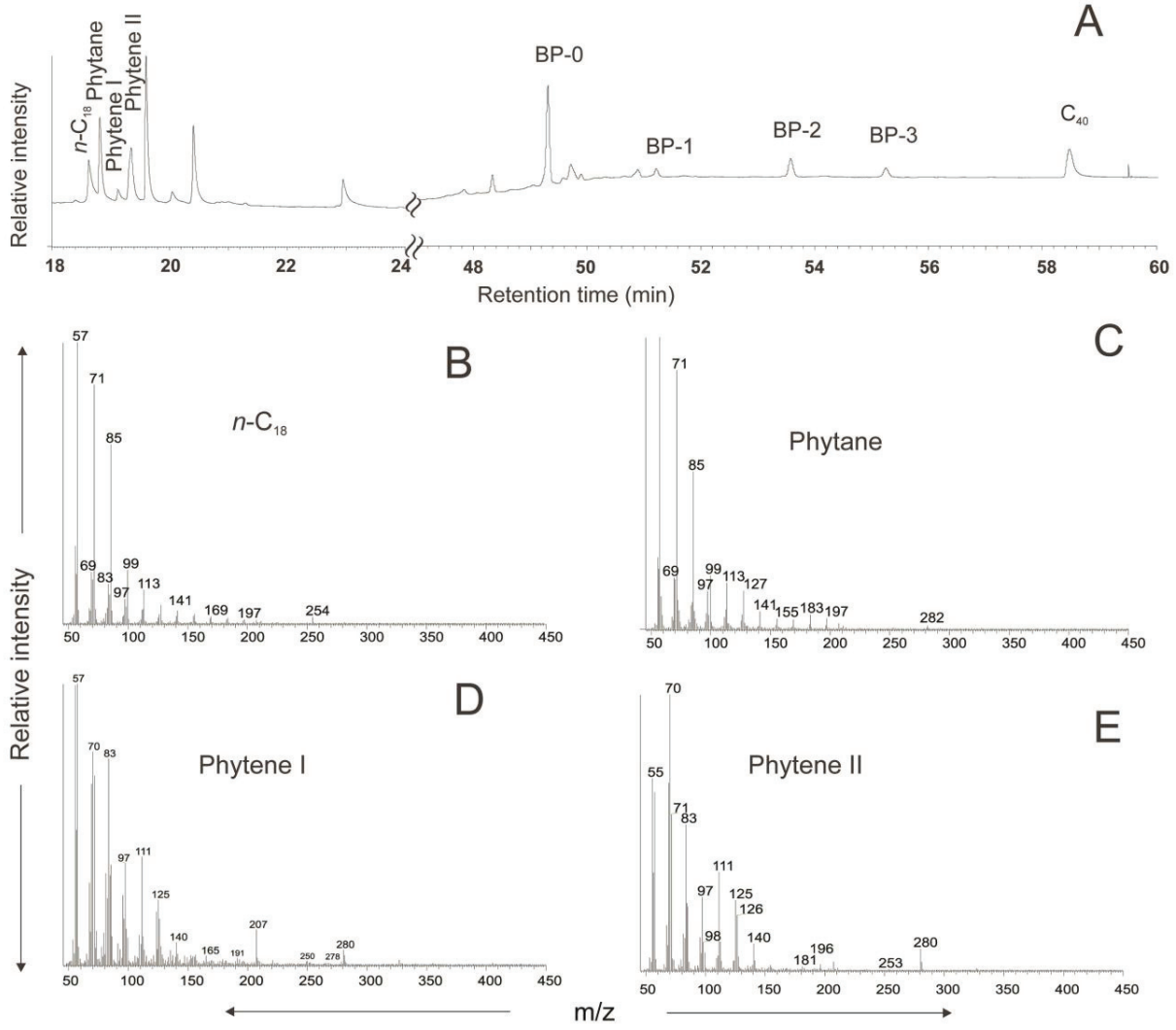

Figure S6. Chromatogram of phytane and phytenes released from intact polar lipid fraction in the incubations of the MZ sample amended with ^{13}C-DIC and unlabeld methanol (A) and the mass spectra of compunds interests (B to E).

Reference

1. Yu Y, Lee C, Kim J, Hwang S. Group-specific primer and probe sets to detect methanogenic communities using quantitative real-time polymerase chain reaction. Biotechnol Bioeng. 2005;89:670-9.

2. Lueders T, Friedrich MW. Effects of amendment with ferrihydrite and gypsum on the structure and activity of methanogenic populations in rice field soil. Appl Environ Microbiol. 2002;68:2484-94.

3. Mori K, Iino T, Suzuki K, Yamaguchi K, Kamagata Y. Aceticlastic and NaCl-requiring methanogen "*Methanosaeta pelagica*" sp. nov., isolated from marine tidal flat sediment. Appl Environ Microbiol. 2012;78:3416-23.

4. Miyazaki J, Higa R, Toki T, Ashi J, Tsunogai U, Nunoura T, et al. Molecular characterization of potential nitrogen fixation by anaerobic methane-oxidizing archaea in the methane seep sediments at the number 8 Kumano Knoll in the Kumano Basin, offshore of Japan. Appl Environ Microbiol. 2009;75:7153-62.

5. Ovreas L, Forney L, Daae FL, Torsvik V. Distribution of bacterioplankton in meromictic Lake sælenvannet, as determined by denaturing gradient gel electrophoresis of PCR-amplified gene fragments coding for 16S rRNA. Appl Environ Microbiol. 1997;63:3367-73.

6. Takai K, Horikoshi K. Rapid detection and quantification of members of the archaeal community by quantitative PCR using fluorogenic probes. Appl Environ Microbiol. 2000;66.

7. Grosskopf R, Janssen PH, Liesack W. Diversity and structure of the methanogenic community in anoxic rice paddy soil microcosms as examined by cultivation and direct 16S rRNA gene sequence retrieval. Appl Environ Microbiol. 1998;64: 960-9.

3.11. Reference

1. Ferry JG, Lessner DJ. Methanogenesis in marine sediments. Ann N Y Acad Sci. 2008;1125:147-57.

2. Thauer RK, Kaster AK, Seedorf H, Buckel W, Hedderich R. Methanogenic archaea: ecologically relevant differences in energy conservation. Nat Rev Microbiol. 2008;6(8):579-91.

3. Mayumi D, Mochimaru H, Tamaki H, Yamamoto K, Yoshioka H, Suzuki Y, et al. Methane production from coal by a single methanogen. Science. 2016;235(6309):222-5.

4. Liu Y, Whitman WB. Metabolic, phylogenetic, and ecological diversity of the methanogenic archaea. Ann N Y Acad Sci. 2008;1125:171-89.

5. Zhuang G-C, Elling FJ, Nigro LM, Samarkin V, Joye SB, Teske A, et al. Multiple evidence for methylotrophic methanogenesis as the dominant methanogenic pathway in hypersaline sediments from the Orca Basin, Gulf of Mexico. Geochim Cosmochim Acta. 2016;187:1-20.

6. Lazar CS, Parkes RJ, Cragg BA, L'Haridon S, Toffin L. Methanogenic diversity and activity in hypersaline sediments of the centre of the Napoli mud volcano, Eastern Mediterranean Sea. Environ Microbiol. 2011;13(8):2078-91.

7. Zhuang G-C, Heuer VB, Lazar CS, Goldhammer T, Wendt J, Samarkin VA, et al. Relative importance of methylotrophic methanogenesis in sediments of the Western Mediterranean Sea. Geochim Cosmochim Acta. 2018;224:171-86.

8. Maltby J, Steinle L, Löscher CR, Bange HW, Fischer MA, Schmidt M, et al. Microbial methanogenesis in the sulfate-reducing zone of sediments in the Eckernförde Bay, SW Baltic Sea. Biogeosciences. 2018;15(1):137-57.

9. Yanagawa K, Tani A, Yamamoto N, Hachikubo A, Kano A, Matsumoto R, et al. Biogeochemical cycle of methanol in anoxic deep-sea sediments. Microbes Environ. 2016;31(2):190-3.

10. Zhuang G-C, Lin Y-S, Elvert M, Heuer VB, Hinrichs K-U. Gas chromatographic analysis of methanol and ethanol in marine sediment pore waters: Validation and implementation of three pretreatment techniques. Mar Chem. 2014;160:82-90.

11. Oremland RS, Polcin S. Methanogenesis and sulfate reduction: competitive and noncompetitive substrates in estuarine sediments. Appl Environ Microbiol. 1982;44(6):1270-6.

12. Florencio L, Field JA, Lettinga G. Importance of cobalt for individual trophic groups in an anaerobic methanol-degrading consortium. Appl Environ Microbiol. 1994;60(1):227-34.

13. Balch WE, Schoberth S, Tanner RS, Wolfe RS. *Acetobacterium*, a new genus of hydrogen-oxidizing, carbon dioxide-reducing, anaerobic bacteria. Int J Syst Evol Microbiol. 1977;27(4):355-61.

14. Lever MA. Acetogenesis in the energy-starved deep biosphere - a paradox? Front Microbiol. 2012;2:284.

15. Oni O, Miyatake T, Kasten S, Richter-Heitmann T, Fischer D, Wagenknecht L, et al. Distinct microbial populations are tightly linked to the profile of dissolved iron in the methanic sediments of the Helgoland mud area, North Sea. Front Microbiol. 2015;6:365.

16. Evans PN, Parks DH, Chadwick GL, Robbins SJ, Orphan VJ, Golding SD, et al. Methane metabolism in the archaeal phylum Bathyarchaeota revealed by genome-centric metagenomics. Science. 2015;350(6259):432-8.

17. Weimer PJ, Zeikus JG. Acetate metabolism in *Methanosarcina barkeri*. Arch Microbiol. 1978;119:175-82.

18. Summons RE, Franzmann PD, Nichols PD. Carbon isotopic fractionation associated with methylotrophic methanogenesis. Org Geochem. 1998;28(7-8):465-75.

19. Hippe H, Caspari D, Fiebig K, Gottschalk G. Utilization of trimethylamine and other N-methyl compounds for growth and methane formation by *Methanosarcina barkeri*. Proc Natl Acad Sci USA. 1979;76(1):494-8.

20. Teeling H, Glockner FO. Current opportunities and challenges in microbial metagenome analysis—a bioinformatic perspective. Brief Bioinform. 2012;13(6):728-42.

21. Singer E, Wagner M, Woyke T. Capturing the genetic makeup of the active microbiome in situ. ISME J. 2017;11(9):1949-63.

22. Neelakanta G, Sultana H. The use of metagenomic approaches to analyze changes in microbial communities. Microbiol Insights. 2013;6:37-48.

23. Thauer RK. Anaerobic oxidation of methane with sulfate: on the reversibility of the reactions that are catalyzed by enzymes also involved in methanogenesis from CO_2. Curr Opin Microbiol. 2011;14(3):292-9.

24. Feijo Delgado F, Cermak N, Hecht VC, Son S, Li Y, Knudsen SM, et al. Intracellular water exchange for measuring the dry mass, water mass and changes in chemical composition of living cells. PLoS One. 2013;8(7):e67590.

25. Friedrich MW. Stable-isotope probing of DNA: insights into the function of uncultivated microorganisms from isotopically labeled metagenomes. Curr Opin Biotechnol. 2006;17(1):59-66.

26. Lueders T. Stable isotope probing of hydrocarbon-degraders. Handbook of Hydrocarbon and Lipid Microbiology2010. p. 4011-26.

27. Grob C, Taubert M, Howat AM, Burns OJ, Dixon JL, Richnow HH, et al. Combining metagenomics with metaproteomics and stable isotope probing reveals metabolic pathways used by a naturally occurring marine methylotroph. Environ Microbiol. 2015;17(10):4007-18.

28. Fortunato CS, Huber JA. Coupled RNA-SIP and metatranscriptomics of active chemolithoautotrophic communities at a deep-sea hydrothermal vent. ISME J. 2016;10(8):1925-38.

29. Manefield M, Whiteley AS, Ostle N, Ineson P, Bailey MJ. Technical considerations for RNA-based stable isotope probing an approach to associating microbial diversity with microbial community function. Rapid Commun Mass Spectrom. 2002;16:2179-83.

30. Vandieken V, Thamdrup B. Identification of acetate-oxidizing bacteria in a coastal marine surface sediment by RNA-stable isotope probing in anoxic slurries and intact cores. FEMS Microbiol Ecol. 2013;84(2):373-86.

31. Lueders T, Wagner B, Claus P, Friedrich MW. Stable isotope probing of rRNA and DNA reveals a dynamic methylotroph community and trophic interactions with fungi and protozoa in oxic rice field soil. Environ Microbiol. 2003;6(1):60-72.

32. Neufeld JD, Schafer H, Cox MJ, Boden R, McDonald IR, Murrell JC. Stable-isotope probing implicates *Methylophaga* spp and novel *Gammaproteobacteria* in marine methanol and methylamine metabolism. ISME J. 2007;1(6):480-91.

33. Weimer PJ, Zeikus JG. One carbon metabolism in methanogenic bacteria. Arch Microbiol. 1978;119:47-57.

34. Wegener G, Kellermann MY, Elvert M. Tracking activity and function of microorganisms by stable isotope probing of membrane lipids. Curr Opin Biotechnol. 2016;41:43-52.

35. Boschker HTS, Nold SC, Wellsbury P, Bos D, de Graaf W, Pel R, et al. Direct linking of microbial populations to specific biogeochemical processes by ^{13}C-labelling of biomarkers. Nature. 1998;392:801-5.

36. Reyes C, Schneider D, Thürmer A, Kulkarni A, Lipka M, Sztejrenszus SY, et al. Potentially active iron, sulfur, and sulfate reducing bacteria in skagerrak and bothnian bay sediments. Geomicrobiol J. 2017:1-11.

37. Widdel F, Pfennig N. Studies on dissimilatory sulfate-reducing bacteria that decompose fatty acids I. Isolation of new sulfate-reducing bacteria enriched with acetate from saline environments. Description of *Desulfobacter postgatei* gen. nov., sp. nov. Arch Microbiol. 1981;134(4):282-5.

38. Widdel F, Kohring GW, Mayer F. Studies on dissimilatory sulfate-reducing bacteria that decompose fatty acids III. Characterization of the filamentous gliding *Desulfonema limicola* gen. nov. sp. nov., and *Desulfonema magnum* sp. nov. Arch Microbiol. 1983;134:286-94.

39. Aromokeye DA, Richter-Heitmann T, Oni OE, Kulkarni A, Yin X, Kasten S, et al. Temperature controls crystalline iron oxide utilization by microbial communities in methanic ferruginous marine sediment incubations. Front Microbiol. 2018;9:2574.

40. Ertefai TF, Heuer VB, Prieto-Mollar X, Vogt C, Sylva SP, Seewald J, et al. The biogeochemistry of sorbed methane in marine sediments. Geochim Cosmochim Acta. 2010;74(21):6033-48.

41. Lueders T, Manefield M, Friedrich MW. Enhanced sensitivity of DNA- and rRNA-based stable isotope probing by fractionation and quantitative analysis of isopycnic centrifugation gradients. Environ Microbiol. 2004;6(1):73-8.

42. Friedrich MW. Methyl-coenzyme M reductase genes: unique functional markers for methanogenic and anaerobic methane-oxidizing Archaea. Methods Enzymol. 2005;397:428-42.

43. Sturt HF, Summons RE, Smith K, Elvert M, Hinrichs KU. Intact polar membrane lipids in prokaryotes and sediments deciphered by high-performance liquid chromatography/electrospray ionization multistage mass spectrometry--new biomarkers for biogeochemistry and microbial ecology. Rapid Commun Mass Spectrom. 2004;18(6):617-28.

44. Zhu C, Lipp JS, Wörmer L, Becker KW, Schröder J, Hinrichs K-U. Comprehensive glycerol ether lipid fingerprints through a novel reversed phase liquid chromatography–mass spectrometry protocol. Org Geochem. 2013;65:53-62.

45. Liu X-L, Lipp JS, Simpson JH, Lin Y-S, Summons RE, Hinrichs K-U. Mono- and dihydroxyl glycerol dibiphytanyl glycerol tetraethers in marine sediments: Identification of both core and intact polar lipid forms. Geochim Cosmochim Acta. 2012;89:102-15.

46. Kellermann MY, Yoshinaga MY, Wegener G, Krukenberg V, Hinrichs K-U. Tracing the production and fate of individual archaeal intact polar lipids using stable isotope probing. Org Geochem. 2016;95:13-20.

47. Boschker HTS, Middelburg JJ. Stable isotopes and biomarkers in microbial ecology. FEMS Microbiol Ecol. 2002;40:85–95.

48. Kato S, Hashimoto K, Watanabe K. Methanogenesis facilitated by electric syntrophy via (semi)conductive iron-oxide minerals. Environ Microbiol. 2012;14(7):1646-54.

49. Kato S, Nakamura R, Kai F, Watanabe K, Hashimoto K. Respiratory interactions of soil bacteria with (semi)conductive iron-oxide minerals. Environ Microbiol. 2010;12(12):3114-23.

50. Bond DR, Lovley DR. Reduction of Fe(III) oxide by methanogens in the presence and absence of extracellular quinones. Environ Microbiol. 2002;4(2):115–24.

51. Lovley DR, Fraga JL, Coates JD, L. B-HE. Humics as an electron donor for anaerobic respiration. Environ Microbiol. 1999;1(1):89-99.

52. Borrel G, Harris HM, Tottey W, Mihajlovski A, Parisot N, Peyretaillade E, et al. Genome sequence of "*Candidatus Methanomethylophilus alvus*" Mx1201, a methanogenic archaeon from the human gut belonging to a seventh order of methanogens. J Bacteriol. 2012;194(24):6944-5.

53. Borrel G, O'Toole PW, Harris HM, Peyret P, Brugere JF, Gribaldo S. Phylogenomic data support a seventh order of methylotrophic methanogens and provide insights into the evolution of Methanogenesis. Genome Biol Evol. 2013;5(10):1769-80.

54. Choquet CG, Richards JC, Patel GB, Sprott GD. Ribose biosynthesis in methanogenic bacteria. Arch Microbiol. 1994a;161:481-8.

55. Choquet CG, Richards JC, Patel GB, Sprott GD. Purine and pyrimidine biosynthesis in methanogenic bacteria. Arch Microbiol. 1994b;161:471-80.

56. Ekiel I, Smith ICP, Sportt GD. Biosynthetic pathways in *Methanospirillum hungatei* as determined by ^{13}C nuclear magnetic resonance. J Bacteriol. 1983;156(1):316-26.

57. Nyce GW, White RH. dTMP biosynthesis in archaea. J Bacteriol. 1996 178(3):914–6.

58. Soderberg T. Biosynthesis of ribose-5-phosphate and erythrose-4-phosphate in archaea: a phylogenetic analysis of archaeal genomes. Archaea. 2005;1:347-52.

59. Sorokin DY, Makarova KS, Abbas B, Ferrer M, Golyshin PN, Galinski EA, et al. Discovery of extremely halophilic, methyl-reducing euryarchaea provides insights into the evolutionary origin of methanogenesis. Nat Microbiol. 2017;2:17081.

60. Aoyagi T, Morishita F, Sugiyama Y, Ichikawa D, Mayumi D, Kikuchi Y, et al. Identification of active and taxonomically diverse 1,4-dioxane degraders in a full-scale activated sludge system by high-sensitivity stable isotope probing. ISME J. 2018;12(10):2376-88.

61. Wegener G, Niemann H, Elvert M, Hinrichs KU, Boetius A. Assimilation of methane and inorganic carbon by microbial communities mediating the anaerobic oxidation of methane. Environ Microbiol. 2008;10(9):2287-98.

62. Nishihara M, Koga Y. Hydroxyarchaetidylserine and hydroxyarchaetidyl-myo-inositol in *Methanosarcina barkeri*: polar lipids with a new ether core portion. Biochim Biophys Acta. 1991;1082:211-7.

63. Nishihara M, Utagawa M, Akutsu H, Koga Y. Archaea contain a novel diether phosphoglycolipid with a polar head group identical to the conserved core of eucaryal glycosyl phosphatidylinosito. J Biol Chem. 1992;267:12432-5.

64. Pancost RD, McClymont EL, Bingham EM, Roberts Z, Charman DJ, Hornibrook ERC, et al. Archaeol as a methanogen biomarker in ombrotrophic bogs. Org Geochem. 2011;42(10):1279-87.

65. Elling FJ, Könneke M, Lipp JS, Becker KW, Gagen EJ, Hinrichs K-U. Effects of growth phase on the membrane lipid composition of the thaumarchaeon *Nitrosopumilus maritimus* and their implications for archaeal lipid distributions in the marine environment. Geochim Cosmochim Acta. 2014;141:579-97.

66. Blumenberg M, Seifert R, Reitner J, Pape T, Michaelis W. Membrane lipid patterns typify distinct anaerobic methanotrophic consortia. Proc Natl Acad Sci USA. 2004;101(30):11111–6.

67. Rossel PE, Lipp JS, Fredricks HF, Arnds J, Boetius A, Elvert M, et al. Intact polar lipids of anaerobic methanotrophic archaea and associated bacteria. Org Geochem. 2008;39(8):992-9.

68. Yu T, Wu W, Liang W, Lever MA, Hinrichs KU, Wang F. Growth of sedimentary Bathyarchaeota on lignin as an energy source. Proc Natl Acad Sci U S A. 2018;115(23):6022-7.

69. Allen MA, Lauro FM, Williams TJ, Burg D, Siddiqui KS, De Francisci D, et al. The genome sequence of the psychrophilic archaeon, *Methanococcoides burtonii*: the role of genome evolution in cold adaptation. ISME J. 2009;3(9):1012-35.

70. Grochowski LL, Xu H, White RH. *Methanocaldococcus jannaschii* uses a modified mevalonate pathway for biosynthesis of isopentenyl diphosphate. J Bacteriol. 2006;188(9):3192-8.

71. Nichols DS, Miller MR, Davies NW, Goodchild A, Raftery M, Cavicchioli R. Cold adaptation in the Antarctic archaeon *Methanococcoides burtonii* involves membrane lipid unsaturation. J Bacteriol. 2004;186(24):8508-15.

72. Thauer RK, Kaster AK, Goenrich M, Schick M, Hiromoto T, Shima S. Hydrogenases from methanogenic archaea, nickel, a novel cofactor, and H_2 storage. Annu Rev Biochem. 2010;79:507-36.

73. Lovley DR. Happy together: microbial communities that hook up to swap electrons. ISME J. 2017;11(2):327-36.

74. Rotaru AE, Shrestha PM, Liu F, Markovaite B, Chen S, Nevin KP, et al. Direct interspecies electron transfer between Geobacter metallireducens and *Methanosarcina barkeri*. Appl Environ Microbiol. 2014;80(15):4599-605.

75. Rotaru A-E, Shrestha PM, Liu F, Shrestha M, Shrestha D, Embree M, et al. A new model for electron flow during anaerobic digestion: direct interspecies electron transfer to *Methanosaeta* for the reduction of carbon dioxide to methane. Energy Environ Sci. 2014;7(1):408-15.

76. Wang LY, Nevin KP, Woodard TL, Mu BZ, Lovley DR. Expanding the diet for DIET: electron donors supporting direct interspecies electron transfer (DIET) in defined co-cultures. Front Microbiol. 2016;7:236.

77. Guan Y, Ngugi D, Blom J, Ali S, Ferry, JG., Stingl U. Draft genome sequence of an obligately methylotrophic methanogen, *Methanococcoides methylutens*, isolated from marine sediment. Genome Announc. 2014;2(6):e01184-14.

78. Kellermann MY, Wegener G, Elvert M, Yoshinaga MY, Lin YS, Holler T, et al. Autotrophy as a predominant mode of carbon fixation in anaerobic methane-oxidizing microbial communities. Proc Natl Acad Sci U S A. 2012;109(47):19321-6.

79. Weiss MC, Sousa FL, Mrnjavac N, Neukirchen S, Roettger M, Nelson-Sathi S, et al. The physiology and habitat of the last universal common ancestor. Nat Microbiol. 2016;1(9):16116.

80. Qin S, Sun Y, Tang Y. Early hydrocarbon generation of algae and influences of inorganic environments during low temperature simulation. Energ Explor Exploit. 2008;26(6):377-96.

81. Koga Y, Morii H. Biosynthesis of ether-type polar lipids in archaea and evolutionary considerations. Microbiol Mol Biol Rev. 2007;71(1):97-120.

82. Ekiel I, Sportt GD, Patel GB. Acetate and CO_2 assimilation by *Methanothrix concilii*. J Bacteriol. 1985;162(3):905-8.

Chapter 4

Asgard archaea are active in marine sediment carbon cycling

Mingwei Cai[1,2,#], Xiuran Yin[3,4,5,#], Yang Liu[1,#], Zhichao Zhou[1,6], Xiaowen Wang[1,2], Wenjin Li[1], Ajinkya Kulkarni[3,4,5], Tim Richter-Heitmann[3], Jie Pan[1], Yuchun Yang[6], Ji-Dong Gu[6], Michael W. Friedrich[3,4,*], and Meng Li[1,*]

[1] Institute for Advanced Study, Shenzhen University, Shenzhen, China

[2] Key Laboratory of Optoelectronic Devices and Systems of Ministry of Education and Guangdong Province, College of Optoelectronic Engineering, Shenzhen University, Shenzhen, China

[3] Microbial Ecophysiology Group, Faculty of Biology/Chemistry, University of Bremen, Bremen, Germany

[4] MARUM, Center for Marine Environmental Sciences, University of Bremen, Bremen, Germany

[5] International Max Planck Research School for Marine Microbiology, Max-Planck-Institute for Marine Microbiology, Bremen, Germany

[6] Laboratory of Environmental Microbiology and Toxicology, School of Biological Sciences, The University of Hong Kong, Pokfulam Road, Hong Kong SAR, China

(In preparation for Science Advances)

Contribution to the manuscript:

Experimental concept and design	33%
Acquisition of experimental data	33%
Data analysis and interpretation	33%
Preparation of figures and tables	33%
Drafting of manuscript	33%

[*]**CORRESPONDENT:**

Meng Li, Room 360, Administration Building, Institute for Advanced Study, Shenzhen University, Shenzhen, China; E-mail: limeng848@szu.edu.cn; Tel: +86-755-26979250

Michael W. Friedrich, Faculty 02 (Chemistry/Biology) & MARUM, University of Bremen, Leobener Straße 3, D-28359, Bremen, Germany; E-mail: michael.friedrich@uni-bremen.de; Tel: +49-421-218-63060

[#] These authors contributed equally to this work.

Abstract

Asgard is an archaeal superphylum that might hold the key to understand the origin of eukaryotes, but its diversity and ecological role remains poorly understood. Here, we propose five new Asgard phyla, including Kariarchaeota, Balderarchaeota, Hodarchaeota, Lagarchaeota and Gerdarchaeota, based on the 16S rRNA genes phylogenetic analysis. Stable-isotope probing (SIP) revealed that Lokiarchaeota actively fix CO_2 and are associated with organic polymers degradation. Supporting the nucleic acid-SIP results, genomics and transcriptomics further evidence that Asgard archaea are active in the metabolism of fatty acids, alcohol, amino acids, proteins, peptides, benzoate and cellulose. Intriguingly, our analyses indicate that the new phylum Gerdarchaeota might utilize organic substrates by aerobic respiration, the Helarchaeota are capable of short-chain alkane oxidation, and Loki- and Thorarchaeota even have potential for medium-chain alkane degradation. Our findings substantially expand the known global diversity of Asgard archaea, and link their metabolic potentials and activities to their extended role in global carbon cycling.

4.1. Introduction

The domain of Archaea constitutes a considerable fraction of the biomass on Earth[1] and have been estimated to account for ~37% of the total microbial cells in the marine biosphere, especially in coastal sediments (up to 69%)[2]. Meanwhile, archaea have been recognized as key players in the global carbon cycle[3], participating in CO_2 fixation and multiple carbon dissimilation pathways such as methanogenesis[4] and the degradation of proteins, carbohydrates, methylated compounds, fatty acids and lipids[5, 6]. Nevertheless, the metabolic, physiological, and evolutionary functions of archaea remain largely unknown, especially for many of the newly discovered archaeal groups in recent years, such as DPANN[7], Bathyarchaeota[8], Verstraetearchaeota[9], and Asgard archaea[10].

Asgard archaea, proposed as the latest archaeal superphylum, are composed Lokiarchaeota[11], Thorarchaeota[12], Odinarchaeota[10], Heimdallarchaeota[10], and Helarchaeota[13], mainly originated from lineages formerly named Marine Benthic Group B (MBG-B)[14], Deep-Sea Archaeal Group (DSAG)[15], Ancient Archaeal Group (AAG) [16], and Marine Hydrothermal Vent Group (MHVG)[16, 17]. Since Asgard archaea contain abundant eukaryotic signature proteins (ESPs) and form a monophyletic group with eukaryotes in the phylogenetic tree, they are regarded as the closest relatives of Eukarya and have attracted increasing research interest[10, 11, 18]. Asgard archaea inhabit various environments (e.g., marine waters and sediment, lake sediment, mangrove sediment, estuarine sediment and mud volcano)[10, 19, 20]. The Asgard-associated rRNA recently identified in natural environments[20] suggests that they might be more diverse than previously known. Based on metagenome analyses, Lokiarchaeota potentially perform hydrogen oxidation[21], Thorarchaeota might be mixotrophic (i.e., using both, inorganic and organic carbon for growth)[19] and acetogenic[12], Heimdallarchaeota harbour novel mechanisms of phototrophy[22, 23], and Helarchaeota might be capable of anaerobic hydrocarbon oxidation[13]. However, knowledge about their metabolic capabilities, activities and ecological roles[10, 12] is still in its infancy due to the shortage of available Asgard archaea genomes[10, 19, 24-26], the lack of cultured representatives, and the limited molecular and physiological data (e.g., metatranscriptomic or stable isotope probing (SIP) analysis).

In the current study, we first investigated Asgard archaea based on all publicly available 16S rRNA gene sequences and expanded the known diversity and global distribution of Asgard archaea. Second, by using nucleic acid-SIP, we successfully revealed metabolic activities of Asgard archaea. Third, we explored the potential metabolic capabilities of Asgard archaea through metagenomics and metatranscriptomics, especially for the new phyla Gerdarchaeota and Helarchaeota. These findings substantially extend our knowledge of the metabolic capabilities and *in situ* activities of Asgard archaea.

4.2. Results and discussion

4.2.1. Asgard archaea are diverse and ubiquitous

To study the diversity of Asgard archaea, 16S rRNA gene sequences (> 600 bp) from all Asgard metagenome-assembled genomes (MAGs, December 2018 updated) and public databases (SILVA SSU 132 and NCBI databases, December 2018 updated), including a recent study of 16S rRNA gene sequences[20], were systematically analysed. After sequence filtering, we obtained >400 Asgard archaeal operational taxonomic units (OTUs, 95% cut-off, 10,448 sequences). The majority of OTUs (79%) and sequences (85%) fell into the Lokiarchaeota lineage (Fig. 1A and Table S2). The phylogenetically broad Lokiarchaeota group with a minimum intragroup similarity of 80% (Table S2) was divided into four subgroups (Lokiarchaeota-1 to Lokiarchaeota-4) based on tree nodes with high bootstrap support (Fig. 1A). Lokiarchaeota-2 and Lokiarchaeota-4 were the most abundant subgroups, accounting for 19% and 59% of the total Asgard 16S rRNA gene sequences, respectively. With a lower minimum intragroup similarity (71%, Table S2) than the recommended phylum-level threshold[27], we divided the lineage of Heimdallarchaeota into two subgroups: Heimdallarchaeota-AAG and Heimdallarchaeota-MHVG, following previous studies[10, 28]. Based on the threshold of 75-83% intragroup similarity of 16S rRNA genes for the phylum level[27], we identified five new Asgard phyla and proposed their names as Kariarchaeota, Balderarchaeota, Hodarchaeota, Lagarchaeota and Gerdarchaeota, respectively (Fig. 1A and Table S3). Most sequences (99.7%) of these new phyla were from expressed 16S rRNA genes[20], indicating that the Asgard archaea are transcriptionally active and more diverse than previously proposed[10].

A high proportion (~92%) of the OTUs of Asgard 16S rRNA gene sequences originated from sediment samples, especially from offshore and coastal sediments (Fig. 1 and Table S1). Besides, Asgard archaea inhabit other environments such as marine water columns, mud volcanos and soil. The global distribution of Asgard archaea appears to follow a biogeographical organization. For example, unique OTUs from hydrothermal environments placed within the Odinarchaeota and several distinct Lokiarchaeota subgroups, while sequences collected from hypersaline habitats (e.g., hypersaline microbial mat and salt-works belt) clustered within the Lokiarchaeota-4 subgroup (Fig. 1A).

4.2.2. Asgard archaea fix CO_2 and degrade organic polymers based on stable isotope probing

The carbon metabolism in Asgard archaea was investigated by RNA- and DNA-SIP in sediment samples from the Helgoland Mud Area (North Sea) by amending ^{13}C-labelled bicarbonate in combination with different electron donors and/or electron acceptors. Due to the general slowness of metabolic processes at 10 °C under energy and carbon pool limitations, we opted for long-term incubations conducted for 255 and 386 days for RNA- and DNA-SIP, respectively.

By applying RNA-SIP, an ultra-high-sensitivity technique with a detection threshold of ≤0.001% of labelled RNA[29], we identified the active members of subgroups Lokiarchaeota-2 and Lokiarchaeota-4 in incubations fed with ^{13}C-labelled bicarbonate and additional electron donors (Figs. 1A, 2A, and S1C). Specifically, the high relative abundance of the Lokiarchaeota-2 subgroup OTUs in ^{13}C-labelled RNA-SIP fractions (>1.80 g/mL) indicated their involvement in the metabolism of elemental sulfur and iron oxide (lepidocrocite) (Figs. 2, S1C, and S1D), although a MAG could not be obtained (Fig. 4). OTUs within subgroup Lokiarchaeota-2 were also associated with the degradation of cellulose (or intermediates) (Figs. 2A and S1C), potentially involving sugar fermentation and acetogenesis as suggested by metagenomic and metatranscriptomic analysis (Fig. 4). OTUs within subgroup Lokiarchaeota-4 were stimulated in the presence of organic polymers (lignin and humic acid, Figs. 2, S1), which was corroborated by a significant increase ($p < 0.05$) in Lokiarchaeota 16S rRNA gene copy numbers (Fig. S1B). More specifically, Lokiarchaeota-4_OTU1 strongly incorporated $^{13}CO_2$ in the presence of lignin (25-50% of all archaeal sequences in fractions >1.80 g/ml, Figs. 2A and S1C), whereas Lokiarchaeota-4_OTU2 incorporated less of the label (in fractions >1.79 g/mL, Figs. 2A and S1C) but made up ~50% of all archaeal sequences. The SIP results revealed highly varied activities of Lokiarchaeota in sulfur metabolism, CO_2 assimilation and organic polymer degradation. The ability to utilize inorganic and recalcitrant carbon, such as lignin and humic acids, reflects a capability for mixotrophic growth in Lokiarchaeota subgroups.

4.2.3. Potential metabolic capabilities of Asgard archaea revealed by metagenomics and metatranscriptomics

To gain in-depth insight into the detailed metabolic capabilities and biological functions of Asgard archaea, especially for the new phyla, we collected isotopically heavy DNA fractions from SIP-incubations and coastal sediments for deep sequencing analysis (totally 2.2 Tbp, Table S4). We recovered

14 high-quality Asgard MAGs with completeness >75% (Table S5). As demonstrated by multi-locus phylogenetic analysis (Fig. 3), 16S rRNA phylogeny (Fig. 1A) and a pan-genome based gene clustering (Fig. S2), we classified six Asgard MAGs as the new Asgard phylum Gerdarchaeota (42-50% AAI to other Asgard MAGs, Fig. S3), one as Helarchaeota (43-47% AAI to other Asgard MAGs, Fig. S3), three as Lokiarchaeota-4, three as Thorarchaeota, and two as Heimdallarchaeota-MHVG, respectively.

All available Asgard MAGs (Table S5, except Odinarchaeota, December 2018 updated) were annotated against databases for function prediction, and the key metabolic pathways were reconstructed to investigate their metabolic capability in combination with the metatranscriptomic data (Fig. 4 and Table S6). Corresponding to the nucleic acid-SIP revealed the active CO_2 fixation in Lokiarchaeota, genes for tetrahydromethanopterin dependent Wood-Ljungdahl (THMPT-WL) and tetrahydrofolate dependent WL (THF-WL) pathways were identified in Lokiarchaeotal MAGs (Fig. 4). Similar with Lokiarchaeota, Thorarchaeotal MAGs also contain genes for both THMPT-WL and THF-WL pathways, however, transcripts for the THMPT-dependent WL pathway in Lokiarchaeota and Thorarchaeota were predominant, especially those for incorporating CO_2 into formyl-methanofuran (Fig. 4). Furthermore, in Lokiarchaeota and other Asgard phyla, the abundant transcripts for the generation of pyruvate from acetyl-CoA and CO_2 elevated the contribution of inorganic carbon to biomass[30]. Additionally, genomic and transcriptomic evidence suggest that Lokiarchaeota and most Asgard phyla have carbon fixation potential via the incomplete rTCA cycle, and the nucleotide salvage pathway using the type III or IV ribulose 1,5-bisphosphate carboxylase (RuBisCO) (Fig. S4)[19, 26, 31, 32]. The ability to perform inorganic carbon assimilation suggests that Asgard archaea are adaptive to various environments, especially in deep marine sediments where the energy supply is extremely low[33] but inorganic carbon is sufficient[34]. We also identified genes involved in degradation of multi-sugar, cellulose, polymeric sugar, and the complete gene sets for benzoate degradation (Fig. 4 and Table S6), which strengthened the observation of active Lokiarchaeota in SIP incubations amended with various organic substrates (Fig. 2A). The presence and the high expression levels of genes involved in acetate, ethanol, 1-alcohol, amino acids, proteins and/or peptides degradation suggest that these compounds are also carbon or energy sources for Lokiarchaeota and other Asgard phyla.

For the new phylum Gerdarchaeota proposed in this study, the near-complete gene sets for only THMPT-WL pathway were identified with detectable transcripts in coastal sediments (Fig. 4), which reveals that members of this new Asgard archaeal phylum may use tetrahydromethanopterin as the single C_1 carrier. The results indicate that Gerdarchaeota are quite different to their neighbourhood Heimdallarchaeota-AAG and Heimdallarchaeota_MHVG (Figs. 3 and S5), which only encode the THF-WL pathway. In

addition, Gerdarchaeota appear to use organic compounds as electron donors (Fig. 4 and Table S6), and the dominant carbohydrate-active enzymes and peptidases were glycosyltransferases and serine peptidases (Fig. S6 and Table S7). Intriguingly, Gerdarchaeota harbour genes encoding cytochrome c oxidase, nitrate reductase and respiratory chain complex I (Fig. 3), suggesting their potentials for organic substrates degradation by aerobic or anaerobic respiration, as reported for Heimdallarchaeota-AAG and Heimdallarchaeota-MHVG[32]. Meanwhile, differ to other Asgard phyla, Gerdarchaeota do not harbour the RuBisCO genes for nucleotide salvage (Fig. 3). Additionally, like Lokiarchaeota, Gerdarchaeota lack Glycerol-1-phosphate dehydrogenase (G1PDH) for the archaeal-type lipid biosynthesis, but contain the bacterial-type Glycerol-3-phosphate dehydrogenase (G3PDH). However, the Asgard archaeal G3PDH is encoded by the *glp* gene, thus it may participate in organic carbon degradation rather than archaeal lipid synthesis[35, 36].

4.2.4. Alkane metabolism

Methane formation is one of the earliest metabolisms on earth[37]. This process was restricted to Euryarchaeota until the discovery of novel *mcr* genes across the domain of archaea, e.g., Bathy-, Verstraete-, Hades-, Nezha-, and Korarchaeaota[8, 9, 38-40]. Notably, genes encoding *mcrABG* were identified in Helarchaeota genome SZ_4_bin10.384, as firstly reported by Seitz et. al.[13], indicating that the MCR complex is widespread in the domain of Archaea. Phylogenetic analysis showed that Asgard archaea *mcrA* genes clustered together within the branch of the butane-oxidizing Syntrophoarchaeum[41] and ethane-oxidizing Argoarchaeum[42] (Fig. S7A), corroborated by the McrB and McrG protein trees (Fig. S7).

Molecular modelling and dynamics studies (see Supplementary Materials and Methods) showed that the MCR complex of Asgard archaea for butane binding was similar to that of *Ca.* Syntrophoarchaeum according to the root mean square deviation (RMSD) values (~5 Å, Fig. S8B). Thus, Asgard archaea might be able to oxidize short-chain alkanes, in which ethane and butane are preferentially used as revealed by the RMSD values (Fig. S8C). Based on the evolutionary analysis, a high percentage (> 10%) of *mcrA* genes in the Helarchaeota MAGs was most likely transferred horizontally from archaea, and most of these genes originated from methanogenic hosts/donors, e.g., Thermococci, Methanomicrobia, and Methanobacteria (Fig. S9). Although *mcrA* gene transcript has not been detected from the MAG SZ_4_bin10.384 (Fig. 3), the expressed Asgard-like *mcrA* genes in the unbinned scaffolds (e.g., SZ_4_scaffold_203331_2, Fig. S10) highlights the involvement in activities of alkane oxidation by Asgard archaea in marine sediments.

For Asgard archaeal C1 alkane degradation, the methyl-CoM formed by MCR might be oxidized to CO_2 via the reverse THMPT-dependent WL pathway[43], while for C2 to C4 alkane degradation, the mechanism of the conversion of $C_nH_{2n+1}CoM$ to $C_nH_{2n-1}CoA$ is enigmatic. Like *Ca.* Syntrophoarchaeum[41], Asgard archaea might use the potential alkyl and methyl transferase, such as MtaA, MtbA or MttB, (Table S6) for this reaction. Additionally, other potential transferases that not identified in *Ca.* Syntrophoarchaeum, such as tetrahydromethanopterin S-methyltransferase (MtrA and MtrH)[41], were also discovered in all Asgard phyla. In the subsequent step, $C_nH_{2n-1}CoA$ is further oxidized to acetyl-CoA through the highly expressed β-oxidation pathway (Fig. 4 and Table S6). Intriguingly, as in ANME[44], Helarchaeota have the genes for assimilatory sulfate reduction, but involvement in anaerobic alkane oxidation linked to sulfate reduction has not been demonstrated yet[38]. In contrast to methanogens[45] and methanotrophs[43], β-oxidation enzymes were also identified in Asgard archaea, Bathyarchaeota[8] and *Ca.* Syntrophoarchaeum[41], suggesting metabolic similarity among the three lineages. Although the MCR complex was not identified in all Asgard MAGs, the presence of β-oxidation enzymes, as well as the Asgard-like *mcrA* genes in the unbinned scaffolds (Fig. S10) revealed their metabolic potential for short-chain hydrocarbon oxidation.

Genes encoding aerobic alkane utilization (*alkB*) were found in Lokiarchaeota and Thorarchaeota MAGs (Fig. 4 and Table S6) retrieved from Shark Bay microbial mat[24]. Hence, Asgard archaea might also participate in medium-chain alkane (C5–C16) oxidation, although the spectrum of alkanes utilized remains unclear. The construction of protein tree indicates that Asgard *alkB* genes are monophyletic with those from the sulfate-reducing bacterium *Desulfatibacillum aliphaticivorans*[46] (46% amino acid identity, Fig. S11). Similar to other sulfate-reducing bacteria[46, 47], Asgard archaea might oxidize medium-chain alkanes via a primary alcohol, which may be further transferred to acetyl-CoA through the incomplete β-oxidation process (Fig. 4). Meanwhile, we identified some auxiliary receiving and transcriptional gene sets, e.g., methyl-accepting chemotaxis proteins (MCPs) and the chemotaxis protein set CheARWY, which might be involved in alkane degradation[48].

Except for the core genes for alkane degradation, genes encoding enzymes for hydrogen metabolism and electron transport, including the [NiFe]-hydrogenase *mvhADG* and the hydrogenase heterodisulfide reductase *hdrABC*[49] were detected in all phyla and were highly expressed in Lokiarchaeota and Thorarchaeota (Fig. 4 and Table S6). Additionally, membrane-bound $F_{420}H_2$ dehydrogenase (Fpo) was identified in all Asgard phyla. The proton gradient generated by Fpo can be used for ATP synthesis through the highly expressed genes encoding V/A-type ATPase (Fig. 4). In contrast to most members of Asgard archaea, Heimdallarchaeota contain cytochrome c oxidase genes, suggesting the potential for electron transfer during respiration[23].

In conclusion, we expand the Asgard archaea diversity by reporting five new Asgard phyla. The wide distribution and large diversity of Asgard archaea suggest that they are globally important components of the microbial community. The experimentally verified ability to perform carbon fixation, organic polymer degradation and transcriptomic activity with a wide spectrum of organic carbon compounds, especially alkanes, indicates that Asgard archaea are important players in the marine sediment carbon cycle. However, their contribution to carbon metabolism remains to be quantified, especially for the newly discovered clades. Overall, our results prove that Asgard archaea are active participants of carbon cycling in the marine environment.

4.3. Methods

4.3.1. Asgard archaea 16S rRNA gene dataset construction

Archaeal 16S rRNA gene sequences were retrieved from the GenBank NCBI nucleotide database (September 2017) and SILVA SSU r132 database[51]. E-utilities[52] was applied to search and retrieve the archaeal 16S rRNA gene sequences from the NCBI nucleotide database using the ESearch function with the following string: "16S AND 800:2000[Sequence Length] AND archaea[organism] AND rrna[Feature Key] AND isolation_source[All fields] NOT genome NOT chromosome NOT plasmid". EFetch function was then used to retrieve the sequences and the corresponding GenBank-formatted flat file, which contained environmental information (e.g., location and isolation source). In the subsequent steps, custom scripts were designed to combine the two datasets and to remove low-quality (i.e., containing 'N' or shorter than 800 bp) and duplicate sequences, resulting in 100,786 archaeal sequences. To obtain potential Asgard 16S rRNA gene sequences, the above sequences were BLAST-searched against genome-based 16S rRNA gene sequences (≥800 bp, Table S2) using BLASTn with a cutoff E-value ≤1e-5, sequence identity ≥75%, and coverage ≥50%. This resulted in a set of 9765 potential Asgard sequences from the public databases. OTUs were assigned using the QIIME UCLUST[53] wrapper, with a threshold of 95% nucleotide sequence identity, and the cluster centroid for each OTU was chosen as the representative OTU sequence. A set of OTU threshold (e.g., 90%, 95% and 97%) was verified to obtain the optimum value for phylogenetic tree building and data analysis.

In addition to public databases, archaeal 16S rRNA gene sequences were also retrieved from a recent study[20]. All expressed 16S rRNA gene sequences in the reference paper were BLASTn-searched against a custom database containing 16S rRNA gene sequences retrieved from Asgard MAGs and potential Asgard OTUs obtained as described above, with a cutoff E-value ≤1e-5, sequence identity ≥50%, and coverage ≥80%. Finally, 5588 potential Asgard sequences were obtained, including eight newly proposed

clusters DAS1–8 (79 sequences)[20]. OTU re-formation of these sequences (15,353 sequences, from both databases and the reference paper) was performed using the QIIME UCLUST[53] wrapper, with a threshold of 95% pair-wise nucleotide sequence identity, resulting in 1836 OTUs.

4.3.2. Phylogenetic position and distribution of Asgard archaea 16S rRNA gene sequences

SINA-aligned[54] archaeal representative OTU sequences obtained in the previous step (1836 OTUs) were pre-filtered using a backbone tree, which was constructed based on updated 16S rRNA archaeal gene datasets[55, 56], using the ARB software (version 5.5) with the "Parsimony (Quick Add Marked)" tool[57]. This resulted in 456 Asgard OTUs. Candidate representative OTU sequences (456 OTUs), genome-based 16S rRNA gene sequences ≥600 bp (17 sequences), and reference sequences were used for phylogenetic tree construction. Maximum-likelihood tree was inferred with IQ-TREE (version 1.6.1)[58] using the GTR+I+G4 mixture model (recommended by the "TESTONLY" model) and ultrafast (-bb 1000). Asgard clade designations were made when either a group was defined in previous publications, or when groups with >20 sequences and intragroup similarity >75%[59] were monophyletic. Attributes [i.e., expressed rRNA gene, biotope, temperature, and salinity (Table S1)] for each representative OTU were extracted and visualized using iTOL software[60]. Calculation of percent identity of new Asgard clades was based on 179 sequences with a long fragment of Asgardarchaeotal 16S rRNA gene. Fragments of 16S rRNA gene from position of *E. coli* 243 to 1414 (~1170 bp) were used for calculating the identity.

The corresponding environmental information (i.e., location and biotopes) for the 16S rRNA gene sequences of Asgard archaea was extracted from the GenBank-formatted flat file using custom scripts. This resulted in 172 libraries with latitude and longitude of sampling sites (Table S1). Information on the sample locations was plotted using the mapdata and ggplot2 packages in R software.

4.3.3. SIP incubations

Sediment for incubations was collected from Helgoland Mud Area methane zone (54°05.23'N, 007°58.04'E) by gravity coring during the RV HEINCKE cruise HE443 in 2015. Sediment from the methanic zone (239-263 cm depth) and artificial sea water (w:v=1:4, 50 mL) were homogenized and incubated anaerobically in sterile 120-mL serum bottles sealed with butyl rubber stoppers, and headspace refilled with N_2. A 10-day pre-incubation was performed by exchanging headspace with N_2 to remove CO_2. Triplicate set ups were supplemented with electron donors (1 g L^{-1} sulfur, 30 mg L^{-1} lignin, 30 mg L^{-1} humic acid, 30 mg L^{-1} cellulose, respectively), electron acceptors (30 mM lepidocrocite) and 10 mM

sodium bicarbonate (^{13}C-labelled bicarbonate provided by Cambridge Isotope Laboratories, Tewksbusry, Massachusetts, USA) and were incubated at 10 °C. An additional set up fed with ^{12}C-bicarbonate was used as a control for comparison. Samples collected at day 255 were used for RNA-SIP analysis and those at day 386 were used for DNA-SIP analysis. DNA and RNA extraction were performed as previously described[50]. Cross-feeding by indirectly utilization of ^{13}C-DIC in these incubations can be neglected for the following reasons: i) organic substrates were unlabelled; ii) no obvious buoyant density shift in nucleic acid-SIP profiles of organic substrates incubations; iii) no considerable increase of bacterial gene copies from incubations amended with organic polymers (Fig. S1d); iv) no significant bacterial community shift between heavy and light fractions in incubations of "sulfur" and "sulfur + lepidocrocite" (Fig. S1c).

4.3.4. Isopycnic centrifugation, gradient fractionation and sequencing

Isopycnic centrifugation and gradient fractionation were performed to separate ^{13}C- labelled from unlabelled nucleic acids as previously described[50]. 0.3– 0.7 µg RNA and 4–6.5 µg DNA were used for DNA- and RNA-SIP, respectively. 13 fractions were obtained from each sample after ultracentrifugation. RNA was reverse transcribed using the high capacity cDNA reverse transcription kit (Applied Biosystems, Foster City, California, USA). cDNA from fractions 4 and 5 (ultra-heavy), 6 and 7 (heavy), 8 and 9 (light), as well as 10 and 11 (ultra-light) were combined for sequencing. DNA samples from fractions without combination were used for high-throughput sequencing. PCR targeting the V4 region of 16S rRNA gene sequences was performed with KAPA HiFi HotStart PCR kit (KAPA Biosystems, Cape Town, South Africa) and barcoded archaeal primer Arc519F (5'-CAGCMGCCGCGGTAA-3') and Arch806R (5'-GGACTACVSGGGTATCTAAT-3'). Thermocycling was performed as follows: 95 °C for 3 min; 35 cycles at 98 °C for 20 sec, 61 °C for 15 sec, and 72 °C for 15 sec; 72 °C for 1 min. PCR products were purified using the Monarch PCR Cleanup Kit (New England Biolabs, Ipswich, Massachusetts, USA) according to the manufacturer. Equimolar amounts of amplicons per samples were combined based on PicoGreen quantification. Amplicon sequencing was conducted using Illumina Hiseq 4000 platform with 150-bp paired-end reads at GATC Biotech (Konstanz, Germany). Raw reads were processed using the QIIME 1.9.0 software package[61]. OTUs were clustered at 97% identity using UPARSE-OTU[62]. Potential Asgard OTUs were taxonomically assigned by BLASTn search against OTUs in Fig. 1a with the following parameters "-perc_identity 97, -qcov_hsp_perc 100, -evalue 1e-5".

4.3.5. Clone library construction

A clone library of archaeal 16S rRNA gene fragments (>800 bp) was constructed to confirm the accuracy of classification by using short Illumina sequences (143 bp). The DNA-SIP samples from heavy fractions of the incubations amended with sulfur and lepidocrocite (density = 1.715 g/ml), lignin and lepidocrocite (1.714 g/ml) as well as humic acid and lepidocrocite (1.714 g/ml) were used for cloning. PCR was performed with the primer set of Arc8F (5'-TCCGGTTGATCCTGCC-3')/Arc912R (5'-GTGCTCCCCCGCCAATTCCTTTA-3') using ALLin RPH polymerase Kit (highQu, Kraichtal, Germany). Thermocycling was performed as follows: 95 °C for 3 min; 40 cycles at 95 °C for 30 sec, 55 °C for 45 sec and 72 °C for 45 sec; 72 °C for 10 min. Purified PCR products were ligated into the pGEM-T vector (Promega, Mannheim, Germany) and transformed into Escherichia coli JM109 competent cells (Promega, Mannheim, Germany) according to the manufacturer. White colonies were randomly picked and cell material was directly subjected to colony PCR with the following cycling parameters: 95 °C for 5 min; 28 cycles at 95 °C for 30 sec, 55 °C for 45 sec, and 72 °C for 1 min; 72 °C for 5 min. Amplicons of 96 clones were submitted to LGC Genomics (Berlin, Germany) for Sanger sequencing. Similarity between OTUs of 16S rRNA gene sequences (Hiseq) and clones ranged from 97.9% to 100% (Fig. 1a), suggesting the accuracy of identification of short Illumina sequences.

4.3.6. Quantitative PCR (qPCR)

16S rRNA genes of Lokiarchaeota in cultures were quantified using the newly designed primer set Loki97F/Loki495R (5'-TTCCCATRGCAAACTGCTCA-3'/5'-CCTTGCCCTCTCCTTTCT-3'), which were designed in ARB using the PROBE DESIGN feature and showed specificity to Lokiarchaeota. qPCR was performed as described previously with modifications[30]. Lokiarchaeota-4 16S rRNA gene clone was used as qPCR standard. Each reaction mixture contained Takyon Master Mix (Eurogentec, Seraing, Belgium), bovine serum albumin (Roche, Mannheim, Germany), 500 nM primers, 1 ng DNA templates or 2 µL of standard. The qPCR protocol comprised an initial denaturation (5 min at 95 °C) and 40-cycle amplification (95 °C for 15 sec, 58 °C for 20 sec and 72 °C for 40 sec). Primer specificity for qPCR was tested by comparison with the known clones including Lokiarchaeota-4 (positive control), Lokiarchaeota-2 (positive control), and clones as negative control selected from Heimdallarchaeota, Odinarchaeota, Bathyarchaeota, Woesearchaeota, and ANME-3. The cycle threshold (Ct) values of Lokiarchaeota-2 was close to Ct values of the Lokiarchaeota-4 clone, while the Ct values of the negative control clones were higher than that of the standard with lowest quantity of DNA, indicating primers were specific for the Lokiarchaeota detected in our samples. Statistically significant differences of gene

abundances between treatments were assessed with the general linear hypothesis test and pairwise Tukey procedures[63] at a threshold of $p < 0.05$. The tests were adjusted for heteroscedasticity, non-Gaussian gene abundance distribution, and for multiple comparisons to control the false discovery rate. Analyses were carried out in R 3.5.2[64].

4.3.7. Sediment sample collection and processing

Samples for metagenome analysis were collected from coast sediment of China (Table S4). They were sampled using custom hollow column, sealed in plastic bags in duplicates, stored in sampling box with ice bags, and transported to the lab within 4 hours. The physiochemical parameters of the samples were determined as previously described[65]. Samples for RNA extraction were preserved in RNALater (Ambion, Life Technologies). For each sample, 10 g sediment each was used for DNA and RNA isolation with the PowerSoil DNA Isolation Kit (MO BIO) and RNA Powersoil™ Total RNA Isolation Kit (QIAGEN), respectively. The rRNA genes were removed from the total RNA using the Ribo-Zero rRNA removal kit (Illumina, Inc., San Diego, CA, USA) and the remaining mRNA was reverse-transcribed. DNA and cDNA were sequenced using an Illumina HiSeq sequencer (Illumina) with 150-bp paired-end reads at BerryGenomics (Beijing, China). Metatranscriptomic reads were quality-trimmed using Sickle (version 1.33)[66] with the quality score ≥25, and the potential rRNA reads were removed using SortMeRNA (version 2.0)[67] against both the SILVA 132 database and the default databases (E-value cutoff ≤1e-5).

4.3.8. Metagenomic assembly, genome binning and gene annotation

Raw metagenomic DNA reads of the mangrove sediments and sediment enrichment were dereplicated (identical reads) and trimmed using sickle (version 1.33)[66] with the option "-q 25". Paired-end Illumina reads for each sample were *de novo* assembled using IDBA-UD (version 1.1.1)[68] with the parameters "-mink 65, -maxk 145, -steps 10". Scaffolds were binned into genomic bins using a combination of MetaBAT[69] and Das Tool[70]. Briefly, twelve sets of parameters were set for MetaBAT binning, and Das Tool was further applied to obtain an optimized, non-redundant set of bins. To improve the quality of the bins (e.g., scaffold length and bin completeness), each Asgard-related bin was remapped with the short-read mapper BWA[75] and re-assembled using SPAdes (version 3.0.0)[71] or IDBA-UD (version 1.1.1)[68], followed by MetaBAT and Das Tool binning. Asgard MAGs with high contamination were further refined with Anvi'o software (version 2.2.2)[72]. The completeness, contamination and strain heterogeneity of the genomic bins were estimated by CheckM (version 1.0.7) software[73]. Anvi'o software (version 2.2.2)[72] was applied for pan-genome analysis of Asgard archaea with the option "--min-occurrence 3".

Protein-coding regions were predicted using Prodigal (version 2.6.3) with the "-p meta" option[74]. The KEGG server (BlastKOALA)[75], eggNOG-mapper[76], InterProScan tool (V60)[77], and BLASTp vs. NCBI-nr database searched on December 2017 (E-value cutoff ≤1e-5) were used to annotate the protein-coding regions. ESP prediction was based on arCOG (eggNOG-mapper) and the eukaryote-specific IPR domains (InterProScan)[10]. Archaeal extracellular peptidases were identified using PRED-SIGNAL[78] and PSORTb[79] (Table S8).

4.3.9. Phylogenetic analyses of Asgard archaea and functional genes

Small subunit 16S rRNA gene sequences and a concatenated set of 122 archaeal-specific conserved marker genes[9] were used for phylogenetic analyses of Asgard archaea. Ribosomal RNA genes in the Asgard bins were extracted by Barrnap (version 0.3, http://www.vicbioinformatics.com/software.barrnap.html). An updated 16S rRNA gene sequence dataset from reference papers[55, 56] with genome-based 16S rRNA genes were aligned using SINA (version 1.2.11)[54]. The 16S rRNA gene sequences and protein maximum-likelihood tree was built with IQ-TREE (version 1.6.1)[58] using the GTR+I+G4 and PMB+F+I+G mixture model (recommended by the "TESTONLY" model), respectively, with opition "-bb 1000". Marker genes for protein tree were identified using hidden Markov models (HMMs) and were aligned separately using hmmalign from HMMER3[80] with default parameters. The 122 archaeal marker genes were identified using hidden Markov models. Each protein was individually aligned using hmmalign[81]. The concatenated alignment was trimmed by BMGE with flags "-t AA -m BLOSUM30"[82]. Then, maximum-likelihood trees were built using IQ-TREE with the best-fit model of "LG+I+G4" followed by extended model selection with FreeRate heterogeneity and 1000 times ultrafast bootstrapping. The final tree was rooted with the DPANN superphylum and Euryarchaeota.

Key genes for enzymes involved in alkane degradation, i.e. *mcrABG* and *alkB*, were extracted from the Asgard MAGs. Amino acid sequences were aligned using MUSCLE (version 3.8.1551)[83] with default parameters. Un-rooted phylogenetic trees for each gene were built with corresponding gene sequences from NCBI database and reference paper[84] using IQ-TREE with model LG+F+I+G4 (*mcrABG*) or LG+F+G4 (*alkB*).

4.3.10. Metabolic pathway construction

Potential metabolic pathways were reconstructed based on the predicted annotations and the reference pathways depicted in KEGG and MetaCyc[85]. Metatranscriptome data from mangrove and mudflat

sediments of Shenzhen Bay (Table S4) were analysed to clarify the transcriptomic activity of Asgard archaea. The abundance of transcripts for each gene was determined by mapping all non-rRNA transcripts to predicted genes using BWA with default setting[6, 86]. Normalized expression was expressed in transcript per million units (TPM), followed by normalization by genome number of each phylum.

4.3.11. Molecular modelling and dynamics simulation

Helarchaeotal MCR amino acid sequences were blasted against the protein data bank (PDB)[87] to obtain high-similarity sequences. The geometry of these sequences were then predicted using MODELLER[88], and those with high DOPE score were kept for analysis. Protein–protein interaction of the MCR complex was predicted using ZDOCK (http://zdock.umassmed.edu/), and the protein–ligand docking was executed by the AutoDock4 (version 4.2.6)[89] with the Lamarckian genetic algorithm[90].

Molecular dynamics (MD) simulations of MCR complexes were performed using GROMACS (version 5.1.1)[91] based on AMBER99SB-ILDN force field[92] and TIP3P water box[93]. The cutoff of non-bonded interactions involving van der Waals and electrostatics was set 10 Å. Long range electrostatic interactions were treated using the Partice-Mesh-Ewald (PME) algorithm[94]. Energy minimization was carried out to obtain initial structure with force $\leq$1000 kJ·mol^{-1}·nm^{-1}. MD simulations were initially carried out using the NVT ensemble for 100 ps (300 K), followed by simulation with NPT ensemble for 100 ps (300 K and 1 bar). Then, 50 ns MD simulations were performed using NPT ensemble (300 K and 1 bar) with the time steps of 2 fs to get the equilibrium trajectories. Snapshot was saved at an interval of 10 ps for subsequent analysis. Snapshots were saved every 10 ps for subsequent analysis.

4.3.12. Evolutionary analysis

All genomes containing MCR complex were downloaded from NCBI (https://www.ncbi.nlm.nih.gov/) databases. CheckM was used to check the genome quality. Genomes with completeness < 70% were removed for the further analysis. We selected 117 genomes for final analysis. The phylogenetic tree of concatenated 122 archaeal marker genes were constructed using IQ-TREE (version 1.6.3) with "-m MFP -mset LG,WAG -mrate E,I,G,I+G -mfreq FU -bb 1000" flags, the genome of a DPANN archaea (Diapherotrites_AR10) was used as outgroup. Putative HGTs were inferred using HGTector[95]. A standard database (version updated on 2017-6-30) were used for homologues searching by using MMseqs2[96]. Quality cutoffs for valid hits were e-value $\leq$1e^{-20}, sequence identity $\geq$30%, and coverage of query sequence $\geq$50%.

4.3.13. Data availability

Archaeal 16S rRNA gene sequences were retrieved from NCBI database, SILVA SSU r132 database, and a reference paper as described in Supplementary Methods. Public Asgard MAGs were from NCBI database and MG-RAST. The newly obtained Asgard MAGs and metatranscriptomic data are available in NCBI database under the project PRJNA495098 and PRJNA360036. Sequencing data of SIP samples have been submitted to GenBank Short Reads Archive with accession numbers from SRR8607872 to SRR8607991. Clone sequences have been deposited at GenBank with accession numbers of MK551261-MK551285.

4.4. Acknowledgements

This research was financed by the National Natural Science Foundation of China (No. 91851105, 31622002, 31600093, and 31700430), the Science and Technology Innovation Committee of Shenzhen (Grant No. JCYJ20170818091727570), the Key Project of Department of Education of Guangdong Province (No. 2017KZDXM071), the China Postdoctoral Science Foundation (No. 2018M633111), the Deutsche Forschungsgemeinschaft (DFG, EXC 309) and the University of Bremen. We thank Ms. Kiley Seitz and Dr. Brett J. Baker for providing the Helarchaeota genomes. We thank Dr. Nidhi Singh for her suggestions in molecular modelling.

4.5. Author contributions

M.L. and M.C. conceived this study. M.C. analysed the 16S rRNA data, metagenomic data and metatranscriptomic data. X.Y., A.K., T.R.H and M.W.F., performed the SIP trials and analysed the 16S rRNA gene data. Y.L. collected samples and analysed the horizontal gene transfer. Z.Z. provided support for diversity analysis. M.C., Y.C.Y., J.P. and Z.Z. prepared the DNA and cDNA for sequencing. W.L. and X.W. analysed MCR complex protein structure and simulated the binding substrates. M.L., M.C., Y.L., and X.Y. wrote, and all authors edited and approved the manuscript.

4.6. Author Information

Reprints and permissions information is available at www.nature.com/reprints. The authors declare no competing financial interests. Readers are welcome to comment on the online version of the paper. Correspondence and requests for materials should be addressed to M.L. (limeng848@szu.edu.cn) or M.W.F. (michael.friedrich@uni-bremen.de).

4.7. Figures

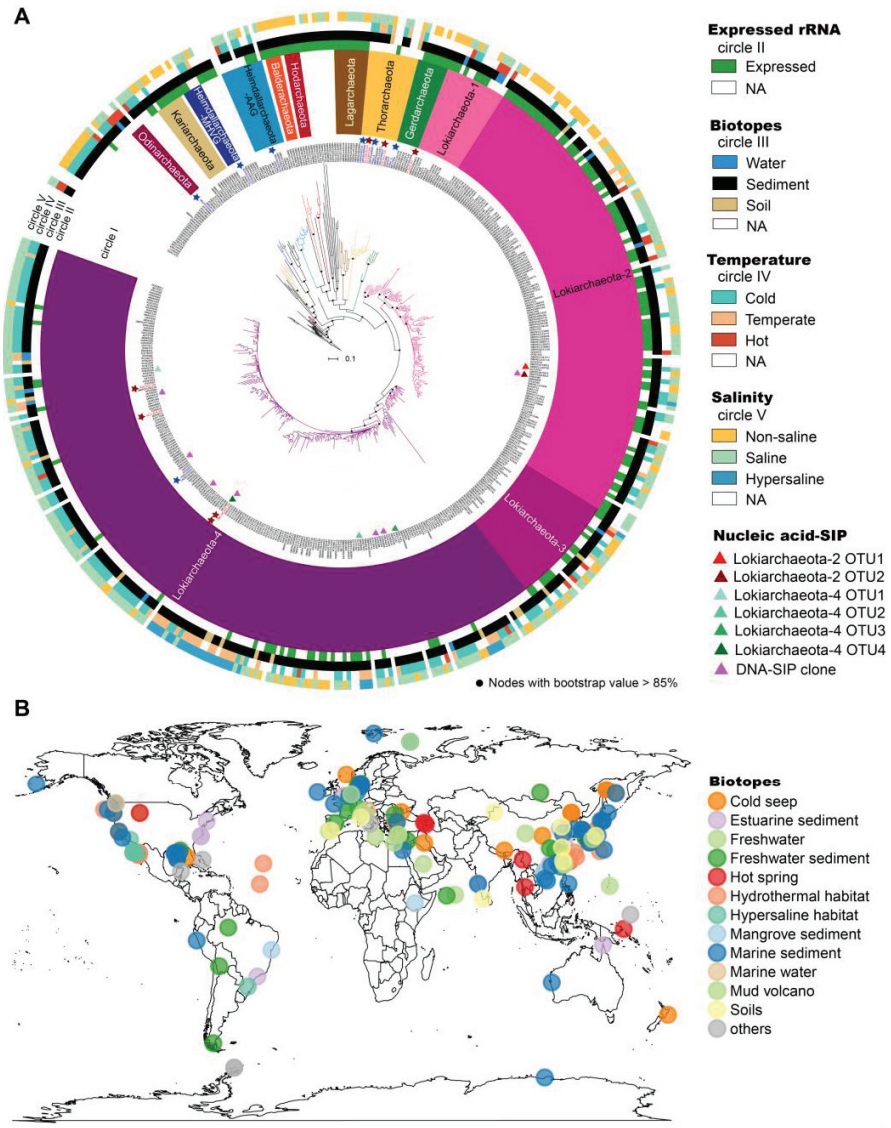

Fig. 1. Diversity and distribution of Asgard archaea. (**A)** Maximum likelihood tree of Asgard archaea constructed using genome-based and publicly available 16S rRNA gene sequences clustered at 95% sequence identity. Groups were designated based on sequences fulfilling the division criteria (see Supplementary Materials and Methods). The colour circles, from the inside to the outside, represent the expressed 16S rRNA gene sequences, habitat, temperature, and salinity, accordingly. Red stars represent 16S rRNA gene sequences from newly discovered Asgard MAGs, and blue stars represent sequences from reference Asgard MAGs. MAGs with the MCR complex and MAGs from ^{13}C-bicarbonate labelled enrichment are highlighted with two red stars. The 16S rRNA gene sequences from DNA-SIP and RNA-

SIP trials are marked with triangles (refer to Fig. 2 for details). The tree was re-rooted with Crenarchaeota. Bootstrap support values >70% are shown. (**B)** Global distribution and biotopes of Asgard archaea from 172 public archaeal libraries. Detailed information can be found in Table S1 and Data S1.

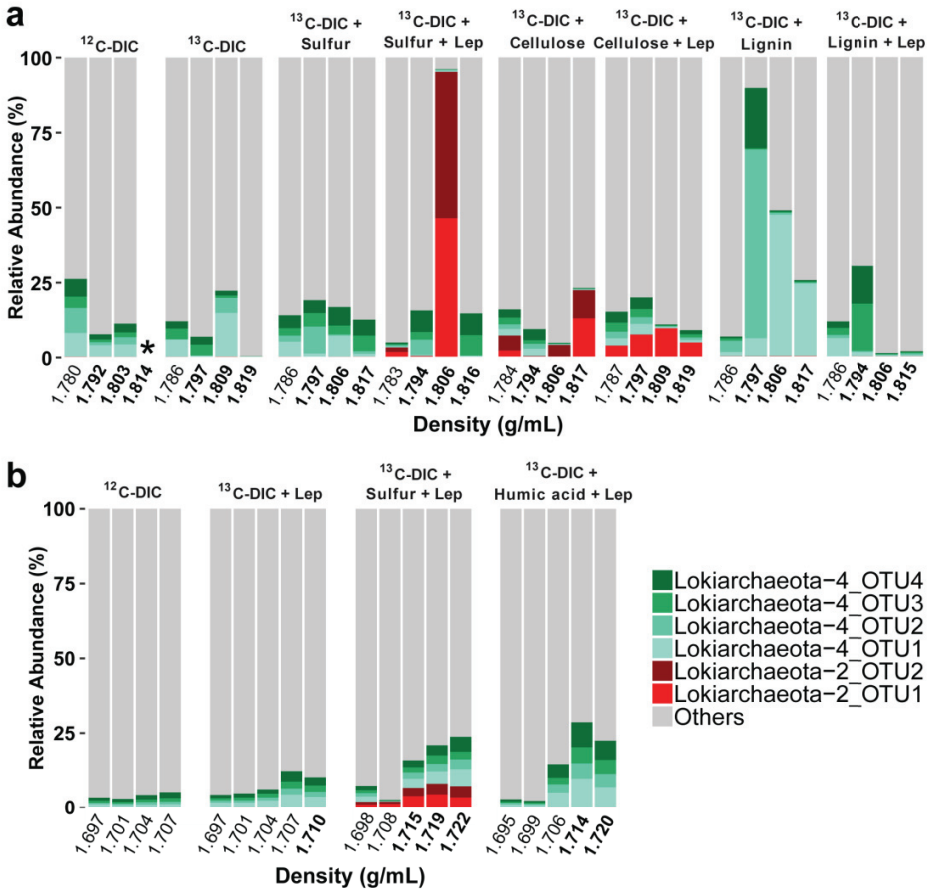

Fig. 2. Total sum scaling of Lokiarchaeota abundances of archaeal 16S rRNA gene sequences from selected "light" and "heavy" gradient fractions of (**a**) RNA- and (**b**) DNA-SIP samples. Considering the limited density shifts in incubations with organic substrates and similar bacterial communities in the RNA fractions of "sulfur" and "sulfur + lepidocrocite" incubations (see Supplementary Methods and Supplementary Fig. 1), cross-feeding was most likely negligible[47]. For RNA-SIP, pairs of fractions (fractions 4 and 5, 6 and 7, 8 and 9, 10 and 11) were combined for Illumina sequencing, whereas individual samples were used for DNA-SIP. Density was indicated as the average density of combined fractions for RNA-SIP samples. The centrifugation gradients densities of RNA >1.79 g/mL and DNA >1.71 g/mL were regarded as containing ^{13}C-labelled nucleic acids (bold)(Lueders et al., 2004a). *

indicates that cDNA synthesis failed because of the low amount of RNA in these fractions. DNA with densities >1.71 g/mL was not obtained from ^{12}C-control incubations. Lep: lepidocrocite. DIC: dissolved inorganic carbon, i.e., bicarbonate.

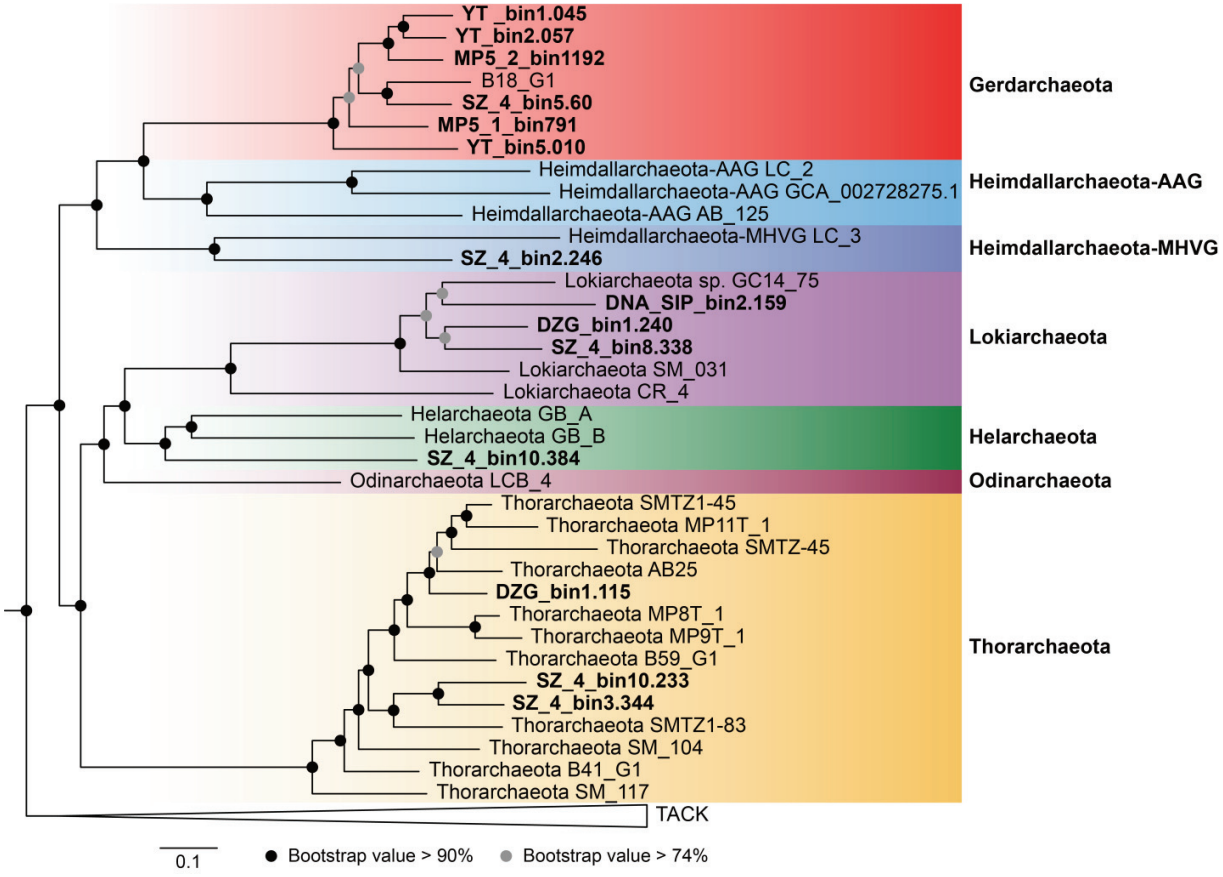

Fig. 3. Maximum likelihood tree of Asgard MAGs inferred from a concatenated alignment of 122 archaeal marker genes and re-rooted with DPANN and Euryarchaeota. The collapsed nodes are represented by triangles and sized in proportion to genome numbers. Asgard MAGs obtained in this study are marked bold.

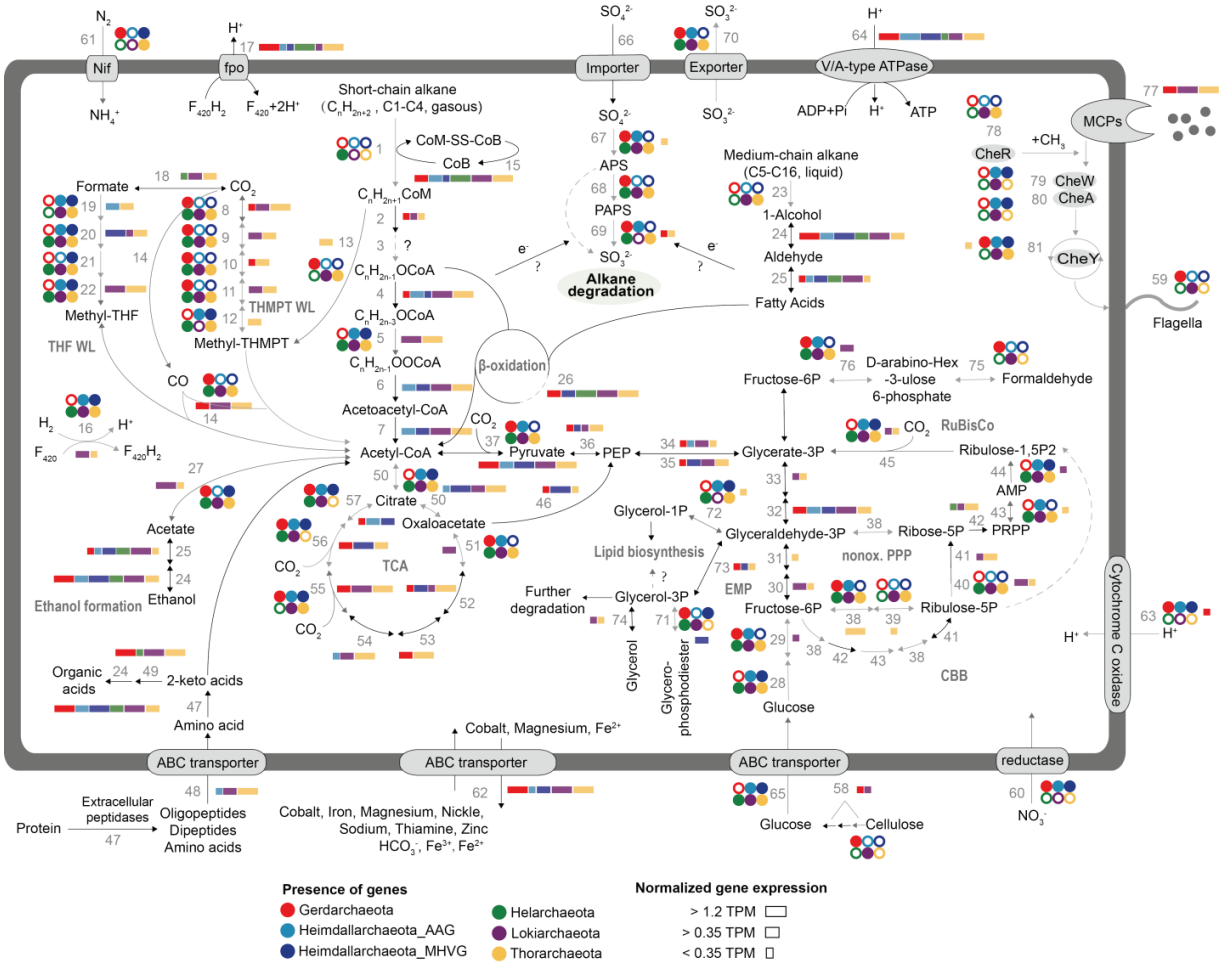

Fig. 4. Key potential metabolic pathways of Asgard archaea. The whole pathway was reconstructed based on all available Asgard MAGs (Table S5). Circles with different colours represent different phyla or MAGs. For comparison purposes, we used arrows of different types and colours. Black arrows indicate genes found in all Asgard MAGs, and grey arrows represent genes that are present in a subset of MAGs. Dashed grey arrows show pathways that are missing from all MAGs. Detailed metabolic information for the MAGs is available in Table S6. The relative abundance of the transcripts (Transcripts Per Million reads, TPM) for each gene was marked with proportionally sized rectangles and represented at the phylum level. Odinarchaeota were excluded because no Odinarchaeota MAG was identified in the present study.

4.8. Supplementary tables

Supplementary Table 1. Overview of 172 archaeal libraries that include Asgard archaeal 16S rRNA sequences.

Library/study	Site location	Biotope	Salinity	Temperatur	Life style	pH	Depth (m
The context of this statement is not immediately apparent (specific instruction a	Mandovi and Zuari river, India	Estuarine sediment	2	2	2	2	5
Please list references, unless that is specified in the table.	Lake Ørn, Denmark	Freshwater sediment	1	1	2	NA	4,5
Microbial methane cycling in a terrestrial mud volcano in eastern Taiwan	Kuan-Shan area, eastern Taiwan	Mud volcano	2	2	2	2	NA
Comparison of archaeal and bacterial community structures in heavily oil-contar	Jidong Oilfield near Bohai Bay, China	Soils	1	1	3	NA	NA
An integrated study reveals diverse methanogens, Thaumarchaeota, and yet-un	Arzakan, Armenia	Hot spring	2	3	2	2	NA
Novel uncultured Chloroflexi dechlorinate perchloroethene to trans-dichloroethe	Jade Bay, Germany	Marine sediment	2	1	2	NA	NA
Archaeal diversity and the prevalence of Crenarchaeota in salt marsh sediments	Long Island Sound, USA	Estuarine sediment	2	2	2	1	NA
Niche Separation of Methanotrophic Archaea (ANME-1 and -2) in Methane-Se	Eastern Japan Sea, Japan	Cold seep	2	1	2	NA	NA
Archaeal diversity in tidal flat sediment as revealed by 16S rDNA analysis	Dongmak, Korea	Marine sediment	1	2	3	1	0,05
An integrated study reveals diverse methanogens, Thaumarchaeota, and yet-un	Jermuk, Armenia	Hot spring	2	3	2	2	NA
Life without light: microbial diversity and evidence of sulfur- and ammonium-ba	Movile Cave, Romania	Freshwater sediment	1	2	2	2	0
Evidence for anaerobic oxidation of methane in sediments of a freshwater syste	Piora valley, Switzerland	Freshwater sediment	1	1	2	NA	13
Comparison of microbial communities associated with phase-separation-induced	Yonaguni Knoll IV hydrothermal field,	Hydrothermal habitat	2	3	2	NA	NA
Stratification of Archaeal communities in shallow sediments of the Pearl River I	Pearl River, China	Estuarine sediment	2	2	2	2	0,5
Enrichment and cultivation of prokaryotes associated with the sulphate-methane	Aarhus Bay, Denmark	Marine sediment	2	1	2	NA	NA
Vertical Distribution and Diversity of Archaea in Nether Sediment from a Mud	Florida Escarpment, USA	Cold seep	2	1	2	NA	3288
Diversity, abundance and distribution of amoA-encoding archaea in deep-sea m	Okhotsk Sea, Pacific Ocean	Cold seep	2	1	2	NA	783
Microbial Communities in Methane- and Short Chain Alkane-Rich Hydrotherma	Guaymas Basin, USA	Hydrothermal habitat	2	3	2	NA	NA
Microbial communities of deep-sea methane seeps at hikurangi continental marg	Wairarapa Takahae, New Zealand	Cold seep	2	1	2	NA	1114
Composition of archaeal community in a paddy field as affected by rice cultivar	Hangzhou, China	Soils	1	2	3	NA	NA
Biogeochemistry and community composition of iron- and sulfur-precipitating m	Nile Deep Sea Fan, Eastern Mediterra	Mud volcano	2	1	2	NA	3024
Biogeochemical processes and microbial diversity of the Gullfaks and Tommeliti	Gullfaks methane seeps, Northern Nor	Cold seep	2	1	2	NA	150
Physiological and molecular characterization of a microbial community establish	Shizuoka, Japan	Soils	1	1	3	2	NA
Stratified communities of active archaea in shallow sediments of the pearl river	Pearl River, China	Estuarine sediment	2	2	2	2	0,6
Diversity of methanogenic archaea in a mangrove sediment and isolation of a ne	Mzinga creek, Tanzania	Mangrove sediment	1	2	2	2	NA
Bacterial sulfur cycling shapes microbial communities in surface sediments of a	Logatchev hydrothermal field, Mid Atla	Hydrothermal habitat	2	3	2	NA	3000
Bacterial and archaeal diversity in surface sediments from the south slope of the	South China Sea, China	Marine sediment	2	1	2	NA	1285
Variability in microbial community and venting chemistry in a sediment-hosted b	Okinawa Trough, Japan	Hydrothermal habitat	2	3	2	1	NA
Taxonomic and Functional Metagenomic Profiling of the Microbial Community i	Laguna de Carrizo, Spain	Freshwater sediment	2	1	2	2	2,4
Culture-Dependent and -Independent Characterization of Microbial Communitie	Taketomi Island, Japan	Hot spring	2	3	2	NA	23
Molecular biological and isotopic biogeochemical prognoses of the nitrification-d	Ogasawara Trench, western Pacific O	Marine sediment	2	1	2	NA	9760
Methanogen diversity evidenced by molecular characterization of methyl coenz	Guaymas Basin, USA	Hydrothermal habitat	2	3	2	NA	NA
Stratified active archaeal communities in the sediments of Jiulong River estuary	Jiulong River Estuary, China	Estuarine sediment	2	1	2	NA	3
Diverse and novel nifH and nifH-like gene sequences in the deep-sea methane	Okhotsk Sea, Pacific Ocean	Cold seep	2	1	2	NA	840
Microbial diversity in sediments associated with surface-breaching gas hydrate	Gulf of Mexico	Marine sediment	2	1	2	NA	NA
Molecular characterization of potential nitrogen fixation by anaerobic methane-o	Kumano Basin, Japan	Mud volcano	2	1	2	NA	2050
Comparison of Archaeal and Bacterial Diversity in Methane Seep Carbonate N	Hydrate Ridge, USA	Cold seep	2	1	2	NA	800
Isolation and Characterization of a Thermophilic, Obligately Anaerobic and Het	Yaeyama Archipelago, Japan	Hydrothermal habitat	2	3	2	NA	NA
Microbial diversity of cold-seep sediments in Sagami Bay, Japan, as determined	Sagami Bay, Japan	Cold seep	2	1	2	NA	NA
Spatial distribution of viruses associated with planktonic and attached microbial	Hatoma Knoll, Japan	Hydrothermal habitat	2	3	1	NA	NA
Use of 16S rRNA gene based clone libraries to assess microbial communities p	Mediterranean Sea	Mud volcano	2	1	2	2	1673
Anaerobic oxidation of methane at different temperature regimes in Guaymas B	Guaymas Basin, USA	Hydrothermal habitat	2	2	2	NA	NA
Influence of deglaciation on microbial communities in marine sediments off the	Tempelfjorden, Arctic Circle	Marine sediment	2	1	2	NA	40
Prokaryotic diversity and metabolically active microbial populations in sediments	Gulf of Mexico	Marine sediment	3	1	2	NA	600
Comparison of the microbial diversity in cold-seep sediments from different dep	Nankai Trough, Pacific ocean	Cold seep	2	1	2	NA	615
Prokaryotic diversity, distribution, and insights into their role in biogeochemical c	Juan de Fuca Ridge, Pacific Ocean	Marine sediment	2	1	2	NA	2135
Diversity and spatial distribution of prokaryotic communities along a sediment ve	Anaximander Mountains, eastern Medi	Mud volcano	2	1	2	NA	NA
Unique clusters of Archaea in Salar de Huasco, an athalassohaline evaporitic ba	Salar de Huasco, Chile	Freshwater sediment	2	1	2	NA	NA
Temporal evolution of methane cycling and phylogenetic diversity of archaea in	Monterey Canyon, California	Marine sediment	2	1	2	NA	2893
A long-term cultivation of an anaerobic methane-oxidizing microbial community	Omine Ridge, Japan	Cold seep	2	1	2	NA	2533
Comparative analysis of archaeal 16S rRNA and amoA genes to estimate the a	East Sea, Korea	Marine sediment	2	1	2	NA	500
Diversity of Archaea in marine sediments from Skan Bay, Alaska, including cul	Skan Bay, USA	Marine sediment	2	1	2	NA	65
Diversity of prokaryotes and methanogenesis in deep subsurface sediments fro	Nankai Trough, Pacific ocean	Marine sediment	2	1	2	NA	4791
An anaerobic methane-oxidizing community of ANME-1b archaea in hypersalin	Gulf of Mexico	Marine sediment	3	1	2	NA	876
Dominance of putative marine benthic Archaea in Qinghai Lake, north-western	Qinghai Lake, China	Freshwater	2	2	1	2	0,1
Diversity and distribution of methanotrophic archaea at cold seeps	Black Sea, Atlantic Ocean	Cold seep	2	1	2	NA	230
Subseafloor microbial communities associated with rapid turbidite deposition in t	Gulf of Mexico	Marine sediment	2	1	2	NA	NA
Diversity and community structure of archaea in deep subsurface sediments fro	Western Pacific	Marine sediment	2	1	2	NA	NA
Variations in archaeal and bacterial diversity associated with the sulfate-methar	Santa Barbara Basin, USA	Marine sediment	2	1	2	NA	587
Cultivation of methanogens from shallow marine sediments at Hydrate Ridge, C	Hydrate Ridge, USA	Marine sediment	2	1	2	NA	1180
Archaeal diversity and distribution along thermal and geochemical gradients in h	Yonaguni Knoll IV hydrothermal field,	Hydrothermal habitat	2	3	2	NA	NA
Characteristics of Microbial Community Structures in the Ulleung Basin, East S	Ulleung Basin, Korea	Marine sediment	2	1	2	NA	NA
Microbial communities associated with geological horizons in coastal subseafloo	Sea of Okhotsk, western Pacific Ocea	Marine sediment	2	1	2	NA	1225
Biogeographical distribution and diversity of microbes in methane hydrate-bearir	Cascadia margin, Pacific Ocean	Marine sediment	2	1	2	NA	900
Biogeographical distribution and diversity of microbes in methane hydrate-bearir	Peru Margin, Pacific Ocean	Marine sediment	2	1	2	NA	5086
16S rDNA diversity analysis of mangrove soil	China	Mangrove sediment	NA	NA	NA	NA	NA
A Microbial Community within a Natural Asphalt Lake	Pitch Lake, Trinidad	Freshwater	NA	NA	NA	NA	NA
Aerobic and anaerobic methane oxidation in terrestrial mud volcanoes in the No	Napoli mud volcano, Eastern Mediterra	Mud volcano	NA	NA	NA	NA	NA

Library/study	Site location	Biotope	Salinity	Temperatur	Life style	pH	Depth (m
Anaerobic methanotrophic communities in shallow permeable sands off the coa	Coast of Elba, Italy	Soils	NA	NA	NA	NA	NA
Anaerobic oxidation of methane by coastal sediment from Marine Lake Greveli	Lake Grevelingen, Pacific ocean	Marine sediment	NA	NA	NA	NA	NA
Analysis of archaeal diversity in surface sediment from the western Pacific	Western Pacific	Marine sediment	NA	NA	NA	NA	NA
Analysis of microbial mat communities from Hamelin Pool, Shark Bay, Western	Hamelin Pool, Australia	Marine sediment	NA	NA	NA	NA	NA
Antarctic permafrost from Bellingshausen (South Shetland Isles) contrasting in	King-George Island, South Shetland Isl	Others	NA	NA	NA	NA	NA
Archaea and Bacteria and their activity in hydrate-bearing deep subsurface sed	Hydrate Ridge, USA	Marine sediment	NA	NA	NA	NA	NA
Archaea Diversity of High Temperature Regions in Guaymas Basin Hydrotherı	Guaymas Basin, USA	Hydrothermal habitat	NA	NA	NA	NA	NA
Archaea of the Miscellaneous Crenarchaeotal Group are abundant, diverse and	White Oak River, USA	Estuarine sediment	NA	NA	NA	NA	NA
Archaeal 16S rRNA gene clones retrieved from bulk environmental DNA of M	Juan de Fuca Ridge, Pacific Ocean	Marine sediment	NA	NA	NA	NA	NA
Archaeal and bacterial communities in Kao-Mei Wetland	Kao-Mei Wetland, Taiwan	Soils	NA	NA	NA	NA	NA
Archaeal and bacterial communities respond differently to environmental gradie	Salton Sea, USA	Hypersaline habitat	NA	NA	NA	NA	NA
Archaeal and methanogenic communities response under bioturbation and oil co	France	Marine sediment	NA	NA	NA	NA	NA
Archaeal communities in mangrove soil characterized by 16S rRNA gene clone	China	Mangrove sediment	1	NA	3	NA	NA
Archaeal Diversity and Lipid Biomarker Profiles in Marine Sediments in the So	South China Sea, China	Marine sediment	NA	NA	NA	NA	NA
Archaeal Diversity in Permafrost Deposits of Bunger Hills Oasis and King Geo	Antarctic	Others	NA	NA	NA	NA	NA
Archaeal diversity in sediments of Victoria Harbour and its adjacent areas	Victoria Harbour, Hong Kong	Marine sediment	NA	NA	NA	NA	NA
Archaeal diversity patterns in relation to hydrocarbon seepage in the Gulf of Me	Gulf of Mexico, Atlantic Ocean	Marine sediment	NA	NA	NA	NA	NA
Biomarker indicators for anaerobic oxidizers of methane in brackish-marine sed	Lagoa Vermelha, Brazil	Marine sediment	NA	NA	NA	NA	NA
Characterization and spatial distribution of methanogens and methanogenic biosı	Exportadora De Sal, S.A. (ESSA)	Hypersaline habitat	NA	NA	NA	NA	NA
Characterization of microbial diversity associated with sulfate-methane transitio	Ulleung Basin, Korea	Marine sediment	NA	NA	NA	NA	NA
Characterizing archaeal diversity and community structure in the surface sedim	Pearl River, China	Estuarine sediment	NA	NA	NA	NA	NA
Community structure of archaea in a freshwater estuarine wetland	Chongqing, China	Estuarine sediment	NA	NA	NA	NA	NA
Comparative study of archaeal diversity in deep marine subsurface sediments o	Nankai Trough, Pacific ocean	Marine sediment	NA	NA	NA	NA	NA
Comparison of microbial communities from deep-sea mud volcanoes in the east	Napoli mud volcano, Eastern Mediterra	Mud volcano	2	2	2	NA	NA
Composition of eukaryotic and prokaryotic rRNA gene phylotypes in guts of ad	Mediterranean Sea	Estuarine sediment	NA	NA	NA	NA	NA
Cultivation of methanogenic community from subseafloor sediments using a con	Japan, Pacific ocean	Marine sediment	NA	NA	NA	NA	NA
Deep-sea benthic archaea recycle relic membrane lipids for their growth	Sagami Bay, Japan	Marine sediment	NA	NA	NA	NA	NA
Different archaeal community composition in root surfaces of Ruppia spp. and I	Lucio del Cangrejo, Spain	Soils	NA	NA	NA	NA	NA
Distribution and phylogenetic diversity of cbbM genes encoding RubisCO form	Suiyo seamount, Pacific Ocean	Hydrothermal habitat	2	3	2	NA	NA
Diversity and abundance of aerobic and anaerobic methane oxidizers at the Haa	Barents Sea, Arctic Ocean	Mud volcano	NA	NA	NA	NA	NA
Diversity and abundance of Bacteria and Archaea in the Bor Khlueng Hot Spri	Bor Khlueng Hot Spring, Thailand	Hot spring	2	3	2	1	NA
Diversity and abundance of functional genes (mcrA, nirS and dsrAB/dsrA gene	Oujiang river, China	Freshwater sediment	NA	NA	NA	NA	NA
Diversity and Distribution of Microbial Communities Potentially Involved in Ana	Okhotsk Sea, Pacific Ocean	Cold seep	NA	NA	NA	NA	NA
Diversity and stratification of archaea in a hypersaline microbial mat	Guerrero Negro	Hypersaline habitat	NA	NA	NA	NA	NA
Diversity of Achaea Communities in Mud Wedge Sediments From Yellow Rive	Yellow River Delta,China	Estuarine sediment	NA	NA	NA	NA	NA
Diversity of Archaea and methanogens in estuarine sediments along a natural sa	Colne Estuary, United Kingdom	Estuarine sediment	NA	NA	NA	NA	NA
Diversity of archeal community from Brazilian mangrove soils	Brazli	Mangrove sediment	NA	NA	NA	NA	NA
Effects of Gas Hydrates on Archaeal Community Structure and Carbon Cycle i	Gulf of Mexico, Atlantic Ocean	Marine sediment	NA	NA	NA	NA	NA
Genotyping of uncultured archaea in a polluted site of Suez Gulf, Egypt, based o	Suez Gulf, Egypt	Marine sediment	NA	NA	NA	NA	NA
Hydrogen and bioenergetics in the Yellowstone geothermal ecosystem	Yellowston Park, USA	Freshwater	NA	NA	NA	NA	NA
Impact of natural oil and higher hydrocarbons on microbial diversity, distribution	Gulf of Mexico, Atlantic Ocean	Cold seep	NA	NA	NA	NA	NA
Investigating anaerobic methane oxidation in Lake Kinneret using geochemical a	Lake Kinneret, Israel	Freshwater sediment	NA	NA	NA	NA	NA
Linking microbial community structure to the S, Fe and N biogeochemical cyclin	Tengchong geothermal fields, China	Hot spring	NA	NA	NA	NA	NA
Lipid biomarker and phylogenetic analyses to reveal archaeal biodiversity and di	Guerrero Negro, Baja California Sur	Hypersaline habitat	NA	NA	NA	NA	NA
Metagenomic analysis of anoxic zone from hydropower plant reservoir in Brazil	Amazon, Brazil	Freshwater sediment	NA	NA	NA	NA	NA
Methane turnve fault (Marmara Sea)	Marmara Sea, Turkey	Cold seep	NA	NA	NA	NA	NA
Microbial assemblages associated with Thioploca sheaths from cold seep setting	Monterey Bay, Pacific Ocean	Cold seep	NA	NA	NA	NA	NA
Microbial communities associated with dolomite formation in a hypersaline lago	Lagoa Vermelha, Brazil	Hypersaline habitat	NA	NA	NA	NA	NA
Microbial communities in the shallow hydrothermal field off Kueishan Island, Ta	Kueishan Island, Taiwan	Hydrothermal habitat	NA	NA	NA	NA	NA
Microbial Communities Reduce Methane Efflux in Mud Volcano Sediments in t	Gulf of Cadiz, Atlantic Ocean	Mud volcano	NA	NA	NA	NA	NA
Microbial community structure and methane-cycling activity of subsurface sedir	Mississippi Canyon, Atlantic Ocean	Marine sediment	NA	NA	NA	NA	NA
Microbial community structure in the oxygen minimum zone of the Northeast su	Northeast subarctic Pacific Ocean	Marine water	NA	NA	NA	NA	NA
Microbial community structures associated with subseafloor sediments off Shim	Shimokita Peninsula	Marine sediment	NA	NA	NA	NA	NA
Microbial community variation in pristine and polluted nearshore Antarctic sedir	Antarctic	Marine sediment	NA	NA	NA	NA	NA
Microbial diversity and community composition of four subseafloor sediments fr	Barents Sea, Arctic Ocean	Marine sediment	NA	NA	NA	NA	NA
Microbial diversity and community structure in deeply buried coral carbonates a	Porcupine Seabight, Atlantic Ocean	Marine sediment	NA	NA	NA	NA	NA
Microbial Diversity Associated with a Paralvinella sulfincola Tube and the Adja	Juan de Fuca Ridge, Pacific Ocean	Hydrothermal habitat	2	3	2	NA	NA
Microbial diversity in alkaline hot springs of Ambitle Island, Papua New Guinea	Ambitle Island, Papua New Guinea	Hot spring	NA	NA	NA	NA	NA
Microbial diversity in surface sediments of the Xisha Trough, the South China S	Xisha Trough, Pacific Ocean	Marine sediment	NA	NA	NA	NA	NA
Molecular and isotopic composition of intact lipid biomarkers in anoxic estuarine	White Oak River, USA	Estuarine sediment	NA	NA	NA	NA	NA
Molecular and microbial ecology of the Grotta Azzurra of Palinuro Cape (Salern	Grotta Azzurra of Palinuro Cape, Italy	Others	NA	NA	NA	NA	NA
Molecular diversity of Archaea in tropical estuarine sediments	Santos-Sao Vicente estuary, Brazil	Estuarine sediment	NA	NA	NA	NA	NA
Molecular Microbial Diversity of Archaea and Bacteria along the Tropical Wes	India	Marine sediment	NA	NA	NA	NA	NA
Novel microbial diversity retrieved by an autonomous rover in the world's deepe	El Zacaton, Mexico	Others	NA	NA	NA	NA	NA
Photosynthesis versus exopolymer degradation in the formation of microbialites	Kiritimati, Republic of Kiribati	Others	NA	NA	NA	NA	NA
Prokaryotic Abundance and Community Composition in a Freshwater Iron-Rich	Hiroshima, Japan	Freshwater sediment	1	2	2	1	NA
Prokaryotic communities of the top 1 m below sea floor sediment in an eastern	Amsterdam mud volcano, Mediterrane	Mud volcano	NA	NA	NA	NA	NA
Prokaryotic community structure and diversity in the sediments of an active sub	Anaximander Mountains, East Mediter	Mud volcano	NA	NA	NA	NA	NA

Library/study	Site location	Biotope	Salinity	Temperatur	Life style	pH	Depth (m
Recording of climate and diagenesis through sedimentary DNA and fossil pigme	Laguna Potrok Aike, Argentina	Freshwater sediment	NA	NA	NA	NA	NA
Seasonal variation of particle-associated and free-living prokaryotic communitie	Gulf of Trieste, Northern Adriatic Sea	Marine water	NA	NA	NA	NA	NA
soil of JingHe saltworks belt in the Lake Ebinur	Lake Ebinur, China	Soils	NA	NA	NA	NA	NA
Spatial and temporal changes in microbial diversity of the Marmara Sea Sedime	Marmara Sea, Turkey	Marine sediment	2	2	2	NA	NA
Spatial and Temporal Changes in the Microbial Communities of Lithifying and N	Bahamas	Others	NA	NA	NA	NA	NA
Spatial distribution of viruses associated with planktonic and attached microbial	Okinawa, Japan	Hydrothermal habitat	NA	NA	NA	NA	NA
Spatial structure and activity of sedimentary microbial communities underlying a	Gulf of Mexico, Atlantic Ocean	Cold seep	NA	NA	NA	NA	NA
Studies on the archaeal diversity in the coconut husk retting zone, Kerala, India	Kerala, India	Soils	NA	NA	NA	NA	NA
The archaea community patterns from sediments of Poyang Lake, China	Poyang Lake, China	Freshwater sediment	NA	NA	NA	NA	NA
The Community Structure of Archaea in Deep Sea Sediment of the Ulleung Ba	Ulleung Basin, Korea	Marine sediment	NA	NA	NA	NA	NA
The Dark Side of the Mushroom Spring Microbial Mat: Life in the Shadow of C	NA	Hot spring	NA	NA	NA	NA	NA
The study of taxonomic composition of microorganisms in surface sediments an	Lake Baikal, Russia	Freshwater sediment	NA	NA	NA	NA	NA
Thermal and geochemical zonation of microbial biogeography in Guaymas Basin	Guaymas Basin, USA	Hydrothermal habitat	NA	NA	NA	NA	NA
Three spatial distribution of microbial communities in the Lei-Gong-Huo mud vo	Lei-Gong-Huo mud volcano, Taiwan	Mud volcano	NA	NA	NA	NA	NA
Tropical aquatic archaea show environment-specific community composition	Ilha Grande, Brazil	Freshwater	NA	NA	NA	NA	NA
Uncultivated archaea from sulfate-reducing cave biofilm	Frasassi cave, Italian	Freshwater	NA	NA	NA	NA	NA
Unexpected diversity and complexity of the Guerrero Negro hypersaline microb	Guerrero Negro	Hypersaline habitat	NA	NA	NA	NA	NA
Vertical distribution and diversity of bacteria and archaea in methane-rich cold s	Okhotsk Sea, Pacific Ocean	Marine sediment	NA	NA	NA	NA	NA
Vertical distribution of prokaryotes and responses to their environment in Hongl	Honghu Lake, China	Freshwater sediment	NA	NA	NA	NA	NA
Archaeal diversity in ODP legacy borehole 892b and associated seawater and s	Cascadia margin, Pacific Ocean	Cold seep	2	1	2	NA	NA
Archaeal diversity in ODP legacy borehole 892b and associated seawater and s	Cascadia margin, Pacific Ocean	Cold seep	2	1	2	NA	600
Mariana forearc serpentine mud volcanos harbor novel communities of extremo	NA	Mud volcano	NA	NA	NA	NA	NA
Novel bacterial and archaeal lineages from an in situ growth chamber deployed	Snake Pit on, Mid-Atlantic Ridge	Hydrothermal habitat	2	3	2	NA	NA
Phylogenetic Diversity of the Archaeal Component in Microbial Mats on Coral-l	Black Sea, Atlantic Ocean	Cold seep	2	1	2	NA	NA
Retrieval of a million high-quality, full-length microbial 16S and 18S rRNA gene	Artificial pond at the Aalborg Universit	Freshwater sediment	NA	NA	NA	NA	NA
Retrieval of a million high-quality, full-length microbial 16S and 18S rRNA gene	Estuary of Mariagerfjord, Denmark.	Estuarine sediment	NA	NA	NA	NA	NA
Retrieval of a million high-quality, full-length microbial 16S and 18S rRNA gene	Madum lake, Denmark	Freshwater sediment	NA	NA	NA	NA	NA
Retrieval of a million high-quality, full-length microbial 16S and 18S rRNA gene	Nors lake, Denmark	Freshwater sediment	NA	NA	NA	NA	NA
Retrieval of a million high-quality, full-length microbial 16S and 18S rRNA gene	Poulstrup lake, Denmark	Freshwater sediment	NA	NA	NA	NA	NA
Retrieval of a million high-quality, full-length microbial 16S and 18S rRNA gene	Seashore close to Dokkedal, Denmark	Marine sediment	NA	NA	NA	NA	NA
Retrieval of a million high-quality, full-length microbial 16S and 18S rRNA gene	Seashore of Fanø, Denmark	Marine sediment	NA	NA	NA	NA	NA
Retrieval of a million high-quality, full-length microbial 16S and 18S rRNA gene	Ulvedybet in Limfjorden, Denmark	Marine sediment	NA	NA	NA	NA	NA
Retrieval of a million high-quality, full-length microbial 16S and 18S rRNA gene	Ulvedybet in Limfjorden, Denmark	Marine sediment	NA	NA	NA	NA	NA
Retrieval of a million high-quality, full-length microbial 16S and 18S rRNA gene	Voer Å, Denmark	Freshwater sediment	NA	NA	NA	NA	NA
Stratification of archaea in the deep sediments of a freshwater meromictic lake:	Lake Pavin, France	Freshwater sediment	1	1	2	NA	NA
The extent of protist diversity: insights from molecular ecology of freshwater eul	NA	Freshwater	NA	NA	NA	NA	NA

For samples collected from marine sediments without specific instructions, the salinity, temperature, and life style scores are presumed to be 2, 1, and 2, respectively. Relative abundance values are from published papers.

Supplementary Table 2. Characteristics of groups within the Asgard archaea.

Groups and subgroups	Minimum intragroup similarity (%)	Number of OTUs	Number of DNA sequences	Number of RNA sequences	RNA proportion (%)	Bootstrap value
Kariarchaeota	81	7	1	157	99.4	100
Balderarchaeota	88	4	0	27	100	100
Hodarchaeota	78	4	0	24	100	100
Lagarchaeota	78	9	0	351	100	100
Gerdarchaeota	85	8	1	97	99.0	100
Lokiarchaeota-1	86	16	12	49	80.3	100
Lokiarchaeota-2	80	121	117	1771	93.8	100
Lokiarchaeota-3	88	28	47	873	94.9	96
Lokiarchaeota-4	83	200	4238	1784	29.7	88
Thorarchaeota	86	13	14	391	96.5	100
Odinarchaeota	92	4	4	0	0	100
Heimdallarchaeota-AAG	87	11	192	78	28.9	100
Heimdallarchaeota-MHVG	80	5	3	5	62.5	100
Heimdallarchaeota	71	16	195	83	29.8	NA
Lokiarchaeota (1-4)	80	365	4414	4477	50.4	98
ungrouped	NA	33	17	199	92.1	NA

Supplementary Table 3. The 16S rRNA gene identity (%) of Asgard groups.

Groups/subgroups	OTUs	Balderarchaeota				Hodarchaeota				Kariarchaeota						Lagarchaeota									Gerdarchaeota					
		P0106434 06	P0107684 81	P0107772 15	P0107809 72	P0106967 48	P0107430 07	P0108456 64	P0108559 42	P0107942 68	P0113005 13	P0107042 39	P0108520 77	P0109197 44	P0106631 14	P0101903 42	P0114522 07	P0102360 85	P0109190 98	P0110414 46	P0110710 51	P0109294 60	P0102583 42	P0112970 44	P0109075 79	P0108535 00	P0108054 04	P0113413 76	P0108271 44	P0113292 19
Balderarchaeota	OBEP0106434	100.0	91.1	94.9	99.0	68.1	68.8	68.5	69.3	71.7	70.3	71.6	70.0	71.4	71.5	70.4	70.8	70.4	71.2	70.3	70.1	71.1	70.3	72.3	70.5	71.1	71.7	72.2	71.3	71.7
	OBEP0107684	91.1	100.0	91.2	91.0	68.3	68.6	69.0	69.3	70.1	69.2	70.6	68.9	70.2	70.0	69.7	70.8	70.8	71.5	70.3	70.1	71.3	70.7	72.5	69.9	69.4	70.3	70.9	71.4	70.2
	OBEP0107772	94.9	91.2	100.0	95.1	68.4	68.8	68.5	69.3	71.4	70.0	71.3	69.9	71.0	71.6	70.7	70.6	71.0	71.2	70.8	69.9	71.1	70.8	71.9	70.0	70.0	71.2	71.5	70.7	71.1
	OBEP0107809	99.0	91.0	95.1	100.0	68.1	69.1	68.5	69.4	71.5	70.1	71.4	69.8	71.1	71.3	70.3	70.8	70.6	71.3	70.6	70.2	71.2	70.5	72.3	70.5	71.2	71.8	72.2	71.4	71.8
Hodarchaeota	OBEP0106967	68.1	68.3	68.4	68.1	100.0	80.8	96.6	93.1	70.6	69.2	70.9	69.4	69.6	69.8	74.2	73.5	72.9	72.7	71.1	70.3	72.6	72.5	70.3	69.4	69.7	69.6	70.6	69.3	69.4
	OBEP0107430	68.8	68.6	68.8	69.1	80.8	100.0	80.6	80.2	70.5	68.3	69.9	69.2	69.9	70.6	71.4	72.5	71.4	71.5	69.1	70.0	71.5	71.1	71.2	69.5	69.4	70.4	69.7	68.6	70.2
	OBEP0108456	68.5	69.0	68.5	68.5	96.6	80.6	100.0	95.6	70.9	68.7	70.9	69.4	70.1	70.3	74.5	74.2	72.9	73.4	72.1	71.5	73.3	72.7	71.0	69.4	69.9	69.8	70.8	69.1	69.6
	OBEP0108559	69.3	69.3	69.3	69.4	93.1	80.2	95.6	100.0	71.2	69.5	70.8	69.3	70.9	70.7	73.1	73.5	72.2	72.8	71.4	71.0	72.7	72.0	71.0	70.5	71.3	71.0	72.2	70.7	70.8
Kariarchaeota	OBEP0107942	71.7	70.1	71.4	71.5	70.6	70.5	70.9	71.2	100.0	92.2	89.0	94.0	93.0	94.4	78.0	77.8	77.2	77.1	75.5	74.6	77.0	77.1	76.2	76.1	75.8	76.8	76.9	75.0	76.6
	OBEP0113005	70.3	69.2	70.0	70.1	69.2	68.3	68.7	69.5	92.2	100.0	87.8	94.5	91.0	92.0	77.1	76.4	76.3	76.4	74.9	74.3	76.2	76.0	74.0	74.9	74.6	75.4	74.9	73.8	75.4
	OBEP0107042	71.6	70.6	71.3	71.4	70.9	69.9	70.9	70.8	89.0	87.8	100.0	89.1	88.0	89.1	78.5	79.0	78.7	78.0	76.6	76.1	77.9	78.3	77.2	76.6	76.4	77.2	78.0	76.9	77.2
	OBEP0108520	70.0	68.9	69.9	69.8	69.4	69.2	69.4	69.3	94.0	94.5	89.1	100.0	94.2	94.0	77.8	77.4	77.1	77.4	75.1	74.8	77.2	76.8	74.8	75.2	74.8	76.0	75.7	74.0	76.0
	OBEP0109197	71.4	70.2	71.0	71.1	69.6	69.9	70.1	70.9	93.0	91.0	88.0	94.2	100.0	95.8	76.8	78.0	77.0	77.4	75.2	74.2	77.3	76.8	75.8	75.7	75.5	76.2	77.3	75.0	76.2
	OBEP0106631	71.5	70.0	71.6	71.3	69.8	70.6	70.3	70.7	94.4	92.0	89.1	94.0	95.8	100.0	77.0	77.9	77.1	77.5	75.6	74.4	77.3	76.9	75.8	76.1	76.2	76.6	77.3	74.9	76.6
Lagarchaeota	OBEP0101903	70.4	69.7	70.7	70.3	74.2	71.4	74.5	73.1	78.0	77.1	78.5	77.8	76.8	77.0	100.0	91.7	92.8	91.5	86.9	86.2	91.7	92.3	85.1	76.5	75.9	77.7	77.5	76.4	77.5
	OBEP0114522	70.8	70.8	70.6	70.8	73.5	72.5	74.2	73.5	77.8	76.4	79.0	77.4	78.0	77.9	91.7	100.0	90.3	92.7	87.5	86.5	92.8	89.8	85.6	76.2	75.9	77.5	77.8	76.4	77.3
	OBEP0102360	70.4	70.8	71.0	70.6	72.9	71.4	72.9	72.2	77.2	76.3	78.7	77.1	77.0	77.1	92.8	90.3	100.0	91.4	86.9	86.1	91.5	99.5	84.8	74.9	75.9	76.3	77.1	75.3	76.3
	OBEP0109190	71.2	71.5	71.2	71.3	72.7	71.5	73.4	72.8	77.1	76.4	78.0	77.4	77.4	77.5	91.5	92.7	91.4	100.0	88.5	87.5	99.8	91.1	86.4	76.4	76.3	77.9	77.8	76.1	77.8
	OBEP0110414	70.3	70.3	70.8	70.6	71.1	69.1	72.1	71.4	75.5	74.9	76.6	75.1	75.2	75.6	86.9	87.5	86.9	88.5	100.0	93.0	88.5	86.8	84.6	74.6	74.0	76.7	75.0	73.8	76.7
	OBEP0110710	70.1	70.1	69.9	70.2	70.3	70.0	71.5	71.0	74.6	74.3	76.1	74.8	74.2	74.4	86.2	86.5	86.1	87.5	93.0	100.0	87.5	85.8	85.7	74.0	73.6	75.4	75.4	73.8	75.4
	OBEP0109294	71.1	71.3	71.1	71.2	72.6	71.5	73.3	72.7	77.0	76.2	77.9	77.2	77.3	77.3	91.7	92.8	91.5	99.8	88.5	87.5	100.0	91.2	86.4	76.5	76.4	78.0	78.0	76.2	77.8
	OBEP0102583	70.3	70.7	70.8	70.5	72.5	71.1	72.7	72.0	77.1	76.0	78.3	76.8	76.8	76.9	92.3	89.8	99.5	91.1	86.8	85.8	91.2	100.0	84.5	74.8	75.6	76.0	76.8	75.0	76.0
	OBEP0112970	72.3	72.5	71.9	72.3	70.3	71.2	71.0	71.0	76.2	74.0	77.2	74.8	75.8	75.8	85.1	85.6	84.8	86.4	84.6	85.7	86.4	84.5	100.0	75.0	74.6	76.4	76.9	75.7	76.3
Gerdarchaeota	OBEP0109075	70.5	69.9	70.0	70.5	69.4	69.5	69.4	70.5	76.1	74.9	76.6	75.2	75.7	76.1	76.5	76.2	74.9	76.4	74.6	74.0	76.5	74.8	75.0	100.0	93.6	94.8	94.6	93.6	94.6
	OBEP0108535	71.1	69.4	70.0	71.2	69.7	69.4	69.9	71.3	75.8	74.6	76.4	74.8	75.5	76.2	75.9	75.9	75.9	76.3	74.0	73.6	76.4	75.6	74.6	93.6	100.0	92.6	92.8	92.8	92.4
	OBEP0108054	71.7	70.3	71.2	71.8	69.6	70.4	69.8	71.0	76.8	75.4	77.2	76.0	76.2	76.6	77.7	77.5	76.3	77.9	76.7	75.4	78.0	76.0	76.4	94.8	92.6	100.0	93.4	92.2	99.8
	OBEP0113413	72.2	70.9	71.5	72.2	70.6	69.7	70.8	72.2	76.9	74.9	78.0	75.7	77.3	77.3	77.5	77.8	77.1	77.8	75.0	75.4	78.0	76.8	76.9	94.6	92.8	93.4	100.0	93.9	93.2
	OBEP0108271	71.3	71.4	70.7	71.4	69.3	68.6	69.1	70.7	75.0	73.8	76.9	74.0	75.0	74.9	76.4	76.4	75.3	76.1	73.8	73.8	76.2	75.0	75.7	93.6	92.8	92.2	93.9	100.0	92.0
	OBEP0113292	71.7	70.2	71.1	71.8	69.4	70.2	69.6	70.8	76.6	75.4	77.2	76.0	76.2	76.6	77.5	77.3	76.3	77.8	76.7	75.4	77.8	76.0	76.3	94.6	92.4	99.8	93.2	92.0	100.0
Heimdallarchaeota-AAG	KP091041	71.6	71.0	71.1	71.6	71.5	71.3	72.7	72.2	71.2	71.3	72.8	70.1	70.5	71.1	73.9	74.2	73.6	74.8	74.9	73.8	74.7	73.1	73.6	72.8	71.9	73.7	72.9	72.2	73.6
	AB019716	70.4	69.2	70.4	70.1	71.9	71.5	72.9	72.2	71.7	71.4	72.6	70.1	70.5	71.1	75.8	75.8	74.7	75.6	74.8	73.4	75.6	74.2	73.4	72.7	71.6	73.1	73.2	72.2	73.0
	AB797480	71.3	70.1	71.0	71.1	71.6	71.6	72.2	71.9	72.5	71.7	73.0	71.0	71.5	71.8	74.6	74.6	73.7	74.8	74.2	73.2	74.8	73.2	73.2	73.1	72.2	74.0	73.3	72.0	73.9
	OBEP0108637	70.8	70.2	70.4	70.5	71.1	70.6	71.6	71.3	71.7	71.2	72.2	70.1	70.7	71.3	74.5	74.8	73.9	74.8	74.3	73.2	74.8	73.4	73.6	72.2	71.2	73.5	72.6	71.6	73.4
	JX000838	71.8	70.8	71.1	71.7	70.6	70.7	71.9	71.8	71.1	71.1	72.1	70.1	70.3	70.8	73.2	73.3	73.0	74.1	74.7	73.5	74.1	72.7	73.4	72.9	71.6	73.9	72.6	71.9	73.8
	DQ640139	71.4	70.6	71.1	71.1	71.1	71.5	71.4	71.4	71.8	71.4	72.8	70.4	70.9	71.1	74.3	74.7	73.6	75.0	74.0	72.9	74.9	73.1	73.6	72.7	71.8	73.7	72.9	72.2	73.6
	GU553642	72.1	71.2	71.7	71.8	71.5	71.5	72.2	72.5	72.0	71.1	72.5	70.2	70.6	71.2	74.0	74.6	73.7	75.0	74.4	73.1	74.9	73.2	73.6	73.1	71.9	74.4	73.3	72.4	74.3
	JQ817966	72.1	71.2	71.3	71.9	71.0	71.2	72.2	72.2	71.3	71.4	72.4	70.2	70.6	71.1	73.3	73.5	73.0	74.3	74.5	73.4	74.2	72.7	73.4	73.1	71.6	74.0	72.8	71.9	73.9
	AB797473	71.5	70.2	71.4	71.3	72.3	71.6	72.8	72.5	72.2	71.0	72.6	70.4	70.9	71.7	74.5	74.6	73.5	74.7	74.3	73.2	74.7	73.1	73.3	73.4	72.3	74.4	74.0	72.4	74.3
Heimdallarchaeota-MHVG	OBEP0113160	69.7	68.6	68.8	70.0	68.0	67.7	69.2	69.2	77.0	76.5	77.3	77.0	76.4	76.8	73.2	73.3	73.0	73.5	73.6	73.3	73.3	72.9	72.2	73.4	72.8	72.8	73.7	71.6	72.8
	OBEP0109184	69.8	67.9	69.4	70.2	66.9	68.2	68.3	68.4	76.4	75.7	76.5	76.2	76.5	76.3	73.2	73.0	72.5	73.9	73.3	73.0	73.8	72.5	72.3	73.3	72.0	72.5	73.8	71.6	72.5
	JX000774	68.6	66.9	68.2	68.5	68.4	68.1	69.8	69.7	75.9	75.2	75.5	75.8	75.6	76.3	72.6	72.4	72.3	73.5	73.1	72.2	73.4	72.1	73.0	71.2	71.1	71.2	72.6	71.7	71.2
	JQ989558	68.1	66.6	68.3	68.4	67.7	67.6	68.6	68.9	75.8	75.0	75.3	75.5	75.7	75.9	72.1	72.8	72.4	73.6	73.4	72.6	73.4	72.3	72.9	72.0	72.1	72.1	73.5	72.1	72.1
Lokiarchaeota-1	OBEP0113942	73.5	72.5	71.9	73.0	72.6	70.9	73.0	72.9	79.1	78.1	80.7	78.9	79.5	80.0	82.4	84.6	81.9	83.9	81.9	81.9	83.7	81.4	82.2	78.2	77.7	79.2	79.8	77.8	79.2
	OBEP0113539	74.0	72.5	72.2	73.5	72.8	71.1	73.6	73.7	79.0	77.6	80.4	78.5	79.1	80.0	81.8	84.1	81.0	83.2	81.5	81.1	83.0	80.5	82.2	78.5	78.0	79.6	80.0	77.8	79.6
	KC682077	72.8	71.9	71.5	72.4	72.3	72.1	73.3	73.5	78.7	77.7	79.1	78.0	78.7	79.8	81.8	83.5	81.7	83.9	81.5	81.1	83.8	81.3	81.8	76.9	76.9	78.0	78.5	77.1	78.0
	AB019721	73.6	72.1	72.2	73.0	72.5	69.8	72.9	72.5	78.8	77.5	79.7	78.0	78.7	79.5	82.0	82.8	81.0	83.3	81.3	81.5	83.1	80.7	82.2	78.2	77.8	79.0	79.6	77.9	79.0
	OBEP0111331	72.6	71.8	71.6	72.3	72.1	71.5	73.2	73.2	78.8	77.8	79.0	78.2	78.6	79.7	82.0	83.6	81.6	83.8	81.4	81.0	83.7	81.2	81.5	76.8	76.7	77.8	78.3	76.5	77.8
	OBEP0110508	72.9	71.8	71.6	72.5	72.6	71.9	73.1	73.3	78.1	77.2	78.9	77.8	78.2	79.4	81.8	83.6	81.6	84.2	81.5	81.1	84.0	81.2	81.7	77.1	77.3	78.2	78.6	77.3	78.2
	OBEP0108298	73.8	72.6	72.7	73.4	72.6	71.5	73.5	73.5	78.8	78.0	79.2	78.5	78.8	79.9	81.8	83.4	81.5	84.0	81.0	80.8	83.8	81.1	81.3	78.2	77.6	78.8	79.3	77.5	78.8
	OBEP0106817	73.8	72.9	72.6	73.2	71.7	70.2	72.3	72.4	78.0	76.7	78.8	77.4	77.8	78.6	81.2	82.8	80.6	82.5	80.6	80.4	82.4	80.3	81.9	77.4	77.1	78.6	78.8	77.1	78.6
	OBEP0113070	73.3	72.3	72.2	72.8	71.6	70.3	72.6	72.7	79.3	77.7	80.1	78.7	79.2	80.1	81.6	83.8	80.8	83.5	81.2	81.0	83.3	80.4	82.6	78.2	77.7	79.4	79.7	77.5	79.4
Lokiarchaeota-2	OBEP0108224	73.7	73.2	72.8	73.5	71.7	71.6	72.9	72.8	77.8	76.2	78.3	77.3	77.5	78.3	82.0	84.4	82.2	84.3	82.0	81.3	84.1	81.7	82.1	77.6	76.7	79.0	79.3	77.0	79.0
	OBEP0106850	72.8	72.9	72.1	72.6	71.9	71.6	73.1	72.5	77.6	76.6	79.0	77.6	77.7	78.4	82.1	84.2	81.3	84.1	82.1	81.0	83.9	80.9	82.2	77.4	76.5	78.5	79.0	76.9	78.5
	OBEP0110437	72.8	72.3	71.8	72.9	72.8	71.8	73.6	72.4	78.3	76.8	78.8	77.8	77.9	78.8	81.3	84.3	81.6	84.1	81.7	80.9	83.9	81.2	81.4	77.6	76.6	78.3	79.1	76.6	78.3
	OBEP0112409	72.8	72.3	72.1	72.7	71.4	71.2	72.7	72.1	78.1	76.6	79.4	77.8	78.2	78.6	81.5	83.8	80.8	83.1	80.9	80.2	82.9	80.4	81.6	77.7	76.6	78.8	79.5	77.0	78.8
	KJ569649	73.1	72.7	72.6	72.9	72.0	72.1	73.2	73.0	78.0	76.9	79.3	77.6	77.9	78.6	82.2	84.2	81.9	84.2	82.1	81.0	84.1	81.4	82.3	77.2	76.3	78.8	78.7	76.8	78.8
	OBEP0112264	72.8	72.8	72.5	72.8	71.9	71.6	73.1	72.9	77.8	77.0	78.9	77.9	77.8	78.3	82.0	84.4	81.6	84.0	82.0	81.1	83.9	81.1	81.9	77.3	76.4	78.8	79.0	76.8	78.8
	OBEP0100591	72.9	72.7	72.5	72.6	71.9	71.2	73.1	72.7	77.9	76.7	78.8	77.6	77.7	78.5	81.7	84.4	82.0	83.8	81.6	81.1	83.6	81.5	82.2	77.7	76.7	78.9	79.0	76.9	78.9
	OBEP0108873	72.8	72.8	72.5	72.8	72.0	71.8	73.2	73.0	78.1	77.1	79.0	78.0	77.9	78.6	82.3	84.8	81.7	84.3	82.3	81.2	84.2	81.2	82.0	77.7	76.8	79.1	79.1	76.9	79.1
	OBEP0112637	73.2	72.7	72.3	73.0	72.7	71.9	73.2	73.6	79.3	77.7	79.3	78.8	79.1	79.7	81.9	84.8	82.0	84.4	82.5	81.5	84.3	81.5	82.3	79.7	78.8	80.5	81.0	78.7	80.5
	JQ989629	72.7	72.3	72.1	72.6	71.8	71.1	72.9	72.7	77.6	76.4	78.7	77.1	77.1	78.0	81.6	83.3	81.4	83.8	81.4	80.7	83.6	80.9	82.0	77.3	76.4	78.6	79.0	76.7	78.6
	OBEP0108657	73.0	72.6	72.3	73.0	72.6	72.0	73.5	73.3	77.8	76.4	78.4	77.5	77.3	78.2	81.9	84.4	81.9	84.1	81.8	81.6	83.9	81.4	81.9	77.8	77.0	79.0	79.4	77.4	79.0
	OBEP0108465	72.5	72.2	72.0	72.4	71.3	71.2	72.5	72.0	78.0	76.3	79.1	77.7	78.3	78.6	81.4	83.7	81.0	83.1	81.0	80.0	82.9	80.6	81.6	77.5	76.4	78.7	79.4	76.7	78.7
	OBEP0106792	73.1	72.6	72.6	73.0	71.7	71.4	73.0	72.8	77.3	76.1	78.4	77.0	77.2	77.9	81.6	83.7	81.8	83.8	81.5	81.0	83.7	81.3	81.8	77.4	76.5	78.6	79.3	76.9	78.6
	OBEP0113039	73.2	72.6	72.3	73.2	72.3	71.9	73.5	73.1	78.2	77.1	79.0	78.0	78.1	78.8	81.8	84.5	81.7	84.0	82.2	81.4	83.9	81.2	81.8	78.4	77.7	79.8	79.5	77.2	79.8
	AB019720	73.2	72.8	72.7	73.0	72.0	72.2	73.2	73.0	78.2	77.1	79.2	77.8	78.1	78.8	82.1	84.0	81.8	84.2	82.1	81.0	84.1	81.3	82.4	77.3	76.4	78.9	78.8	76.9	78.9
Lokiarchaeota-3	OBEP0100530	72.8	72.3	72.0	72.7	70.8	69.7	71.5	71.5	77.3	76.5	78.2	77.0	77.4	78.3	80.2	81.9	79.7	82.0	80.6	79.1	81.8	79.4	80.0	76.7	76.6	78.2	78.6	76.4	78.2
	OBEP0101668	72.7	72.1	71.7	72.5	71.7	70.4	72.2	72.5	78.1	76.9	79.0	77.7	77.9	78.9	80.9	83.4	81.0	82.9	81.0	80.4	82.8	80.5	80.8	77.6	77.0	78.5	79.4	77.3	78.5
	OBEP0102313	72.3	71.7	71.5	72.2	71.5	70.0	71.9	72.0	78.0	76.7	78.2	77.4	77.3	78.5	81.0	82.9	80.9	82.8	80.7	79.9	82.7	80.4	79.8	76.8	76.7	77.8	78.8	76.7	77.8
	OBEP0110714	72.2	71.4	71.0	72.0	71.8	70.0	72.4	72.1	78.7	77.4	78.1	77.4	77.6	78.8	79.8	82.0	79.1	81.7	80.6	78.9	81.5	78.8	78.8	77.6	76.6	79.0	79.0	76.3	79.0
	OBEP0112264	72.5	72.0	71.2	72.2	71.1	70.4	71.8	71.9	77.4	76.4	78.3	77.1	77.4	78.2	80.3	82.8	80.3	82.5	80.4	79.2	82.4	79.9	80.0	76.6	76.4	77.6	78.1	76.2	77.6
	OBEP0110576	71.9	72.2	71.4	71.8	71.1	70.6	71.7	72.3	77.2	76.4	77.3	76.8	77.3	78.0	80.6	83.1	80.2	82.2	80.8	80.0	82.0	79.9	80.1	77.7	77.1	78.7	78.8	77.1	78.7
	OBEP0100714	72.7	72.2	71.7	72.4	71.0	70.0	71.3	72.0	77.4	76.3	77.9	77.0	77.1	77.8	79.5	82.0	79.3	81.1	79.4	78.9	80.9	78.9	79.0	76.5	76.7	77.4	78.7	76.6	77.4
	OBEP0113924	73.3	72.7	72.1	73.1	71.5	70.8	72.2	72.2	78.5	76.9	78.8	77.5	77.9	78.8	80.4	83.0	80.8	82.8	80.9	79.9	82.7	80.4	80.1	77.4	77.0	78.6	78.9	77.0	78.6
	OBEP0111211	71.3	71.0	70.5	71.3	71.9	70.8	72.4	72.9	77.7	77.1	78.4	77.9	78.4	78.9	80.7	83.2	81.0	83.1	81.1	80.3	83.0	80.5	80.3	76.6	76.7	77.8	78.4	76.3	77.8
	OBEP0110627	72.2	71.6	71.0	72.0	71.1	69.7	71.3	71.5	78.7	77.5	78.7	78.3	78.0	79.2	80.8	83.5	80.4	82.4	81.0	79.8	82.2	80.2	80.4	78.0	76.7	79.1	78.9	76.7	79.1
	OBEP0110597	72.0	71.3	70.9	71.9	71.4	71.0	72.1	72.5	77.6	77.3	78.8	78.3	78.1	78.5	81.0	83.2	80.9	83.1	81.1	80.2	82.9	80.4	80.8	76.8	76.6	78.0	78.5	76.6	78.0
	OBEP0111518	72.3	71.2	71.0	72.0	71.6	69.9	71.6	71.8	76.9	76.3	77.0	76.7	76.8	77.4	80.1	82.0	79.3	81.8	80.0	78.8	81.6	78.9	78.7	77.5	77.0	78.9	79.0	76.9	78.9
	OBEP0100244	73.2	72.6	72.1	73.0	71.1	70.0	71.9	71.8	77.7	76.8	78.6	77.4	77.7	78.5	80.3	82.2	80.2	82.4	80.8	79.4	82.2	79.9	80.3	77.0	76.8	78.2	78.8	76.7	78.2
	OBEP0110714	71.9	71.6	71.1	71.8	70.0	69.7	70.9	71.8	77.4	77.2	77.3	77.3	77.5	78.1	81.2	83.2	80.5	83.0	81.7	80.7	82.8	80.2	80.5	76.9	76.3	77.8	77.9	76.0	77.8
	OBEP0111127	72.6	72.0	71.6	72.6	71.9	71.2	72.6	72.7	78.5	77.4	79.3	78.0	78.0	79.2	81.4	83.9	81.2	83.2	81.0	80.8	83.0	80.8	81.3	77.6	76.9	78.6	79.3	76.7	78.6
	OBEP0112829	73.3	72.7	72.0	73.1	71.6	70.8	72.3	72.3	78.5	77.0	78.8	77.6	77.8	78.7	80.6	83.3	81.1	83.1	81.1	80.2	83.0	80.6	80.3	77.2	76.8	78.6	78.9	76.8	78.6
	OBEP0110314	72.3	71.7	71.2	72.3	70.7	70.4	71.7	71.6	78.4	77.1	78.2	77.6	77.6	78.6	80.8	83.6	80.5	82.3	81.4	80.8	82.2	80.2	80.3	77.5	76.3	78.7	78.5	76.2	78.7
	AF068822	72.4	71.7	71.3	72.2	71.6	70.4	72.0	72.5	77.7	76.9	78.9	77.5	77.9	78.7	80.7	83.2	80.7	82.7	81.0	79.8	82.6	80.3	80.1	77.4	77.0	78.7	79.3	77.0	78.7
	OBEP0111317	72.2	71.6	71.2	72.0	71.8	71.1	72.0	72.6	78.1	77.2	78.8	78.3	78.2	79.1	80.2	82.9	80.5	82.3	81.0	79.8	82.1	80.1	80.5	76.7	76.5	78.1	78.4	76.1	78.1
	AF419642	73.0	72.2	71.7	72.8	71.4	70.9	72.2	72.1	77.9	76.5	78.6	76.9	77.3	78.2	80.5	83.0	80.8	82.9	80.8	79.6	82.7	80.5	79.8	77.4	77.2	79.0	79.0	77.1	79.0
	OBEP0108758	72.1	71.3	70.4	71.9	70.6	69.5	71.1	71.1	77.7	76.7	77.2	77.1	76.8	77.8	79.6	81.7	79.8	81.3	80.2	79.4	81.1	79.3	78.6	75.9	76.1	77.3	77.6	75.9	77.3
	OBEP0111126	71.7	71.2	70.5	71.6	71.1	70.7	71.3	71.6	78.0	76.8	78.3	77.6	77.2	78.5	80.7	83.1	80.8	82.1	80.4	79.6	81.9	80.3	80.2	77.8	76.7	78.8	79.2	76.7	78.8
	OBEP0110637	71.8	71.2	71.3	71.8	71.0	70.2	71.6	71.8	78.7	77.3	78.4	77.8	78.2	78.8	81.0	83.5	80.8	82.6	81.4	80.1	82.4	80.5	80.7	77.7	76.3	78.5	79.0	76.6	78.5
	OBEP0102552	73.1	72.7	72.1	73.0	71.1	70.1	72.0	71.9	77.8	76.8	78.6	77.4	77.8	78.6	80.3	82.4	80.2	82.4	80.8	79.5	82.3	79.9	80.4	77.1	76.9	78.3	78.9	76.7	78.3
	OBEP0101481	72.1	71.4	71.0	71.9	71.3	70.7	72.0	72.4	78.2	77.4	79.3	78.4	78.6	79.4	80.8	83.4	80.8	82.8	81.1	80.4	82.7	80.4	80.6	76.9	76.8	78.2	78.5	76.6	78.2

Groups/subgroups		Balderarchaeota				Hodarchaeota				Kariarchaeota						Lagarchaeota									Gerdarchaeota					
	OTUs	P010643406	P010768481	P010777215	P010780972	P010696748	P010743007	P010845664	P010855942	P010794268	P011300513	P010704239	P010852077	P010919744	P010663114	P010190342	P011452207	P010236085	P010919098	P011041446	P011071051	P010929460	P010258342	P011297044	P010907579	P010853500	P010805404	P011341376	P010827144	P011329219
Lokiarchaeota-4	OBEP0108336	72.9	71.8	71.1	72.7	71.2	70.3	72.0	71.9	77.4	76.2	78.0	76.7	76.6	77.6	80.0	82.0	80.2	81.4	80.1	79.6	81.2	79.7	79.4	76.5	76.7	78.0	78.2	76.5	78.0
	OBEP0101481	73.3	72.6	72.0	73.1	71.9	70.5	72.6	72.8	77.8	77.2	79.0	77.7	77.7	78.7	80.9	83.1	80.8	82.9	81.1	79.9	82.7	80.4	80.5	77.1	76.8	78.3	78.7	76.8	78.3
	OBEP0110651	71.7	71.2	70.8	71.6	71.2	71.1	72.0	72.2	77.6	76.7	78.3	77.6	78.0	78.8	80.5	82.9	80.8	82.4	81.2	80.4	82.2	80.3	80.3	76.6	76.4	77.9	78.2	75.9	77.9
	OBEP0113317	72.8	72.4	71.8	73.2	72.1	70.6	72.5	72.4	78.1	77.2	78.4	77.2	77.6	78.2	80.6	82.5	80.0	82.3	80.6	79.0	82.1	79.6	80.0	76.9	76.4	78.1	78.6	76.3	78.1
	OBEP0107862	73.1	72.7	72.2	73.1	71.3	70.6	72.0	72.6	78.3	77.3	78.5	77.6	78.0	78.6	79.8	82.2	79.5	81.2	79.5	78.8	81.0	79.3	79.0	77.0	76.3	77.8	78.8	76.5	77.8
	OBEP0106579	72.8	71.7	71.5	72.6	71.3	70.7	72.0	72.2	78.4	77.1	79.4	78.0	78.4	79.3	80.7	83.1	80.6	82.9	81.0	80.1	82.8	80.3	80.9	77.1	76.9	78.5	79.1	76.7	78.5
	OBEP0110475	72.0	71.1	70.9	71.9	71.2	70.1	71.7	71.5	78.1	77.3	78.4	77.9	78.0	79.0	80.5	82.8	79.9	81.9	81.1	79.3	81.8	79.6	79.4	78.3	77.1	79.5	79.2	76.8	79.5
	OBEP0110225	72.3	71.8	70.9	72.0	71.1	69.8	71.7	71.8	77.9	77.2	78.6	78.1	77.6	78.9	81.3	83.1	80.9	82.7	81.1	79.8	82.5	80.5	80.4	77.1	76.6	78.1	78.8	76.4	78.1
	OBEP0112218	72.7	71.9	71.6	72.5	70.8	69.4	71.7	71.5	77.8	76.5	78.2	77.4	77.3	78.2	79.8	81.5	79.9	81.2	80.0	78.4	81.0	79.4	79.4	75.9	76.2	77.6	78.2	75.7	77.6
	AY835409	73.3	72.1	71.6	73.3	71.5	70.6	72.0	72.4	78.2	76.6	78.5	76.9	77.0	78.1	80.0	82.3	79.7	81.6	80.8	80.1	81.4	79.2	79.5	77.2	76.9	78.0	79.1	77.1	78.0
	GU553554	73.6	72.6	71.9	73.4	71.9	70.5	72.5	72.6	78.3	77.2	78.8	77.5	77.5	78.7	80.9	82.8	80.5	82.5	81.0	79.6	82.3	80.0	80.3	77.2	77.6	78.5	79.0	77.1	78.5
	OBEP0106507	73.1	72.0	71.6	72.9	70.7	69.8	71.3	71.8	77.9	76.3	78.3	76.9	77.0	78.0	80.5	82.7	80.7	81.7	80.6	80.4	81.5	80.3	80.1	78.0	77.6	78.5	79.5	77.4	78.5
	AY822005	72.5	71.5	71.1	72.5	71.3	70.6	71.9	72.0	77.7	76.8	78.2	76.8	76.8	78.1	80.5	82.5	80.4	82.0	79.8	79.1	81.8	80.0	79.6	76.6	76.5	77.5	78.5	76.6	77.5
	OBEP0110790	72.9	71.9	71.4	72.7	71.8	70.9	72.5	72.5	78.3	77.1	78.4	77.4	77.4	78.4	80.6	82.9	80.7	82.7	80.3	79.8	82.5	80.4	80.0	77.5	77.1	78.3	79.3	77.1	78.3
	OBEP0106257	72.7	71.9	71.3	72.5	69.8	70.0	70.1	70.7	76.9	75.9	77.2	76.4	76.5	77.2	79.4	82.3	79.9	82.2	79.5	79.6	82.0	79.5	79.4	75.3	75.9	76.9	77.0	75.9	76.9
	OBEP0106720	73.2	72.1	71.4	73.0	71.5	70.6	72.3	72.0	77.9	76.6	78.2	77.1	77.2	78.0	80.1	82.3	80.0	81.6	80.6	79.7	81.4	79.6	79.3	76.4	76.8	77.3	78.3	76.6	77.3
	OBEP0110171	72.5	71.9	71.4	72.5	71.5	70.5	72.4	72.0	79.2	77.7	79.1	78.3	78.3	79.3	81.8	84.1	81.0	82.9	81.6	80.9	82.7	80.7	81.1	77.7	76.4	78.9	78.8	76.6	78.9
	OBEP0110899	72.6	72.0	71.2	72.4	71.2	69.9	72.3	72.0	78.2	77.4	78.8	78.0	78.3	79.0	80.3	82.4	80.2	82.6	80.9	79.5	82.4	80.0	79.9	77.1	76.8	78.0	78.9	76.8	78.0
	EU910616	72.2	71.4	71.0	71.9	71.9	70.8	72.3	72.9	78.6	77.7	79.6	78.4	78.4	79.6	80.9	83.4	80.9	83.2	81.0	80.2	83.1	80.4	80.6	77.5	77.4	78.8	79.3	77.0	78.8
	OBEP0112873	73.0	72.5	71.9	73.1	72.3	70.7	72.9	72.8	78.4	77.3	78.8	77.6	77.8	78.5	80.7	82.7	80.4	82.4	80.8	79.3	82.2	80.0	80.1	77.0	76.6	78.2	78.7	76.4	78.2
	OBEP0109211	72.9	72.3	71.7	72.8	71.4	70.3	71.9	72.0	78.0	76.5	78.5	77.2	77.2	78.3	80.7	82.9	81.1	82.8	80.8	79.7	82.6	80.6	80.1	76.5	76.6	78.1	78.3	76.4	78.1
	OBEP0101367	72.8	71.7	71.5	72.5	71.7	70.0	72.0	71.8	78.1	77.0	78.6	77.9	77.8	78.8	81.2	83.4	81.0	83.0	80.6	80.1	82.9	80.5	80.4	77.6	77.0	78.3	79.3	77.0	78.3
	OBEP0110426	70.5	70.3	69.3	70.4	70.6	70.5	71.3	71.5	76.7	76.3	77.7	77.3	77.3	78.0	80.0	83.0	79.9	82.2	80.9	79.8	82.0	79.4	79.8	76.1	76.0	77.5	77.4	75.7	77.5
	OBEP0113140	72.7	72.1	71.6	72.5	71.0	69.5	71.4	71.5	78.0	76.7	78.3	77.3	77.5	78.3	80.6	82.6	80.5	81.7	80.5	79.2	81.5	80.0	80.0	76.2	76.5	77.8	78.5	76.6	77.8
	OBEP0110456	72.6	72.0	71.5	72.5	71.0	70.5	71.9	71.8	78.6	77.3	78.4	77.8	77.7	78.7	81.0	83.6	80.5	82.5	81.4	80.6	82.3	80.2	80.5	77.6	76.4	78.8	78.6	76.3	78.8
	OBEP0110380	72.4	72.0	71.3	72.2	71.8	71.1	72.3	72.7	78.1	77.0	78.4	77.8	77.8	79.0	80.7	83.4	80.4	82.4	81.3	80.4	82.2	80.0	80.5	77.1	76.2	78.4	78.5	76.2	78.4
	OBEP0101667	72.7	72.0	71.6	72.6	71.1	70.0	71.7	71.9	78.2	77.4	78.6	77.5	77.7	78.8	80.6	82.7	80.5	82.7	80.3	79.3	82.5	80.2	80.1	77.0	76.5	78.2	78.6	76.3	78.2
	EU420711	72.9	72.5	71.8	72.7	70.9	69.7	71.4	71.6	77.8	76.7	78.7	77.3	77.7	78.5	80.8	82.5	80.5	82.0	80.6	79.4	81.8	80.0	80.5	76.2	76.6	77.7	78.4	76.9	77.7
	OBEP0110145	71.9	71.2	70.8	71.6	70.2	69.7	71.0	71.3	77.7	77.3	78.2	78.1	78.6	78.9	80.6	83.3	80.2	82.3	80.5	79.9	82.1	79.7	80.2	77.3	76.1	77.9	78.8	76.5	77.9
	OBEP0108994	72.7	72.0	71.8	72.5	71.3	69.8	71.1	71.5	78.5	77.7	79.0	78.3	78.1	79.2	81.3	83.7	81.2	83.2	81.0	79.8	83.1	80.8	80.1	78.5	77.4	79.1	79.9	77.6	79.1
	OBEP0100043	71.6	71.5	70.7	71.2	71.3	70.6	72.0	71.0	76.7	75.3	76.8	76.8	76.4	77.5	80.0	81.5	79.4	80.1	79.9	78.5	79.9	79.2	78.6	76.8	76.0	76.9	78.3	76.3	76.9
	OBEP0110175	72.7	71.6	71.0	72.5	70.5	70.5	71.3	71.5	78.5	77.7	78.7	78.4	78.0	79.2	80.6	82.9	80.1	82.6	81.0	80.4	82.4	79.8	80.6	77.5	76.4	78.6	78.8	76.4	78.6
	OBEP0108952	73.0	72.3	71.8	72.9	71.5	70.5	72.5	72.3	77.7	76.8	78.8	77.3	77.8	78.6	81.0	83.2	80.7	83.0	81.3	80.1	82.8	80.3	80.4	77.2	76.8	78.2	78.9	76.7	78.2
	OBEP0113085	71.4	71.8	70.9	71.6	71.1	70.9	71.6	71.7	77.7	76.6	76.3	77.0	77.9	77.8	78.0	80.0	77.6	78.9	79.1	78.4	78.7	77.3	78.1	77.8	76.6	78.4	78.1	78.0	78.4
	OBEP0100803	73.1	72.1	71.6	73.0	71.9	70.3	72.6	72.1	78.1	77.0	78.9	77.6	77.9	79.0	81.2	83.1	81.0	83.2	80.7	79.9	83.1	80.5	80.8	77.6	77.0	78.4	79.4	77.3	78.4
	OBEP0112781	72.4	71.6	71.2	72.2	72.0	71.0	72.6	72.5	78.8	77.6	79.1	78.4	78.0	79.2	80.8	83.5	80.9	82.3	81.3	80.1	82.1	80.6	80.1	77.7	76.8	79.3	79.1	76.6	79.3
	JF268336	73.1	72.1	71.5	73.0	71.6	70.5	71.7	71.7	78.2	77.1	78.8	77.4	77.4	78.3	80.9	83.2	80.5	82.3	80.8	79.9	82.1	80.1	79.7	77.5	77.6	78.3	79.4	77.6	78.3
	OBEP0107194	72.6	72.1	71.4	72.4	71.2	70.4	71.3	71.4	78.2	77.1	78.9	78.0	77.6	78.9	80.4	82.9	80.4	82.7	80.5	79.5	82.5	80.0	80.6	78.4	77.1	79.3	79.7	77.4	79.3
	OBEP0100987	72.5	72.2	71.5	72.4	70.7	69.7	71.5	71.4	77.4	76.3	78.5	77.1	77.4	78.2	79.8	81.9	79.6	81.9	80.4	79.0	81.7	79.3	79.7	76.8	76.6	78.1	78.7	76.4	78.1
	OBEP0101055	73.0	72.3	71.9	72.8	71.5	70.5	71.8	72.6	78.7	77.4	78.8	78.3	78.1	78.9	81.4	83.6	81.5	83.3	81.2	80.4	83.1	81.0	80.7	77.6	77.4	78.8	79.3	77.2	78.8
	OBEP0113032	73.0	72.2	71.9	72.8	71.3	70.1	71.5	71.6	78.8	77.9	79.1	78.5	78.4	79.5	81.2	83.7	81.3	83.2	81.0	79.9	83.1	80.8	80.1	78.5	77.2	78.9	79.7	77.2	78.9
	OBEP0110396	71.5	70.8	70.1	71.2	70.6	69.9	71.3	71.5	77.1	76.9	78.4	78.1	77.8	78.4	80.4	82.4	80.2	82.3	80.7	79.6	82.2	79.7	80.1	76.1	76.0	77.6	77.9	75.8	77.6
	OBEP0100258	73.1	72.4	71.9	72.9	71.6	70.4	72.0	72.4	78.7	77.7	79.2	78.4	78.7	79.6	81.3	83.7	81.3	83.3	81.3	80.4	83.2	80.9	80.5	77.7	77.3	78.3	79.4	77.3	78.3
	OBEP0112407	73.0	72.1	71.3	72.8	71.1	69.9	71.9	71.7	78.6	77.2	78.3	77.9	77.8	78.8	80.4	82.6	80.5	82.7	81.0	79.7	82.5	80.1	79.9	77.0	77.2	78.3	78.8	76.7	78.3
	OBEP0106677	72.5	71.8	71.5	72.3	71.3	70.2	71.8	72.2	77.7	76.8	78.6	77.4	77.7	78.6	80.4	82.5	80.3	82.7	80.2	79.2	82.5	79.9	80.5	77.1	76.8	78.1	78.9	76.8	78.1
	OBEP0114807	72.7	72.7	72.2	72.6	71.3	70.5	71.8	72.0	77.7	76.2	78.4	77.4	77.4	78.2	80.0	82.6	79.7	81.8	79.8	79.5	81.7	79.3	79.5	76.8	76.9	77.7	79.1	76.9	77.7
	KP814621	73.0	72.4	71.9	72.7	71.4	69.9	71.5	71.7	78.3	77.2	78.9	77.8	77.8	78.6	81.1	83.0	81.0	82.3	80.9	79.4	82.1	80.5	80.4	76.6	76.9	78.3	79.0	76.9	78.3
	OBEP0112234	73.2	72.3	71.6	73.0	71.6	70.5	72.4	72.1	77.8	77.0	78.7	77.5	77.7	78.6	80.6	82.8	80.4	82.6	80.7	79.5	82.4	80.1	80.1	77.1	76.8	78.3	78.8	76.9	78.3
	JX000783	72.7	71.3	71.1	72.4	71.1	70.1	71.0	71.5	77.6	76.4	77.6	77.0	77.0	77.7	80.3	82.5	80.0	81.9	80.4	79.5	81.7	79.6	79.7	76.8	77.5	77.9	78.9	77.4	77.9
	OBEP0107458	72.8	71.8	71.2	72.6	71.0	69.8	71.4	71.4	78.3	77.1	78.1	77.6	77.4	78.6	80.2	82.2	80.2	82.2	80.6	79.2	82.0	79.7	79.7	76.8	76.9	78.1	78.5	76.4	78.1
	OBEP0101437	73.2	72.3	71.5	73.1	71.3	70.0	72.3	72.1	78.1	77.0	78.8	77.7	78.0	78.8	80.6	82.8	80.4	82.8	81.0	79.6	82.7	80.1	80.2	77.3	76.8	78.3	79.0	76.9	78.3
	OBEP0110289	72.0	71.4	71.1	71.9	71.7	71.0	72.2	72.5	77.4	76.7	78.3	77.5	77.8	78.5	80.4	82.8	80.8	82.7	81.1	80.1	82.5	80.3	80.5	76.6	76.7	78.2	78.5	76.4	78.2
	OBEP0114788	72.7	71.9	71.6	72.5	70.7	69.8	71.3	71.6	77.5	76.6	78.5	77.3	77.5	78.3	80.5	82.2	80.1	82.5	80.6	79.7	82.3	79.7	80.0	76.6	76.5	77.6	78.4	76.3	77.6
Lokiarchaeota-4	OBEP0110905	72.9	73.0	71.8	72.8	72.0	70.4	72.3	71.8	77.7	77.4	77.9	78.2	78.1	78.7	80.3	82.1	79.6	82.6	80.4	79.4	82.5	79.4	79.9	79.7	78.9	80.5	80.0	79.1	80.5
	FJ655658	73.3	73.2	72.0	72.9	71.8	70.6	71.9	72.1	77.7	77.2	77.9	77.6	78.0	78.4	80.3	82.2	79.5	82.8	80.7	79.7	82.7	79.0	80.3	79.1	79.3	80.1	79.9	78.9	80.1
	OBEP0109115	73.5	73.0	72.4	73.1	72.4	70.7	73.1	72.9	77.9	77.5	78.7	78.2	78.2	78.9	80.8	82.8	79.9	82.9	81.0	80.5	82.7	79.4	80.4	78.8	78.6	79.6	79.8	78.5	79.6
	GU553522	73.3	73.2	72.3	72.8	71.9	70.5	72.5	72.4	77.7	77.2	78.6	77.8	78.0	78.6	80.2	82.3	79.6	82.6	80.8	80.3	82.5	79.1	80.3	78.4	78.3	79.1	79.3	78.5	79.1
	JQ989539	73.1	73.1	72.0	72.8	71.2	70.4	71.9	71.7	77.8	77.4	78.4	77.9	78.2	78.8	79.9	81.5	79.0	82.4	80.1	79.0	82.2	78.5	79.9	78.9	79.0	79.8	79.6	78.6	79.8
	AB800140	73.5	73.1	72.4	73.0	71.5	70.9	72.2	72.4	77.6	77.2	78.3	77.6	77.9	78.5	80.3	81.9	79.1	82.5	80.4	79.7	82.3	78.6	80.4	78.7	78.7	79.9	79.6	78.3	79.9
	AF412942	72.6	72.4	71.6	72.1	70.8	70.1	71.5	71.7	76.7	76.5	77.6	76.9	77.1	77.8	80.3	81.9	79.1	82.5	80.4	79.7	82.3	78.6	79.7	78.5	78.5	79.6	79.4	78.3	79.6
	OBEP0106345	73.0	72.8	72.5	72.5	71.5	70.4	72.3	72.5	77.4	77.3	78.1	77.5	77.5	78.2	79.9	81.9	79.6	82.6	80.4	79.9	82.5	79.1	79.7	78.6	78.5	79.5	79.3	78.0	79.5
	OBEP0113210	72.9	72.6	71.8	72.5	71.6	70.1	71.9	71.9	77.5	77.2	77.9	77.7	77.6	78.3	79.9	81.8	79.1	82.2	79.9	79.2	82.0	78.6	79.3	78.7	78.5	79.3	79.5	78.3	79.3
	JQ817971	73.1	71.9	72.2	72.6	71.9	70.8	72.5	72.2	77.5	77.0	78.7	77.5	77.7	78.4	81.1	82.5	80.6	83.1	81.0	80.3	82.9	80.1	81.1	77.7	77.6	78.9	79.0	77.9	78.9
	JN123687	72.4	72.1	71.3	71.8	70.9	70.4	71.5	71.6	76.7	76.2	77.5	76.7	76.8	77.5	79.3	80.8	78.2	81.4	79.5	78.9	81.2	77.7	78.8	77.3	77.6	78.7	78.5	77.4	78.7
	HM480259	71.8	71.4	71.0	71.6	71.6	70.3	71.7	71.3	76.7	76.4	77.2	76.7	77.6	78.0	79.6	80.5	78.9	81.8	79.1	77.6	81.6	78.4	78.6	78.0	78.4	79.2	79.1	78.0	79.2
	AF412944	72.9	72.6	72.4	72.6	71.8	70.8	72.2	72.4	77.4	76.8	78.3	77.6	77.9	78.4	80.3	81.8	80.0	82.6	80.8	79.9	82.4	79.5	80.0	78.0	78.2	79.4	79.3	78.0	79.4
	JN123682	73.2	73.0	72.1	72.6	71.4	70.7	72.2	72.2	77.8	77.1	78.3	77.6	78.0	78.6	80.4	82.1	79.6	82.6	80.7	80.1	82.4	79.1	80.1	78.8	79.0	79.9	79.8	79.0	79.9
	OBEP0106182	72.4	72.1	71.2	72.0	71.6	70.9	72.4	71.6	77.2	76.6	77.3	77.2	77.8	78.1	79.5	81.2	78.5	81.7	79.6	78.7	81.5	78.0	78.9	78.1	78.1	78.8	78.7	77.6	78.8
	OBEP0110767	72.5	72.3	71.5	72.1	71.9	70.6	72.4	72.0	77.4	76.6	77.5	77.2	77.3	77.9	80.2	82.5	79.5	82.5	80.7	79.8	82.3	79.2	79.6	78.8	78.2	79.6	79.0	77.9	79.6
	JQ989549	72.5	72.0	71.5	72.0	71.0	70.3	71.5	71.7	77.1	76.6	78.0	77.1	77.5	78.0	79.9	81.3	78.6	82.0	79.8	79.0	81.8	78.1	79.5	77.9	78.0	79.3	78.9	77.8	79.3
	JN123610	72.6	72.2	71.6	72.2	71.5	70.3	72.0	72.1	77.0	76.6	77.7	77.0	77.4	78.0	80.4	81.6	79.1	82.4	80.2	79.6	82.2	78.6	79.7	78.4	78.3	79.4	79.5	78.4	79.4
	AB800489	73.4	72.8	72.2	73.0	71.9	70.9	72.6	72.8	77.2	76.9	78.5	77.2	77.5	78.1	80.5	82.3	79.4	82.5	81.1	80.4	82.3	78.9	80.2	78.4	78.6	79.6	79.5	78.4	79.6
	OBEP0106699	73.1	72.6	72.2	72.6	71.6	70.4	71.9	72.1	77.1	76.8	77.5	77.4	77.6	77.9	80.8	82.0	79.7	82.9	81.0	80.3	82.8	79.2	80.0	78.5	78.4	79.5	79.4	78.3	79.5
	OBEP0113561	73.2	72.9	72.2	72.7	71.8	70.7	72.6	72.7	77.5	77.1	78.6	77.7	77.9	78.5	80.6	82.5	79.6	82.5	80.9	80.2	82.3	79.1	80.1	78.6	78.7	79.9	79.6	78.5	79.9
	AB800193	73.2	72.0	72.3	72.7	71.9	70.8	72.5	72.2	77.5	77.0	78.7	77.5	77.7	78.4	81.2	82.6	80.7	83.2	81.1	80.4	83.0	80.2	81.2	77.8	77.7	79.0	79.1	78.0	79.0
	AM992695	69.0	69.1	68.2	68.5	67.6	66.4	68.5	69.2	72.6	72.3	73.6	72.5	72.8	73.7	75.9	77.0	75.1	78.2	75.1	75.0	78.2	74.7	75.9	75.2	75.3	75.5	75.8	74.8	75.5
	OBEP0106368	72.9	73.0	72.0	72.6	71.4	69.7	71.7	71.8	77.1	76.8	77.5	77.4	77.3	77.8	80.0	81.9	78.7	82.2	80.3	78.8	82.0	78.4	78.8	78.0	77.5	78.9	78.6	76.9	78.9
	AB799355	73.1	72.7	72.1	72.6	71.4	70.3	72.1	72.3	77.4	76.9	78.2	77.4	77.7	78.3	80.3	82.0	79.1	82.5	80.5	79.8	82.3	78.6	80.1	78.4	78.6	79.8	79.5	78.4	79.8
	GU553813	73.5	73.3	72.7	73.1	71.8	70.4	72.4	72.5	77.7	77.2	78.3	77.7	78.1	78.6	80.1	82.1	79.4	82.5	81.0	80.1	82.3	79.0	80.2	77.9	78.1	79.2	79.0	78.1	79.2
	DQ522906	73.6	73.0	72.4	73.2	72.1	70.9	72.8	73.0	77.5	77.0	78.7	77.5	77.7	78.4	80.5	82.3	79.5	82.5	81.1	80.4	82.3	79.0	80.2	78.5	78.7	79.7	79.6	78.5	79.7
	OBEP0107794	73.1	73.4	72.0	72.6	71.9	70.9	72.3	72.4	77.7	76.8	78.3	77.5	77.8	78.4	80.1	82.1	79.6	82.7	80.9	80.2	82.5	79.1	80.5	78.2	78.5	79.3	79.0	78.3	79.3
	OBEP0107777	73.3	72.9	72.2	72.9	72.0	71.0	72.3	72.5	78.3	77.8	78.5	78.5	78.4	79.3	80.7	82.5	79.9	83.0	80.9	80.4	82.8	79.4	80.0	79.2	79.1	80.1	80.1	78.7	80.1
	OBEP0114711	72.8	72.3	71.8	72.3	71.6	70.4	72.4	72.4	77.3	76.6	78.1	77.2	77.4	77.9	80.6	82.7	79.7	83.1	80.6	80.1	82.9	79.2	79.9	78.6	78.4	79.4	79.5	78.1	79.4
	OBEP0106540	73.2	72.8	72.1	72.8	71.8	70.4	72.2	72.7	77.6	77.1	78.5	77.8	77.8	78.2	80.6	82.3	79.8	82.5	80.7	80.2	82.3	79.3	80.0	78.4	78.7	79.6	79.7	78.6	79.6
Odinarchaeota	KX764885	72.5	71.8	72.3	72.4	71.8	73.0	71.8	72.2	80.0	79.0	80.7	78.6	78.8	79.3	81.3	81.4	81.4	81.1	80.4	79.8	80.9	81.1	81.0	79.9	78.2	80.6	80.0	78.6	80.6
	AB019719	71.6	71.6	71.3	71.4	71.9	72.4	71.7	72.2	80.0	78.8	80.6	78.6	78.9	79.5	80.8	80.9	80.9	80.5	79.2	78.6	80.3	80.4	80.9	80.1	79.2	80.7	80.4	79.0	80.7
Thorarchaeota	OBEP0113149	70.7	69.8	70.3	70.6	69.7	71.5	70.4	70.3	74.0	73.4	75.7	74.0	74.4	74.6	77.7	78.1	76.8	78.0	77.7	77.1	77.9	76.4	77.5	74.1	74.0	75.8	76.2	73.9	75.7

Calculation of percent identity of new Asgard groups was based on 179 sequences with a long fragment of Asgardarchaeotal 16S rRNA gene. Fragments of 16S rRNA gene from position of *E. coli* 243 to 1414 (~1170 bp) were used for calculating the identity. Novel clades are marked with colored background.

Supplementary Table 4. Information of sediment samples analyzed in this study.

Sample	Combined samples for metagenomic assembly	Biotope	Sampling Location	DNA Data size (Gbp)	cDNA Data size (Gbp)	Sampling time	latitude and longitude
				99.2	NA		
DZ	NA	Mangrove sediment	Xinying Bay, Danzhou, China (10-20 cm)	105.6	NA	Jan, 2018	19.7410 N, 109.2727 E
DZG	NA	Mangrove sediment	Dongzhai Bay, Haikou, China (10-20 cm)	107.6	NA	Jan, 2018	19.9516 N, 110.5764 E
LZ	NA	Mangrove sediment	Leizhou Bay, China (10-20cm)	112.1	NA	Jan, 2018	20.9262 N, 110.1628 E
Maipo_7	MP_5	Mangrove sediment	Shenzhen Bay, Hong Kong, China (0-2 cm)	126.9	8.6	Sep, 2014	22.4979 N, 114.0295 E
Maipo_8		Mangrove sediment	Shenzhen Bay, Hong Kong, China (10-15 cm)	91.1	8.6	Sep, 2014	22.4979 N, 114.0295 E
Maipo_9		Mangrove sediment	Shenzhen Bay, Hong Kong, China (20-25 cm)	88.6	8.9	Sep, 2014	22.4979 N, 114.0295 E
Maipo_10		Mudflat sediment	Shenzhen Bay, Hong Kong, China (0-5 cm)	98.1	9.5	Sep, 2014	22.4992 N, 114.0276 E
Maipo_11		Mudflat sediment	Shenzhen Bay, Hong Kong, China (13-16 cm)	86.0	12.2	Sep, 2014	22.4992 N, 114.0276 E
SZ_1	NA	Mangrove sediment	Shenzhen Bay, Shenzhen, China (0-2 cm)	105.6	12.4	Jan, 2018	22.5288 N, 114.0300 E
SZ_2	NA	Mangrove sediment	Shenzhen Bay, Shenzhen, China (6-8 cm)	121.1	12.4	Jan, 2018	22.5288 N, 114.0300 E
SZ_3	NA	Mangrove sediment	Shenzhen Bay, Shenzhen, China (12-14 cm)	90.6	11.7	Jan, 2018	22.5288 N, 114.0300 E
SZ_4	NA	Mangrove sediment	Shenzhen Bay, Shenzhen, China (28-30 cm)	96.6	NA	Jan, 2018	22.5288 N, 114.0300 E
XMD	NA	Mangrove sediment	Ximen Island, Leqing, China (10-20 cm)	114.3	NA	Jan, 2018	28.3484 N, 121.1782 E
YX	NA	Mangrove sediment	Zhangjiang Estuary, Yunxiao, China (10-20 cm)	96.9	NA	Jan, 2018	25.9179 N, 117.4215 E
C1-1	YT	seagrass sediment	Rongcheng Swan Lake (0-4cm)	119.5	NA	Nov, 2018	37.3502 N, 122.5781 E
C1-7		seagrass sediment	Rongcheng Swan Lake (21-26cm)	105.4	NA	Nov, 2018	37.3502 N, 122.5781 E
C1-10		seagrass sediment	Rongcheng Swan Lake (36-41cm)	101.1	NA	Nov, 2018	37.3502 N, 122.5781 E
FC1-1		mudflat sediment	Rongcheng Swan Lake (0-4cm)	150.9	NA	Nov, 2018	37.3464 N, 122.5700 E
FC1-7		mudflat sediment	Rongcheng Swan Lake (21-26cm)	123.7	NA	Nov, 2018	37.3464 N, 122.5700 E
FC1-10		mudflat sediment	Rongcheng Swan Lake (36-41cm)	96.7	NA	Nov, 2018	37.3464 N, 122.5700 E

Table S5. Overview of Asgard archaea genomic bins.

Metagenomic bins		Bin size (Mbp)	Number of scaffolds	Largest scaffold (Mbp)	N50 (Kbp)	Number of ORFs	Completeness (%)[1]	Contamination (%)[1]	Strain heterogeneity (%)[*]	GC (%)	rRNA[#]
Gerdarchaeota	MP5_1_bin791	4.8	441	0.08	20.8	4,598	90.65	18.69	0.00	31.7	NA
	MP5_2_bin1192	3.2	580	0.03	32.5	3,394	88.47	8.72	23.08	30.1	NA
	SZ_4_bin5.60	3.4	68	0.37	69.1	3,206	93.46	8.88	0.00	30.5	NA
	YT _bin1.045	3.7	240	0.10	25.2	2,427	83.29	8.88	0.00	31.1	NA
	YT_bin2.057	4.3	223	0.15	31.6	4,042	94.86	9.81	0.00	32.2	SSU+LSU
	YT_bin5.010	2.6	599	0.02	4.9	2,841	75.24	9.63	23.53	34.1	NA
	B18_G1	2.9	261	0.06	18.4	2,921	86.45	7.94	0.00	38.9	LSU
Helarchaeota	SZ_4_bin10.384	4.4	54	0.48	215.6	4,343	96.26	4.21	0.00	30.1	LSU
	Hel_GB_A^	3.8	333	0.05	15.2	3,574	82.40	2.80	0.00	35.3	NA
	Hel_GB_B^	3.5	180	0.07	28.9	3,164	86.92	1.40	0.00	28.0	NA
Lokiarchaeota	DNA_SIP_bin2.159	3.4	362	0.04	12.5	3,716	75.23	6.22	41.18	29.3	SSU
	DZG_bin1.240	3.9	112	0.21	66.1	3,706	87.85	3.74	0.00	33.0	SSU
	SZ_4_bin8.338	3.7	198	0.11	33.5	3,596	86.45	2.34	0.00	30.6	SSU+LSU
	CR4	4.3	1,904	0.09	4.1	4,413	80.45	2.34	0.00	44.0	SSU+LSU
	GC14_75	5.1	504	0.07	15.4	5,384	90.29	45.15	78.21	31.1	SSU+LSU
	SM_031	4.8	728	0.05	8.7	5,404	85.21	5.14	0.00	30.1	LSU
Thorarchaeota	DZG_bin1.115	3.1	95	0.19	53.2	2,956	82.78	3.27	0.00	45.0	SSU
	SZ_4_bin3.344	1.7	22	0.47	222.1	1,674	83.57	2.34	0.00	45.5	SSU+LSU
	SZ_4_bin10.233	3.5	98	0.27	71.9	3,344	83.18	2.8	0.00	47.2	SSU+LSU
	AB_25	2.3	264	0.09	15.4	2,914	90.12	3.19	33.33	44.6	SSU+LSU
	B41_G1	3.0	559	0.09	7.0	3,154	94.86	8.88	0.00	51.9	SSU+LSU
	B59_G1	4.3	523	0.20	34.0	4,344	95.33	9.42	5.26	48.9	SSU+LSU
	MP8T	3.5	148	0.24	51.5	3,612	92.06	5.30	11.11	41.6	SSU+LSU

	MP9T	4.4	390	0.11	12.5	4,513	85.05	1.01	0.00	41.5	NA
	MP11T	3.5	235	0.12	18	3,693	90.19	2.34	0.00	42.6	SSU+LSU
	SMTZ1_45	3.5	119	0.18	51.2	3,208	87.69	5.14	0.00	42.2	SSU+LSU
	SMTZ1_83	3.3	266	0.07	15.3	3,029	90.19	6.54	14.29	49.3	SSU+LSU
	SM_104	4.3	243	0.10	35.6	4,337	91.30	5.14	14.29	39.5	LSU
	SM_117	4.0	320	0.14	28.2	4,363	86.45	6.83	14.29	45.3	NA
Odinarchaeota	LCB_4	1.5	9	1.18	1181.4	1,584	96.3	1.4		38.1	SSU+LSU
Heimdallarchaeota-AAG	AB_125	2.3	225	0.04	10.8	2,348	79.37	2.34	0.00	33.4	SSU+LSU
	GCA_002728275.1	1.4	76	0.07	26.4	1,386	83.18	1.87	50	30.1	SSU+LSU
	LC_2	4.8	177	0.15	38.7	4,586	72.43	4.21	40	32.6	LSU
Heimdallarchaeota-MHVG	SZ_4_bin2.246	3.0	16	0.65	525.5	2,686	87.38	1.94	0.00	34.9	NA
	LC_3	5.7	157	0.22	59.3	5,514	91.59	5.61	12.5	29.7	SSU+LSU

[*] Completeness and contamination were assessed using lineage-specific maker sets with checkM.
[#] rRNA genes were predicted using Barrnap (version 0.9, https://github.com/tseemann/barrnap) with the parameter "1e-5".
[^] These MAGs were from Guaymas Basin hydrothermal vent sediments.
Asgard MAGs with completeness > 70% were chosen for analyses and those retrieved in this study are marked red.

4.9.Supplementary figures

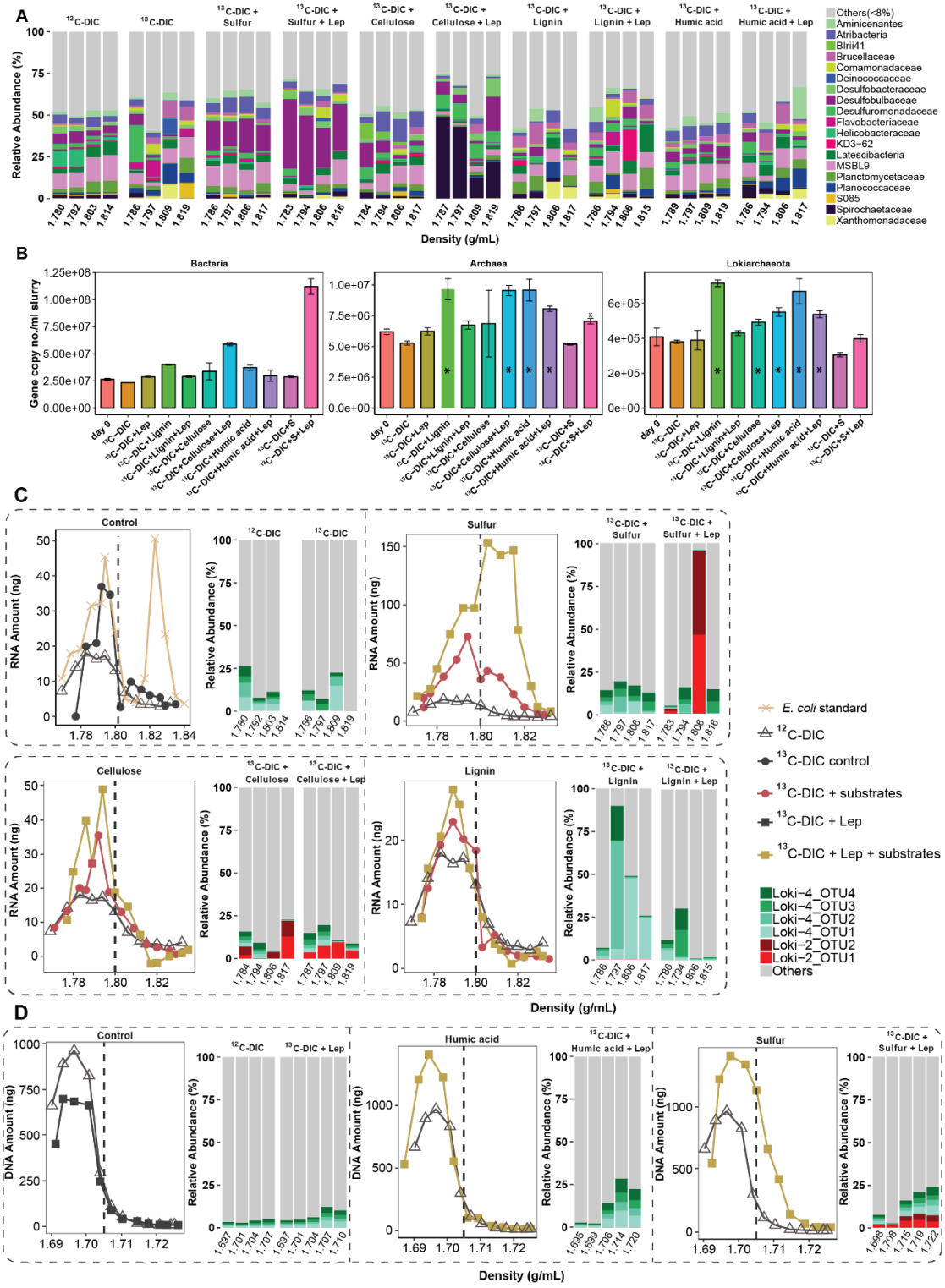

Supplementary Fig. 1. (a) Total sum scaling of abundances of bacterial 16S rRNA gene sequences from selected "light" and "heavy" gradient fractions of RNA-SIP samples. Before Illumina sequencing, 2 fractions (fraction 4 and 5, 6 and 7, 8 and 9, 11 and 10) were combined together as one sample for library preparation. Density is indicated by the average density of combined fractions for RNA-SIP samples. Relative abundances are shown at the family level as taxonomic threshold. (b) 16S rRNA gene copy numbers of Lokiarchaeota of DNA extracts from SIP incubations on day 0 and 255. * indicates significant increase of gene copies compared to control incubations i.e., "day 0" and "^{13}C-DIC" (c) RNA-SIP profiles and relative abundances of Lokiarchaeota 16S rRNA gene sequences. (d) DNA-SIP profiles and relative abundances of Lokiarchaeota 16S rRNA gene sequences. DIC: dissolved inorganic carbon (i.e. bicarbonate); S: sulfur; Lep: lepidocrocite. Dashed lines indicate starting density before ultracentrifugation.

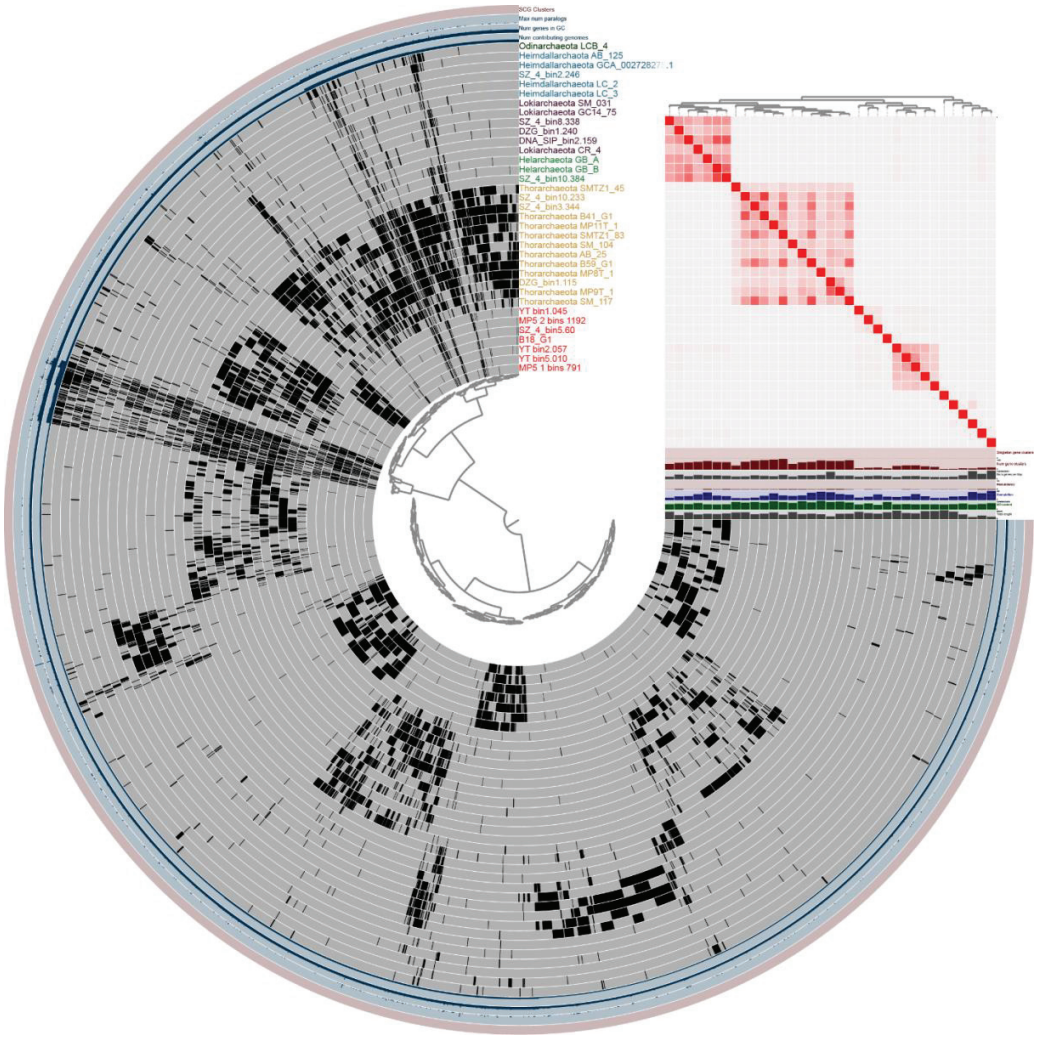

Fig. S2. Pan-genome analysis of protein clusters within all Asgard MAGs and their amino acid identity (ANI) using the Anvi'o software. The inner and upper trees were clustered using "Gene cluster presence

absence". Asgard MAGs with red stars are from this study. Those with MCR complex or from ^{13}C-labelled enrichment were highlighted with two red stars. The ANI ranges from 60% to 100%, with deeper colour represent higher identity.

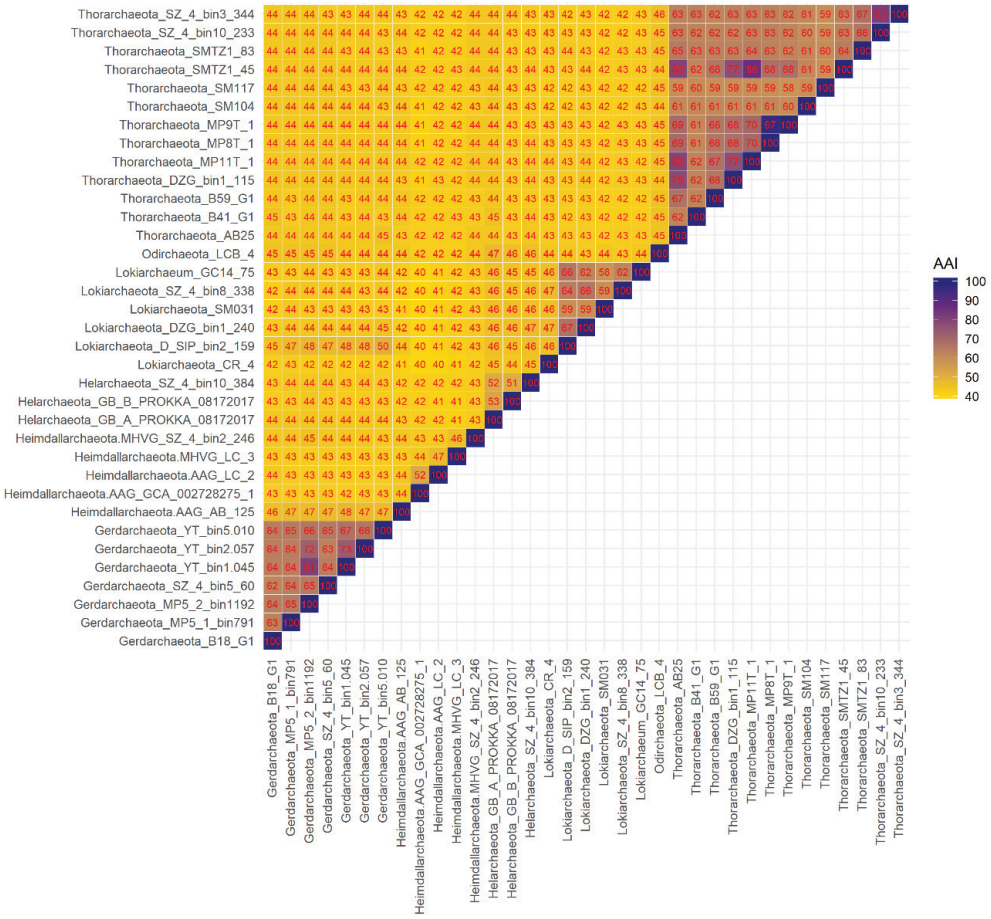

Fig. S3. Amino acid identity (AAI) of Asgard MAGs. AAI was calculated using CompareM (https://github.com/dparks1134/CompareM).

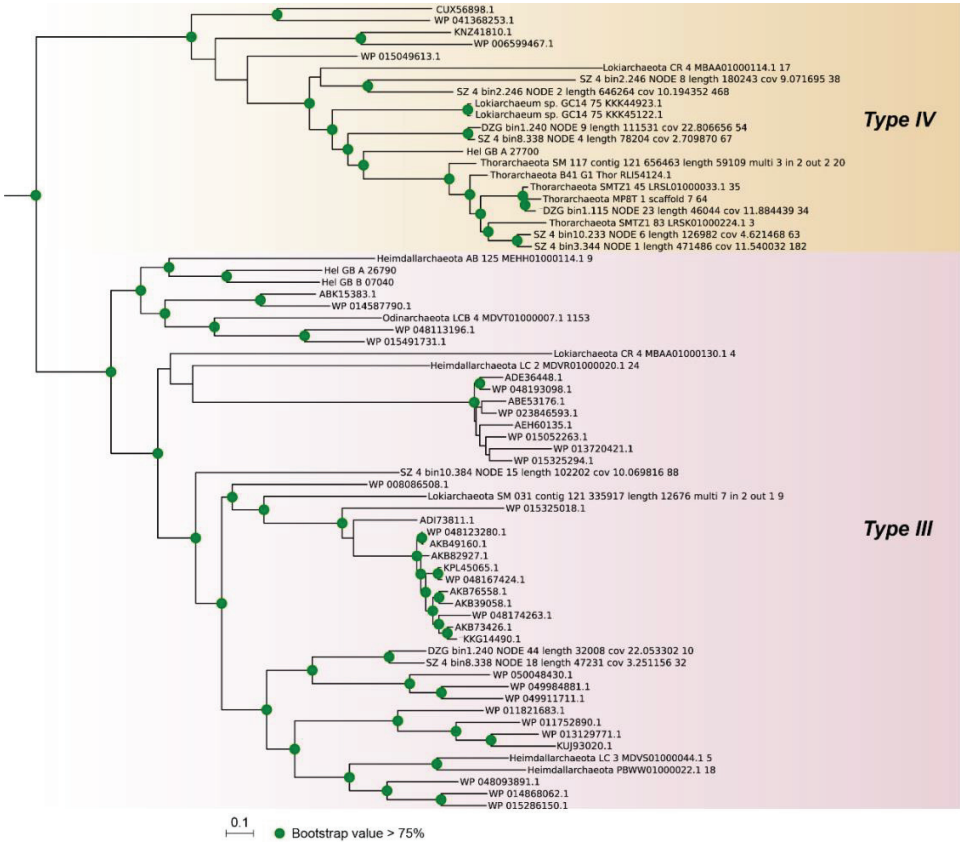

Fig. S4. Phylogenetic maximum likelihood tree of RuBisCO amino acid sequences (the large subunit). The tree was build using IQ-TREE with model LG+I+G4 and parameter "-bb 1000".

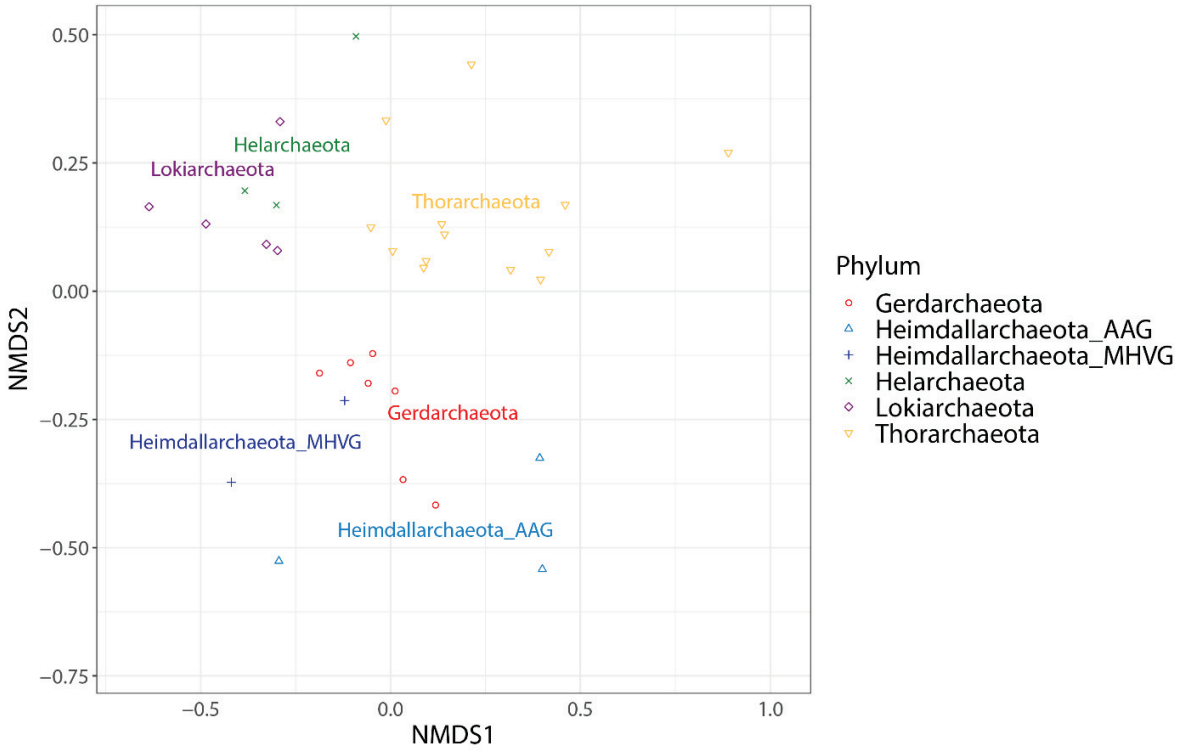

Fig. S5. Non-metric multidimensional scaling (NMDS) plot of KEGG in all available Asgard MAGs (December 2018 updated). Odinarchaeota was excluded because it has one MAG and it is not representative. KEGG data was analyzed by Bray–Curtis dissimilarity.

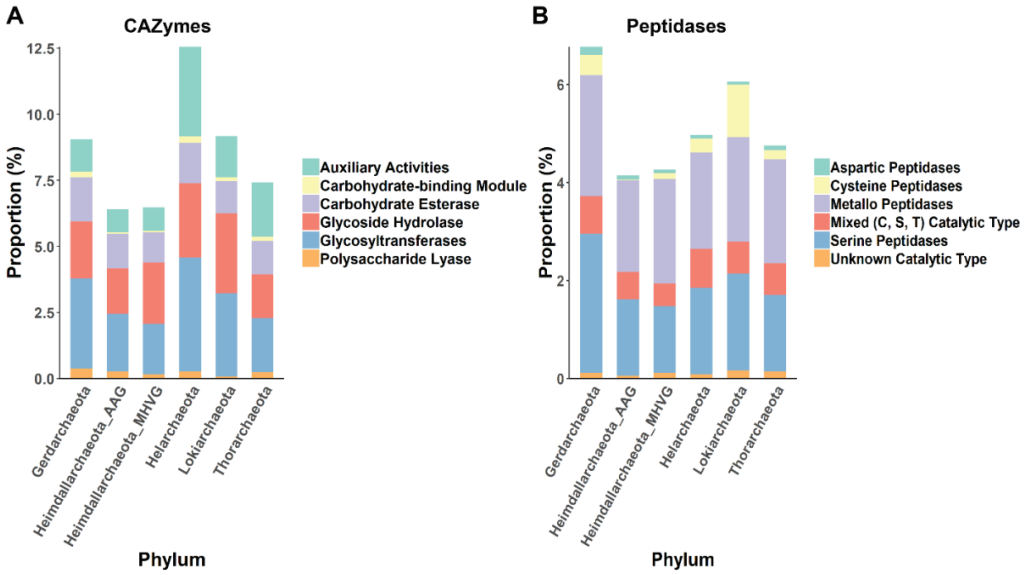

Fig. S6. Abundance of (A) carbohydrate-active enzymes and (B) peptidases in Asgard phyla. Carbohydrate-active enzymes (CAZymes) and peptidases were annotated using the dbCAN webserver and MEROPs database, respectively. The e-value cutoff is 1e-5 for both cases. Proportion was calculated by normalizing the MAGs number and the average protein numbers in each phylum. Detailed information is available in Table S7.

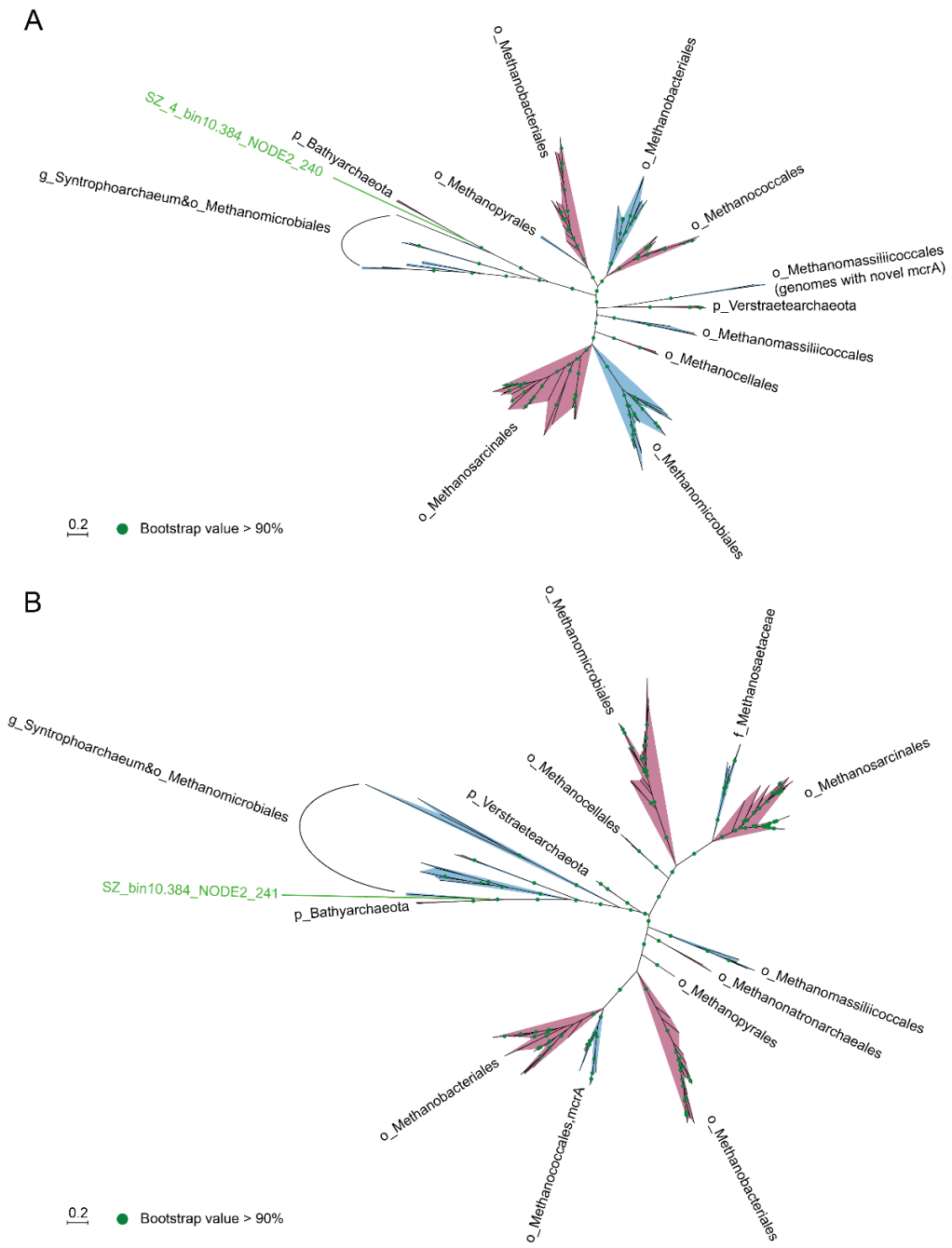

Fig. S7. Protein trees of (A) McrB and (B) McrG. Asgard archaea McrA gene obtained in this study is marked with green line. The maximum-likelihood trees were inferred using IQ-TREE tree with model LG+F+I+G4 and parameter "-bb 1000". The background-colour is added to differentiate adjacent groups.

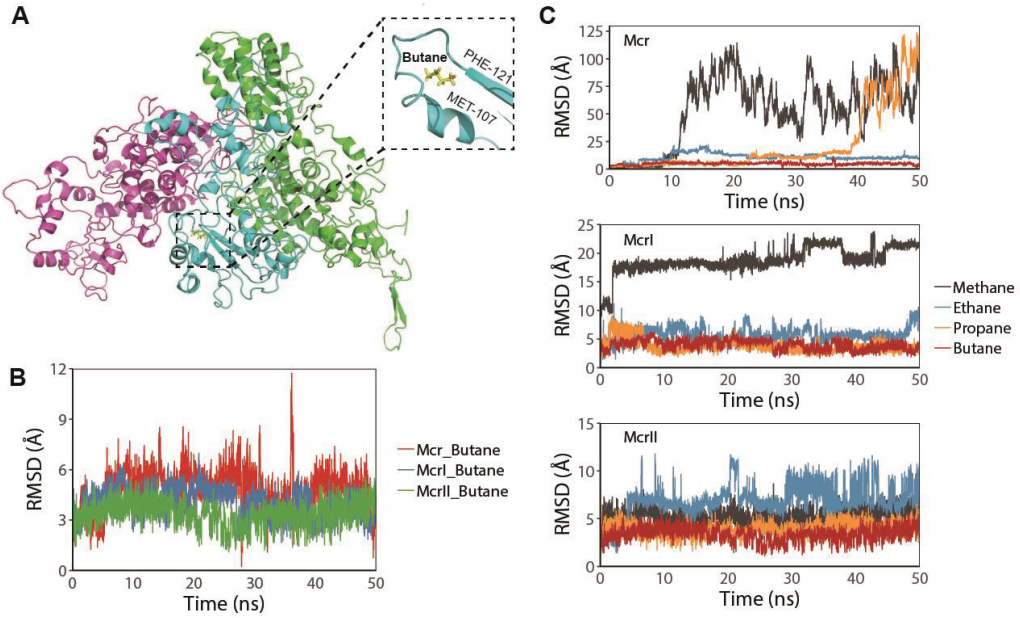

Fig. S8. (A) Equilibrium structure of the Lokiarchaeotal MCR complex and the docking model of butane (yellow). McrA, McrB and McrG are marked in green, magenta, and cyan, respectively. Magnified structure of butane binding with the pocket of McrG shown as inset. The main residues interacting with butane are from MET107 to PHE121 of McrG. (B) The RMSD of butane in Mcr (red), McrI (blue) and McrII (green) complexes as a function of time. The RMSD of butane in the three complexes are of the same magnitude (~5Å). (C) The RMSD of methane (black), ethane (blue), propane (yellow) and methane (red) in Mcr (top), McrI (middle) and McrII (bottom) complexes as a function of time. The RMSD of butane in all the three complexes are of smaller magnitude than the ones of methane, which implies that the binding affinities of butane to all the three Mcr complexes are higher than the ones of methane. Here, Mcr represents the Lokiarchaeotal MCR complex, while McrI and McrII represent the complexes from the *Ca.* Syntrophoarchaeum butanivorans. The RMSD is estimated as the distance deviation of methane/butane to the center of mass of each Mcr complex.

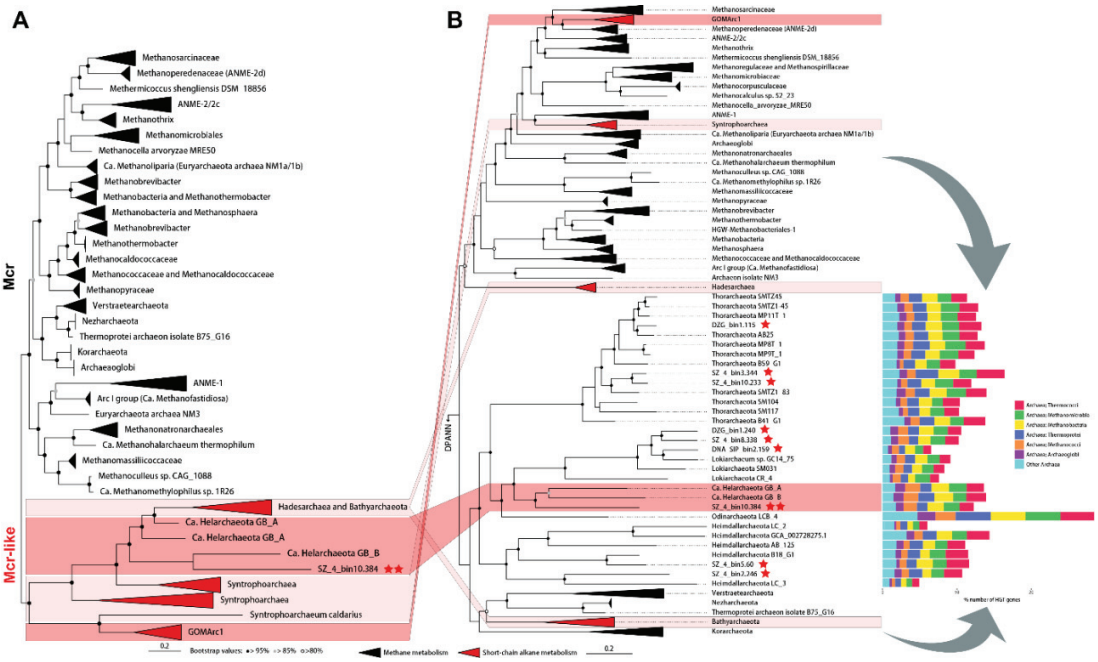

Fig. S9. Phylogenetic position and evolution of Asgard archaea *mcrA* genes. (**A)** Maximum likelihood phylogenetic tree of the *mcrA* genes. (**B)** Ancestral genome content reconstruction with the concatenated 122 archaeal marker gene tree inferred from IQ-TREE. Bar plot of the percentage of genes horizontally transferred from archaea to their genomes. The genes and MAGs obtained in this article are marked with red stars, and those with the MCR complex are highlighted with two red stars. The two grey arrows indicate genes that underwent extensive horizontal transfer from archaea.

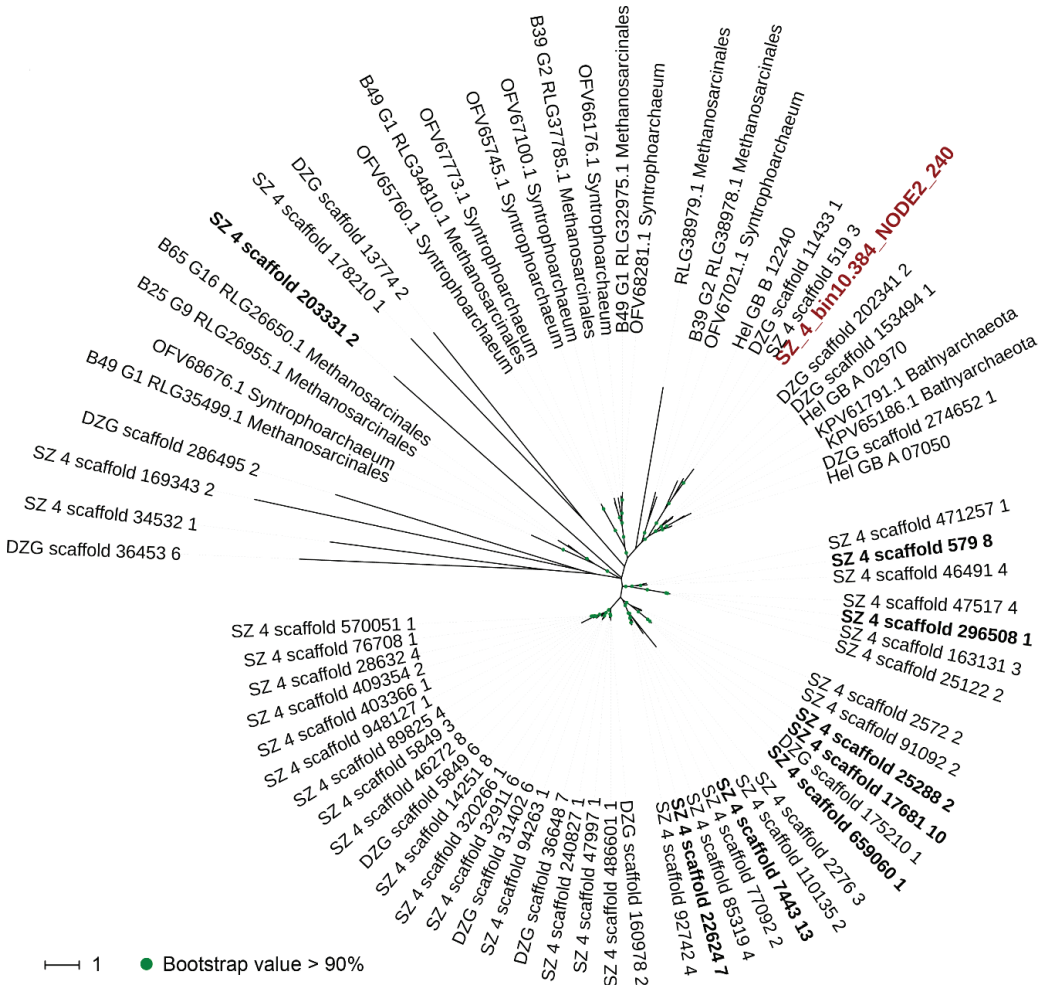

Fig. S10. Protein tree based on *mcrA* gene sequences as identified in the scaffolds. The protein sequences were obtained through BLASTP against novel McrA protein sequences of Asgard with E-value cutoff ≤1e-5. Amino acids > 400 aa were kept for tree building. The tree was re-rooted with Euryarchaeotal and Verstraetearchaeotal McrA protein sequences. McrA sequences deduced from transcripts are marked in bold.

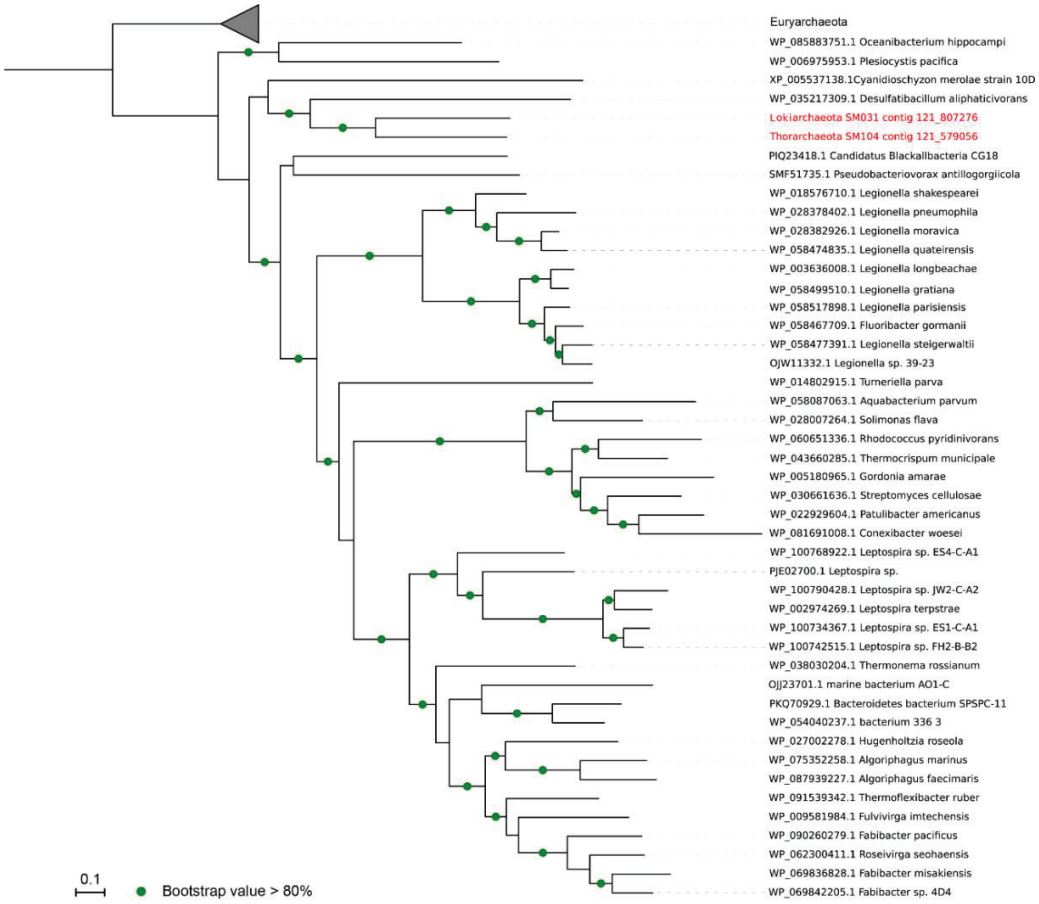

Fig. S11. Protein tree of *alkB* genes. The reference sequences were obtained through BLASTP search with NCBI nr protein database and clustered at 90% sequence identity with Usearch.

4.10. References

1. Lipp, J. S., Morono, Y., Inagaki, F. & Hinrichs, K. U. Significant contribution of Archaea to extant biomass in marine subsurface sediments. *Nature* **454**, 991-994 (2008).

2. Hoshino, T. & Inagaki, F. Abundance and distribution of Archaea in the subseafloor sedimentary biosphere. *ISME J.* **13**, 227-231 (2018).

3. Offre, P., Spang, A. & Schleper, C. Archaea in biogeochemical cycles. *Annu. Rev. Microbiol.* **67**, 437-457 (2013).

4. Ferry, J. G. Methanogenesis: ecology, physiology, biochemistry & genetics. In Springer Science & Business Media: 2012.

5. Baker, B. J. *et al.* Community transcriptomic assembly reveals microbes that contribute to deep-sea carbon and nitrogen cycling. *ISME J.* **7**, 1962-1973 (2013).

6. Li, M. *et al.* Genomic and transcriptomic evidence for scavenging of diverse organic compounds by widespread deep-sea archaea. *Nat. Commun.* **6**, 8933 (2015).

7. Rinke, C. *et al.* Insights into the phylogeny and coding potential of microbial dark matter. *Nature* **499**, 431-437 (2013).

8. Evans, P. N. *et al.* Methane metabolism in the archaeal phylum Bathyarchaeota revealed by genome-centric metagenomics. *Science* **350**, 434-438 (2015).

9. Vanwonterghem, I. *et al.* Methylotrophic methanogenesis discovered in the archaeal phylum Verstraetearchaeota. *Nat. Microbiol.* **1**, 16170 (2016).

10. Zaremba-Niedzwiedzka, K. *et al.* Asgard archaea illuminate the origin of eukaryotic cellular complexity. *Nature* **541**, 353-358 (2017).

11. Spang, A. *et al.* Complex archaea that bridge the gap between prokaryotes and eukaryotes. *Nature* **521**, 173-179 (2015).

12. Seitz, K. W. *et al.* Genomic reconstruction of a novel, deeply branched sediment archaeal phylum with pathways for acetogenesis and sulfur reduction. *ISME J.* **10**, 1696-1705 (2016).

13. Seitz, K. W. *et al.* Asgard archaea capable of anaerobic hydrocarbon cycling. *Nat. Commun.* **10**, 1822 (2019).

14. Vetriani, C. *et al.* Population structure and phylogenetic characterization of marine benthic archaea in deep-sea sediments. *Appl. Environ. Microbiol.* **65**, 4375-4384 (1999).

15. Inagaki, F. *et al.* Archaeology of Archaea: geomicrobiological record of Pleistocene thermal events concealed in a deep-sea subseafloor environment. *Extremophiles* **5**, 385-392 (2001).

16. Takai, K. & Horikoshi, K. Genetic diversity of archaea in deep-sea hydrothermal vent environments. *Genetics* **152**, 1285-1297 (1999).

17. Inagaki, F. *et al.* Microbial communities associated with geological horizons in coastal subseafloor sediments from the Sea of Okhotsk. *Appl. Environ. Microbiol.* **69**, 7224-7235 (2003).

18. Zhou, Z., Liu, Y., Li, M. & Gu, J. D. Two or three domains: a new view of tree of life in the genomics era. *Appl. Microbiol. Biot.* **102**, 3049-3058 (2018).

19. Liu, Y. *et al.* Comparative genomic inference suggests mixotrophic lifestyle for Thorarchaeota. *ISME J.* **12**, 1021-1031 (2018).

20. Karst, S. M. *et al.* Retrieval of a million high-quality, full-length microbial 16S and 18S rRNA gene sequences without primer bias. *Nat. Biotechnol.* **36**, 190-195 (2018).

21. Sousa, F. L. *et al.* Lokiarchaeon is hydrogen dependent. *Nat. Microbiol.* **1**, 16034 (2016).

22. Pushkarev, A. *et al.* A distinct abundant group of microbial rhodopsins discovered using functional metagenomics. *Nature*, 1 (2018).

23. Bulzu, P.-A. *et al.* Casting light on Asgardarchaeota metabolism in a sunlit microoxic niche. *Nat. Microbiol.*, doi: 10.1038/s41564-019-0404-y (2019).

24. Wong, H. L. *et al.* Disentangling the drivers of functional complexity at the metagenomic level in Shark Bay microbial mat microbiomes. *ISME J.* **12**, 2619-2639 (2018).

25. Parks, D. H. *et al.* Recovery of nearly 8,000 metagenome-assembled genomes substantially expands the tree of life. *Nat. Microbiol.* **2**, 1533-1542 (2017).

26. Dombrowski, N., Teske, A. P. & Baker, B. J. Expansive microbial metabolic versatility and biodiversity in dynamic Guaymas Basin hydrothermal sediments. *Nat. Commun.* **9**, 4999 (2018).

27. Konstantinidis, K. T., Rosselló-Móra, R. & Amann, R. Uncultivated microbes in need of their own taxonomy. *ISME J.* **11**, 2399 (2017).

28. Eme, L. *et al.* Archaea and the origin of eukaryotes. *Nat. Rev. Microbiol.* **15**, 711-723 (2017).

29. Aoyagi, T. *et al.* Ultra-high-sensitivity stable-isotope probing of rRNA by high-throughput sequencing of isopycnic centrifugation gradients. *Environ. Microbiol. Rep.* **7**, 282-287 (2015).

30. Yin, X. *et al.* CO_2 conversion to methane and biomass in obligate methylotrophic methanogens in marine sediments. *ISME J.* doi.org/10.1038/s41396-019-0425-9 (2019).

31. Sato, T., Atomi, H. & Imanaka, T. Archaeal type III RuBisCOs function in a pathway for AMP metabolism. *Science* **315**, 1003-1006 (2007).

32. Spang, A. *et al.* Proposal of the reverse flow model for the origin of the eukaryotic cell based on comparative analyses of Asgard archaeal metabolism. *Nat. Microbiol.*, doi: 10.1038/s41564-019-0406-9 (2019).

33. Magnabosco, C. *et al.* A metagenomic window into carbon metabolism at 3 km depth in Precambrian continental crust. *ISME J.* **10**, 730-741 (2016).

34. D'hondt, S. *et al.* Distributions of microbial activities in deep subseafloor sediments. *Science* **306**, 2216-2221 (2004).

35. Villanueva, L., Schouten, S. & Damsté, J. S. S. Phylogenomic analysis of lipid biosynthetic genes of Archaea shed light on the 'lipid divide'. *Environ. Microbiol.* **19**, 54-69 (2017).

36. Williams, T. J., Allen, M., Tschitschko, B. & Cavicchioli, R. Glycerol metabolism of haloarchaea. *Environ. Microbiol.* **19**, 864-877 (2017).

37. Battistuzzi, F. U., Feijao, A. & Hedges, S. B. A genomic timescale of prokaryote evolution: insights into the origin of methanogenesis, phototrophy, and the colonization of land. *BMC Evol. Biol.* **4**, 44 (2004).

38. McKay, L. J. *et al.* Co-occurring genomic capacity for anaerobic methane and dissimilatory sulfur metabolisms discovered in the Korarchaeota. *Nat. Microbiol.* **4**, 614-622 (2019).

39. Wang, Y. *et al.* Expanding anaerobic alkane metabolism in the domain of Archaea. *Nat. Microbiol.* **4**, 595-602 (2019).

40. Borrel, G. *et al.* Wide diversity of methane and short-chain alkane metabolisms in uncultured archaea. *Nat. Microbiol.* **4**, 603-613 (2019).

41. Laso-Pérez, R. *et al.* Thermophilic archaea activate butane via alkyl-coenzyme M formation. *Nature* **539**, 396-401 (2016).

42. Chen, S.-C. *et al.* Anaerobic oxidation of ethane by archaea from a marine hydrocarbon seep. *Nature* **568**, 108-111 (2019).

43. Meyerdierks, A. *et al.* Metagenome and mRNA expression analyses of anaerobic methanotrophic archaea of the ANME-1 group. *Environ. Microbiol.* **12**, 422-439 (2010).

44. Yu, H. *et al.* Comparative Genomics and Proteomic Analysis of Assimilatory Sulfate Reduction Pathways in Anaerobic Methanotrophic Archaea. *Front. Microbiol.* **9**, 2917 (2018).

45. Kumar, V. S., Ferry, J. G. & Maranas, C. D. Metabolic reconstruction of the archaeon methanogen Methanosarcina Acetivorans. *BMC Evol. Biol.* **5**, 28 (2011).

46. Grossi, V. *et al.* Anaerobic 1-alkene metabolism by the alkane-and alkene-degrading sulfate reducer Desulfatibacillum aliphaticivorans strain CV2803T. *Appl. Environ. Microbiol.* **73**, 7882-7890 (2007).

47. Kleindienst, S. *et al.* Diverse sulfate-reducing bacteria of the *Desulfosarcina*/*Desulfococcus* clade are the key alkane degraders at marine seeps. *ISME J.* **8**, 2029-2044 (2014).

48. Lanfranconi, M. P., Alvarez, H. M. & Studdert, C. A. A strain isolated from gas oil-contaminated soil displays chemotaxis towards gas oil and hexadecane. *Environ. Microbiol.* **5**, 1002-1008 (2003).

49. Greening, C. *et al.* Genomic and metagenomic surveys of hydrogenase distribution indicate H_2 is a widely utilised energy source for microbial growth and survival. *ISME J.* **10**, 761-777 (2016).

50. Lueders, T., Manefield, M. & Friedrich, M. W. Enhanced sensitivity of DNA- and rRNA-based stable isotope probing by fractionation and quantitative analysis of isopycnic centrifugation gradients. *Environ. Microbiol.* **6**, 73-78 (2004).

51. Quast, C. *et al.* The SILVA ribosomal RNA gene database project: improved data processing and web-based tools. *Nucleic Acids Res.* **41**, D590 (2012).

52. Kans, J. Entrez direct: E-utilities on the UNIX command line. (2017).

53. Edgar, R. C. Search and clustering orders of magnitude faster than BLAST. *Bioinformatics* **26**, 2460-2461 (2010).

54. Pruesse, E., Peplies, J. & Glöckner, F. O. SINA: accurate high-throughput multiple sequence alignment of ribosomal RNA genes. *Bioinformatics* **28**, 1823-1829 (2012).

55. Spang, A., Caceres, E. F. & Ettema, T. J. Genomic exploration of the diversity, ecology, and evolution of the archaeal domain of life. *Science* **357**, eaaf3883 (2017).

56. Durbin, A. M. & Teske, A. Archaea in organic-lean and organic-rich marine subsurface sediments: an environmental gradient reflected in distinct phylogenetic lineages. *Front. Microbiol.* **3**, 168 (2012).

57. Ludwig, W. *et al.* ARB: a software environment for sequence data. *Nucleic Acids Res.* **32**, 1363-1371 (2004).

58. Nguyen, L. T., Schmidt, H. A., von Haeseler, A. & Minh, B. Q. IQ-TREE: a fast and effective stochastic algorithm for estimating maximum-likelihood phylogenies. *Mol. Biol. Evol.* **32**, 268-274 (2014).

59. Yarza, P. *et al.* Uniting the classification of cultured and uncultured bacteria and archaea using 16S rRNA gene sequences. *Nat. Rev. Microbiol.* **12**, 635-645 (2014).

60. Letunic, I. & Bork, P. Interactive Tree Of Life (iTOL): an online tool for phylogenetic tree display and annotation. *Bioinformatics* **23**, 127-128 (2006).

61. Caporaso, J. G. *et al.* QIIME allows analysis of high-throughput community sequencing data. *Nat. Methods* **7**, 335-336 (2010).

62. Edgar, R. C. UPARSE: highly accurate OTU sequences from microbial amplicon reads. *Nat. Methods* **10**, 996-998 (2013).

63. Herberich, E., Sikorski, J. & Hothorn, T. A robust procedure for comparing multiple means under heteroscedasticity in unbalanced designs. *PLoS One* **5**, e9788 (2010).

64. Team, R. C. R: A language and environment for statistical computing. (2013).

65. Zhou, Z. *et al.* Stratified bacterial and archaeal community in mangrove and intertidal wetland mudflats revealed by high throughput 16S rRNA gene sequencing. *Front. Microbiol.* **8**, 2148 (2017).

66. Joshi, N. & Fass, J. Sickle: A sliding-window, adaptive, quality-based trimming tool for FastQ files (Version 1.33)[Software]. (2011).

67. Kopylova, E., Noé, L. & Touzet, H. SortMeRNA: fast and accurate filtering of ribosomal RNAs in metatranscriptomic data. *Bioinformatics* **28**, 3211-3217 (2012).

68. Peng, Y., Leung, H. C., Yiu, S. M. & Chin, F. Y. IDBA-UD: a de novo assembler for single-cell and metagenomic sequencing data with highly uneven depth. *Bioinformatics* **28**, 1420-1428 (2012).

69. Kang, D. D., Froula, J., Egan, R. & Wang, Z. MetaBAT, an efficient tool for accurately reconstructing single genomes from complex microbial communities. *PeerJ* **3**, e1165 (2015).

70. Sieber, C. M. *et al.* Recovery of genomes from metagenomes via a dereplication, aggregation and scoring strategy. *Nat. Microbiol.* **3**, 836-843 (2018).

71. Bankevich, A. *et al.* SPAdes: a new genome assembly algorithm and its applications to single-cell sequencing. *J. Comput. Biol.* **19**, 455-477 (2012).

72. Delmont, T. O. & Eren, A. M. Linking pangenomes and metagenomes: the *Prochlorococcus* metapangenome. *PeerJ* **6**, e4320 (2018).

73. Parks, D. H. *et al.* CheckM: assessing the quality of microbial genomes recovered from isolates, single cells, and metagenomes. *Genome Res.* **25**, 1043-1055 (2015).

74. Hyatt, D. *et al.* Prodigal: prokaryotic gene recognition and translation initiation site identification. *BMC Bioinformatics* **11**, 119 (2010).

75. Kanehisa, M., Sato, Y. & Morishima, K. BlastKOALA and GhostKOALA: KEGG tools for functional characterization of genome and metagenome sequences. *J. Mol. Biol.* **428**, 726-731 (2016).

76. Huerta-Cepas, J. *et al.* Fast genome-wide functional annotation through orthology assignment by eggNOG-mapper. *Mol. Biol. Evol.* **34**, 2115-2122 (2017).

77. Jones, P. *et al.* InterProScan 5: genome-scale protein function classification. *Bioinformatics* **30**, 1236-1240 (2014).

78. Bagos, P. *et al.* Prediction of signal peptides in archaea. *Protein Eng. Des. Sel.* **22**, 27-35 (2008).

79. Yu, N. Y. *et al.* PSORTb 3.0: improved protein subcellular localization prediction with refined localization subcategories and predictive capabilities for all prokaryotes. *Bioinformatics* **26**, 1608-1615 (2010).

80. Mistry, J. *et al.* Challenges in homology search: HMMER3 and convergent evolution of coiled-coil regions. *Nucleic Acids Res.* **41**, e121 (2013).

81. Eddy, S. R. Accelerated Profile HMM Searches. *PLOS Computational Biology* **7**, e1002195 (2011).

82. Criscuolo, A. & Gribaldo, S. BMGE (Block Mapping and Gathering with Entropy): a new software for selection of phylogenetic informative regions from multiple sequence alignments. *BMC Evol. Biol.* **10**, 210 (2010).

83. Edgar, R. C. MUSCLE: multiple sequence alignment with high accuracy and high throughput. *Nucleic Acids Res.* **32**, 1792-1797 (2004).

84. Speth, D. R. & Orphan, V. J. Metabolic marker gene mining provides insight in global mcrA diversity and, coupled with targeted genome reconstruction, sheds further light on metabolic potential of the *Methanomassiliicoccales*. *PeerJ* **6**, e5614 (2018).

85. Caspi, R. *et al.* The MetaCyc Database of metabolic pathways and enzymes and the BioCyc collection of Pathway/Genome Databases. *Nucleic Acids Res.* **36**, D623-D631 (2007).

86. Li, H. & Durbin, R. Fast and accurate short read alignment with Burrows–Wheeler transform. *Bioinformatics* **25**, 1754-1760 (2009).

87. Berman, H. M. *et al.* The Protein Data Bank. *Nucleic Acids Res.* **28**, 235-242 (2000).

88. Eswar, N. *et al.* Comparative protein structure modeling using modeller. *Curr. Protoc. Bioinformatics.* **15**, 5.6.1-5.6.30 (2006).

89. Morris, G. M. *et al.* AutoDock4 and AutoDockTools4: Automated docking with selective receptor flexibility. *J. Comput. Chem.* **30**, 2785-2791 (2009).

90. Morris, G. M. *et al.* Automated docking using a Lamarckian genetic algorithm and an empirical binding free energy function. *J. Comput. Chem.* **19**, 1639-1662 (1998).

91. Van Der Spoel, D. *et al.* GROMACS: Fast, flexible, and free. *J. Comput. Chem.* **26**, 1701-1718 (2005).

92. Lindorff-Larsen, K. *et al.* Improved side-chain torsion potentials for the Amber ff99SB protein force field. *Proteins* **78**, 1950-1958 (2010).

93. Jorgensen, W. L. *et al.* Comparison of simple potential functions for simulating liquid water. *J. Chem. Phys.* **79**, 926-935 (1983).

94. Darden, T., York, D. & Pedersen, L. Particle mesh Ewald: An N·log(N) method for Ewald sums in large systems. *J. Chem. Phys.* **98**, 10089-10092 (1993).

95. Zhu, Q., Kosoy, M. & Dittmar, K. HGTector: an automated method facilitating genome-wide discovery of putative horizontal gene transfers. *BMC genomics* **15**, 717 (2014).

96. Steinegger, M. & Söding, J. MMseqs2 enables sensitive protein sequence searching for the analysis of massive data sets. *Nat. Biotechnol.* **35**, 1026-1028 (2017).

Chapter 5

General Discussion

The main goal of the thesis was to examine the carbon metabolism in methylotrophic methanogens and Asgard archaea, especially for inorganic carbon assimilation. Based on nucleic acid-SIP, we have clearly shown that ^{13}C-DIC is required as the co-substrate for identifying archaea (methylotrophic methanogens and Lokiarchaeota-4) and detecting their activities in marine sediments, which indicates that inorganic carbon is the main carbon source for nucleic acid synthesis in these archaea.

In methylotrophic methanogens (Chapter 2 and 3), the low methanogenesis rate is associated with methane production from CO_2. This mixotrophic methanogenesis from both methanol and CO_2 in utilizing both substrates kinetically alters inorganic carbon assimilation into biomass, which is indicated by lipid-SIP. Thus, in marine sediments, the low methane production rate *in situ* most likely alters carbon utilization patterns in obligate methylotrophic methanogens. Presently, it is unknown whether methanogens can benefit from the process or whether it is only due to reaction kinetics. However, it is clear that carbon metabolism of methylotrophic methanogens is more divergent *in situ* than that in pure cultures under optimized conditions, and the large pool of inorganic carbon in sediments could alter carbon incorporation patterns of archaea.

Similarly, the ^{13}C-DIC-dependent nucleic acid-SIP is also feasible for identifying uncultivated Asgard archaea (Lokiarchaeota) (Chapter 4). By amending organic polymers, i.e., lignin, humic acid and cellulose, activities of Lokiarchaeota were successfully detected in SIP incubations. In combination with metagenomic sequencing, we have shown that Lokiarchaeota might degrade the polymeric sugar part of these organic compounds via Embden–Meyerhof–Parnas pathway or potentially use the products of polymer breakdown (benzoate) as carbon or energy source. Asgard archaea harbor a more complex carbon metabolism than methanogens, which is indicated by the observation of oxidation pathways of both, short- and medium-chain alkanes. The finding of methyl-coenzyme M reductase genes in Asgard archaea widely extends the phylogenetic distribution of microorganisms involved in short-chain alkane oxidation way beyond methane as a substrate. Taken together, the new findings about activities and potential capabilities of Asgard archaea suggest multiple carbon utilization potentials and versatile activities in alkane oxidation, potentially linked to environmental adaption.

Both methylotrophic methanogens and Asgard archaea have genes encoding methyl-CoM reductase (MCR) for alkane metabolisms. Because of the reversible reactions catalyzed by relevant enzymes

including the Wood-Ljungdahl pathway and alkane metabolisms (Friedrich 2005; Hallam et al., 2004; Scheller et al., 2010), the presence of these relevant enzymes in archaea harbor versatile activities. In the case of methylotrophic methanogenesis, the reverse reactions of CO_2 to methyl-H_4SPT and further to methane suggest CO_2 conversion to methane in obligate methylotrophic methanogens, which will alter carbon incorporation patterns as methyl-H_4SPT can be used for biomass synthesis. Initially, MCR catalyzes the reaction of methane formation. In this process, methanogens can obtain decent amounts of energy for cell growth. However, the extension of *mcr* genes to anaerobic methanotrophs (ANMEs) indicates the reversibility of the methanogenesis (Hallam et al., 2004; Scheller et al., 2010). Furthermore, findings about alkane oxidation via the catalysis of MCR expanded the function of the MCR cluster in archaea (Evans et al., 2019). Therefore, alkane metabolism in methylotrophic methanogens and Asgard archaea offers a glimpse of the versatile abilities of archaea regarding to the survival in a variety of environments. It is likely that archaea can use many reversible activities to adapt to adverse environmental conditions.

Carbon fixation into organic carbon is the determining factor for existence of biosphere on earth. Although the origin of life is unclear, the lack of organic carbon and oxygen on the primitive earth (Lyons et al., 2014; Zahnle et al., 2010) indicates the importance of anaerobic inorganic carbon utilization. Phylogenetic analysis of prokaryotic genes encoding protein depicts the physiology of CO_2 fixation via the Wood–Ljungdahl pathway and methyl compound metabolisms in the last universal common ancestor (LUCA) (Weiss et al., 2016). Thus, the utilization of C1 substrates (methanol) and organic polymers as well as the activity of inorganic carbon assimilation by methylotrophic methanogens and Asgard archaea is potentially associated with the evolution of life.

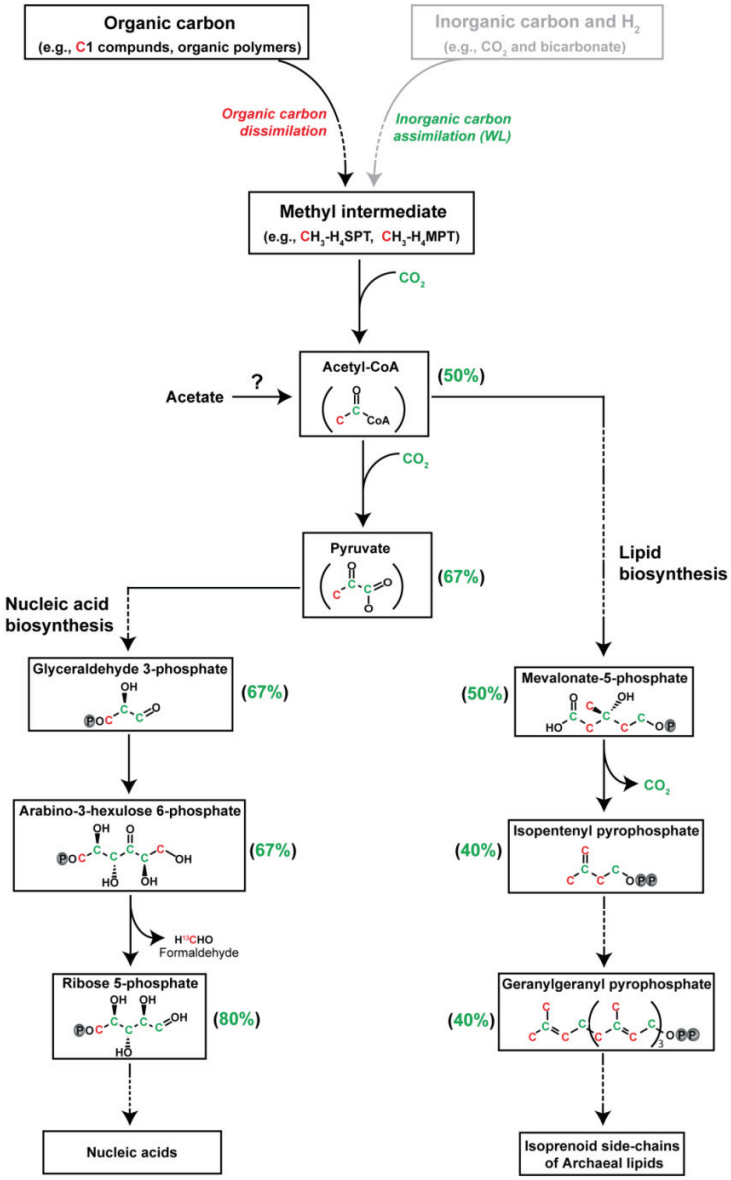

Fig. 1 Summary of the organic carbon dissimilation and carbon assimilation into nucleic acid and lipid biosynthesis in archaea from anoxic marine sediments

WL: Wood–Ljungdahl pathway; CH_3-H_4SPT, methyl-tetrahydrosarcinapterin; CH_3-H_4MPT, methyl-tetrahydromethanopterin. Square with black outline indicates utilization of organic substrates and carbon fixation in archaea. A combination of different reaction steps is indicated by dashed line. Grey color shows autotrophic CO_2 fixation via the reductive WL pathway, potentially by hydrogenotrophic methanogens and Asgard archaea. Red represents carbon assimilation of organic compounds into archaea. Green shows inorganic carbon assimilation and contribution of inorganic carbon to intermediates. Question marker denotes the potential acetate incorporation for biomass.

5.1. Carbon metabolism in methylotrophic methanogens and Asgard archaea

5.1.1. Methyl metabolism

Methylated compounds are the reduced carbon sources and are involved in carbon and energy metabolisms in archaea (Weiss et al., 2016). In the presence of C1 compounds or organic polymers, archaea preferentially use these organic substrates to generate methyl groups, which are the key intermediate of carbon source for biosynthesis (Fig. 1). For example, methanol conversion to CH_3-H_4SPT and methane in methylotrophic methanogens provides energy and methyl intermediate for cell growth. In contrast, Asgard archaea harbor more complex methyl sources. With organic polymers (lignin, humic acid and cellulose), the methyl intermediate originates from organic carbon dissimilation (Fig. 1), which might be involved in utilization of intermediates (fatty acids and benzoate) during the degradation of these organic polymers as shown in Chapter 4 (Fig. 2 and 3). Microorganisms would uptake organic carbon for producing methyl intermediate if methylated compounds or organic carbon are available, since CO_2 reduction to CH_3-H_4SPT is endergonic (Berg et al., 2010). On the contrary, dissimilation of methanol or organic compounds to methyl group and further to CO_2 provides energy for cell activities (Kleerebezem et al., 1999; Thauer et al., 2008; Watkins et al., 2014). Therefore, organic carbon is necessary for triggering the activity of archaea. For example, the standard free energy for methylotrophic methanogenesis from methanol is -105 kJ/mol CH_4 (Liu and Whitman 2008), which can provide sufficient energy for cell growth. For Asgard archaea, participating in degradation of organic polymers such as lignin, humic acids and cellulose or their products of polymer breakdown also provides energy for Asgard activities. As adaption strategy, Asgard archaea might harbor a low growth rate and participate in the degradation of complex compounds existing in sediments. The environmental filtering under the intricate conditions with low energy and carbon availability might lead to the characteristics of these archaea such as long doubling time and the difficulty of enrichment and isolation from sediments.

Marine sediment is a large pool of organic compounds originating from terrigenous sources and water column (Burdige 2005; Schlünz and Schneider 2000; Schubert and Calvert 2001). The continuous precipitation and sedimentation provide organic carbon for microbial growth. Archaea with a slow activity and long doubling time (e.g., Asgard archaea, Bathyarchaeota and ANMEs) might have a similar lifestyle considering the limitation of organic carbon utilization. With a long-time scale, these archaea might have a high abundance in marine sediments (Danovaro et al., 2016; Hoshino and Inagaki 2019), as shown that archaea and bacteria even have a similar abundance in marine sediments (Lloyd et al., 2013a; Schippers et al., 2012).

For carbon assimilation, the methyl intermediate generated from methyl substrates and organic polymers in methylotrophic methanogens and Asgard archaea, respectively, while CO_2 is utilized for the synthesis of carboxyl groups of acetyl-CoA in the presence of methyl intermediate (Fig.2; Fig. 5 and 6 in Chapter 3). The methyl group will be further delivered to acetyl-CoA for biosynthesis of lipid and nucleic acids. The scenario is like that C1 substrates such as methanol and methylamines are the small-molecule compounds without carbon–carbon bond, lacking the diversity of functional groups, which result in inorganic carbon assimilation to replenish carbon source for cell growth. In addition, because of carbon availability in organic polymers, inorganic carbon incorporation might be important for carbon utilization by archaea.

5.1.2. Inorganic carbon assimilation

Inorganic carbon assimilation by microorganisms is ubiquitous in marine sediments, including autotrophic, mixotrophic and heterotrophic carbon fixation (Jones et al., 2016; Sakai et al., 2011; Santruckova et al., 2005). As chemolithoautotrophs, microorganisms affiliated to sulfur-oxidizing bacteria (*Gammaproteobacteria*) fix inorganic carbon in dark sediments under energy supply from sulfur oxidation (Dyksma et al., 2016). For archaea, hydrogenotrophic methanogens in deeper marine sediments also perform dark carbon fixation with reduction of CO_2 to biomass by H_2 (Sakai et al., 2011). Mixotrophs are defined as having the similar contribution of carbon source from organic and inorganic carbon, such as methylotrophic bacteria with serine cycle, some acetogens (*Clostridium ljungdahlii*) and methylotrophic methanogens (Chistoserdova et al., 2009; De Marco 2004; Weimer and Zeikus 1978). Heterotrophs can fix CO_2 via anaplerotic reactions of the citric acid cycle and fermentation pathway (Krebs 1941; Santruckova et al., 2005).

Therefore, inorganic carbon utilization by microorganisms is intricate, especially for archaea in which the carbon source and activity are unclear. However, in consistence with the typical physiology of the LUCA, Euryarchaeota, Bathyarchaeota and Asgard archaea harbor the Wood-Ljungdahl pathway involving in CO_2 fixation (Weiss et al., 2016), which is followed by the reaction to pyruvate from acetyl-CoA and CO_2 (Santiago-Martinez et al., 2016). Methyl group of acetyl-CoA might be formed from organic substrate, i.e., methyl group of methanol by methylotrophic methanogens (Chapter 2) and fatty acids or alkane by Asgard archaea (Chapter 4). However, for the reactions such as acetyl-CoA and pyruvate synthesis, CO_2 incorporation is inevitable in archaea, indicating inorganic carbon is crucial for biomass synthesis. In marine sediments, the presence of organic substrates such as methyl compounds and recalcitrant

compounds might stimulate the activities of these archaea but the organic carbon availability is low. In this case, CO_2 fixation is the carbon replenishment of the limited organic carbon for archaeal growth.

5.2. Carbon incorporation in other archaea

Our study about carbon metabolism in methylotrophic methanogens and Asgard archaea provides insight into the potentials of carbon utilization pattern in archaea, which allows us to have a further discussion about carbon metabolism in other archaea. In Helgoland Mud area, archaea placed within the phyla of Thaumarchaeota, Euryarchaeota, Bathyarchaeota, Lokiarchaeota and Odinarchaeota were detected (Chapter 1). However, knowledge about carbon incorporation by the other archaea found in Helgoland Mud sediments is still limited to date, including Bathyarchaeota, anaerobic methanotrophs (ANMEs), marine benthic group D and DHVEG-1 (MBG-D and DHVEG-1), *Methanomassiliicoccales* and SG8-5.

5.2.1. Carbon metabolism in Bathyarchaeota

Bathyarchaeota is a ubiquitous phylum which is found in a variety of anaerobic marine sediments (He et al., 2016; Kubo et al., 2012; Zhou et al., 2018b). Except for ungrouped Bathyarchaeota, this phylum is classified into 17 subgroups (Kubo et al., 2012), indicating a high diversity in sediments. However, the activity of this archaea phylum has not been known before, only long-term incubations suggest that members of the subgroup Bathy-8 participate in lignin degradation and CO_2 fixation (Yu et al., 2018). Although two genes involved in the degradation of aromatic compounds are detected including catalase peroxidase and 4-oxalocrotonate tautomerase (Meng et al., 2014; Yu et al., 2018), carbon assimilation into biomass is unclear. Arguments such as incorporation of methoxy group and CO_2 into acetyl-CoA and further to biomass indicate that Bathy-8 is an autotroph (Yu et al., 2018) although the relevant gene was not shown for methoxy metabolism. However, it is not feasible to conclude that Bathy-8 are "organoautotrophs" since the methyl or methoxy group from lignin are apparently metabolized. Chapter 3 and Fig. 1 indicate that the methyl group will be assimilated into acetyl-CoA and further to biomass, suggesting a mixotrophic activity of these Bathyarchaeota in utilizing both organic carbon and inorganic carbon source for biomass synthesis. For archaea in anoxic sediments, the methyl group, as a reduced carbon source, and CO_2 as oxidized carbon source are necessary for synthesis of acetyl-CoA. Via the Wood-Ljungdahl pathway with lowest energetic cost (Berg et al., 2010), archaea most likely use both organic and inorganic carbon to produce acetyl-CoA for biomass, because only utilizing CO_2 would require more reducing equivalents (H_2 in the case of hydrogenotrophic methanogens) and energy. Therefore, similar to methylotrophic methanogens and Lokiarchaeota, Bathyarchaeota very likely harbor a mixotrophic carbon utilization pattern rather than solely autotrophic carbon fixation.

5.2.2. Carbon metabolism in anaerobic methanotrophs (ANMEs)

In ANMEs, methane generated from deeper marine sediments can be converted into CO_2 in presence of electron acceptors such as sulfate, iron oxides and nitrate (Fig. 2) (Yan et al., 2018). In the sulfate methane transition zone (SMTZ) of marine sediments, the syntrophic consortia between ANMEs and sulfate reducers is formed, in which ANMEs deliver electrons generated during anaerobic methane oxidation (AOM) to microorganisms for sulfate reduction (Hinrichs et al., 1999; Knittel and Boetius 2009). The reactions of anaerobic methane oxidation are as followed:

$CH_4 + SO_4^{2+} \rightarrow HCO_3^- + HS^- + H_2O$ $\Delta G^{\circ\prime} = -16.6$ KJ/mol CH_4 (Valentine and Reeburgh 2000)

Although energy formation from AOM coupled to sulfate reduction is feasible, carbon incorporation into biomass in ANMEs is not well estimated. Incubation-dependent AOM indicates that methane oxidation by ANME-1 strongly accelerates CO_2 incorporation into archaeal lipids (Kellermann et al., 2012). Lipid analysis with dual labeling strategy of ^{13}C-DIC and D suggests that ANME-1 is "chemoorganoautotrophic" according to the ratio of inorganic carbon assimilation to lipid production (Kellermann et al., 2012). However, methane oxidation via the catalysis of methyl-CoM reductase (MCR) to methyl intermediate (CH_3-H_4MPT) will be used for acetyl-CoA synthesis and then for biomass (Fig. 2) (Meyerdierks et al., 2010), indicating a mixotrophic growth during AOM, which is supported by previous studies (Nauhaus et al., 2007; Weber et al., 2017; Wegener et al., 2008). In addition, it is unclear whether the dual labeling technique is feasible to assess carbon assimilation patterns in ANME-1, since the calculation of produced lipid is based on deuterium assimilation from D_2O, while hydrogen incorporation into biomass (lipid) from methane is complicated and unclear because four hydrogen atoms are available in methane. Therefore, it is very likely that ANMEs, as mixotrophs, harbor the similar carbon utilization patterns to methylotrophic methanogens as they share the similar methyl incorporation.

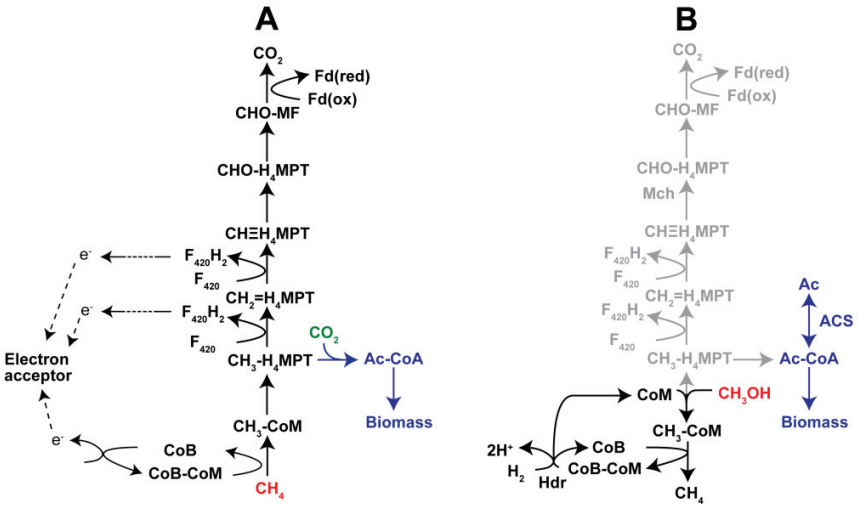

Fig. 2 Pathway of anaerobic methane oxidation (AOM) in ANMEs (A) and methanogenesis in *Methanomassiliicoccales* spp (B). Electron acceptor in Fig. A indicates that the reduction of potential electron acceptors such as sulfate, iron oxides and nitrate coupled to AOM. Ac-CoA: acetyl-CoA; Ac: acetate; ACS: acetyl-CoA synthase. Grey represents the methanogenic pathway absent in *Methanomassiliicoccales*. Pathway construction is based on the KEGG metabolic pathways and the previous studies (Borrel et al., 2013; Borrel et al., 2014; Cai et al., 2018; Chistoserdova et al., 2005; Havelsrud et al., 2011; Lang et al., 2015; Li et al., 2016; Meyerdierks et al., 2010).

5.2.3. Carbon metabolism in Thermoplasmata and potential acetate metabolism in archaea

Thermoplasmata including *Thermoprofundales* (i.e., former marine benthic group D; MBG-D), SG8-5 (RC-III) and *Methanomassiliicoccales* are found in Helgoland Mud sediments. Metagenomic analysis suggests that *Thermoprofundales* and SG8-5 are anaerobic protein degraders (Lazar et al., 2017; Lloyd et al., 2013b; Zhou et al., 2018a). *Thermoprofundales* might fix CO_2 via the Wood–Ljungdahl pathway, which is identified in metagenome-assembled genomes (Zhou et al., 2018a).

As the seventh order of methanogens, *Methanomassiliicoccales* have been identified in human feces, rumen, termite gut and waste treatment sludge (Mihajlovski et al., 2008; Paul et al., 2012; Tajima 2001; Wright et al., 2004). *Methanomassiliicoccales* are able to produce methane by using H_2 and methyl substrates such as methanol, methylamins, methanethiol and dimethyl sulfide (Borrel et al., 2014). The reaction of methanol dependent methanogenesis is followed:

$CH_3OH + H_2 \rightarrow CH_4 + H_2O$ $\Delta G^{\circ\prime} = -113$ kJ/mol CH_4 (Liu and Whitman 2008)

Given that H_2 is directly used to reduce the methyl group and the pathway of oxidation of methyl group to CO_2 is absent, methyl intermediate (CH_3-H_4MPT) cannot be obtained during methane formation in *Methanomassiliicoccales* (Fig. 2), indicating that methane metabolism in these archaea is only involved in energy generation rather than carbon assimilation. Metagenomic analysis and the culture medium further suggest an additional carbon source, i.e., acetate, is necessary for cell carbon incorporation into biomass. This observation suggests *Methanomassiliicoccales* were not detected by RNA-SIP in methanol incubations without H_2 (Chapter 2 and 3), although evidences show that *Methanomassiliicoccales*-like group is detected in marine sediments (Zhou et al., 2015). Hence, unlike other obligate methylotrophic methanogens (*Methanococcoides* spp.), *Methanomassiliicoccales* likely to use acetate as carbon source, which is incorporated into acetyl-CoA via the catalysis of acetyl-CoA synthase (Fig. 2).

Apart from *Methanomassiliicoccales*, the functional genes involved in acetate assimilation or generation are detected in most archaea (Table 1 in Chapter 1), indicating acetate metabolism potentially plays an important role in carbon utilization in archaea. Previous studies from the perspective of energy metabolism suggest that archaea should produce acetate to obtain ATP instead of acetate assimilation (He et al., 2016; Lazar et al., 2017; Liu et al., 2018; Spang et al., 2019; Zhou et al., 2018a). For example, ANME-1 might perform methanogenesis with acetate or grow on acetate (Beulig et al., 2018; Jagersma et al., 2012). Based on the capability of acetate metabolism in *Methanomassiliicoccales* and ANME-1, our studies propose that except for CO_2 as the replenishment carbon source for archaeal growth when carbon availability is low, acetate might be the second crucial carbon source as the acetate metabolism genes are ubiquitous in archaea. Without participation of methanogens or additional electron acceptors, acetate degradation is intricate since acetate is the primary terminal product of organic decomposition in anaerobic conditions (Duddleston et al., 2002). In addition, acetate as the key intermediate for organic carbon degradation, is detectable (up to ~20 μM) (Beulig et al., 2018; King 1991; Zhuang et al., 2018) and does not directly link to methanogenesis in marine sediments (Beulig et al., 2018). Therefore, SIP technique should be applied based on incubations with ^{13}C-labeled acetate as the co-substrate to target uncultured archaea in marine sediments.

5.3. Nucleic acid-SIP for detecting archaea-high sensitivity meets low activity

Nucleic acid-SIP based on ^{13}C-labeled carbon incorporation is applied to detect the activity of microorganisms in a variety of environments. During nucleic acid-SIP, specific carbon source should be used to stimulate microorganisms in incubation setups, but for uncultured microorganisms with unknown

carbon source or complex carbon utilization, nucleic acid-SIP is not able to detect them. Cross-feeding of label might occur if a high molecular carbon source is supplied. Since next generation sequencing after nucleic acid-SIP provides a high phylogenetic resolution, the direct detection of microbial activity by SIP attracts the interests of scientists, especially combining with further analysis such as metagenomic or metatranscriptomic sequencing and Raman-FISH (Fortunato and Huber 2016; Grob et al., 2015; Huang et al., 2007).

In general, 12 to 14 fractions will be obtained after density gradient separation of nucleic acids. In order to have a successful separation of ^{13}C-labeled nucleic acid, density shifts require a high labeling level in RNA or DNA (more than 10 atom% of C) (Manefield et al., 2002). However, nucleic acid-SIP harbors an ultra-high sensitivity as indicated by the successful separation of a mixture of 0.001% of ^{13}C-labeled RNA (Aoyagi et al., 2015). This ultra-high sensitivity in identifying active microorganisms has been applied to detect dioxane degraders with a low activity (Aoyagi et al., 2018). Considering the high sensitivity of nucleic acid-SIP and low activity of Asgard archaea in marine sediments, the higher relative abundance of Lokiarchaeota in heavy fractions than light fractions suggests inorganic carbon assimilation into nucleic acids of these Lokiarchaeota (Fig. 2 in Chapter 4). Therefore, nucleic acid-SIP is a crucial technique to identify microorganisms with low activity.

Additionally, apart from methylotrophic methanogens and Lokiarchaeota, it is very likely that the nucleic acid-SIP method together with using ^{13}C-labeled bicarbonate can detect other archaea such as Bathyarchaeota, some Thermoplasmata, ANMEs and so on. In marine sediments, these archaea are detectable and potentially active after feeding some organic substrates combining with ^{13}C-DIC. Given that archaea activity in deeper marine sediment is very low, nucleic acid-SIP technique might be very useful to detect their activities.

5.4. Carbon fixation in bacteria in anoxic marine sediments

In the Helgoland mud sediments, divergent bacteria groups were detected. Specifically in the SIP incubations without amending electron donor, bacteria affiliated to Atribacteria, Planctomycetes (*Planctomycetaceae* and MSBL9), and Deltaproteobacteria (*Desulfobacteraceae*, *Desulfobulbaceae* and *Desulfuromonadaceae*) were identified, indicating the potential activity *in situ*. However, relative abundances of these bacteria did not show a substantial increase in the heavy fractions. Indeed, metagenomic analysis of these detected bacteria shows that Atribacteria are potentially heterotrophs in fermentation carbohydrates and organic acids (Nobu et al., 2016). Planctomycetes are also regarded as heterotrophs growing on carbohydrates or sugar polymers (Robbins et al., 2016; Woebken et al., 2007).

For the family of *Desulfobacteraceae*, *Desulfobulbaceae* and *Desulfuromonadaceae*, most members are heterotrophs, although some groups harbor the complete WL pathway and reverse citric acid cycle for carbon fixation with the reduction by H_2 (Brysch et al., 1987; Dorries et al., 2016; Finster et al., 2013), suggesting H_2 is required for autotrophic growth. Therefore, it seems that nucleic-SIP combining with incubations amended ^{13}C-DIC is feasible for identifying active archaeal groups in marine sediments. The explanation is that some archaea such as methylotrophic methanogens, Lokiarchaeota, ANMEs and even Bathyarchaeota are mixotrophically assimilating both organic substrates and CO_2 as carbon source, coupling methyl intermediate production from organic carbon and CO_2 for biomass biosynthesis.

Based on these findings, further work should focus on the topics as follows:

1) Is it ubiquitous that CO_2 conversion to methane occurs in all methanogens? Except for hydrogenotrophic methanogens, methylotrophic methanogens can use CO_2 for methane production. But it is unknown whether acetoclastic methanogens can produce methane from CO_2 without syntrophic partners, although the complete acetyl-CoA pathway is detected in these methanogens.

2) RNA-SIP has shown that Lokiarchaeota is able to degrade lignin but the corresponding pathway was not detected. More evidence should be collected to prove how Asgard archaea participate in lignin degradation such as specific functional group of lignin molecular and secondary products of organic polymer degradation by obtaining highly complete metagenomes, enriching Asgard archaea and measuring intermediates.

3) Carbon fixation in other archaeal phyla. It is well known that some Euryarchaeota (hydrogenotrophic methanogens) and Thaumarchaeota (ammonia oxidizer) incorporate inorganic carbon for carbon source, but carbon assimilation such as in Bathyarchaeota, Woesearchaeota, ANMEs is not well studied. Nucleic acid- and lipid-SIP should be applied to study carbon assimilation patterns by these archaea from incubated samples. Further studies should explore factors influencing carbon fixation by archaea in marine sediments such as organic carbon content, geochemical profiles of sediments.

4) It is likely that archaea activities are associated with organic carbon degradation since organic carbon is necessary for archaea growth, i.e., methanol utilization in methylotrophic methanogens and organic polymer degradation by Lokiarchaeota. However, how organic compounds affect archaeal diversity and distribution in marine sediments is unclear. For example, is there any relationship between distributions of some specific archaea and organic carbon content, specific molecular structures of organic compounds or C:O:N:H ratios? Therefore, archaeal distributions, activities and organic carbon characteristics from different marine sediments should be investigated to establish their correlations.

5.5. Reference

Aoyagi, T., Hanada, S., Itoh, H., Sato, Y., Ogata, A., Friedrich, M. W., Kikuchi, Y. and Hori, T. (2015) Ultra-high-sensitivity stable-isotope probing of rRNA by high-throughput sequencing of isopycnic centrifugation gradients. *Environ Microbiol Rep,* 7, 282-287.

Aoyagi, T., Morishita, F., Sugiyama, Y., Ichikawa, D., Mayumi, D., Kikuchi, Y., Ogata, A., Muraoka, K., Habe, H. and Hori, T. (2018) Identification of active and taxonomically diverse 1,4-dioxane degraders in a full-scale activated sludge system by high-sensitivity stable isotope probing. *ISME J,* 12, 2376-2388.

Berg, I. A., Kockelkorn, D., Ramos-Vera, W. H., Say, R. F., Zarzycki, J., Hugler, M., Alber, B. E. and Fuchs, G. (2010) Autotrophic carbon fixation in archaea. *Nat Rev Microbiol,* 8, 447-460.

Beulig, F., Roy, H., Glombitza, C. and Jorgensen, B. B. (2018) Control on rate and pathway of anaerobic organic carbon degradation in the seabed. *Proc. Natl. Acad. Sci. U. S. A.,* 115, 367-372.

Borrel, G., O'Toole, P. W., Harris, H. M., Peyret, P., Brugere, J. F. and Gribaldo, S. (2013) Phylogenomic data support a seventh order of methylotrophic methanogens and provide insights into the evolution of methanogenesis. *Genome Biol. Evol.,* 5, 1769-1780.

Borrel, G., Parisot, N., Harris, H. M., Peyretaillade, E., Gaci, N., Tottey, W., Bardot, O., Raymann, K., Gribaldo, S., Peyret, P., O'Toole, P. W. and Brugere, J. F. (2014) Comparative genomics highlights the unique biology of *Methanomassiliicoccales*, a *Thermoplasmatales*-related seventh order of methanogenic archaea that encodes pyrrolysine. *BMC Genomics,* 15, 679, doi: 10.1186/1471-2164-15-679.

Brysch, K., Schneider, C., Fuchs, G. and Widdel, F. (1987) Lithoautotrophic growth of sulfate-reducing bacteria, and description of *Desulfobacterium autotrophicum* gen. nov., sp. nov. *Arch Microbiol,* 148, 264-274.

Burdige, D. J. (2005) Burial of terrestrial organic matter in marine sediments: A re-assessment. *Global Biogeochem. Cy.,* 19, GB4011 doi:10.1029/2004GB002368.

Cai, C., Leu, A. O., Xie, G. J., Guo, J., Feng, Y., Zhao, J. X., Tyson, G. W., Yuan, Z. and Hu, S. (2018) A methanotrophic archaeon couples anaerobic oxidation of methane to Fe(III) reduction. *ISME J,* 12, 1929-1939.

Chistoserdova, L., Kalyuzhnaya, M. G. and Lidstrom, M. E. (2009) The expanding world of methylotrophic metabolism. *Annu Rev Microbiol,* 63, 477-499.

Chistoserdova, L., Vorholt, J. A. and Lidstrom, M. E. (2005) A genomic view of methane oxidation by aerobic bacteria and anaerobic archaea. *Genome Biol,* 6, 208, doi: 10.1186/gb-2005-6-2-208.

Danovaro, R., Molari, M., Corinaldesi, C. and Dell'Anno, A. (2016) Macroecological drivers of archaea and bacteria in benthic deep-sea ecosystems. *Sci. Adv.,* 2, e1500961, doi: 10.1126/sciadv.1500961.

De Marco, P. (2004) Methylotrophy versus heterotrophy: a misconception. *Microbiology,* 150, 1606-1607.

Dorries, M., Wohlbrand, L., Kube, M., Reinhardt, R. and Rabus, R. (2016) Genome and catabolic subproteomes of the marine, nutritionally versatile, sulfate-reducing bacterium *Desulfococcus multivorans* DSM 2059. *BMC Genomics,* 17, 918, doi: 10.1186/s12864-016-3236-7.

Duddleston, K. N., Kinney, M. A., Kiene, R. P. and Hines, M. E. (2002) Anaerobic microbial biogeochemistry in a northern bog: Acetate as a dominant metabolic end product. *Global Biogeochemical Cycles,* 16, 1063, doi:10.1029/2001GB0014022.

Dyksma, S., Bischof, K., Fuchs, B. M., Hoffmann, K., Meier, D., Meyerdierks, A., Pjevac, P., Probandt, D., Richter, M., Stepanauskas, R. and Mussmann, M. (2016) Ubiquitous *Gammaproteobacteria* dominate dark carbon fixation in coastal sediments. *ISME J.,* 10, 1939-1953.

Evans, P. N., Boyd, J. A., Leu, A. O., Woodcroft, B. J., Parks, D. H., Hugenholtz, P. and Tyson, G. W. (2019) An evolving view of methane metabolism in the Archaea. *Nat. Rev. Microbiol.* **17**, 219–232

Finster, K. W., Kjeldsen, K. U., Kube, M., Reinhardt, R., Mussmann, M., Amann, R. and Schreiber, L. (2013) Complete genome sequence of *Desulfocapsa sulfexigens*, a marine deltaproteobacterium specialized in disproportionating inorganic sulfur compounds. *Stand Genomic Sci,* 8, 58-68.

Fortunato, C. S. and Huber, J. A. (2016) Coupled RNA-SIP and metatranscriptomics of active chemolithoautotrophic communities at a deep-sea hydrothermal vent. *ISME J.,* 10, 1925-1938.

Friedrich, M. W. (2005) Methyl-coenzyme M reductase genes: unique functional markers for methanogenic and anaerobic methane-oxidizing Archaea. *Methods in Enzymology,* 397, 428-442.

Grob, C., Taubert, M., Howat, A. M., Burns, O. J., Dixon, J. L., Richnow, H. H., Jehmlich, N., von Bergen, M., Chen, Y. and Murrell, J. C. (2015) Combining metagenomics with metaproteomics and stable isotope probing reveals metabolic pathways used by a naturally occurring marine methylotroph. *Environ Microbiol,* 17, 4007-4018.

Hallam, S. J., Putnam, N., Preston, C. M., Detter, J. C., Rokhsar, D., Richardson, P. M. and DeLong, E. F. (2004) Reverse methanogenesis: testing the hypothesis with environmental genomics. *Science,* 305, 1457-1462.

Havelsrud, O. E., Haverkamp, T. H., Kristensen, T., Jakobsen, K. S. and Rike, A. G. (2011) A metagenomic study of methanotrophic microorganisms in Coal Oil Point seep sediments. *BMC Microbiol,* 11, 221 doi: 10.1186/1471-2180-11-221.

He, Y., Li, M., Perumal, V., Feng, X., Fang, J., Xie, J., Sievert, S. M. and Wang, F. (2016) Genomic and enzymatic evidence for acetogenesis among multiple lineages of the archaeal phylum Bathyarchaeota widespread in marine sediments. *Nat. Microbiol.,* 1, 16035, doi: 10.1038/nmicrobiol.2016.35.

Hinrichs, K. U., Hayes, J. M., Sylva, S. P., Brewer, P. G. and DeLong, E. F. (1999) Methane-consuming archaebacteria in marine sediments. *Nature,* 389, 802-805.

Hoshino, T. and Inagaki, F. (2019) Abundance and distribution of Archaea in the subseafloor sedimentary biosphere. *ISME J,* 13, 227-231.

Huang, W. E., Stoecker, K., Griffiths, R., Newbold, L., Daims, H., Whiteley, A. S. and Wagner, M. (2007) Raman-FISH: combining stable-isotope Raman spectroscopy and fluorescence in situ hybridization for the single cell analysis of identity and function. *Environ Microbiol,* 9, 1878-1889.

Jagersma, C. G., Meulepas, R. J., Timmers, P. H., Szperl, A., Lens, P. N. and Stams, A. J. (2012) Enrichment of ANME-1 from Eckernforde Bay sediment on thiosulfate, methane and short-chain fatty acids. *J Biotechnol,* 157, 482-489.

Jones, S. W., Fast, A. G., Carlson, E. D., Wiedel, C. A., Au, J., Antoniewicz, M. R., Papoutsakis, E. T. and Tracy, B. P. (2016) CO_2 fixation by anaerobic non-photosynthetic mixotrophy for improved carbon conversion. *Nat Commun,* 7, 12800, doi: 10.1038/ncomms12800.

Kellermann, M. Y., Wegener, G., Elvert, M., Yoshinaga, M. Y., Lin, Y. S., Holler, T., Mollar, X. P., Knittel, K. and Hinrichs, K. U. (2012) Autotrophy as a predominant mode of carbon fixation in anaerobic methane-oxidizing microbial communities. *Proc. Natl. Acad. Sci. U. S. A.,* 109, 19321-19326.

King, G. M. (1991) Measurement of acetate concentrations in marine pore waters by using an enzymatic approach. *Appl Environ Microbiol,* 57, 3476-3481.

Kleerebezem, R., Hulshoff Pol, L. W. and Lettinga, G. (1999) Energetics of product formation during anaerobic degradation of phthalate isomers and benzoate. *FEMS Microbiol Ecol,* 29, 273-282.

Knittel, K. and Boetius, A. (2009) Anaerobic oxidation of methane: progress with an unknown process. *Annu Rev Microbiol,* 63, 311-334.

Krebs, H. A. (1941) Carbon dioxide assimilation in heterotrophic organisms. *Nautre,* 147, 560-563.

Kubo, K., Lloyd, K. G., J, F. B., Amann, R., Teske, A. and Knittel, K. (2012) Archaea of the Miscellaneous Crenarchaeotal Group are abundant, diverse and widespread in marine sediments. *ISME J,* 6, 1949-1965.

Lang, K., Schuldes, J., Klingl, A., Poehlein, A., Daniel, R. and Brunea, A. (2015) New mode of energy metabolism in the seventh order of methanogens as revealed by comparative genome analysis of "*Candidatus* Methanoplasma termitum". *Appl. Environ. Microbiol.,* 81, 1338-1352.

Lazar, C. S., Baker, B. J., Seitz, K. W. and Teske, A. P. (2017) Genomic reconstruction of multiple lineages of uncultured benthic archaea suggests distinct biogeochemical roles and ecological niches. *ISME J.,* 11, 1118-1129.

Li, Y., Leahy, S. C., Jeyanathan, J., Henderson, G., Cox, F., Altermann, E., Kelly, W. J., Lambie, S. C., Janssen, P. H., Rakonjac, J. and Attwood, G. T. (2016) The complete genome sequence of the methanogenic archaeon ISO4-H5 provides insights into the methylotrophic lifestyle of a ruminal representative of the *Methanomassiliicoccales*. *Stand Genomic Sci,* 11, 59, doi: 10.1186/s40793-016-0183-5.

Liu, X., Li, M., Castelle, C. J., Probst, A. J., Zhou, Z., Pan, J., Liu, Y., Banfield, J. F. and Gu, J. D. (2018) Insights into the ecology, evolution, and metabolism of the widespread Woesearchaeotal lineages. *Microbiome,* 6, 102, doi: 10.1186/s40168-018-0488-2.

Liu, Y. and Whitman, W. B. (2008) Metabolic, phylogenetic, and ecological diversity of the methanogenic archaea. *Ann. NY. Acad. Sci.,* 1125, 171-189.

Lloyd, K. G., May, M. K., Kevorkian, R. T. and Steen, A. D. (2013a) Meta-analysis of quantification methods shows that archaea and bacteria have similar abundances in the subseafloor. *Appl Environ Microbiol,* 79, 7790-7799.

Lloyd, K. G., Schreiber, L., Petersen, D. G., Kjeldsen, K. U., Lever, M. A., Steen, A. D., Stepanauskas, R., Richter, M., Kleindienst, S., Lenk, S., Schramm, A. and Jorgensen, B. B. (2013b) Predominant archaea in marine sediments degrade detrital proteins. *Nature,* 496, 215-218.

Lyons, T. W., Reinhard, C. T. and Planavsky, N. J. (2014) The rise of oxygen in Earth's early ocean and atmosphere. *Nature,* 506, 307-315.

Manefield, M., Whiteley, A. S., Griffiths, R. I. and Bailey, M. J. (2002) RNA stable isotope probing, a novel means of linking microbial community function to phylogeny. *Appl. Environ. Microbiol.,* 68, 5367-5373.

Meng, J., Xu, J., Qin, D., He, Y., Xiao, X. and Wang, F. (2014) Genetic and functional properties of uncultivated MCG archaea assessed by metagenome and gene expression analyses. *ISME J.,* 8, 650-659.

Meyerdierks, A., Kube, M., Kostadinov, I., Teeling, H., Glockner, F. O., Reinhardt, R. and Amann, R. (2010) Metagenome and mRNA expression analyses of anaerobic methanotrophic archaea of the ANME-1 group. *Environ. Microbiol.,* 12, 422-439.

Mihajlovski, A., Alric, M. and Brugere, J. F. (2008) A putative new order of methanogenic Archaea inhabiting the human gut, as revealed by molecular analyses of the mcrA gene. *Res Microbiol,* 159, 516-521.

Nauhaus, K., Albrecht, M., Elvert, M., Boetius, A. and Widdel, F. (2007) *In vitro* cell growth of marine archaeal-bacterial consortia during anaerobic oxidation of methane with sulfate. *Environ Microbiol,* 9, 187-196.

Nobu, M. K., Dodsworth, J. A., Murugapiran, S. K., Rinke, C., Gies, E. A., Webster, G., Schwientek, P., Kille, P., Parkes, R. J., Sass, H., Jorgensen, B. B., Weightman, A. J., Liu, W. T., Hallam, S. J., Tsiamis, G., Woyke, T. and Hedlund, B. P. (2016) Phylogeny and physiology of candidate phylum 'Atribacteria' (OP9/JS1) inferred from cultivation-independent genomics. *ISME J,* 10, 273-286.

Paul, K., Nonoh, J. O., Mikulski, L. and Brune, A. (2012) "*Methanoplasmatales*," *Thermoplasmatales*-related archaea in termite guts and other environments, are the seventh order of methanogens. *Appl Environ Microbiol,* 78, 8245-8253.

Robbins, S. J., Evans, P. N., Parks, D. H., Golding, S. D. and Tyson, G. W. (2016) Genome-centric analysis of microbial populations enriched by hydraulic fracture fluid additives in a coal bed methane production well. *Front Microbiol,* 7, 731, doi: 10.3389/fmicb.2016.00731.

Sakai, S., Takaki, Y., Shimamura, S., Sekine, M., Tajima, T., Kosugi, H., Ichikawa, N., Tasumi, E., Hiraki, A. T., Shimizu, A., Y., K., Nishiko, R., Mori, K., Fujita, N., Imachi, H. and Takai, K. (2011) Genome sequence of a mesophilic hydrogenotrophic methanogen *Methanocella paludicola*, the first cultivated representative of the order *Methanocellales*. *PLoS ONE,* 6, e22898, doi: 10.1371/journal.pone.0022898.

Santiago-Martinez, M. G., Encalada, R., Lira-Silva, E., Pineda, E., Gallardo-Perez, J. C., Reyes-Garcia, M. A., Saavedra, E., Moreno-Sanchez, R., Marin-Hernandez, A. and Jasso-Chavez, R. (2016) The nutritional status of *Methanosarcina acetivorans* regulates glycogen metabolism and gluconeogenesis and glycolysis fluxes. *FEBS J,* 283, 1979-1999.

Santruckova, H., Bird, M. I., Elhottova, D., Novak, J., Picek, T., Simek, M. and Tykva, R. (2005) Heterotrophic fixation of CO_2 in soil. *Microb Ecol,* 49, 218-225.

Scheller, S., Goenrich, M., Boecher, R., Thauer, R. K. and Jaun, B. (2010) The key nickel enzyme of methanogenesis catalyses the anaerobic oxidation of methane. *Nature,* 465, 606-608.

Schippers, A., Kock, D., Hoft, C., Koweker, G. and Siegert, M. (2012) Quantification of microbial communities in subsurface marine sediments of the Black Sea and off Namibia. *Front Microbiol,* 3, 16, doi: 10.3389/fmicb.2012.00016.

Schlünz, B. and Schneider, R. R. (2000) Transport of terrestrial organic carbon to the oceans by rivers: re-estimating flux- and burial rates. *IRJES,* 88, 599-606.

Schubert, C. J. and Calvert, S. E. (2001) Nitrogen and carbon isotopic composition of marine and terrestrial organic matter in Arctic Ocean sediments: implications for nutrient utilization and organic matter composition. *Deep Sea Res. Part 1,* 48, 789-810.

Spang, A., Stairs, C. W., Dombrowski, N., Eme, L., Lombard, J., Caceres, E. F., Greening, C., Baker, B. J. and Ettema, T. J. G. (2019) Proposal of the reverse flow model for the origin of the eukaryotic cell based on comparative analyses of Asgard archaeal metabolism. *Nat Microbiol*. doi: 10.1038/s41564-019-0406-9.

Tajima, K. (2001) Phylogenetic analysis of archaeal 16S rRNA libraries from the rumen suggests the existence of a novel group of archaea not associated with known methanogens. *FEMS Microbiology Letters,* 200, 67-72.

Thauer, R. K., Kaster, A. K., Seedorf, H., Buckel, W. and Hedderich, R. (2008) Methanogenic archaea: ecologically relevant differences in energy conservation. *Nat. Rev. Microbiol.,* 6, 579-591.

Valentine, D. L. and Reeburgh, W. S. (2000) New perspectives on anaerobic methane oxidation. *Environ Microbiol,* 2, 477-484.

Watkins, A. J., Roussel, E. G., Parkes, R. J. and Sass, H. (2014) Glycine betaine as a direct substrate for methanogens (*Methanococcoides* spp.). *Appl. Environ. Microbiol.,* 80, 289-293.

Weber, H. S., Habicht, K. S. and Thamdrup, B. (2017) Anaerobic methanotrophic archaea of the ANME-2d cluster are active in a low-sulfate, iron-rich freshwater sediment. *Front Microbiol,* 8, 619, doi: 10.3389/fmicb.2017.00619.

Wegener, G., Niemann, H., Elvert, M., Hinrichs, K. U. and Boetius, A. (2008) Assimilation of methane and inorganic carbon by microbial communities mediating the anaerobic oxidation of methane. *Environ Microbiol,* 10, 2287-2298.

Weimer, P. J. and Zeikus, J. G. (1978) One carbon metabolism in methanogenic bacteria. *Arch. Microbiol.,* 119, 47-57.

Weiss, M. C., Sousa, F. L., Mrnjavac, N., Neukirchen, S., Roettger, M., Nelson-Sathi, S. and Martin, W. F. (2016) The physiology and habitat of the last universal common ancestor. *Nat. Microbiol.,* 1, 16116, doi: 10.1038/nmicrobiol.2016.116.

Woebken, D., Teeling, H., Wecker, P., Dumitriu, A., Kostadinov, I., Delong, E. F., Amann, R. and Glockner, F. O. (2007) Fosmids of novel marine *Planctomycetes* from the Namibian and Oregon coast upwelling systems and their cross-comparison with planctomycete genomes. *ISME J,* 1, 419-435.

Wright, A. D. G., Williams, A. J., Winder, B., Christophersen, C. T., Rodgers, S. L. and Smith, K. D. (2004) Molecular diversity of rumen methanogens from sheep in western Australia. *Appl. Environ. Microbiol,* 70, 1263-1270.

Yan, Z., Joshi, P., Gorski, C. A. and Ferry, J. G. (2018) A biochemical framework for anaerobic oxidation of methane driven by Fe(III)-dependent respiration. *Nat Commun,* 9, 1642, doi: 10.1038/s41467-018-04097-9.

Yu, T., Wu, W., Liang, W., Lever, M. A., Hinrichs, K. U. and Wang, F. (2018) Growth of sedimentary Bathyarchaeota on lignin as an energy source. *Proc. Natl. Acad. Sci. U. S. A.,* 115, 6022-6027.

Zahnle, K., Schaefer, L. and Fegley, B. (2010) Earth's earliest atmospheres. *Cold Spring Harb Perspect Biol,* 2, a004895, doi: 10.1101/cshperspect.a004895.

Zhou, Z., Chen, J., Cao, H., Han, P. and Gu, J. D. (2015) Analysis of methane-producing and metabolizing archaeal and bacterial communities in sediments of the northern South China Sea and coastal Mai Po Nature Reserve revealed by PCR amplification of mcrA and pmoA genes. *Front Microbiol,* 5, 789, doi: 10.3389/fmicb.2014.00789.

Zhou, Z., Liu, Y., Lloyd, K. G., Pan, J., Yang, Y., Gu, J. D. and Li, M. (2018a) Genomic and transcriptomic insights into the ecology and metabolism of benthic archaeal cosmopolitan, *Thermoprofundales* (MBG-D archaea). *ISME J.* 13, 885–901

Zhou, Z., Pan, J., Wang, F., Gu, J. D. and Li, M. (2018b) Bathyarchaeota: globally distributed metabolic generalists in anoxic environments. *FEMS Microbiol Rev,* 42, 639-655.

Zhuang, G.-C., Heuer, V. B., Lazar, C. S., Goldhammer, T., Wendt, J., Samarkin, V. A., Elvert, M., Teske, A. P., Joye, S. B. and Hinrichs, K.-U. (2018) Relative importance of methylotrophic methanogenesis in sediments of the Western Mediterranean Sea. *Geochim. Cosmochim. Acta,* 224, 171-186.

Acknowledgements

First of all, I would like to thank my supervisor, professor Friedrich, who immediately accepted me to have my PhD study after sending the application. Although I had a hard time in detecting methylotrophic methanogens using ^{13}C-methanol when I started my PhD, professor Friedrich fully supported me to develop the labeling strategy and finally we had success with RNA-SIP. Except for knowledge, I also broaden my scope of vision in science from you. Thank you, professor.

Secondly, I am deeply grateful to my PhD committee. Thank you for your time to review my thesis and attending my PhD defense.

I am also sincerely thankful to all of my great colleagues and friends including Prof. Karl-Heinz Blotevogel, Dr. Tetsuro Miyatake, Dr. Rolf Nimzyk, Dr. Oluwatobi Oni, Dr. Saar Sztejrenszus, Dr. Tim Richter-Heitmann, Dr. David Aromokeye, Dr. Weichao Wu, Charlotte Holz, Celina Schreiber, Martina Stickan, Ajinkya Kulkarni, Annika Schnakenberg, Shreya Tilve, Lea Wunder and Qingzeng Zhu. Thanks to all of my collaborators and partner Prof. Meng Li, Weichao Wu, Mara Maeke, Jenny Wendt, Mingwei Cai, Yang Liu, Xavier Prieto Mollar. Thank you for your support.

Lastly, I would like to thank my family, my wife, my parents, my sister and my parents-in-law. Without your support, I could not imagine how I could have finished my thesis.

Universität Bremen

Ort, Datum: _____

Versicherung an Eides Statt

Ich, _____ (Vorname, Name, Anschrift, Matr.-Nr.)

versichere an Eides Statt durch meine Unterschrift, dass ich die vorstehende Arbeit selbständig und ohne fremde Hilfe angefertigt und alle Stellen, die ich wörtlich dem Sinne nach aus Veröffentlichungen entnommen habe, als solche kenntlich gemacht habe, mich auch keiner anderen als der angegebenen Literatur oder sonstiger Hilfsmittel bedient habe.
Ich versichere an Eides Statt, dass ich die vorgenannten Angaben nach bestem Wissen und Gewissen gemacht habe und dass die Angaben der Wahrheit entsprechen und ich nichts verschwiegen habe.
Die Strafbarkeit einer falschen eidesstattlichen Versicherung ist mir bekannt, namentlich die Strafandrohung gemäß § 156 StGB bis zu drei Jahren Freiheitsstrafe oder Geldstrafe bei vorsätzlicher Begehung der Tat bzw. gemäß § 161 Abs. 1 StGB bis zu einem Jahr Freiheitsstrafe oder Geldstrafe bei fahrlässiger Begehung.

_____
Ort, Datum Unterschrift